AEROTHERM CORPORATION

RESEARCH & DEVELOPMENT IN AEROTHERMOCHEMISTRY

Final Report No. 67-16, Part II

EXPERIMENTAL AND ANALYTICAL EVALUATION OF THE APOLLO THERMAL PROTECTION SYSTEM UNDER SIMULATED REENTRY CONDITIONS

by

John W. Schaefer
Donald T. Flood
John J. Reese, Jr.
Kimble J. Clark

[redacted]

[redacted]

AEROTHERM FINAL REPORT NO. 67-16 PART II

EXPERIMENTAL AND ANALYTICAL EVALUATION OF THE APOLLO THERMAL PROTECTION SYSTEM UNDER SIMULATED REENTRY CONDITIONS

by

John W. Schaefer
Donald T. Flood
John J. Reese, Jr.
Kimble J. Clark

July 15, 1967

PART II
ANALYSIS OF RESULTS

Prepared for

National Aeronautics and Space Administration

NASA Manned Spacecraft Center
Houston, Texas
Structures and Mechanics Division
Donald J. Tillian/ES

Contract NAS9-5430

Aerotherm Project 6007

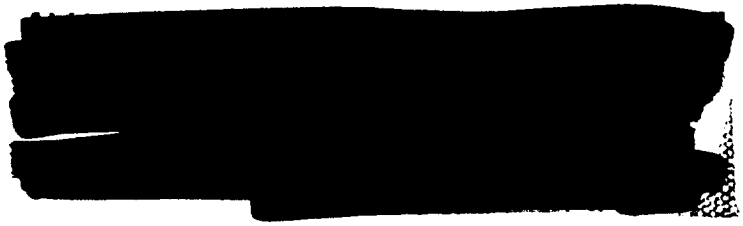

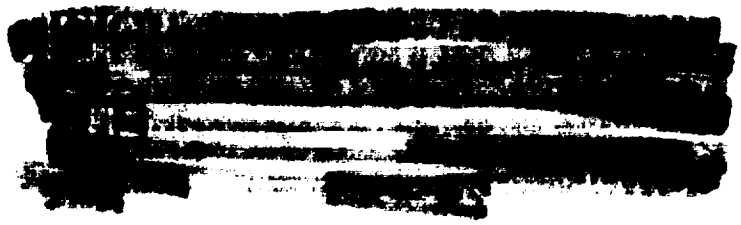

TABLE OF CONTENTS

TABLE OF CONTENTS (continued)

LIST OF FIGURES

LIST OF FIGURES (concluded)

LIST OF TABLES

LIST OF SYMBOLS

A	area (ft^2), or asymptotic calorimeter identification
a	channel (duct) height (inch), or a constant
B	pre-exponential factor (1/sec)
B'	dimensionless recession rate parameter
BH	blunt hemisphere model shape identification
C_p	specific heat (Btu/lb-^oR)
D	model body diameter (inch), or diameter (inch), or duct
D_c	model core diameter (inch)
d_e	nozzle exit diameter (inch)
E_a/R	activation energy factor (^oR)
FF	flat face model shape identification
H	hemisphere model shape identification
h	enthalpy (Btu/lb)
K	mass fraction
K_c	char thermal conductivity (Btu/ft-sec-^oR)
K_p	virgin material thermal conductivity (Btu/ft-sec-^oR)
$\tilde{K}$	elemental mass fraction
Le	Lewis number
M	mass loss (gm)
m	mass (gm)
$\dot{m}$	mass flow rate of gas (lb/sec)
$\dot{m}_c$	mass loss rate of char (lb/sec)
$\dot{m}_g$	mass loss rate of pyrolysis gases (lb/sec)
$\mathcal{M}$	molecular weight (lb/lb-mol)
N	number of mols
Pr	Prandtl number
p_e	nozzle exit pressure (atm), or local static pressure (atm)
p_o	plenum (chamber) pressure (atm)
p_s	model stagnation pressure (atm)
p_v	vapor pressure (atm)
Q_{in}	arc input power (Btu/sec)

LIST OF SYMBOLS (continued)

Q_{loss}	total energy transfer rate to cooling water (Btu/sec)
q	heat flux (Btu/ft^2sec)
q_c	convective heat flux (Btu/ft^2sec)
$q_c\sqrt{R}$	stagnation point heating rate ($Btu/ft^{3/2}sec$)
R	effective spherical nose radius (ft), or radius (ft), or gas constant ($ft\text{-}lb_f/lb_m$)
$\bar{R}$	universal gas constant ($ft\text{-}lb_f/lb\text{-}mol\,^oR$)
RAD	radiation probe identification
r	nozzle radius (inch)
r_e	nozzle radius at exit (inch)
SUBS	subsonic anode arc configuration identification
SUPS	supersonic anode arc configuration identification
s	surface recession (inch)
$\dot{s}$	average surface recession rate (mils)
T	absolute temperature (^oR), or transient calorimeter identification
T_{ref}	reference temperature (^oR)
Z	compressibility
α	angle from stagnation point for a spherical nose
ΔT	temperature difference (^oR)
$\Delta\theta$	time increment (sec)
ϵ	emissivity
θ	exposure time or time (sec)
γ	blowing reduction parameter
μ	viscosity (lb/sec-ft)
ρ	density (lb/ft^3)
ρ_c	residual or fully-charred material density (lb/ft^3)
ρ_p	virgin material density (lb/ft^3)
$\rho_e u_e C_H$	heat transfer coefficient (lb/ft^2sec)
$\rho_e u_e C_M$	mass transfer coefficient (lb/ft^2sec)
τ_w	wall shear stress (lb/ft^2)
ψ	density factor exponent

Subscripts

cal	(based on) calorimeter
cpi	char-pyrolysis zone interface
cw	cold wall
eb	energy balance
hf	heat flux
hw	hot wall
mb	mass balance
n	nose
O	oxygen
o	non-ablating
ppi	pyrolysis zone - virgin material interface
N	nitrogen
r	radiative
t	total
w	wall
*	condensed phase, or evaluated at sonic throat conditions
0	centerline
1,2	species 1, species 2

SECTION 8
INTRODUCTION

All experimental and analytical results obtained under this program, a study of the Apollo thermal protection system under simulated reentry conditions, were presented in Part I together with all the necessary support information on test apparatus, technique, and models, and on the analytical prediction techniques. Part II, contained herein, presents the analysis and interpretation of these results. For the sake of continuity within this part of the report, Part II is written as a separate document and includes essentially all material response information necessary to the interpretation and analysis of the results. The general background information and program description is also included for completeness in this introductory section. Section 8.1 presents a general introduction which is basically the introduction to Part I, and Section 8.2 presents a brief program outline. As noted in Section 8.1, Section 9 which follows presents the analysis of the material response, Section 10 presents a summary of this analysis in the form of a descriptive characterization of the material response, and Section 11 presents recommendations for future work.

8.1 GENERAL INTRODUCTION

The design and qualification of the Apollo thermal protection system requires an accurate knowledge of the system ablative material response to atmospheric entry conditions. For entry from the Apollo lunar mission, these conditions encompass a broad spectrum of enthalpy, pressure, heat flux, both convective and radiative, and shear. The response of the thermal protection material to this reentry environment must be known so that the system design has adequate protection capabilities but minimum weight. In order to define and evaluate this material response, ground tests that closely simulate the conditions of manned lunar return are required. Arc plasma generator testing provides an ideal means for simulating these conditions. An extensive test program on the Apollo thermal protection system material, using an arc plasma generator to simulate the broad spectrum of conditions experienced by the Apollo vehicle, was therefore performed. The results of this test program are presented in this report.

Because of scaling problems and the time variation of the above mentioned environmental parameters, it is not possible to exactly duplicate simultaneously all trajectory conditions in a ground test facility. The test results must therefore be related to empirical or theoretical prediction techniques which can then in turn be used to predict the thermal protection system response to flight trajectories. An analysis of the test results in the light of this requirement is also included herein.

This report is divided into two basic parts, Part I which presents all results obtained under the program and Part II which discusses and analyzes these results. Part I is a separate document and is divided into seven sections. Section 2 presents an outline of the overall program to provide the reader a brief but complete look at the total program. Section 3 presents the descriptions of the test facilities in which the reentry simulation tests were performed. Section 4 presents a detailed description of all test models of the thermal protection system material used in the program. Section 5 presents all instrumentation and the data reduction techniques. Section 6 presents all test results obtained under the program including the test model response to the broad spectrum of conditions to which they were exposed, the test conditions calibration results, and the results of chemical and physical properties tests on some of the tested models. Finally, Section 7 presents the results of analytical predictions of material performance made for a broad spectrum of conditions including several corresponding to model tests.

Part II, contained herein, provides the discussion and analysis of the test results. Section 9 provides the interpretation and analysis of all results obtained under the program including the reentry simulation test results, the analytical prediction results, and the chemical and physical properties test results. Section 10 presents a summary of all results in the form of a descriptive characterization of the material response based on all program results. Finally, Section 11 presents recommendations for future work.

The authors express their appreciation to the many NASA and Aerotherm personnel who have contributed to the program. The contributions of Mr. Donald J. Tillian, the NASA-MSC Technical Monitor, and Mr. Donald M. Curry, also of NASA-MSC, are gratefully acknowledged. Particular thanks go to Mr. Roy M. Wakefield of the Gasdynamics Branch of NASA-Ames who conducted the combined convective and radiative heating test program in the NASA-Ames Entry Heating Simulator. The Aerotherm staff members who contributed to the program include Mr. Roald A. Rindal and Dr. Robert M. Kendall of the techical staff, Mr. Thomas Wong who performed all design work and assisted in the testing, and Mr. Francis J. McKinley who served as chief technician; their efforts are gratefully acknowledged.

8.2 PROGRAM DESCRIPTION

The complete program performed under this contract, NAS9-5430, is outlined briefly below. The program was divided into three basic efforts for

study of the Apollo thermal protection material as follows, the first of which being the main program effort:

Test and evaluation under simulated reentry conditions.
Analytical predictions of performance under test and reentry conditions.
Chemical and physical properties tests on models exposed to simulated reentry conditions.

The 5026-39HCG material was considered almost exclusively in the program; a few tests were also performed on other similar materials.

The reentry simulation test program was divided into seven phases. These phases are outlined below and the nominal range of test conditions noted.

Phase I Shear

Study of the effect of shear on material performance

Enthalpy	3000 to 10,000 Btu/lb
Local pressure	1 to 3 atm
Shear stress	3 to 20 psf
Convective heat flux	175 to 525 Btu/ft^{2}sec
Chemical environment	Air and Nitrogen

Phase II Combined Convective and Radiative Heating

Study of the effect of combined convective and radiative heating and radiative - only heating on material performance

Enthalpy	3000 to 6250 Btu/lb
Stagnation pressure	0.10 atm
Convective heat flux	0 to 175 Btu/ft^{2}sec
Radiative heat flux	0 to 600 Btu/ft^{2}sec
Chemical environment	Air

Phase III High Stagnation Pressure

Study of the effect of high heat flux and high pressure on material performance

Enthalpy	3500 to 5000 Btu/lb
Stagnation pressure	1 to 3 atm
Convective heat flux	800 to 1800 Btu/ft^{2}sec
Chemical environment	Air and Nitrogen

Phase IV A Low Stagnation Pressure and Exposure Time

Study of material performance at low stagnation pressure and study of the effect of exposure time on material performance

Enthalpy	3500 to 25,000 Btu/lb
Stagnation pressure	0.008 atm
Convective heat flux	30 to 250 Btu/ft^{2}sec
Chemical environment	Air

Phase IV B Low Stagnation Pressure and Chemical Environment

Study of the effect of chemical environment on material performance at low pressure

Enthalpy	5000 to 17,500 Btu/lb
Stagnation pressure	0.028 atm
Convective heat flux	90 to 300 Btu/ft^{2}sec
Chemical environment	Air, Nitrogen, Helium, various Oxygen concentrations in Nitrogen

Phase V Model Size and Exposure Time

Study of material performance at low stagnation pressure, study of the effect of model size on test results, and study of the effect of exposure time on material performance

Enthalpy	5000 to 17,500 Btu/lb
Stagnation pressure	0.008 to 0.028 atm
Convective heat flux	60 to 450 Btu/ft^{2}sec
Chemical environment	Air

Phase VI A Model Shape, Constant Enthalpy and Constant Stagnation Pressure

B Model Shape, Constant Stagnation Pressure and Constant Stagnation Heating Rate

Study of material performance at low stagnation pressure, study of the effect of model shape on test results

Enthalpy	3500 to 25,000 Btu/lb
Stagnation pressure	0.028 atm
Convective heat flux	60 to 450 Btu/ft^{2}sec
Chemical environment	Air

Phase VII Enthalpy and Stagnation Pressure at Constant Heating Rate

Study of material performance at constant heating rate with enthalpy and pressure variable

Enthalpy	3500 to 25,000 Btu/lb
Stagnation pressure	0.028 to 0.4 atm
Convective heat flux	450 Btu/ft^{2}sec
Chemical environment	Air

A total of 158 models were tested over the above spectrum of conditions. The program also included a complete calibration of these test conditions.

The analytical predictions of material performance were made using the Aerotherm ablation computer programs and input information based on data provided by NASA-MSC. Predictions were made at conditions corresponding to several of the model tests and for a parametric array of environmental conditions.

The chemical and physical properties tests were performed on several models tested under simulated reentry conditions. These properties tests included microchemical quantitative analysis and X-ray diffraction studies of the surface materials and in-depth char, density distribution measurements as determined by X-ray transmission, infrared spectra measurements of the in-depth char and surface materials, and surface and in-depth photomicrographs.

The analysis and interpretation of the results obtained under the program are presented in the following sections.

SECTION 9
ANALYSIS OF MATERIAL RESPONSE

The analysis of the 5026-39HCG material response, based on all experimental and analytical results obtained under the program, are presented in this section. The results of the reentry simulation tests, presented in Section 6.2, are discussed in Section 9.1, this discussion covering all phases of the test program. The results are analyzed both qualitatively and quantitatively and two basic correlations of the results are presented. The analytical predictions, presented in Section 7.4, are discussed in Section 9.2. Comparisons are made with the measured material performance, and the material response mechanisms are analyzed in the light of these comparisons. The results of the chemical and physical properties tests, presented in Section 6.3, are discussed in Section 9.3. The material response mechanisms and the theoretical model used in the analytical predictions are analyzed in terms of these results.

9.1 REENTRY SIMULATION TEST RESULTS

The results of all reentry simulation model tests performed under the contract are discussed in the following sections. This discussion is directed primarily towards the surface recession rate and surface temperature results; the internal response is discussed briefly below but the major discussion is deferred to Section 9.2.1 which presents the comparisons between test results and analytical predictions. The discussion of model test results presented below is divided into two sections. Section 9.1.1 is concerned with the complete program results taken in total and presents correlations of these results. Section 9.1.2 discusses the effects of the various test variables on material response according to the various phases of the test program.

9.1.1 Correlation of Results

In order to provide an overall look at the test results and to provide a basis for discussing the effects of the various test variables on material performance, the results from all phases of the program are discussed below as a group. Empirical correlations of the complete set of results are presented and the validity of these correlations discussed. The material response results are presented in terms of average surface recession rate and surface temperature where average surface recession rate is defined as total centerline measured surface recession divided by exposure time (s/θ) and average surface temperature is the average measured temperature once the surface has reached a relatively stable temperature level. The internal response is also discussed briefly at the end of this section.

A summary of the model response and test conditions for all tests in each program phase is presented in Table 9-1. All subsequent plots of the experimental results presented in this and following sections are based on these results. The hot-wall convective heat transfer coefficients presented in the table correspond to the assumption that the ratio $(\rho_e u_e C_H)_{hw}/(\rho_e u_e C_H)_{cw}$ is 0.925 as discussed in Section 7.3.2.7. These coefficients were therefore calculated from

$$(\rho_e u_e C_H)_{hw} = 0.925 \frac{(q_c \sqrt{R})_{cal}}{\sqrt{R_m}\,(h - h_w)} = 0.925 \frac{(q_c)_m}{h - h_w} \qquad (9\text{-}1)$$

where R_m is the model effective nose radius and h_w is the enthalpy at the calorimeter wall temperature, assumed to be $300^{\circ}F$ in all cases.

The test results obtained under the program and presented in subsequent figures cover a broad spectrum of conditions. Because many of these figures include almost all these results, it was necessary to define a special set of symbols to identify the pertinent model and test variables. This symbol key is presented in Table 9-3 and is on a fold-out page for convenience in reviewing the following figures. The circle symbol is used for illustrative purposes in demonstrating the keys for variables other than enthalpy. This special key is used throughout the report to provide continuity in the plots.

Plots of all results obtained under the program for stagnation point, convective-only heating in air are presented in Figures 9-1 through 9-8. Before discussing these figures, a comment on the effect of exposure time on average surface recession rate and temperature is in order since the results presented cover a broad spectrum of exposure times. From all results except those at low surface recession rate, $\dot{s} < 1$ mil/sec, and low surface temperature, $T_w < 3000^{\circ}R$, the material response is essentially independent of exposure time. Exposure time is therefore not a significant variable in these plots except for the few points at the above conditions. The effects of exposure time are discussed in detail in Section 9.2.4. It should also be noted that the results at moderate and low recession rate cover the entire enthalpy spectrum from 3000 Btu/lb to 25,000 Btu/lb whereas the results at high recession rate correspond to enthalpies of 5000 Btu/lb or less. Also the high recession rate results were obtained at moderate and high stagnation pressure and the moderate and low recession rate results at low stagnation pressure. Note that wherever the surface recession was highly irregular (high pressure) the maximum and minimum recession was measured (Table 9-1); for these cases both results are plotted in the figures and the points connected by a line.

TABLE 9-1

ABLATION MODEL RESPONSE RESULTS

(A) PHASE I SHEAR

Model No.	Enthalpy h (Btu/lb)	Chamber Pressure P_c (atm)	Model Heating Rate $(\dot{q}_c)_{cw}$ (Btu/ft sec)	Model Heat Transfer Coefficient $(\rho_e u_e C_H)_{cw}$ (lb/ft sec)	Shear Stress τ (c) (psf)	Chemical Environment	Exposure Time t (sec)	Surface Recession s (inch)	Average Recession Rate $\dot{s}$ (mils/sec)	Average Surface Temperature T_w (°R)	Inverse of Surface Temperature $1/T_w \times 10^3$ ($°R^{-1}$)	Char Depth (a) (inch)	Pyrolysis Zone Depth (a) (inch)	Mass Loss Δ (gm)	Recession Rate Parameter B'	Post Test Surface Description (b)	Test Condition	Test No.
6/D/.22	5,430	1.38	161	0.030	2.67	Air	29.6	0.308	10.4	4,725	2.12	0.386	—	0.807	0.941	—	50	377
9/D/.22	"	1.40	"	"	"	"	29.7	0.283	9.52	4,575	2.19	0.345	—	1.04	1.20	—	"	378
12/D/.22	5,220	1.41	"	"	"	"	30.4	0.096	3.16	4,700	2.13	0.221	—	0.729	0.434	—	"	379
1/D/.22	5,310	2.25	282	0.075	10.50	"	16.1	0.280	17.4	4,650	2.15	0.340	—	0.866	0.631	—	51	1,481
8/D/.22	4,750	2.32	"	"	"	"	"	0.233	14.5	4,625	2.16	0.279	—	0.949	0.734	—	"	1,482
11/D/.22	5,800	2.76	"	"	"	"	17.5	0.155	8.86	5,000	2.00	0.201	—	0.849	0.489	—	"	1,495
2/D/.22	4,780	5.08	500	0.136	19.10	"	10.7	0.428	40.0	4,875	2.05	0.448	—	1.20	0.805	—	52	1,483
7/D/.22	4,500	5.11	"	"	"	"	12.1	0.353	29.2	4,650	2.15	0.368	—	1.24	0.819	—	"	1,484
10/D/.22	4,310	"	"	"	"	"	5.9	0.154	26.1	4,800	2.08	0.159	—	0.609	0.796	—	"	1,499
5/D/.22	5,250	1.16	160	0.044	2.67	Nitrogen	30.2	0.011	0.36	4,225	2.37	0.229	—	0.382	0.012	—	53	482
3/D/.22	4,740	2.48	278	0.070	10.00	"	16.4	0.231	14.1	5,000	2.00	0.261	—	0.659	0.551	—	54	1,490
4/D/.22	4,740	5.62	484	0.141	18.70	"	11.9	0.333	28.0	5,050	1.98	0.379	—	1.28	0.544	—	55	1,491
07/D/.22	4,230	1.38	237	0.065	7.16	Air	11.6	0.210/0.295	18.1/25.4	4,700	2.13	0.245/0.330	0.260/0.345	0.695	0.756/0.616	G,(M)	8	712
08/D/.22	4,050	1.42	"	"	"	"	11.4	0.175/0.270	15.3/23.6	4,800	2.08	0.245/0.340	0.255/0.350	0.612	0.639/0.986	"	"	713
01/D/.22	3,030	1.65	211	0.062	7.95	Nitrogen	27.4	0.05/0.38	1.82/13.9	4,900	2.04	0.120/0.68	0.130/0.69	0.743	0.081/0.617	LG,(DG),NM	7	710
02/D/.22	3,970	1.64	"	"	"	"	28.8	0.26/0.465	9.02/16.1	5,100	1.96	0.400/0.605	0.420/0.625	0.934	0.401/0.715	G,NM	"	711
7/D/.22	3,730	1.14	192	0.047	2.71	Air	8.3	0.061	7.35	4,500	2.22	0.141	0.151	0.242	0.427	G,(M)	9	721
6/D/.22	3,240	1.12	"	"	"	"	15.7	0.165/0.210	10.5/13.4	4,700	2.12	0.220/0.265	0.235/0.280	0.630	0.610/0.778	G,M	"	722
03/D/.22	4,340	1.20	179	0.045	3.38	Nitrogen	27.9	0.011	0.50	4,075	2.46	0.204	0.254	0.420	0.030	G,NM	11	720
5/D/.22	10,140	1.10	321	0.038	3.25	Air	12.5	0.086	6.88	4,650	2.15	0.166	0.186	0.833	0.498	"	10	723
11/D/.22	10,140	"	"	"	"	"	15.7	0.110	7.00	4,675	2.14	0.210	0.230	0.426	0.507	"	"	724
09/D/.22	9,210	1.13	326	"	2.91	Nitrogen	28.7	0.021	0.73	4,750	2.10	0.241	0.291	0.399	0.053	BR,NM	12	719

(a) Based on $(\rho_e u_e C_H)_{cw} = 0.92 \times (\rho_e u_e C_H)_{cw}$

(b) Nominal initial shear stress

( ) Referenced to original surface

(c) See Surface Description Key, Table 9-2

TABLE 9-1

ABLATION MODEL RESPONSE RESULTS

(b) PHASE II — COMBINED CONVECTIVE AND RADIATIVE HEATING

Model No.	Enthalpy h (Btu/lb)	Stagnation Pressure P_s (atm)	Model Heating Rate: Convective $(q_c)_{cw}$ (Btu/ft²sec)	Model Heating Rate: Radiative q_r (-) (lb/ft sec)	Model Heat Transfer Coefficient $(\rho_e u_e C_H)_{nw}(a)$ (lb/ft²sec)	Chemical Environment	Exposure Time τ (sec)	Surface Recession s (inch)	Average Recession Rate $\dot{s}$ (mils/sec)	Average Surface Temperature T_w (°R)	Inverse of Surface Temperature $1/T_w \times 10^3$ ($°R^{-1}$)	Char Depth (-) (inch)	Pyrolysis Zone Depth (-) (inch)	Mass Loss M (gm)	Recession Rate Parameter B'	Post Test Surface Description (b)	Test Condition	Test No.
40/FF/1.25	3,090	0.112	163	0	0.051	Air	20.1	0.070	3.48	3,775	2.65	0.130	0.160	0.063	0.186	DG,M	56	66
38/FF/1.25	3,100	"	164	81.5	0.049	"	"	0.095	4.73	3,900	2.56	0.195	0.215	0.104	0.264	DG,(M)	57	69
45/FF/1.25	3,210	"	168	153	0.048	"	15.0	0.090	6.00	4,200	2.38	0.160	0.180	0.076	0.339	DG,NM	58	72
50/FF/1.25	3,120	"	"	336	"	"	10.1	0.068	6.73	4,550	2.20	0.138	0.158	0.065	0.383	"	59	73
62/FF/1.25	3,050	"	170	500	0.052	"	8.1	0.105	12.96	4,600	2.18	0.185	0.205	0.068	0.675	G,NM	60	76
51/FF/1.25	3,290	"	148	0	0.043	"	30.2	0.112	3.71	3,625	2.76	0.212	0.232	0.088	0.234	G,M	56	216
61/FF/1.25	3,260	"	"	0	"	"	—	0.110	—	—	—	—	—	—	—	G,NM	"	217
46/FF/1.25	3,250	"	"	150	"	"	20.2	0.138	6.83	4,050	2.47	0.218	0.238	0.099	0.431	"	58	218
56/FF/1.25	3,420	"	"	352	"	"	20.1	0.121	6.02	4,400	2.28	0.231	0.251	0.096	0.379	DG,NM	59	219
63/FF/1.25	5,020	0.071	102	0	0.019	"	25.1	0.025	1.00	3,800	2.63	0.095	0.115	0.070	0.144	G,M	61	156
59/FF/1.25	5,130	"	"	66	"	"	26.0	0.081	3.12	4,000	2.50	0.181	0.211	0.064	0.448	G,NM	62	157
53/FF/1.25	5,120	"	95	107	0.017	"	25.1	0.032	1.27	4,100	2.44	0.132	0.172	0.083	0.207	DG,NM	64	160
60/FF/1.25	5,130	"	"	214	"	"	25.2	0.072	2.86	4,400	2.28	0.192	0.212	0.086	0.467	"	64	161
47/FF/1.2	5,060	"	"	472	"	"	15.1	0.090	5.96	4,800	2.08	0.190	0.210	0.093	0.972	"	65	162
49/FF/1.25	6,290	0.099	214	0	0.032	"	25.3	0.103	4.07	4,100	2.44	0.183	0.213	0.092	0.350	"	66	201
58/FF/1.25	6,780	"	"	111	"	"	"	0.140	5.53	4,500	2.22	0.220	0.240	0.105	0.476	"	67	203
66/FF/1.25	6,810	"	"	215	"	"	20.2	0.082	4.06	4,600	2.18	0.182	0.202	0.094	0.350	"	68	204
42/FF/1.25	6,390	"	"	349	"	"	15.1	0.065	4.30	4,700	2.12	0.175	0.195	0.078	0.369	"	69	207
44/FF/1.25	6,170	"	"	390	"	"	15.2	0.082	5.39	4,750	2.10	0.182	0.202	0.094	0.465	"	70	208
48/FF/1.25	—	—	0	96	—	Vacuum	20.8	0.012	0.58	3,075	3.26	0.062	0.092	0.045	—	LG,NM	71	220
42/FF/1.25	—	—	"	218	—	"	20.0	0.032	1.60	3,800	2.63	0.112	0.132	0.065	—	"	72	221
46/FF/1.25	—	—	"	295	—	"	"	0.022	1.10	4,150	2.41	0.122	0.152	0.047	—	"	73	222
7/FF/1.25	—	—	"	487	—	"	15.0	0.059	3.93	4,925	2.03	0.169	0.189	0.059	—	"	74	223
58/FF/1.25	—	—	"	569	—	"	15.1	0.104	6.89	4,825	2.07	0.214	0.234	0.130	—	"	75	224

(a) Average of prerun and postrun radiative heating rates

( ) Based on $(\rho_e u_e C_H)_{nw} = 0.75 (\rho_e u_e C_H)_{cw}$

(-) Referenced to original surface

(b) See Surface Description Key, Table 9-2

TABLE 9-1

ABLATION MODEL RESPONSE RESULTS

(c) PHASE III - HIGH STAGNATION PRESSURE

Model No.	Enthalpy h (Btu/lb)	Stagnation Pressure P_s (atm)	Model Heating Rate $(q_c)_{cw}$ (Btu/ft sec)	Model Heat Transfer Coefficient $(\rho_e u_e C_H)_{hw}$ (a) (lb/ft sec)	Chemical Environment	Exposure Time (sec)	Surface Recession s (inch)	Average Recession Rate $\dot{s}$ (mils/sec)	Average Surface Temperature T_w (°R)	Inverse of Surface Temperature $1/T_w \times 10$ ($°R^{-1}$)	Char Depth ( ) (inch)	Pyrolysis Zone Depth ( ) (inch)	Mass Loss M (gm)	Recession Rate Parameter B'	Post Test Surface Description (b)	T/C	Test No.
154/BH/1.0	5,681	1.06	1,170	0.217	Air	15.2	0.585	38.5	4,600	2.17	0.625	0.643	0.670	0.484	DG,NM	43	869A
158/BH/1.0	"	"	"	"	"	10.2	0.509	50.0	——	——	0.549	0.559	0.833	0.629	"	"	869B
113/BH/1.0	5,047	1.05	1,200	0.222	"	5.1	0.240	47.0	4,960	2.02	0.260/0.290	0.265/0.295	0.383	0.579	G,NM	"	870A
141/BH/1.0	4,975	1.11	1,110	0.208	Nitrogen	20.2	0.435/0.465	21.5/23.0	4,700	2.12	0.495/0.565	0.505/0.600	0.797	0.282/0.301	DG,NM	42	867A
152/BH/1.0	"	"	"	"	"	10.1	0.275/0.435	27.2/43.0	——	——	0.295/0.495	0.305/0.505	0.617	0.355/0.563	G,NM	"	867B
156/BH/1.0	5,456	1.02	805	0.219	Air	20.6	0.635/0.735	30.8/35.6	4,800	2.08	0.665/0.765	0.670/0.770	1.086	0.385/0.446	"	40	868A
157/BH/1.0	"	"	"	"	"	10.5	0.355/0.525	33.8/50.0	——	——	0.388/0.558	0.395/0.565	0.643	0.424/0.626	"	"	868B
134/BH/1.0	3,310	1.01	836	0.238	"	5.1	0.311	61.0	4,600	2.17	0.331	0.336	0.442	0.702	DG,NM	"	870B
149/BH/1.0	3,556	"	884	0.233	Nitrogen	30.1	0.595/0.875	19.8/29.0	4,800	2.08	0.595/0.935	0.600/0.945	1.266	0.232/0.125	——	41	866A
150/BH/1.0	"	"	"	"	"	15.0	0.292	19.4	——	——	0.357	0.377	0.522	0.227	G,NM	"	866B
159/BH/1.0	3,251	1.93	1,150	0.333	Air	7.3	——	——	5,000	2.00	——	——	——	——	——	44	875A
160/BH/1.0	"	"	"	"	"	5.4	0.485/0.875	90.0/162	5,070	1.97	0.485/0.900	0.490/0.905	0.952	0.738/1.33	G,NM	"	875B
143/BH/1.0	3,115	1.94	1,120	0.338	"	1.9	0.203	107	4,960	2.02	0.218	0.223	0.390	0.866	DG,NM	"	876A
145/BH/1.0	"	"	"	"	"	"	0.305/0.515	160/271	4,920	2.04	0.315/0.535	0.323/0.533	0.582	1.30/2.19	G,NM	"	876B
146/BH/1.0	3,000	2.05	1,060	0.288	Nitrogen	10.2	0.759	74.4	4,960	2.02	0.784	0.789	1.23	0.705	"	45	874A
147/BH/1.0	"	"	"	"	"	5.4	0.220	40.7	5,000	2.00	0.260	0.265	0.524	0.385	DG,NM	"	874B
161/BH/1.0	3,015	3.16	1,820	0.339	Air	3.2	0.365	114	4,760	2.10	0.365/0.380	0.370/0.385	0.730	0.918	G,NM	49	882A
162/BH/1.0	3,224	3.08	1,800	0.322	"	"	0.375/0.545	117/186	——	——	0.375/0.595	0.380/0.600	0.795	0.992/1.58	"	"	885A
155/BH/1.0	3,367	3.10	1,770	0.308	"	1.84	0.227	123	——	——	0.234	0.239	0.17	1.09	"	"	886
142/BH/1.0	3,015	3.16	1,820	0.339	"	2.8	0.365/0.455	130/162	5,030	1.99	0.365/0.465	0.370/0.470	0.648	1.05/1.31	"	"	882B
144/BH/1.0	3,224	3.08	1,800	0.322	"	1.8	0.205/0.335	114/186	——	——	0.210/0.365	0.213/0.380	0.428	0.937/1.53	"	"	885B
136/BH/1.0	3,151	3.10	1,770	0.321	"	2.9	0.418	144	4,850	2.06	0.428	0.428	0.17	1.22	"	"	884B
133/BH/1.0	3,602	3.16	1,790	0.364	Nitrogen	3.98	0.405/0.632	101/158	——	——	0.405/0.662	0.410/0.667	0.92	0.757/1.19	DG,NM	48	881A
135/BH/1.0	"	"	"	"	"	"	0.275/0.365	68.8/91.3	——	——	0.295/0.405	0.300/0.410	0.39	0.516/0.686	G,NM	"	881B
132/BH/1.0	3,518	3.01	1,230	0.328	Air	4.28	0.405/0.525	94.2/122	——	——	0.415/0.535	0.420/0.540	0.78	0.784/1.02	"	46	883A
137/BH/1.0	"	"	"	"	"	2.54	0.255/0.445	101/175	——	——	0.262/0.452	0.267/0.457	0.17	0.842/1.46	"	"	883B
131/BH/1.0	3,519	3.08	1,210	0.323	"	3.40	0.345/0.475	101/140	——	——	0.355/0.385	0.360/0.390	0.39	0.856/1.19	"	"	884A
130/BH/1.0	3,471	3.13	1,180	0.312	Nitrogen	3.67	0.384	104	4,730	2.12	0.394	0.402	0.594	0.806	"	47	880A
131/BH/1.0	3,532	3.28	1,280	0.341	"	2.90	0.232/0.495	81.0/171	4,725	"	0.260/0.520	0.265/0.525	0.640	0.650/1.37	"	"	880B

(a) Based on $(\rho_e u_e C_H)_{hw} = 0.924 \times (\rho_e u_e C_H)_{cw}$

(b) Reference to original surface

(c) See Surface Description Key, Table 9-2

TABLE 9-1

ABLATION MODEL RESPONSE RESULTS

(d) PHASE IV A LOW STAGNATION PRESSURE AND EXPOSURE TIME

Model No.	Enthalpy h (Btu/lb)	Stagnation Pressure P_s (atm)	Model Heating Rate $(q_c)_{cw}$ (Btu/ft^{2}sec)	Model Heat Transfer Coefficient $(\rho_e u_e C_H)_{hw}$(1) (lb/ft^{2}sec)	Chemical Environment	Exposure Time t_e (sec)	Surface Recession s (inch)	Average Recession Rate $\dot{s}$ (mils/sec)	Average Surface Temperature T_w ($^\circ$R)	Inverse of Surface Temperature $1/T_w \times 10^4$ ($^\circ R^{-1}$)	Char Depth (2) (inch)	Pyrolysis Zone Depth (2) (inch)	Mass Loss M (gm)	Recession Rate Parameter B'	Post Test Surface Description (3)	Test Condition	Test No.
93/BH/2.0	3,442	0.0082	33.0	0.0090	Air	210.2	0.100	0.48	2,650	3.78	0.320	0.420	1.689	0.146	S	26	772B
95/BH/2.0	3,539	″	34.0	″	″	120.3	0.076	0.63	2,675	3.74	0.236	0.286	1.187	0.191	″	″	773B
94/BH/2.0	″	″	″	″	″	60.6	0.049	0.81	2,700	3.70	0.149	0.199	0.713	0.245	″	″	773A
89/BH/2.0	4,944	0.0090	48.0	0.0091	″	210.5	0.114	0.54	2,900	3.45	0.374	0.444	1.882	0.163	″	24	769A
88/BH/2.0	5,044	0.0110	46.0	0.0085	″	121.1	0.077	0.64	2,850	3.51	0.237	0.327	1.349	0.205	″	″	768A
87/BH/2.0	4,910	0.0112	47.0	0.0090	″	61.0	0.055	0.90	2,875	3.48	0.155	0.195	0.823	0.273	″	″	767A
92/BH/2.0	10,193	0.0079	123	0.0112	″	120.3	0.300	2.49	3,350	2.98	0.480	0.540	2.361	0.607	DG,M	25	772A
91/BH/2.0	10,969	″	116	0.0098	″	60.5	0.152	2.51	3,250	3.08	0.237	0.317	1.274	0.700	″	″	770B
90/BH/2.0	″	″	″	″	″	30.3	0.077	2.54	3,200	3.12	0.147	0.177	0.723	0.708	″	″	770A
106/BH/2.0	16,880	0.0082	162	0.0089	″	90.4	0.217	2.40	3,500	2.86	0.357	0.407	1.832	0.366	DG,(M)	37	856A
108/BH/2.0	16,301	0.0080	154	0.0088	″	60.4	0.147	2.44	3,550	2.82	0.247	0.317	1.515	0.760	——	″	855B
99/BH/2.0	″	″	″	″	″	30.3	0.078	2.57	3,475	2.88	0.178	0.218	0.800	0.801	DG,(M)	″	855A
163/BH/2.0	25,800	0.0085	251	0.0091	″	31.5	——	——	——	——	——	——	——	——	DG,NM	36	857B
166/BH/2.0	29,400	″	286	0.0090	″	70.0	0.184	2.63	3,900	2.56	0.444	0.504	2.129	0.694	″	″	859B
162/BH/2.0	25,800	″	251	″	″	60.5	0.153	2.53	3,850	2.60	0.293	0.353	2.697	0.768	DG,NM,(BD)	″	857A
109/BH/2.0	25,600	″	249	″	″	30.3	0.076	2.50	3,825	2.62	0.186	0.226	0.930	0.757	DG,NM	″	856B

(1) Based on $(\rho_e u_e C_H)_{hw} = 0.925\ (\rho_e u_e C_H)_{cw}$

(2) Referenced to original surface

(3) See Surface Description Key, Table 9-2

TABLE 9-1

ABLATION MODEL RESPONSE RESULTS

(c) PHASE IV B — LOW STAGNATION PRESSURE AND CHEMICAL ENVIRONMENT

Model No.	Enthalpy h_s (Btu/lb)	Stagnation Pressure P_s (atm)	Model Heating Rate $(q_c)_{cw}$ (Btu/ft sec)	Model Heat Transfer Coefficient $(\rho_e u_e C_H)_{mw}$ (a) (lb/ft sec)	Chemical Environment	Exposure Time τ (sec)	Surface Recession s (inch)	Average Recession Rate $\dot{s}$ (mils/sec)	Average Surface Temperature T_w (°R)	Inverse of Surface Temperature $1/T_w \times 10$ ($°R^{-1}$)	Char Depth (b) (inch)	Pyrolysis Zone Depth (b) (inch)	Mass Loss M (gm)	Recession Rate Parameter B'	Post Test Surface Description (c)	Test Condition	Test No.
74/BH/2.0	6,322	0.0261	130	0.019	Air	60.7	0.100	2.64	3,525	2.84	0.260	0.360	1.531	0.377	G,M	1	746A
79/BH/2.0	5,736	0.0276	99	0.016	0.70 N_2/0.30 O_2	61.0	0.196	3.21	3,450	2.90	0.286	0.326	1.66	0.544	"	14	748B
78/BH/2.0	5,640	0.0283	89	0.015	0.85 N_2/0.15 O_2	60.6	0.144	2.38	3,475	2.88	0.294	0.334	1.299	0.443	"	15	748A
77/BH/2.0	5,511	0.0296	76	0.013	0.93 N_2/0.07 O_2	61.4	0.114	1.86	3,350	2.98	0.274	0.314	1.232	0.394	"	16	747B
73/BH/2.0	5,801	0.0278	151	0.024	Nitrogen	60.8	0.050	0.82	3,725	2.68	0.260	0.320	2.273	0.092	G,NM	17	751A
76/BH/2.0	5,961	0.0297	188	0.029	"	60.5	0.082	1.36	3,750	2.67	0.292	0.342	1.230	0.126	DG,NM	1	747A
81/BH/2.0	10,918	0.0298	"	0.024	Helium	60.3	0.023	0.38	3,875	2.58	0.213	0.333	1.024	0.065	LG,NM	22	758A
82/BH/2.0	"	"	"	0.016	"	60.9	0.022	0.36	3,800	2.64	0.272	0.331	1.071	0.062	"	"	758B
75/BH/2.0	11,208	0.0283	201	"	Air	60.6	0.301	4.97	4,050	2.47	0.401	0.431	2.152	0.842	G,NM	2	746B
83/BH/2.0	10,100	0.0269	190	0.017	0.70 N_2/0.30 O_2	60.4	0.316	5.23	4,100	2.44	0.406	0.446	2.203	0.817	"	18	749B
84/BH/2.0	10,860	0.0290	174	0.015	0.85 N_2/0.15 O_2	61.0	0.242	3.97	4,275	2.34	0.382	0.422	1.982	0.727	BG,NM	19	750B
85/BH/2.0	10,442	"	214	0.019	0.93 N_2/0.07 O_2	60.3	0.215	3.57	4,350	2.30	0.375	0.415	1.912	0.511	"	20	750A
80/BH/2.0	9,907	0.0276	271	0.025	Nitrogen	60.6	0.172	2.84	4,425	2.26	0.292	0.402	1.767	0.306	"	21	749A
24/BH/2.0	11,013	0.0264	279	0.024	"	60.4	0.109	1.80	4,225	2.37	0.329	0.379	1.748	0.209	"	1	751B
101/BH/2.0	17,000	0.0287	311	0.017	Air	45.2	0.215	4.76	4,525	2.21	0.295	0.335	1.746	0.784	G,(BD),NM	30	834A
104/BH/2.0	17,000	0.0266	218	0.013	0.70 N_2/0.30 O_2	44.9	0.229	5.10	4,425	2.26	0.309	0.349	1.768	1.04	G,NM	32	841A
103/BH/2.0	17,000	0.0284	289	0.016	0.85 N_2/0.15 O_2	45.0	0.181	4.02	4,650	2.15	0.311	0.351	1.641	0.689	DG,(BD),NM	33	842A
102/BH/2.0	17,000	0.0275	297	"	0.93 N_2/0.07 O_2	"	0.135	3.00	4,600	2.18	0.295	0.335	1.527	0.522	"	34	843A
105/BH/2.0	17,000	0.0264	363	0.026	Nitrogen	45.3	0.120	2.65	4,875	2.05	0.310	0.370	1.563	0.393	BD,NM	35	841B
106/BH/2.0	17,000	0.0258	386	0.022	"	45.1	0.121	2.68	4,650	2.15	0.311	0.381	1.488	0.333	"	"	842B
107/BH/2.0	17,000	0.0254	418	0.023	"	44.9	0.107	2.38	4,575	2.19	0.307	0.327	1.347	0.276	"	"	843B
86/BH/2.0	18,019	0.0278	360	0.017	Helium	45.0	0.029	0.64	4,600	2.18	0.299	0.349	1.242	0.112	LG,BD,NM	23	759

(a) Based on $(\rho_e u_e C_H)_{mw} = 0.92 \cdot (\rho_e u_e C_H)_{cw}$

(b) Perpendicular to original surface

(c) See Surface Description Key, Table 9-2

TABLE 9-1

ABLATION MODEL RESPONSE RESULTS

(I) PHASE V MODEL SIZE AND EXPOSURE TIME

Model No.	Enthalpy h (Btu/lb)	Stagnation Pressure P_s (atm)	Model Heating Rate $(q_c)_{cw}$ (Btu/ft sec)	Model Heat Transfer Coefficient $(\rho_e u_e C_H)_{hw}$ (1) (lb/ft sec)	Chemical Environment	Exposure Time θ (sec)	Surface Recession s (inch)	Average Recession Rate $\dot{s}$ (mils/sec)	Average Surface Temperature T_w (°R)	Inverse of Surface Temperature $1/T_w \times 10^3$ ($°R^{-1}$)	Char Depth (-) (inch)	Pyrolysis Zone Depth (-) (inch)	Mass Loss M (gm)	Recession Rate Parameter	Post Test Surface Description (2)	Test Condition	Test No.
114/BH/4.0	4,910	0.0112	33.0	0.0064	Air	211.4	0.095	0.40	2,825	3.54	0.305	0.455	1.624	0.175	LG,S	24	767B
115/BH/4.0	5,044	0.0110	32.0	0.0059	|	120.5	0.061	0.51	2,800	3.57	0.231	0.381	1.185	0.235	|	|	768B
116/BH/4.0	4,944	0.0090	34.0	0.0064	|	60.4	0.035	0.58	|	|	0.115	0.195	0.735	0 246	G,S	|	769B
120/BH/4.0	13,500	0.0081	91.0	0.0063	|	90.2	0.137	1.52	4,250	3.08	0.267	0.327	1.641	0 664	G,(M)	38	859B
127/BH/4.0	14,386	|	97.0	0.0062	|	59.9	0.082	1.37	|	|	0.252	0.312	1.189	0 604	|	|	858B
126/BH/4.0	|	|	|	|	30.6	0.043	1.40	3,200	3.12	0.141	0.163	0.696	0.615	|	|	858A
120/BH/4.0	4,510	0.0275	90.0	0.0104	|	90.3	—	—	—	—	—	—	1.213	—	LG,S,M	28	821B
118/BH/4.0	4,612	0.0279	96.6	0.0114	|	54.2	—	—	—	—	—	—	0.930	—	G,(S),M	|	820B
117/BH/4.0	|	|	|	|	30.3	0.026	0.86	3,200	3.12	0.106	0.146	0.582	0.208	LG,S,(M)	|	820A
122/BH/4.0	10,434	0.0275	134	0.0119	|	60.6	0.168	2.77	3,800	2.63	0.308	0.348	1.724	0.634	G,NM	29	822B
121/BH/4.0	11,119	0.0283	117	0.0099	|	28.0	—	—	—	—	—	—	1.393	—	—	|	822A
119/BH/4.0	10,976	0.0279	119	|	|	30.8	0.096	3.12	4,000	2.50	0.196	0.236	0.990	0.861	G,NM	|	821A
123/BH/4.0	15,186	0.0283	191	0.0117	|	45.2	0.096	2.12	3,800	2.63	0.256	0.316	1.172	0.497	G,BD,NM	30	835B
125/BH/4.0	15,891	0.0279	198	0.0116	|	29.8	0.056	1.88	3,825	2.62	0.196	0.236	1.058	0.445	G,(BD),NM	|	836B
124/BH/4.0	19,040	|	238	|	|	20.0	0.045	2.25	3,775	2.65	0.125	0.165	0.717	.530	G,NM	|	836A

(1) Based on $(\rho_e u_e C_H)_{hw} = 0.925\ (\rho_e u_e C_H)_{cw}$

(-) Referenced to original surface

( ) See Surface Description Key, Table 9-2

TABLE 9-1

ABLATION MODEL RESPONSE RESULTS

(a) PHASE VI A MODEL SHAPE, CONSTANT ENTHALPY AND CONSTANT STAGNATION PRESSURE

Model No.	Enthalpy h (Btu/lb)	Stagnation Pressure P_s (atm)	Model Heating Rate $(q_c)_{cw}$ (Btu/ft²)	Model Heat Transfer Coefficient $(\rho_e u_e C_H)_{hw}$ (1) (lb/ft²sec)	Chemical Environment	Exposure Time θ (sec)	Surface Recession s (inch)	Average Recession Rate $\dot{s}$ (mils/sec)	Average Surface Temperature T_w (°R)	Inverse of Surface Temperature $1/T_w \times 10^3$ ($°R^{-1}$)	Char Depth (-) (inch)	Pyrolysis Zone Depth (-) (inch)	Mass Loss M (gm)	Recession Rate Parameter B'	Post Test Surface Description (2)	Test Condition	Test No.
16/BH/2.0	5,937	0.0275	116	0.018	Air	90.0	0.218	2.42	3,660	2.78	0.388	0.458	2.153	0.363	G(M)	1	675A
25/BH/2.0	5,447	0.0270	121	0.021	|	45.6	0.112	2.46	3,575	2.80	0.232	0.262	1.154	0.322	|	|	676A
19/BH/2.0	5,582	|	83.0	0.011	|	90.0	0.139	1.54	3,600	2.78	0.309	0.339	1.701	0.399	|	|	674B
33/BH/2.0	5,640	0.0275	159	0.026	|	93.5	0.356	3.81	3,750	2.67	0.466	0.506	2.860	0.396	|	|	675B
28/BH/2.0	10,357	0.0281	190	0.017	|	90.0	0.384	4.27	—	—	0.504	0.544	3.182	0.683	BD,(G),NM	2	673B
29/BH/2.0	9,594	0.0283	159	0.015	|	45.2	0.171	3.78	4,175	2.40	0.281	0.321	1.717	0.667	(BD),G,NM	|	676B
17/BH/2.0	10,357	0.0281	142	0.013	|	90.0	0.293	3.26	—	—	0.413	0.453	2.627	0.700	BD,G,NM	|	673A
35/BH/2.0	10,463	|	241	0.021	|	|	0.499	5.54	4,400	2.32	0.609	0.629	3.998	0.708	BD,(G),NM	|	674A
101/BH/2.0	15,000	0.0285	242	0.017	|	27.3	0.132	4.84	4,550	2.22	0.222	0.242	0.995	0.798	(BD,NM)	30	831B
102/BH/2.0	13,760	0.0283	205	|	|	45.4	0.177	3.90	4,150	2.41	0.307	0.347	1.929	0.645	|	|	835A
103/BH/2.0	14,860	0.0285	222	0.012	|	30.5	0.106	3.48	4,500	2.22	0.210	0.250	1.350	0.574	G,(BD),NM	|	831A
31/BH/2.0	14,283	0.0287	225	0.012	|	45.7	0.117	4.22	4,400	2.27	0.267	0.317	1.553	0.713	BD,NM	|	832B
30/BH/2.0	14,634	|	242	|	|	30.4	0.083	2.73	|	|	0.183	0.223	1.073	0.601	|	|	832A
109/BH/2.0	17,204	0.0279	310	0.022	|	30.0	0.154	5.13	4,175	2.39	0.241	0.264	1.557	0.626	G,(BD),NM	|	833B

(1) Based on $(\rho_e u_e C_H)_{hw} = 0.925\ (\rho_e u_e C_H)_{cw}$

(2) Referenced to original surface

( ) See Surface Description Key, Table 9-2

TABLE 9-1

ABLATION MODEL RESPONSE RESULTS

(b) PHASE VI – MODEL SCALE, CONSTANT STAGNATION PRESSURE AND CONSTANT STAGNATION HEATING RATE

Model No.	Enthalpy h (Btu/lb)	Stagnation Pressure P_s (atm)	Model Heating Rate $(q_c)_{cw}$ (Btu/ft² sec)	Model Heat Transfer Coefficient $(\rho_e u_e C_H)_{hw}$ (1) (lb/ft² sec)	Chemical Environment	Exposure Time θ (sec)	Surface Recession s (inch)	Average Recession Rate $\dot{s}$ (mils/sec)	Average Surface Temperature T_w (°R)	Inverse of Surface Temperature $1/T_w \times 10^3$ (°R^{-1})	Char Depth (2) (inch)	Pyrolysis Zone Depth (2) (inch)	Mass Loss M (gm)	Recession Rate Parameter B'	Post Test Surface Description (3)	Test Condition	Test No.
26/BH/2.0	5,549	0.0269	85.0	0.010	Air	90.0	0.255	2.84	3,700	2.70	0.415	0.435	2.286	0.530	G,(M)	1	682B
22/FF/2.0	7,336	0.0265	86.0	0.012	"	"	0.205	2.28	3,650	2.74	0.345	0.485	2.029	0.563	DG	4	683B
3/H/2.0	5,092	0.0289	115	0.031	"	"	0.241	2.68	3,500	2.86	0.371	0.421	2.352	0.251	G,M	6	691
27/BH/2.0	10,269	0.0282	181	0.018	"	"	0.391	4.34	4,175	2.40	0.551	0.611	3.219	0.724	BD,(G),NM	2	683A
16/FF/2.0	11,200	0.0271	170	0.012	"	90.1	0.300	3.33	4,200	2.38	0.410	0.450	2.851	0.820	G,(BD),NM	31	833A
5/H/2.0	7,145	0.0272	172	0.024	"	90.0	0.402	4.47	4,000	2.50	0.492	0.522	3.330	0.544	G	3	682A
102/BH/2.0	16,517	0.0271	288	0.017	"	44.7	0.218	4.88	4,450	2.24	0.328	0.388	1.687	0.825	G,(BD),NM	30	834B
18/FF/2.0	19,201	0.0293	259	0.013	"	42.5	0.165	3.88	4,275	2.34	0.295	0.325	0.891	0.847	BD,G,NM	27	804
12/H/2.0	10,692	0.0286	327	0.033	"	45.0	0.261	5.80	4,300	2.32	0.371	0.401	2.258	0.508		5	684

(1) Based on $(\rho_e u_e C_H)_{hw} = 0.925\ (\rho_e u_e C_H)_{cw}$

(2) Referenced to original surface

(3) See Surface Description Key, Table 9-2

TABLE 9-1

ABLATION MODEL RESPONSE RESULTS

(b) PHASE VII – ENTHALPY AND STAGNATION PRESSURE AT CONSTANT HEATING RATE

Model No.	Enthalpy h (Btu/lb)	Stagnation Pressure P_s (atm)	Model Heating Rate $(q_c)_{cw}$ (Btu/ft² sec)	Model Heat Transfer Coefficient $(\rho_e u_e C_H)_{hw}$ (1) (lb/ft² sec)	Chemical Environment	Exposure Time θ (sec)	Surface Recession s (inch)	Average Recession Rate $\dot{s}$ (mils/sec)	Average Surface Temperature T_w (°R)	Inverse of Surface Temperature $1/T_w \times 10^3$ (°R^{-1})	Char Depth (2) (inch)	Pyrolysis Zone Depth (2) (inch)	Mass Loss M (gm)	Recession Rate Parameter B'	Post Test Surface Description (3)	Test Condition	Test No.
90/BH/2.0	18,869	0.0285	337	0.018	Air	30.8	0.148	4.81	4,575	2.18	0.258	0.288	0.643	0.793	G,BD,NM	27	803A
97/BH/2.0	"	"	"	"	"	31.0	0.155	5.00	"	"	0.285	0.395	1.350	0.825	"	"	803B
111/BH/1.0	10,588	0.0817	577	0.054	"	39.6	0.388	9.80	4,750	2.10	0.468	0.488	0.724	0.527	G,NM	13	732
112/BH/1.0	10,548	0.0831	562	0.053	"	40.7	0.382	9.39	4,725	2.12	0.462	0.482	0.711	0.519	—	"	733
110/BH/1.0	10,167	0.0827	570	0.056	"	24.6	0.232	9.43	4,750	2.10	0.292	0.302	0.448	0.495	G,NM	"	731
91/BH/1.0	10,334	0.0842	563	0.048	"	40.5	0.338	8.35	4,650	2.15	0.383	0.413	2.538	0.508	BD,NM	"	734
129/BH/1.0	4,515	0.073	510		"	20.1	0.325	16.2	4,800	2.08	0.365	0.375	0.586	0.325	DG,NM	39	889A
130/BH/1.0	"	"			"	15.4	0.247	16.0	4,775	2.10	0.302	0.417	0.422	0.422	"	"	889B

(1) Based on $(\rho_e u_e C_H)_{hw} = 0.925\ (\rho_e u_e C_H)_{cw}$

(2) Referenced to original surface

(3) See Surface Description Key, Table 9-2

TABLE 9-2

SURFACE DESCRIPTION KEY

Code	Surface Description
NM	No Melt
M	Melt Globules
S	Scab
G	Gray
DG	Dark Gray
LG	Light Gray
BD	Black, Apparent Carbon Deposition

Note: Parentheses indicate small quantities, e.g., (M).

A-327

TABLE 9-3

MASTER SYMBOL KEY FOR PLOTS

ENTHALPY, h (BTU/LB)		STAGNATION PRESSURE P_s (ATM)	
△	3,000	♀	.001
▷	3500 & 4,000	♁	.008 - .010
○	5,000	○	.028
△	6250	♌	.07 - .11
□	7500	♌	0.4
□	10,000 & 9,000	♌	1.0
◇	12,500	♌	2.0
◇	14,000	♌	3.0
◇	17,500	♂	10
△	25,000		
×	0 (VACUUM)		

SIZE		SHAPE	
⊗	1 IN	○	BH
⊙	1¼ IN	○	FF
○	2 IN	○	H
⊘	4 IN	●	DUCT

CHEMICAL ENVIRONMENT		SHEAR STRESS T_w (PSF)	
○	AIR	♌	3
◐	NITROGEN	♌	7-10
		♁	20

ANALYTICAL PREDICTION
●

NOTE :

THE CIRCLE SYMBOL IS USED FOR ILLUSTRATIVE PURPOSES IN DEMONSTRATING THE KEYS FOR VARIABLES OTHER THAN THE ENTHALPY.

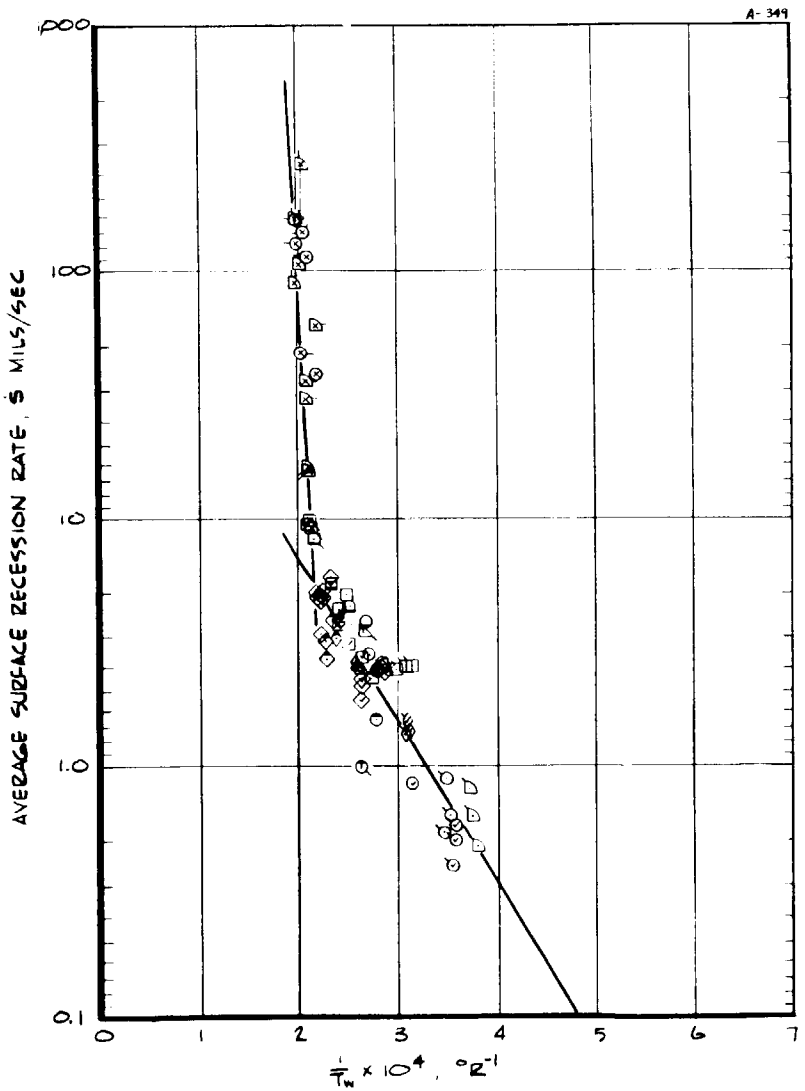

FIGURE 9-1 SURFACE RECESSION RESPONSE AS A FUNCTION OF THE INVERSE OF SURFACE TEMPERATURE

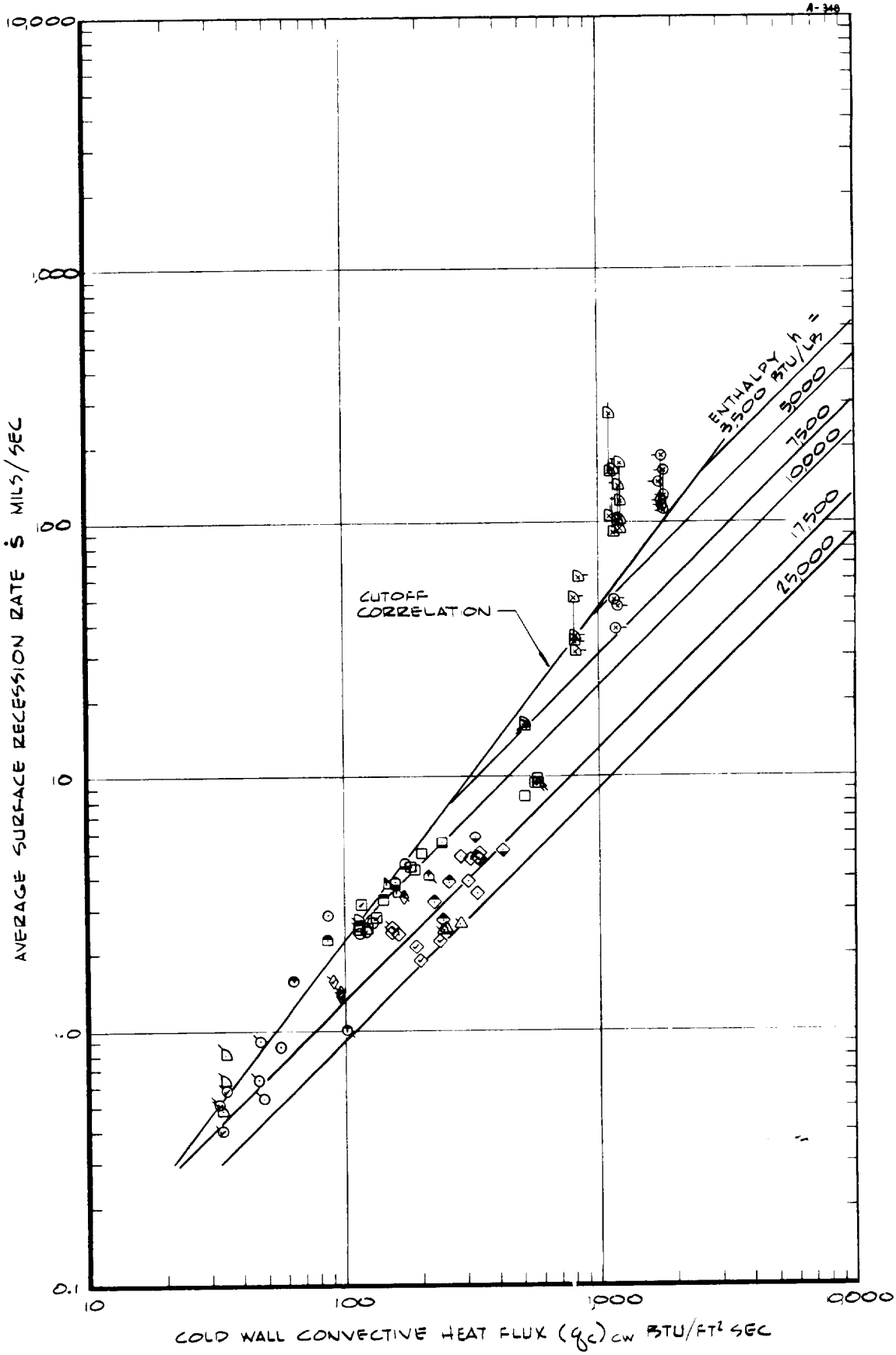

FIGURE 9-2 SURFACE RECESSION RESPONSE AS A FUNCTION OF COLD WALL CONVECTIVE HEAT FLUX.

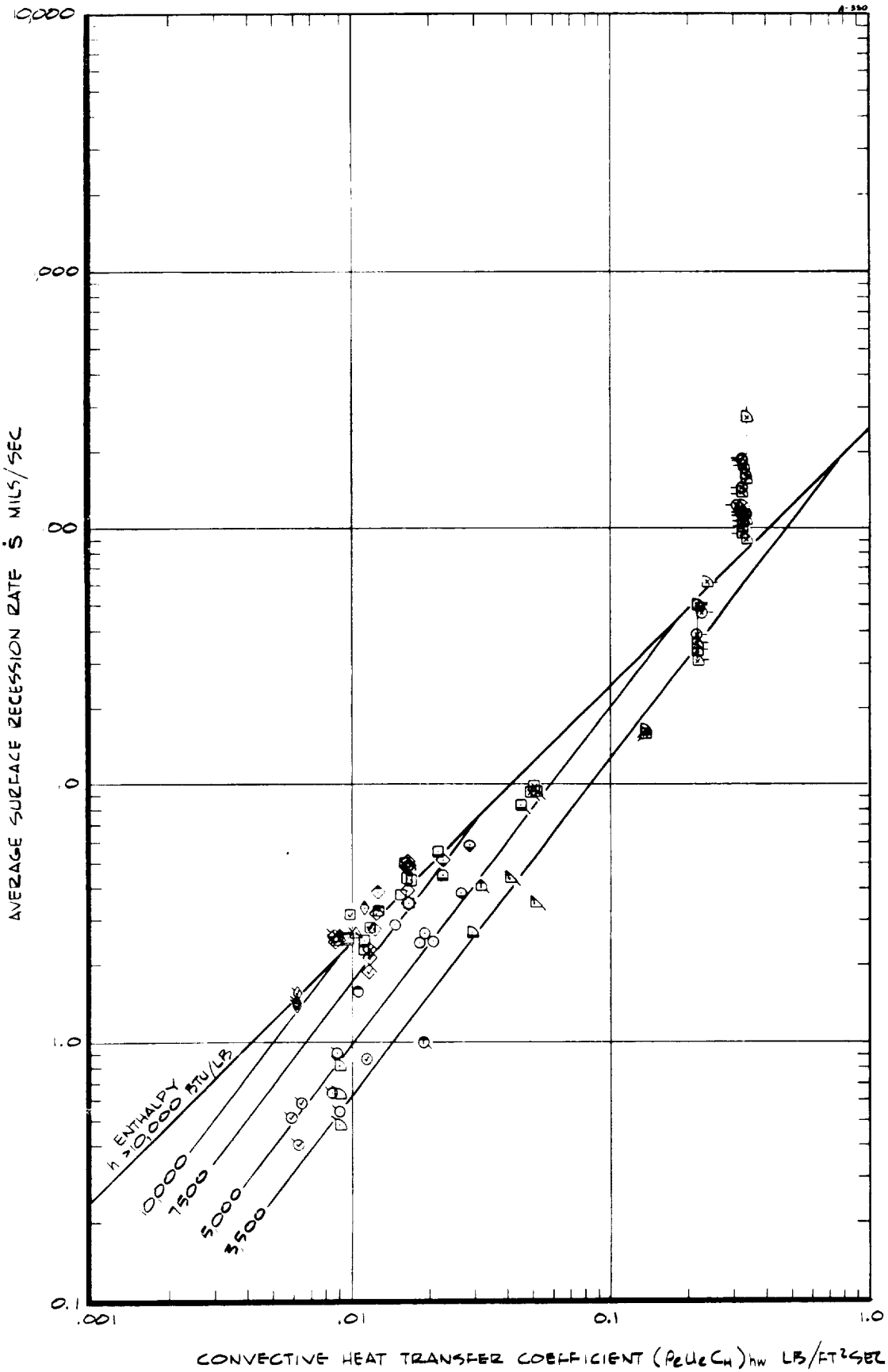

FIGURE 9-3 SURFACE RECESSION RESPONSE AS A FUNCTION OF CONVECTIVE HEAT TRANSFER COEFFICIENT.

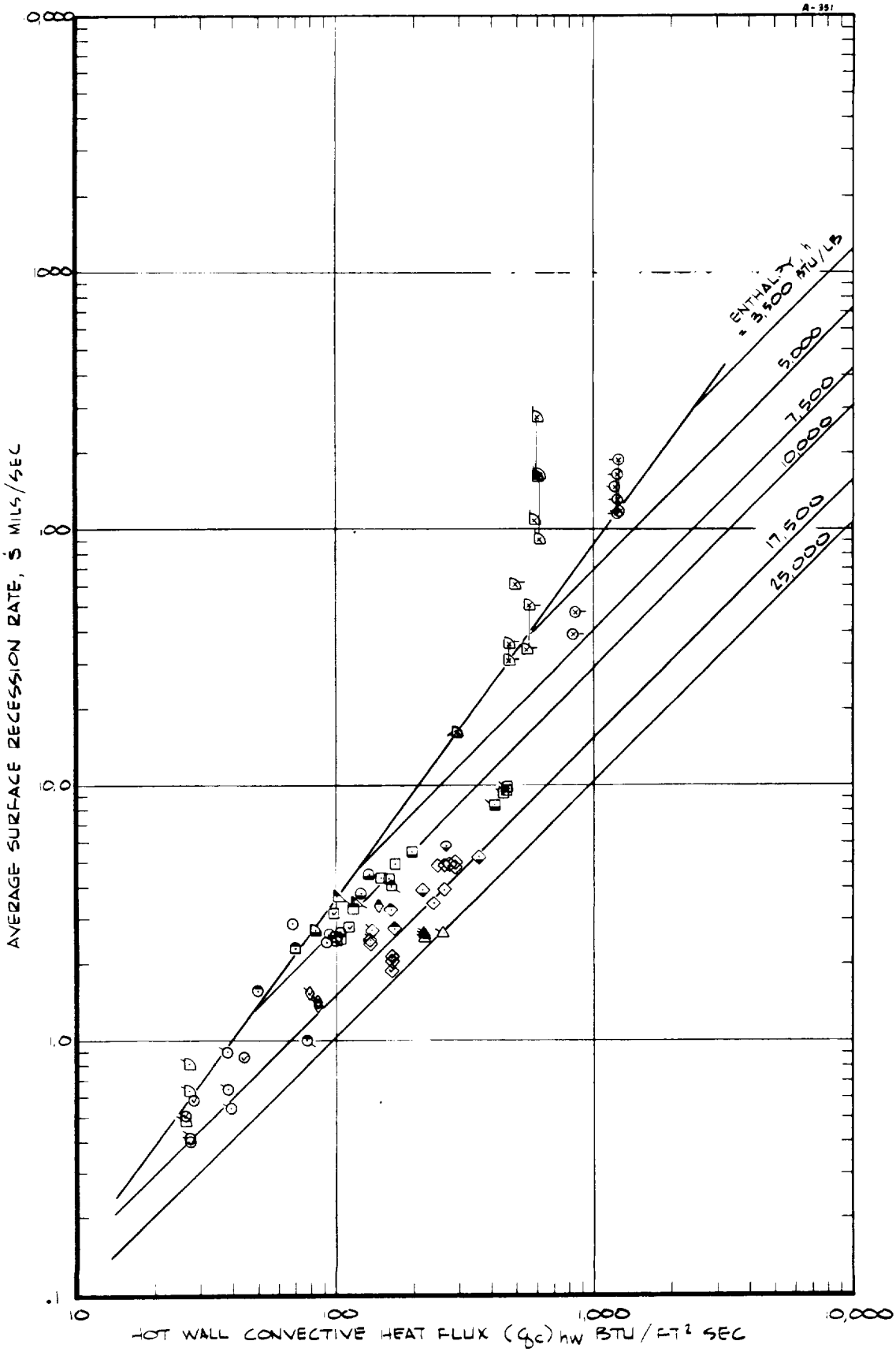

FIGURE 9-4 SURFACE RECESSION RESPONSE AS A FUNCTION OF HOT WALL CONVECTIVE HEAT FLUX.

FIGURE 9-5 SURFACE TEMPERATURE RESPONSE AS A FUNCTION OF COLD WALL CONVECTIVE HEAT FLUX.

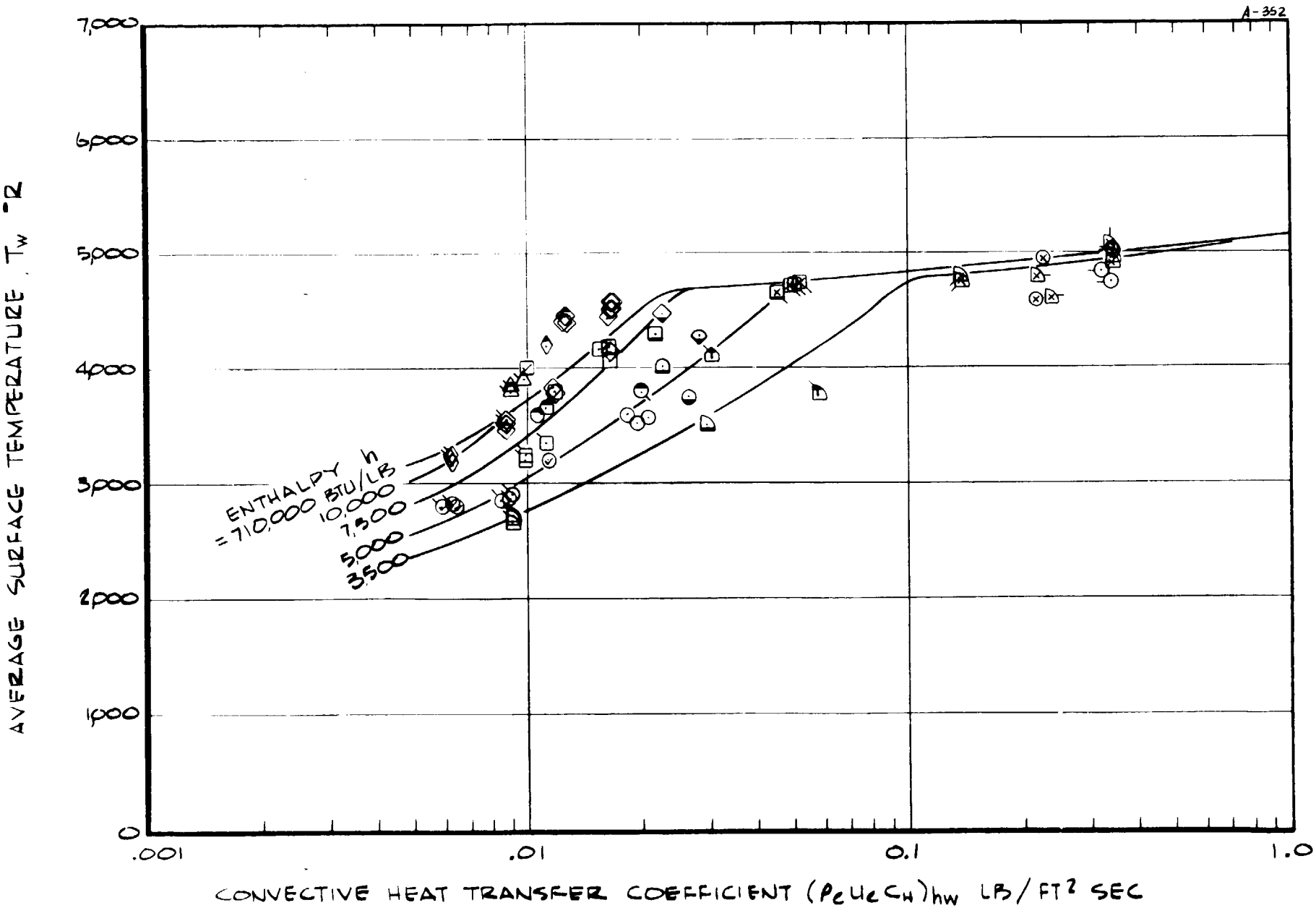

FIGURE 9-6 SURFACE TEMPERATURE RESPONSE AS A FUNCTION OF CONVECTIVE HEAT TRANSFER COEFFICIENT

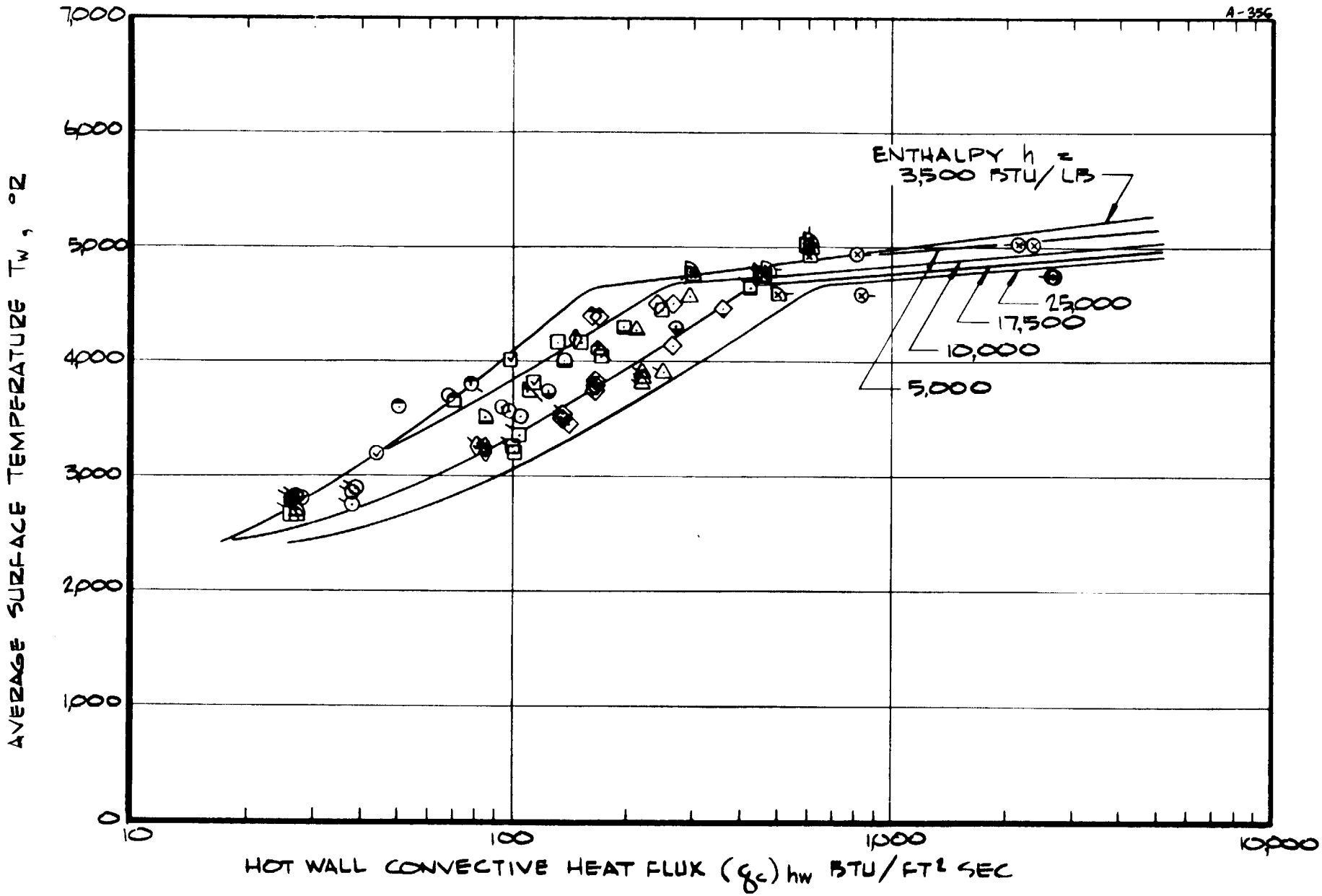

FIGURE 9-7 SURFACE TEMPERATURE RESPONSE AS A FUNCTION OF HOT WALL CONVECTIVE HEAT FLUX.

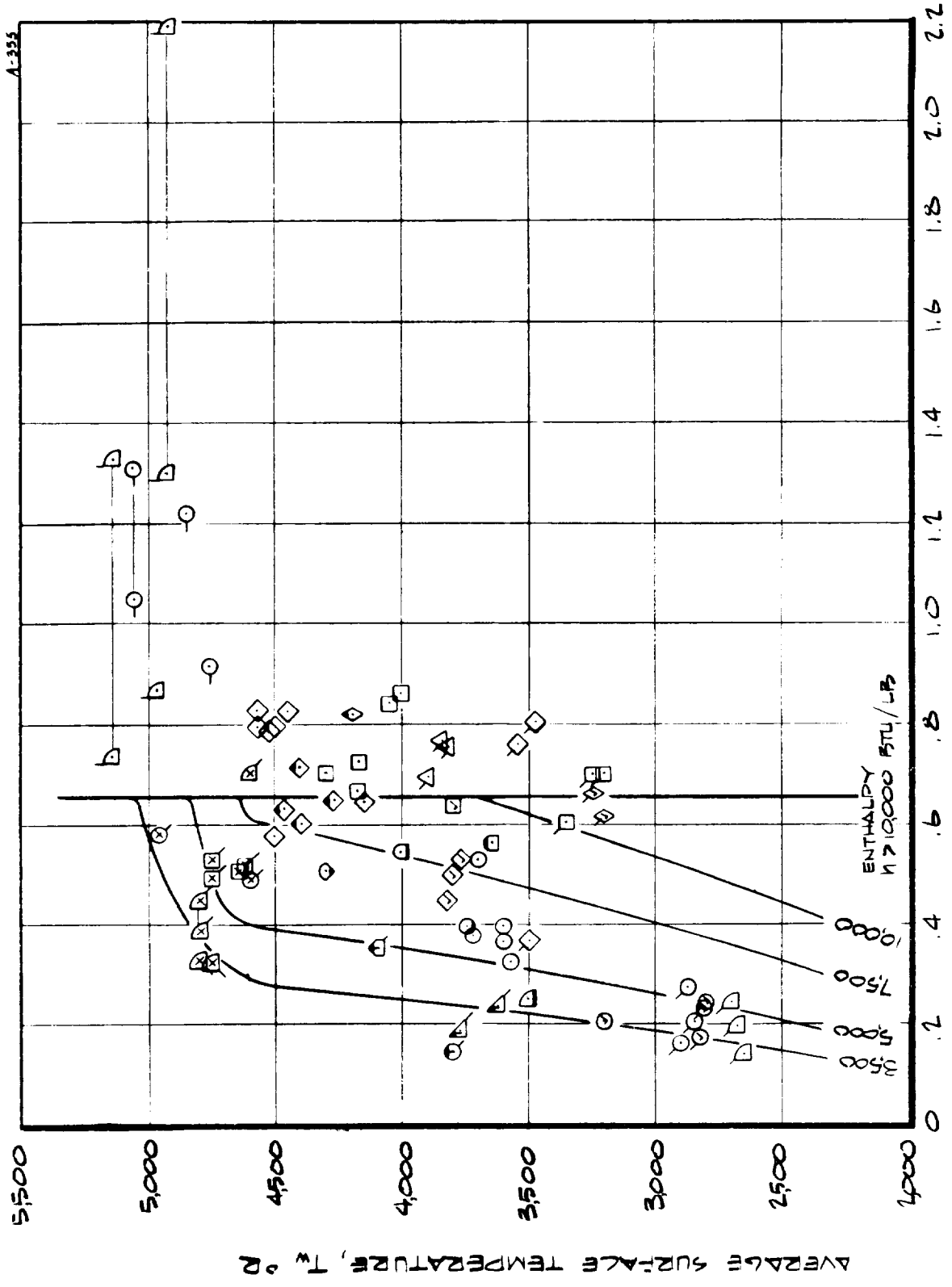

FIGURE 9-8 SURFACE TEMPERATURE RESPONSE AS A FUNCTION OF THE RECESSION RATE PARAMETER B'.

Figure 9-1 presents the plot of average surface recession rate as a function of the inverse of the average surface temperature. This plot is the classic kinetically controlled surface removal plot, any straight line on the plot corresponding to

$$\dot{s} = Be^{-a/T_w} \tag{9-2}$$

where B and a are constants. The experimental results fall into two distinct groups as shown by the lines drawn through the data. The transition point between these two variations is an $\dot{s}$ of about 5 mils/sec and a T_w of about $4650^{\circ}R$. The results exhibit considerable scatter about the two correlation lines and there is no apparent test variable that correlates with this scatter. Note that at high recession rate, the high surface temperature results were favored in defining the line. At stagnation pressures of 1 atm and greater it was difficult to obtain a definitive surface temperature measurement because of the high recession rate; the measured values in some cases are felt to be lower than actual. The apparent kinetically controlled correlation of the results as shown in Figure 9-1 should not be interpreted as an indication that the surface chemical reactions are, in fact, kinetically controlled. It is however an indication of the strong effect of surface temperature on surface recession for the 5026-39HCG material. In any case, the two lines of Figure 9-1 represent a reasonable correlation of the results, at least for the conditions of this test program. The character of the material response and the parameters governing it are discussed further in this and subsequent sections.

The average surface recession rate is plotted as a function of the cold wall heat flux to the model in Figure 9-2. The results follow the expected trend of increasing recession rate with increasing heat flux. The scatter of the results is significant; however, some sense can be made of it through a simple empirical correlation. The basic correlation assumes that the recession rate is directly proportional to heat transfer coefficient (and mass transfer coefficient)

$$\dot{s} \propto \rho_e u_e C_H = \frac{0.925(q_c)_{cw}}{h - h_w} \tag{9-3}$$

where, for a cold wall, h_w is negligible. Note that Equation (9-3) corresponds to

$$B' = \frac{\dot{s}\rho_p}{\rho_e u_e C_H} = \text{constant.} \tag{9-4}$$

Equation (9-3) defined the slope of the constant enthalpy lines on the plot of Figure 9-2. Their position was determined by fitting the 10,000 Btu/lb points with a line of this slope. This fit then uniquely defined the position of all other constant enthalpy lines within the assumption of Equation (9-3). As seen from Figure 9-2, this simple assumption does a surprisingly good job of correlating many of the results. It was also apparent, however, that an upper limit on recession rate was required independent of the $\dot{s} \propto \rho_e u_e C_H$ correlation. This "cutoff" line is also included on the plot. The complete correlation is a reasonable representation of the experimental results except at high heat flux and high stagnation pressure. At these conditions, mechanical removal occurred at the surface and therefore the results would be expected to be higher than the correlation, as observed. These high pressure results will be discussed in detail in Section 9.1.2.2. The correlation has, of course, been demonstrated only for the range of conditions obtained under this program. Study of the results indicates that the cutoff line is probably a weak function of pressure. This line would probably have a lower slope, closer to that of the $\dot{s} \propto \rho_e u_e C_H$ correlation lines, if it were plotted at constant pressure. The cutoff line is therefore felt to be a family of lines that are a weak function of pressure such that the cutoff line occurs at higher $\dot{s}$ with increasing pressure.

The two basic correlations shown in Figures 9-1 and 9-2 are presented in various forms throughout the following discussion. The correlation of Figure 9-1 provides a relation between the surface response parameters: surface recession rate as a function of surface temperature. The correlation of Figure 9-2 then relates the surface response parameters to the environmental conditions: surface recession rate as a function of heat flux or heat transfer coefficient or, in combination with the correlation of Figure 9-1, surface temperature as a function of heat flux or heat transfer coefficient.

The average surface recession rate is plotted as a function of model heat transfer coefficient in Figure 9-3. The correlation of Figure 9-2 is also included where the $\dot{s} \propto \rho_e u_e C_H$ correlation is the single upper line and the cutoff correlation is the family of lines at constant enthalpy. Plotted in this form, the correlation again demonstrates a reasonable representation of the experimental results except at high heat flux and pressure. The observations and conclusions presented above for Figure 9-2 also apply here.

The average surface recession rate is plotted as a function of the hot wall convective heat flux to the model in Figure 9-4. This heat flux is defined by

$$(q_c)_{hw} = (\rho_e u_e C_H)_{hw} (h - h_w) \qquad (9\text{-}5)$$

where h_w is the enthalpy of air (in equilibrium) at the measured average surface temperature and stagnation pressure. This heat flux is therefore the flux to a non-ablating wall and does not consider the effects of differing chemical composition and of blowing at the wall due to ablation. Again an empirical correlation is presented and is defined by the same procedures and rationale as discussed in conjunction with Figure 9-2. The correlation of Figure 9-1, relating surface recession rate and surface temperature, was also used to define h_w (Equation (9-5)) in the correlation. The cutoff line is also included and corresponds closely to the similar line of Figure 9-2. The complete correlation of Figure 9-4 is a reasonable representation of the experimental results but, overall, does no better than the simpler correlation of Figure 9-2 in tieing the results together. The observations discussed with reference to Figure 9-2 also apply to Figure 9-4.

A plot of average surface temperature as a function of cold wall convective heat flux to the model is presented in Figure 9-5. The results demonstrate a considerable scatter but the expected trend of increasing surface temperature with heat flux is certainly apparent. Two different correlations are included in the plot. One, the dashed line, consists of two straight line segments with their point of intersection being arbitrarily chosen as $4650^{\circ}R$, the similar intersection point found in Figure 9-1. The solid-lines correlation is the combination of the correlations of Figures 9-1 and 9-2, the latter defining the $\dot{s}$ for a given heat flux and enthalpy and the former relating this $\dot{s}$ to surface temperature. Both correlations represent a reasonable fit of the experimental results although some scatter is certainly apparent, particularly at low and moderate enthalpies.

The average surface temperature is plotted as a function of heat transfer coefficient in Figure 9-6. Plotted in this form, the surface temperature results exhibit more scatter than when plotted against cold wall heat flux, Figure 9-5. Again a correlation of the results is included and relates to the more detailed correlation of Figure 9-5. The correlation represents the low and moderate enthalpy results quite accurately but is not as effective at high enthalpy. Based on the results of Figures 9-5 and 9-6, it appears that the surface temperature at high enthalpy is reasonably well correlated by the cold wall heat flux (Figure 9-5) whereas the surface temperature at moderate and low enthalpies is reasonably well correlated by the heat transfer coefficient (Figure 9-6). It should be remembered that these correlations depend on the correlations of Figures 9-1 and 9-2 and therefore the above conclusions must be viewed in the light of these earlier correlations.

The average surface temperature as a function of non-ablating, hot wall convective heat flux is plotted in Figure 9-7. The correlation included is the surface temperature counterpart of the recession rate correlation presented

in Figure 9-4. The results exhibit the same scatter observed in Figure 9-5 and the correlation also exhibits the same deficiencies noted with reference to that figure.

Finally, Figure 9-8 presents a plot of the surface temperature as a function of the dimensionless recession rate parameter $B' = \dot{s}\rho_p/\rho_e u_e C_H$ where ρ_p is the density of the virgin material, taken as 32.8 lb/ft^3. A correlation which is the combined correlations of Figures 9-1 and 9-3 is also presented in the figure. Based on this correlation, the recession rate parameter B' at high enthalpy is a constant at the value 0.655, this vertical line corresponding to the $\dot{s} \propto \rho_e u_e C_H$ correlation presented previously. The correlation exhibits the general trend of the results although the scatter is considerable. The high heat flux, high pressure results again appear out of line with the rest of the results as discussed previously.

The above figures have provided an overall look at the complete set of experimental results for surface recession and surface temperature and have also demonstrated two basic empirical correlations of these results, the first relating the surface response in terms of surface recession rate and surface temperature,

$$\dot{s} \propto e^{-a/T_w}$$

and the second relating this surface response to the environmental parameters

$$\dot{s} \propto \rho_e u_e C_H$$

where there is a cutoff limit to this latter correlation. These correlations though empirical, have a rational basis and provide in most cases a reasonable characterization of the results. The test results are discussed further below in terms of the other response parameters.

The measured char depths and pyrolysis zone depths are also presented in Table 9-1, these depths being referenced to the original surface. For almost all test conditions of this program, the in-depth response did not achieve steady state conditions; the surface, char, and pyrolysis zone recession rates were equal only for the high pressure, high heat flux tests. Contrary to the bulk of the surface recession results, the char and pyrolysis zone depth results are therefore a strong function of exposure time. These results must therefore be considered quantitatively through comparisons with transient calculations of the in-depth response considering the actual exposure times and surface boundary conditions. Such comparisons are presented in Section 9.2 and further discussion is deferred to that section. A few qualitative observations, available from Table 9-1, are of interest however and are presented below. The total char depth for a given exposure time is primarily a function of heat flux; it is relatively independent of enthalpy and of surface recession. These same conclusions also apply to the total pyrolysis zone depth.

The thicknesses of the char and pyrolysis zones (char depth minus surface recession and pyrolysis zone depth minus char depth, respectively) decrease with increasing heat flux, these thicknesses being almost negligible at high pressure and heat flux. Further discussion on the char and pyrolysis zone is presented in Section 9-2.

In addition to all measurements made on the models tested, the post-test surface condition was also noted as a further description of the model response. The observations are summarized in Table 9-1 and repeated for the air results only in Table 9-4 in order of increasing surface temperature. These surface conditions are discussed briefly below. At low surface temperature in the range 2,600°R to 2,900°R, which also corresponded to low heat flux, enthalpy, and stagnation pressure, the surface consisted of a fibrous "scab" which adhered rather loosely to the char surface underneath, this underneath surface having a light gray, fibrous appearance. This surface condition has been illustrated previously in Figure 6-32 and is discussed further in Section 9.1.2.1 and 9.3. At surface temperatures in the approximate range, 3,200°R to 3,800°R, a flowing melt occurred on the surface and consisted of globules covering a broad spectrum of size. Based on the broad range of conditions corresponding to the results in this temperature range, surface temperature certainly appears to be the important variable in defining the surface condition. There apparently is a very small effect of enthalpy and/or heat flux on the occurrence of a surface melt, however; for a given surface temperature, the higher the enthalpy and/or heat flux the less likely a melt will occur. At temperatures above 3,800°R no melt is observed and in many cases a black surface deposit occurs over a part or all of the model surface. This deposit has the appearance of carbon black and may be the result of coking of the pyrolysis cases at the surface during the test or at the start of the cooldown period after test.

The above discussions have provided an overall look at the test results. A more detailed view of these results, particularly in terms of the effect of the test variables on material performance, is presented in the following section.

9.1.2 Effects of Test Variables

The effects of the various test variables on the material response are discussed in this section. The test results are presented for the most part by test phase and the correlations presented in the previous section are used as the baseline for analysis of the test variables effects wherever appropriate. Section 9.1.2.1 discusses the low pressure results and Section 9.1.2.2 the high pressure results. The effect of free stream chemistry is discussed in Section 9.1.2.3, exposure time in Section 9.1.2.4, and model

TABLE 9-4

EFFECT OF SURFACE TEMPERATURE AND TEST CONDITIONS ON MODEL SURFACE CONDITION
(Air Environment Only)

Average Surface Temperature T_w (^oR)	Post Test Surface Description (1)	Enthalpy h (Btu/lb)	Stagnation Pressure p_s (atm)	Convective Heating Rate q_c (Btu/ft^{2}sec)	Model No.
2650	S	3442	0.0082	33	93
2675	|	3539	|	34	95
2700	|	|	|	|	94
2800	G,S	4944	0.0090	|	116
|	LG,S	5044	0.0110	32	115
2825	|	4910	0.0112	33	114
2850	S	5044	0.0110	46	88
2875	|	4910	0.0112	47	87
2900	|	4944	0.0090	48	89
3200	LG,(S),M	4612	0.0279	56	117
|	G,M	14480	0.0081	97	126
|	DG,M	10969	0.0079	116	90
3250	G,M	13500	0.0081	91	128
|	|	14480	|	97	127
|	DG,M	10969	0.0079	116	91
3350	|	10193	|	123	92
3475	|	16301	0.0080	154	99
3500	|	16880	0.0082	162	106
|	G,M	3692	0.0289	115	34
3525	|	6322	0.0261	130	74
3575	|	5447	0.0270	121	25
3600	|	5582	|	63	19
|	|	5937	0.0275	116	30
3625	|	3290	0.112	148	51
3650	DG	7236	0.0265	86	22
3700	G,M	5549	0.0269	87	26
3750	|	5640	0.0275	159	33
3775	DG,M	3090	0.112	163	46
|	G,NM	19040	0.0279	238	124
3800	G,M	5020	0.071	102	37
|	G,NM	10434	0.0275	134	122
|	G,BD,NM	15186	0.0283	191	123
3825	|	15891	0.0279	198	125
|	DG,NM	25600	0.0085	249	109
3850	DG,NM,(BD)	25800	|	251	162
3900	DG,NM	29400	|	286	166
4000	G,NM	11119	0.0283	117	121
|	G	7145	0.0272	172	36
4050	G,NM	11578	0.0283	201	75
4100	DG,NM	6290	0.099	214	49
4150	BD,NM	17300	0.0283	305	165
4175	BD,(G),NM	9554	|	159	29
|	|	10269	0.0282	181	27
4200	G,(BD),NM	14200	0.0271	170	16
4275	BD,(G),NM	19201	0.0293	259	18
4300	|	10692	0.0286	327	32
|	|	10463	0.0281	241	35
4400	BD,NM	14287	0.0287	225	21

TABLE 9-4. (concluded)

Average Surface Temperature T_w (^oR)	Post Test Surface Description (1)	Enthalpy h (Btu/lb)	Stagnation Pressure p_s (atm)	Convective Heating Rate q_c (Btu/ft^{2}sec)	Model No.
4400	BD,NM	14844	0.0287	245	20
4450	G,(BD),NM	16517	0.0271	288	102
4475	G,(BD),NM	17204	0.0279	416	159
4500	BD,NM	15800	0.0285	332	100
|	G,BD,NM	|	|	|	164
4525	G,(BD),NM	17400	0.0287	311	101
4575	G,BD,NM	18860	0.0285	337	97
|	|	|	|	|	96
4600	DG,NM	5031	1.06	1170	154
|	|	3310	1.01	836	134
4650	BD,NM	10443	0.0842	505	31
4750	G,NM	10588	0.0817	577	111
4750	|	10167	0.0827	570	110
4760	|	5015	3.16	1820	136
4775	DG,NM	3515	0.373	510	138
4800	G,NM	3456	1.02	805	156
|	DG,NM	3515	0.373	510	129
4850	G,NM	5151	3.10	1770	140
4920	|	3115	1.94	1120	145
4960	|	5047	1.05	1200	113
|	DG,NM	3115	1.44	1120	144
5030	G,NM	5015	3.16	1820	137
5070	|	3251	1.93	1150	153

(1) See Surface Description Key, Table 9-2.

size and shape in Section 9.1.2.5. The combined convective and radiative heating results are discussed in Section 9.1.2.6 and finally the shear results are discussed in Section 9.1.2.7.

9.1.2.1 Low Pressure

The low pressure test results obtained under the program encompass Phases IV - VI and part of Phase VII. These results and corresponding test conditions were tabulated previously in Tables 9-1d-i and covered the range of stagnation pressures from 0.008 to 0.028 atm and enthalpies from 3,500 to 25,000 Btu/lb. Results for several different free stream chemical environments were obtained. However, only the results for air are discussed in this section; the results for the non-air environments are discussed in Section 9.1.2.3. The model body diameters were 2 and 4 inches, both with 1-inch instrumented cores, both the shroud and core were 5026-39HCG material, the model shapes were blunt hemisphere, flat face, and full hemisphere (see Figure 4-2), and the nozzle exit diameters were 3.5, 4.5, 6.0, and 8.0 inches, the 4-inch models being tested with the last two nozzle sizes only. There were no apparent problems in defining the test conditions, in the conduct of tests, and in the measurements of model response which would affect the interpretation of the test results. The test results are presented and discussed in the following paragraphs. The correlations presented in the previous section are included in the subsequent figures as a basis for comparison. The discussions of the previous section are not repeated except where they are particularly pertinent to the further presentation of the low pressure test results.

Figure 9-9 presents the "kinetically controlled" correlation of the low pressure test results presented previously in Figure 9-1 for the complete spectrum of results. The plot is presented in a linear scale to allow a closer look at these results. The results exhibit some scatter and there are no test variables that definitively correlate with this scatter. It is, however, possible to interpret a small effect of enthalpy and pressure on the results: at a given recession rate the surface temperature may decrease with decreasing enthalpy and pressure.

The surface recession rate and surface temperature response are presented in Figure 9-10 as a function of cold wall heat flux. At constant heat flux, the recession rate and temperature increase with decreasing enthalpy (to a point as indicated by the < 10,000 Btu/lb cutoff correlation) and, at constant enthalpy, they increase with increasing heat flux. In both cases, the results exhibit some scatter although in general the correlation appears quite effective. For surface recession rate, the scatter is most significant for the results in the 17,500 Btu/lb range but they at least fall around the correlation line. There is no apparent test variable that pulls these results

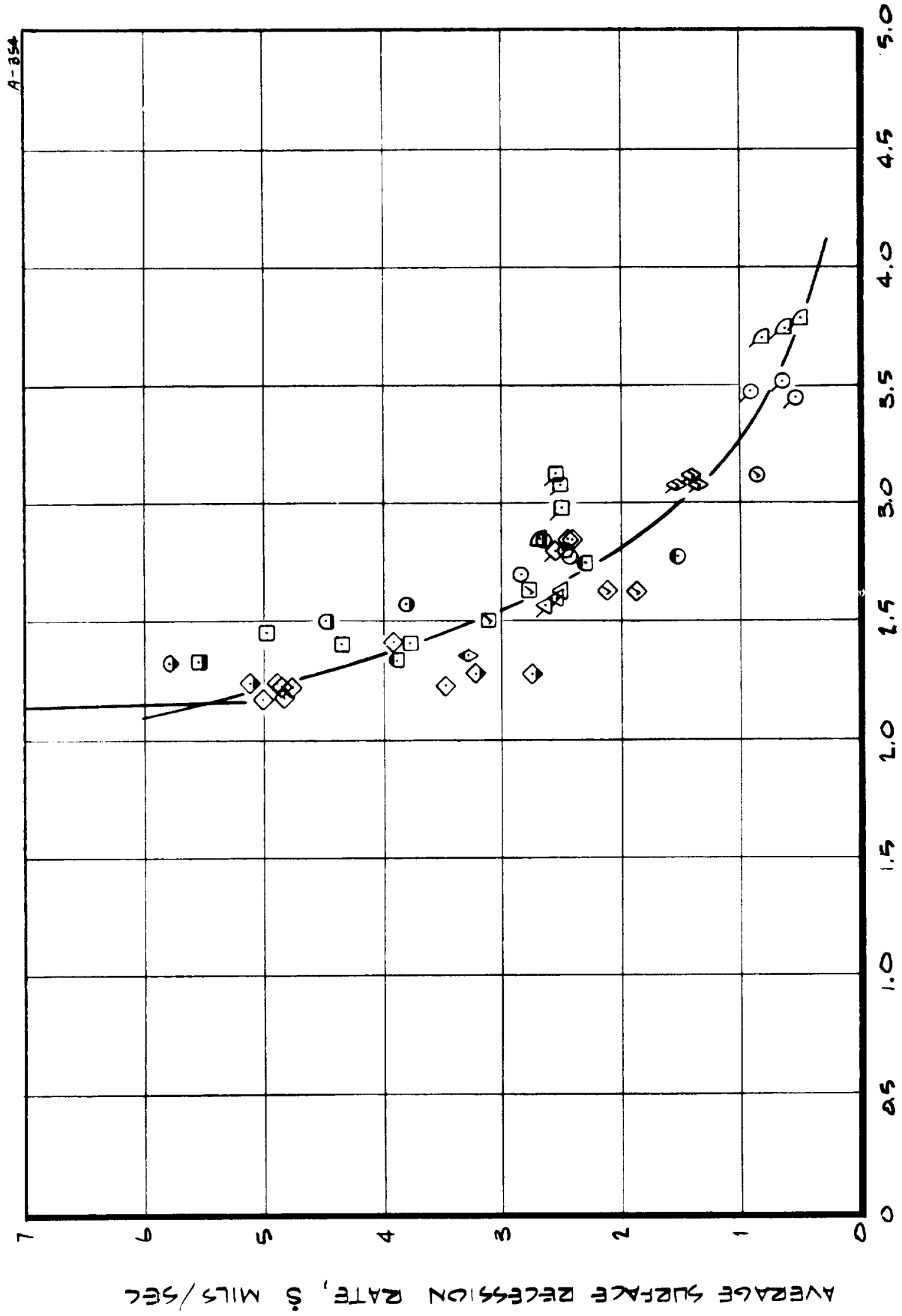

FIGURE 9-9 SURFACE RECESSION RATE - SURFACE TEMPERATURE VARIATION FOR THE LOW PRESSURE TESTS.

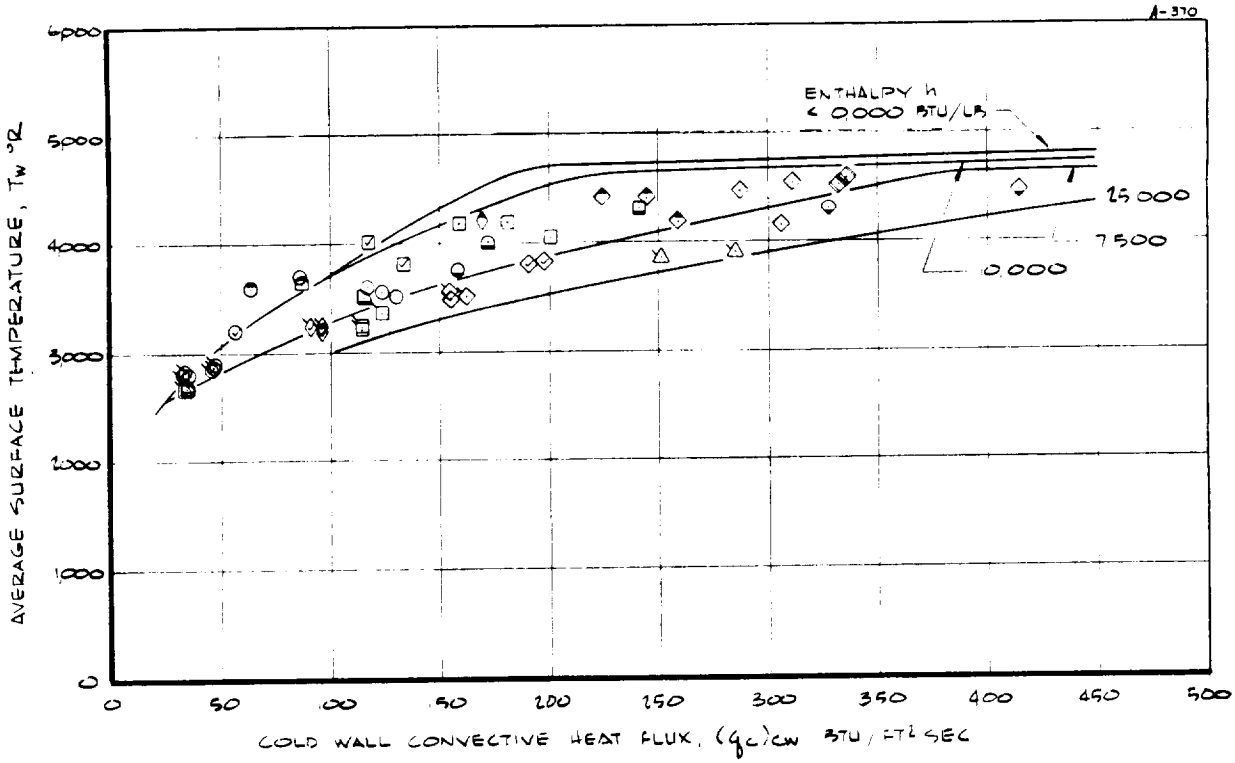

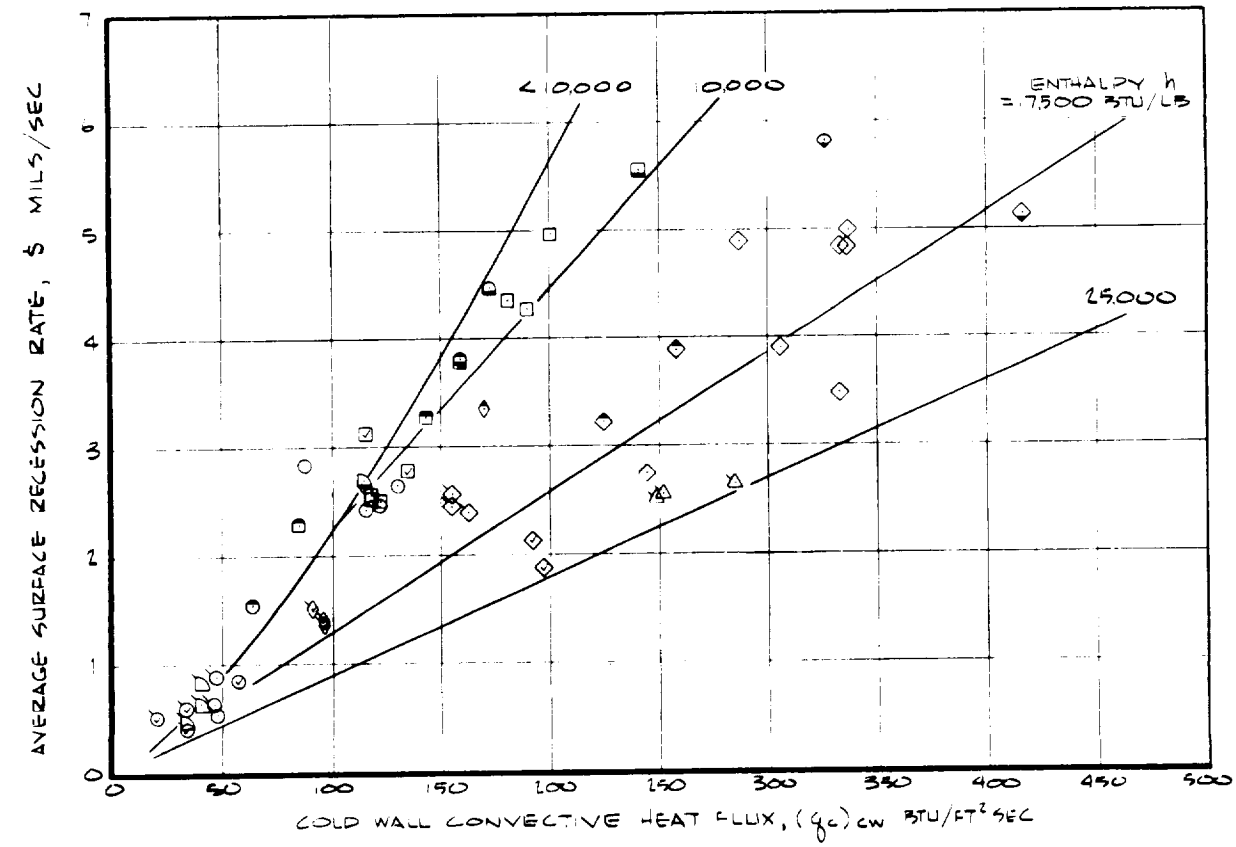

FIGURE 9-10 EFFECT OF COLD WALL CONVECTIVE HEAT FLUX ON MATERIAL PERFORMANCE LOW PRESSURE TESTS.

together and therefore the observed scatter apparently is simply experimental or due to nonuniformities in the material. All other recession results follow a generally consistent pattern and agree quite favorably with the correlation. There is no apparent effect of pressure on the results. For surface temperature, the results exhibit some scatter but again the correlation is a reasonable fit of the results.

Figure 9-11 presents the variation of surface recession rate and temperature with heat transfer coefficient. At constant heat transfer coefficient, the recession rate and surface temperature increase with increasing enthalpy - again to a point as indicated by the > 10,000 Btu/lb, $\dot{s} \propto \rho_e u_e C_H$ line. The results exhibit some scatter, it again being greatest for the 17,500 Btu/lb points, but the correlations fit the results reasonably well.

The variation of surface recession rate and surface temperature with enthalpy is presented in Figure 9-12. The results in this form exhibit a classic "shotgun" pattern. The two basic correlations presented in the previous figures and included in Figure 9-12 in appropriate form provide the proper interpretation of the results, however. The actual experimental heat fluxes, available from Table 9-1 and Figure 9-10 agree reasonably well with the correlation lines presented.

As noted previously, the results at low heat flux exhibited a significant variation in average surface recession rate with exposure time. This effect is illustrated in Figure 9-13 which presents the only three test conditions for which the effect of exposure time was significant. The recession rate decreased with increasing exposure time, this being contrary to what might be expected on consideration of the transient response of the material. At all three conditions, and only at these three conditions, a silica, filament-like scab formed on the surface as shown previously in Figure 6-32. The scab covered the entire surface of each honeycomb cell and, after test, was found to be essentially separate from and only loosely attached to the underneath char surface. The scab was rather fragile and therefore definitive thickness measurements could not be made; however, the scab apparently provided protection to the underneath char surface, this protection increasing as the scab thickness increased with time. This phenomenon is discussed further in Sections 9.2 and 9.3. In all three cases, the surface temperature was not a function of exposure time (see Table 9-1); the approximate values were 2,700°R for the 3,500 Btu/lb condition and 2,850°R for the two 5,000 Btu/lb conditions. Note that they were the lowest surface temperatures achieved in the test program. The next highest measured surface temperature was 3,200°R for which a flowing silica melt occurred. It should also be noted that study of the motion pictures taken for the tests in which the scab formed revealed no melt removal and no unusual performance. The scab material is

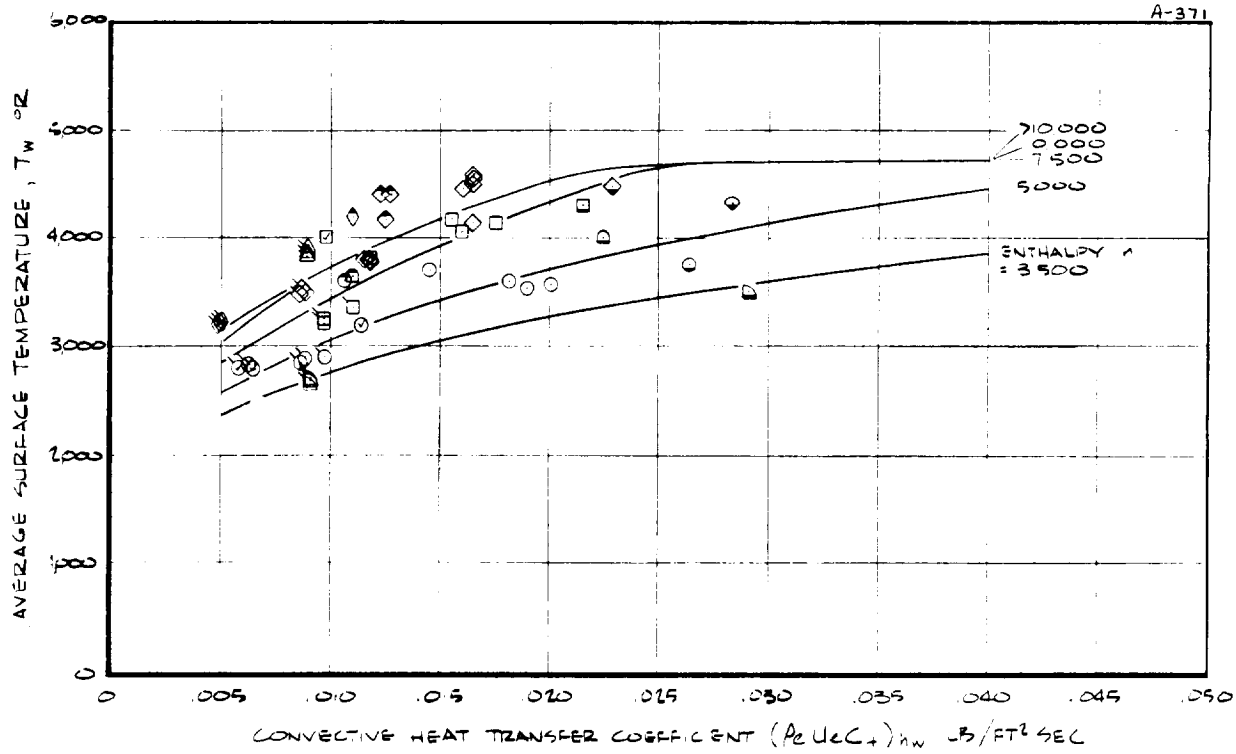

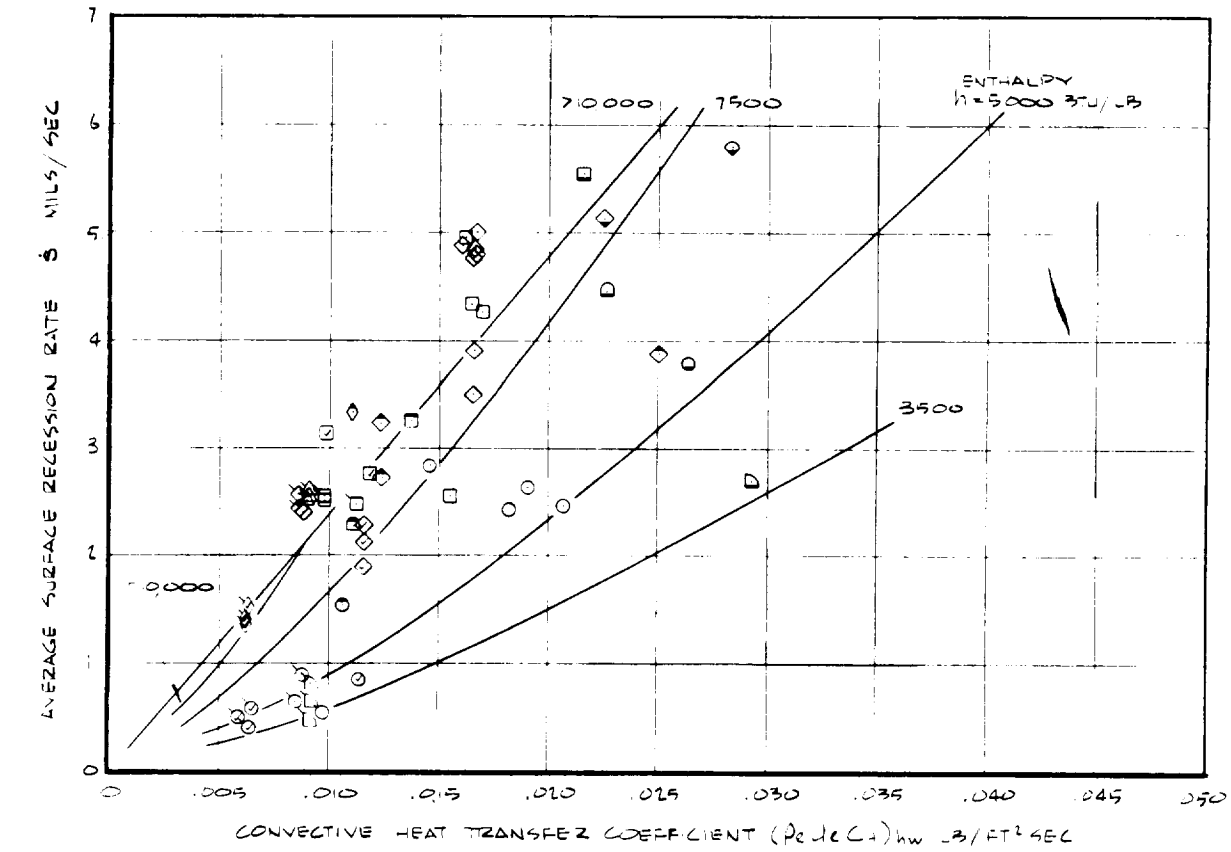

FIGURE 9-11 EFFECT OF HEAT TRANSFER COEFFICIENT ON MATERIAL PERFORMANCE, LOW PRESSURE TESTS.

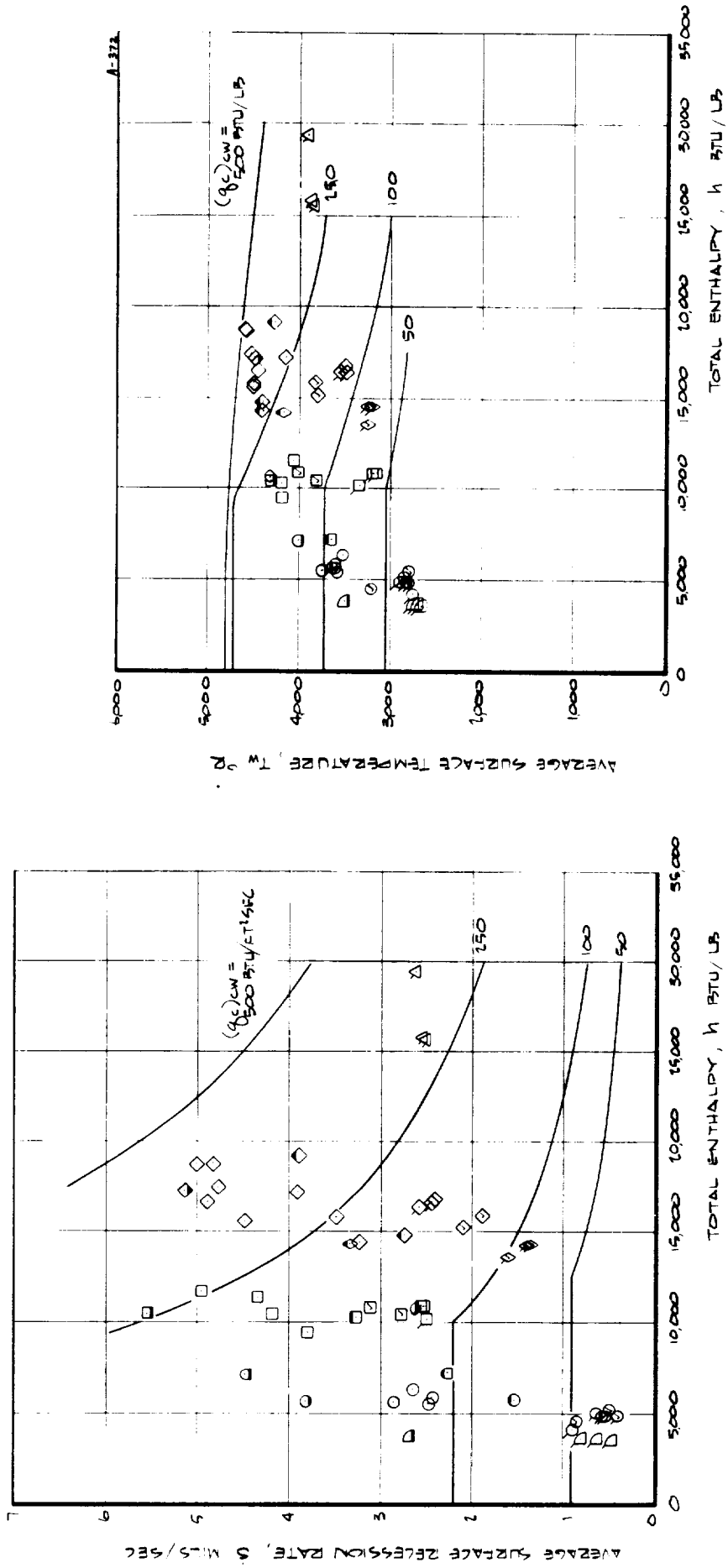

FIGURE 9.12 EFFECT OF ENTHALPY ON MATERIAL PERFORMANCE, LOW PRESSURE TESTS.

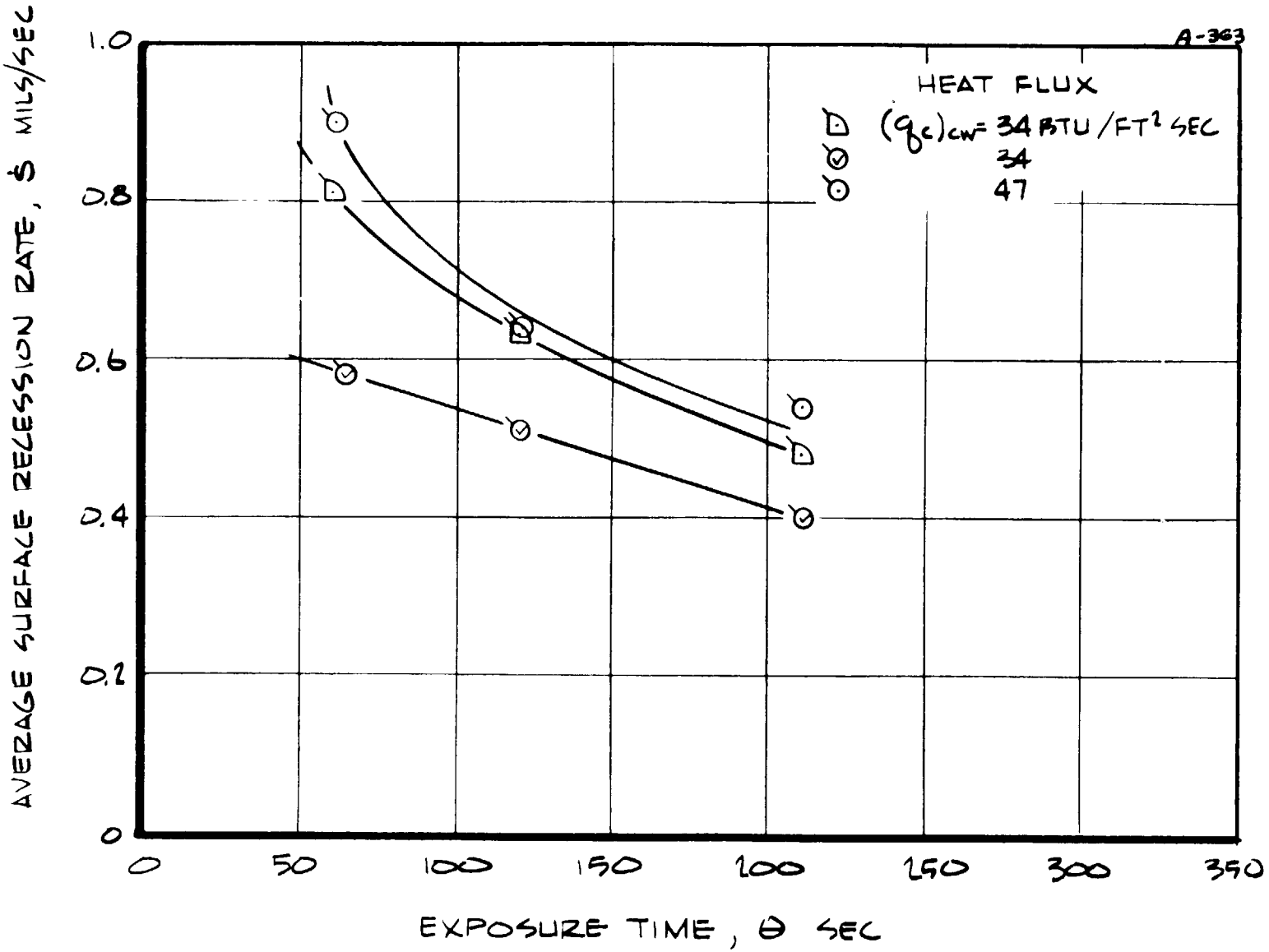

FIGURE 9-13 EFFECT OF EXPOSURE TIME ON RECESSION RATE AT LOW HEAT FLUX.

described further in Section 9.3, Chemical and Physical Properties Tests Results.

9.1.2.2 High Pressure

The high pressure testing was performed as Phase III of the test program and the model response and test conditions were presented previously in Table 9-1c. The test conditions covered the range of stagnation pressures from 1 to 3 atmospheres and enthalpies from 3,500 to 5,000 Btu/lb. Results were obtained for both air and nitrogen as the free stream chemical environment; only the air results are discussed in this section, the nitrogen results being discussed in Section 9.1.2.3. The model body diameter was 1 inch, with a 1/2 inch instrumented core, and the nose shape was the blunt hemisphere configuration (see Figures 4-2 and 4-3). The shroud was the molded material, 5026-39M, to prevent pyrolysis off-gases blowing out the side walls. The shroud therefore had a higher density than the 5026-39HCG honeycomb material used in the core. The nozzle exit diameter was 0.8 inch for the 1 and 2 atm stagnation pressure conditions and 0.6 inch for the 3 atm condition. The high density shroud and the small nozzle exit diameters represent potential problems in obtaining definitive test results as discussed below.

For given material chemical composition and environmental conditions, the mass loss rate of surface material is ideally a constant independent of density and therefore the surface recession rate is inversely proportional to density ($\dot{s} = \dot{m}_c/\rho_c$). Because of this, the molded shroud material would be expected to recede at a lower rate than the honeycomb core material. This was in fact observed after test in almost all the high pressure models and also observed in the motion pictures during the tests in that in some tests the external flow had a component in the opposite direction of the main flow as shown in the sketch. The original blunt hemisphere nose shape was of course not retained through a test and the flow field was complex and ill-

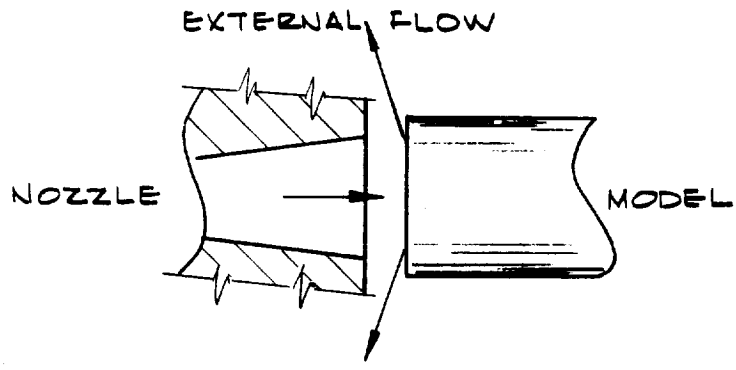

defined. The convective heat flux corresponding to the model tests is therefore ill-defined, probably being lower than that presented in Table 9-1c which corresponds to the original model shape. In addition, the response of the core material was probably directly influenced by the relatively lower inherent recession of the shroud material. All things considered, the measured recession performance is probably somewhat lower than would be expected at the conditions indicated in Table 9-1c had the above problems not existed. The small nozzle exit diameters (e.g., see the above sketch) also presented a potential problem in that the models were not fully immersed in the test flow. The effective nose radius was smaller, and therefore the convective heat flux higher, than would be expected for totally immersed flow (the heating rate results of Table 9-1 reflect this effect). Also the smaller flow area probably contributed to the differential recession between the shroud and instrumented plug. Small inaccuracies in exposure time were also magnified because of the short exposure times required and, because of the relatively large total recessions which occurred, the results may be affected by axial nonuniformities in the flow field if they existed.

In summary, the accuracy of the high pressure test results may be compromised by a number of potential problems as discussed above. The measured surface recession was generally erratic. This response may be due to the above mentioned problems or it may be that this response is inherent in the material thus making these potential problems appear important. In any case, the measured material performance is probably somewhat optimistic in terms of characterizing the material response at these conditions. The results are, however, felt to be sufficiently definitive to allow at least semi-quantitative conclusions to be made from them. The test results are presented and discussed in detail in the following paragraphs.

The surface recession rate and surface temperature variations with convective heat flux are presented in Figure 9-14. At 1 atm stagnation pressure, the recession rate is high, in the 50 mils/sec range, but, based on the correlation, is also close to what would be expected for the two test enthalpies, 3,500 and 5,000 Btu/lb. At 2 and 3 atm stagnation pressure, however, the results fall significantly above the correlation and are erratic both between tests at the same conditions and in terms of the maximum and minimum recession for a single test. The measured recession is as much as a factor of 5 above what would be expected according to the correlation, a factor of 2 to 2.5 being a good "average" for these results. It therefore appears that above 1 atm stagnation pressure mechanical removal of the surface material occurs; the material becomes pressure sensitive. A basic change in char structure or chemistry at high temperature is another possible explanation. The mechanism of

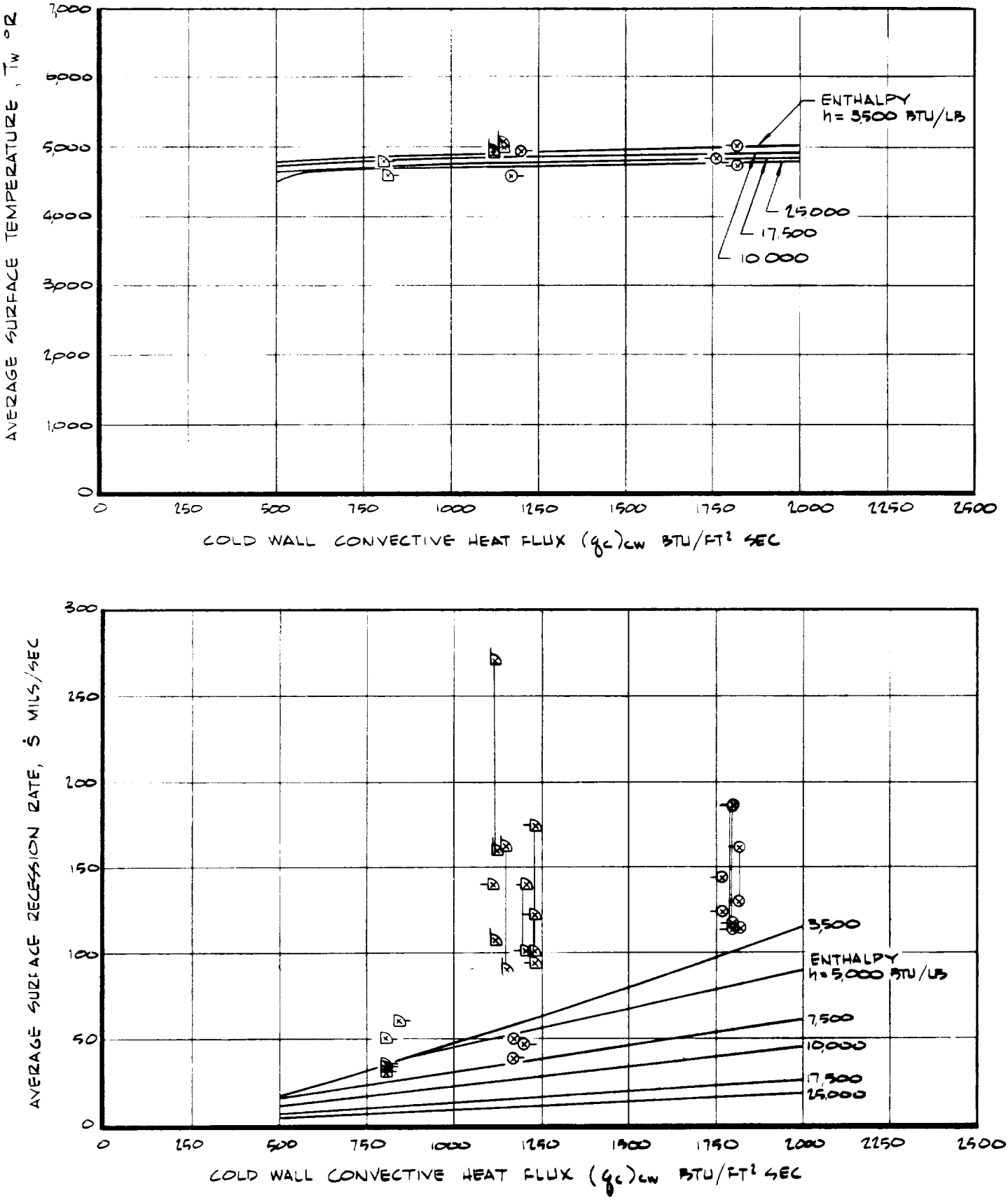

FIGURE 9-14 EFFECT OF COLD WALL CONVECTIVE HEAT FLUX ON MATERIAL PERFORMANCE, HIGH PRESSURE TESTS.

any mechanical removal is difficult to define, the possibilities including thermal stress, internal pressure generation, surface shear, and surface pressure gradients. The temperature gradient through the char is severe therefore resulting in high thermal stress and the possibility of mechanical failure of the char. The high pyrolysis off-gas rate could cause high internal pressures and result in char blowoff (e.g., see Reference 9-1). At off-stagnation-point locations, the shear could be sufficiently high to cause mechanical removal. (Shear effects are discussed further in Section 9.1.2.7.) Note that because of the erractic recession the stagnation point location varied through a test. Finally, surface and the resultant internal pressure gradients could be sufficiently high to cause structural failure of the char.

The surface temperature results also presented in Figure 9-14 fall on or below the correlation lines, these temperatures being in the 5,000°R range. As noted previously, it was difficult to obtain definitive measurements of surface temperature because of the high recession rates. Therefore, for a given test condition, the higher surface temperature result is felt to be closest to the expected temperature.

The variations of surface recession rate and temperature with heat transfer coefficient are presented in Figure 9-15. The same observations and conclusions discussed with reference to Figure 9-14 are also apparent here.

9.1.2.3 Free Stream Chemistry

The effects of free stream chemistry on material response were studied as part of the low pressure tests (Phases IV and VI) and the high pressure tests (Phase III). These results and corresponding test conditions were tabulated previously in Tables 9-1d and e, g and h, and c, respectively. In the low pressure test series, tests were performed for the range of enthalpy from 5,000 to 17,500 Btu/lb at a stagnation pressure of 0.028 atm and for the free stream chemical environments of helium, nitrogen, 0.07 O_2/0.93 N_2, 0.15 O_2/0.85 N_2, air and 0.30 O_2/0.70 N_2. The 2-inch blunt hemisphere model configuration was used in all these tests. Note that for the 17,500 Btu/lb conditions in the low pressure tests, no theoretical calculations of heat transfer coefficient were made for the non-air conditions. It was therefore not possible to relate heat flux directly to enthalpy (h_{hf}) for these non-air conditions, heat flux enthalpy being the standard for these conditions. It was therefore assumed that

$$h_{hf} = (h_{hf})_{air} \frac{h_{eb}}{(h_{eb})_{air}} \qquad (9\text{-}6)$$

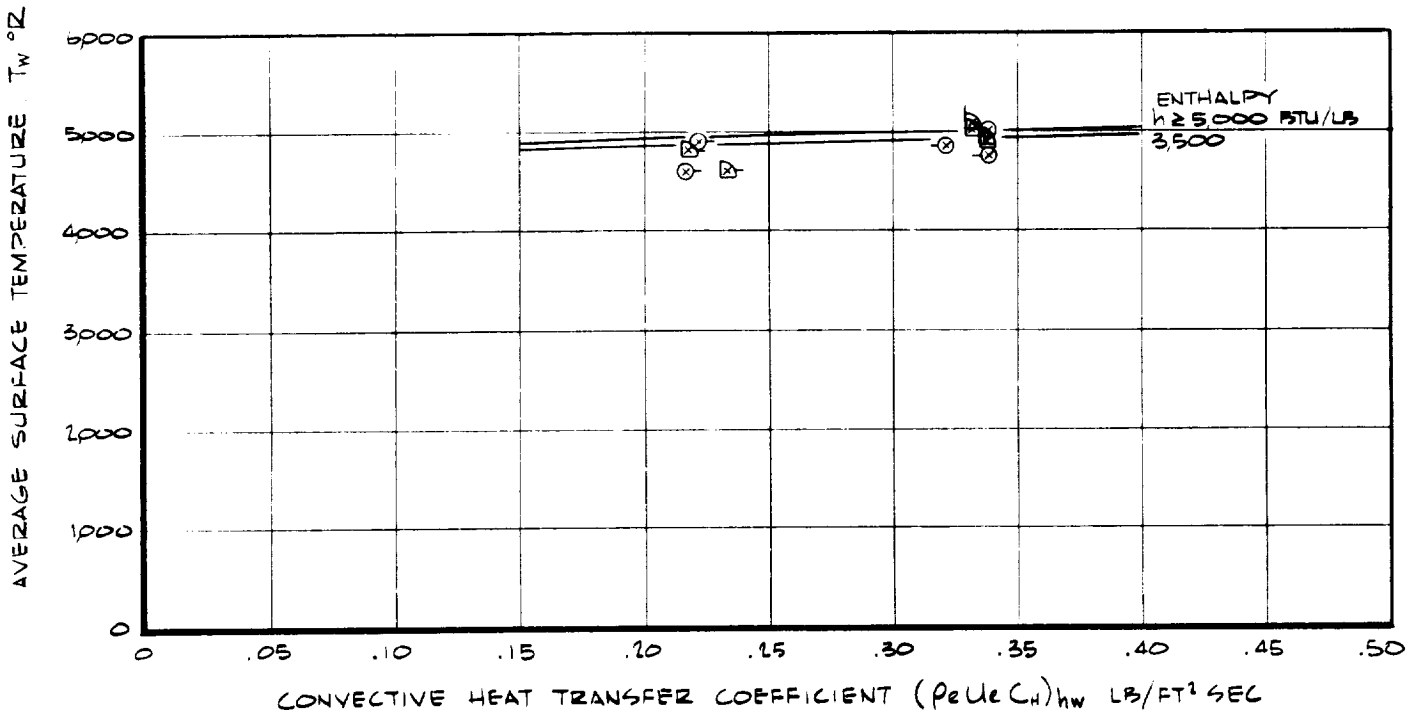

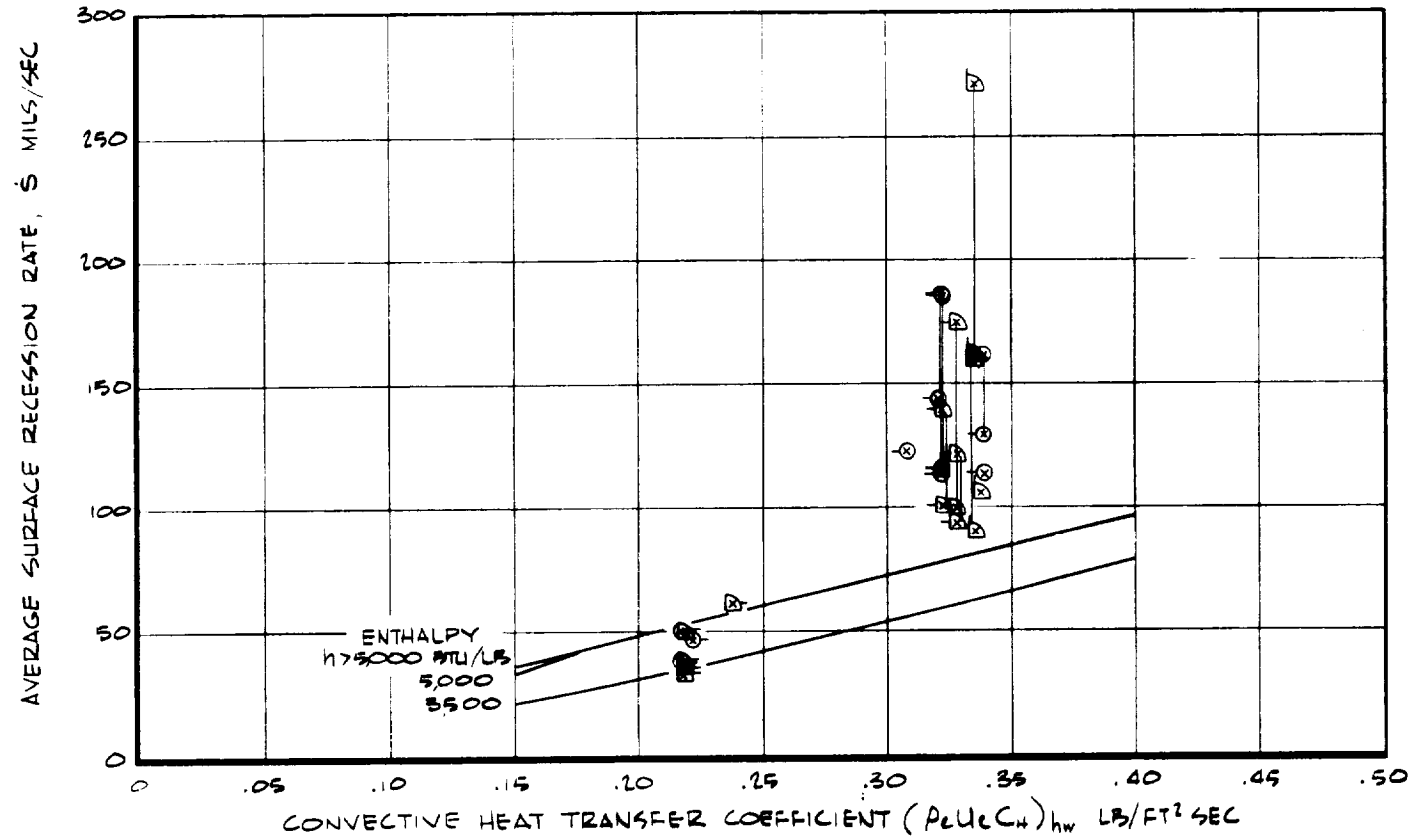

FIGURE 9-15 EFFECT OF HEAT TRANSFER COEFFICIENT ON MATERIAL PERFORMANCE, HIGH PRESSURE TESTS.

which says that the heat flux enthalpy is proportional to the energy balance enthalpy independent of the chemical environment. No theoretical basis is offered for this assumption; however it is felt to be reasonable. In the high pressure test series, tests were performed at enthalpies of 3500 to 5000 Btu/lb stagnation pressures of 1, 2, and 3 atm, and free stream chemical environments of nitrogen and air. The 1-inch blunt hemisphere model configuration was used in all these tests. In the low pressure test series, there were no apparent problems which compromised the validity of the results; in the high pressure test series, the comments of Section 9.1.2.2 apply. The test results are presented and discussed in the following paragraphs.

The effect of oxygen mass fraction on the response of the 5026-39HCG material is presented in Figure 9-16 for the low pressure test results (p_s = 0.028 atm). The results for helium are also included on the right. At each enthalpy, the heat fluxes were approximately constant with variations in chemistry except for the nitrogen tests for which the heat fluxes were somewhat higher (see Table 9-1e). At all three enthalpy levels the average surface recession rate decreases approximately linearly with decreasing oxygen content. The recession rate is significant even for the pure nitrogen environment, decreasing by a factor of about 2 over that at 30 percent oxygen content. Above 10,000 Btu/lb there is no significant effect of enthalpy on the recession rate; the 5,000 Btu/lb results, however, fall below those for the higher enthalpies. This result is consistent with the $\dot{s} \propto \rho_e u_e C_H$ and cut-off correlations presented, for example, in Figure 9-2 and indicates that the correlations are approximately valid independent of oxygen mass fraction at least for the conditions of Phase IVB.

The helium environment also exhibits a finite recession but the rate is about a factor of 5 lower than that for nitrogen. Note also that a similar comparison between argon and nitrogen was also observed in Reference 9-2. Since helium represents a chemically inert environment, the recession measured in the helium environment might well be attributed to shrinkage of the material.[1] Such shrinkage could well occur after test as the model cools down or it could be a phenomenon associated with heating of the material during test. In any case the effective recession rate is small, 0.64 mils/sec or less in

[1] Actually, decomposition of the 5026-39HC material is predicted to occur in the helium environment above temperatures of about 5,000°R. The surface temperatures for the three helium tests did not exceed 4,600°R however.

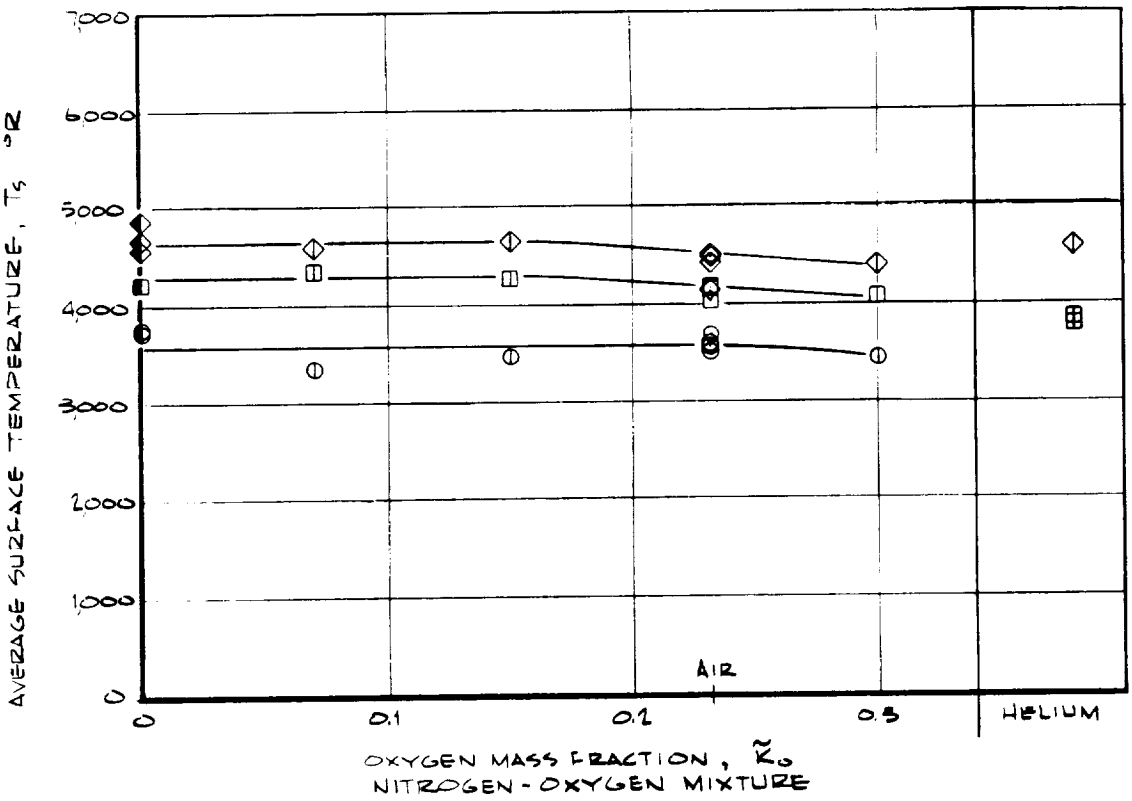

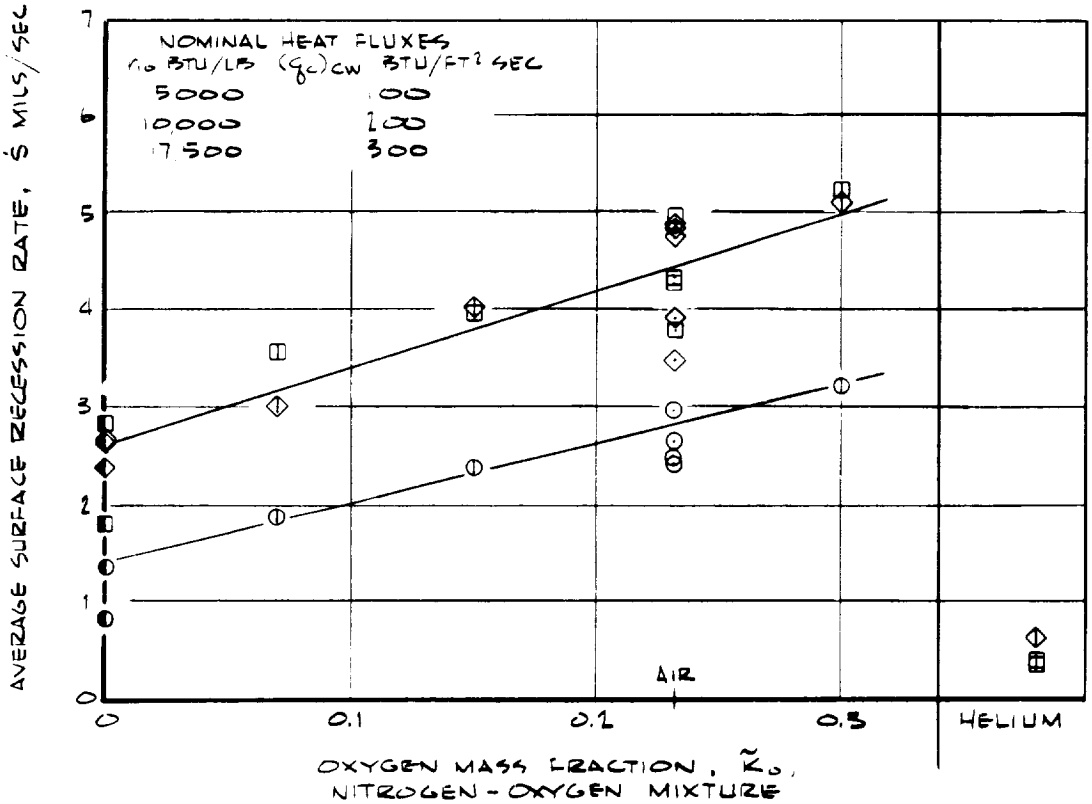

FIGURE 9-16 EFFECT OF CHEMICAL ENVIRONMENT ON MATERIAL PERFORMANCE.

the tests performed herein, this being about 10 to 15 percent of the recession rate observed in air at comparable conditions. These helium results and the implications of shrinkage on the comparisons of experimental measurements and analytical predictions are discussed further in Sections 9.2 and 9.3.

The surface temperature results, also presented in Figure 9-16, exhibit a general decrease in temperature with increasing oxygen content, which also corresponds to increasing recession rate and surface chemical removal. The surface temperature increases with increasing enthalpy which also corresponds to increasing heat flux. The helium results exhibit a stronger effect of enthalpy (and/or heat flux) than do the results for the nitrogen/oxygen gas systems.

Figure 9-17 presents a comparison of the air and nitrogen results at all conditions for which comparisons can be made. The nitrogen results generally fall below the results for air although the difference in surface recession rate between the two environments is not large. Note that this trend also holds at 3 atm stagnation pressure where mechanical removal may be important.

At high stagnation pressures the surface temperatures were comparable for the two chemical environments and are not presented here (see Table 9-1). The low pressure results are included in Figure 9-16.

The effects of free stream chemistry on material performance are discussed further in Sections 9.2 and 9.3.

9.1.2.4 Exposure Time

The effect of exposure time on material performance was studied as part of all test phases except Phase II. In the high pressure tests (Phase III) the results were sufficiently erratic to preclude any comments regarding the effects of exposure time. Based on the other results however, no effect would be expected. The shear results (Phase I) are discussed separately in Section 9.1.2.7 and are not included here. Representative results from the other test phases are included in Figure 9-18 which presents surface recession, surface recession rate, and surface temperature as a function of exposure time. All results exhibit an approximately constant surface recession rate except at the conditions for which the surface scab was observed, the lowest set of test points in all plots. (This effect was discussed previously in Section 9.1.2.1 and is not repeated here.) As seen in Figure 9-18c, the surface temperature is independent of exposure time for all test conditions. The effect of exposure time on the surface response of the material is therefore negligible except for surface recession at low heat flux and enthalpy where the surface scab occurred. The effect of exposure time on the surface and in-depth response is discussed further in the light of the analytical predictions in Section 9.2.

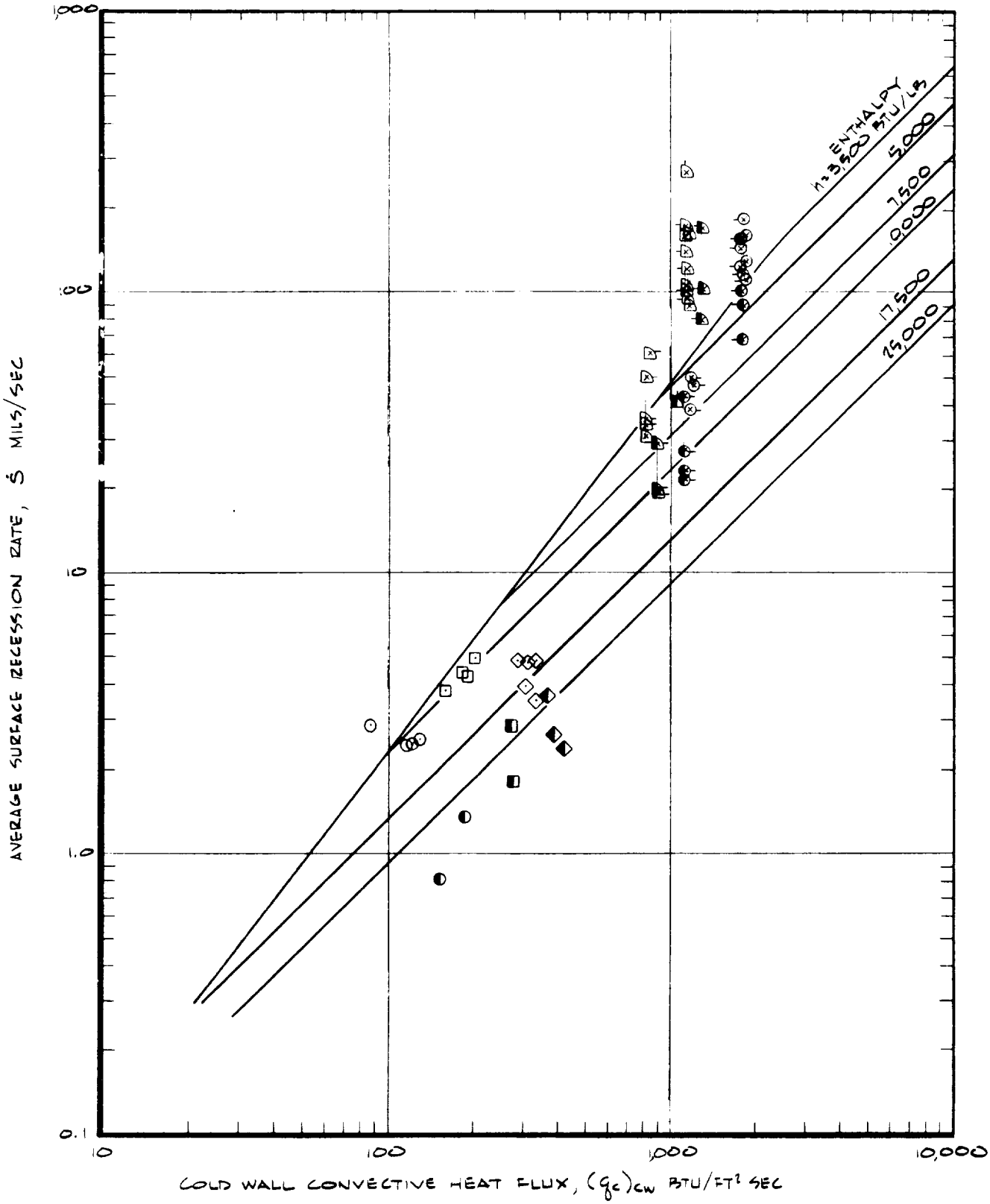

FIGURE 9-17 COMPARISON OF SURFACE RECESSION RATE IN AIR AND NITROGEN ENVIRONMENT.

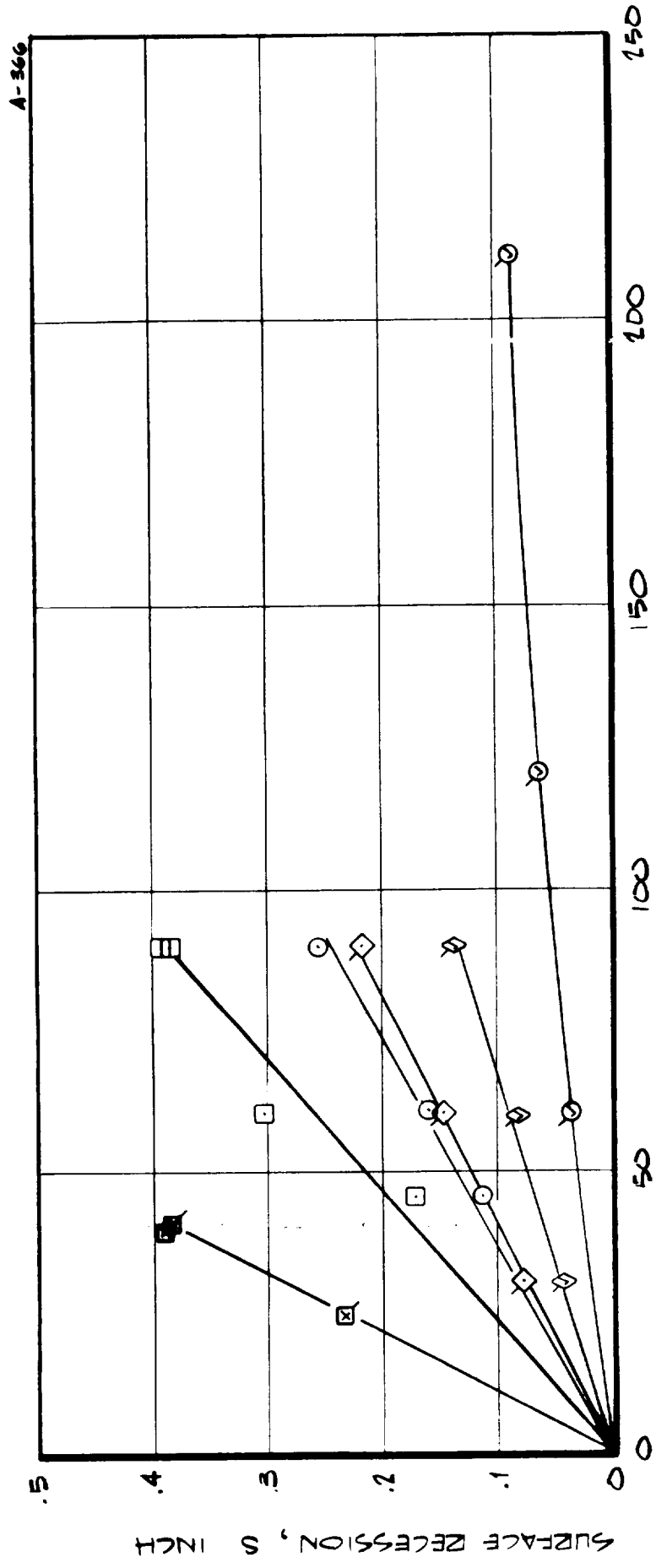

(a) SURFACE RECESSION.

FIGURE 9-18 EFFECT OF EXPOSURE TIME ON MATERIAL PERFORMANCE.

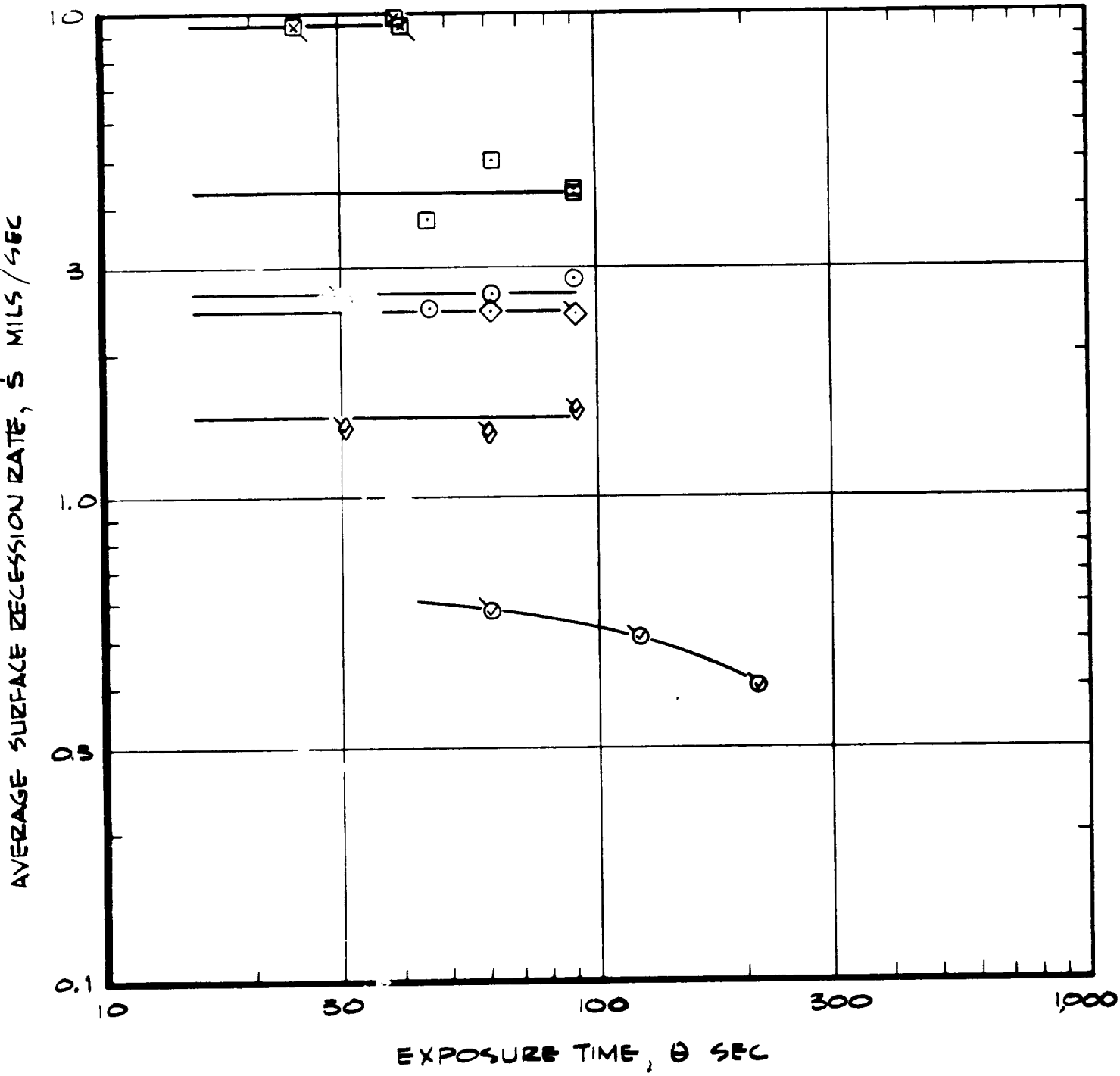

(b) SURFACE RECESSION RATE

FIGURE 9-18 CONTINUED

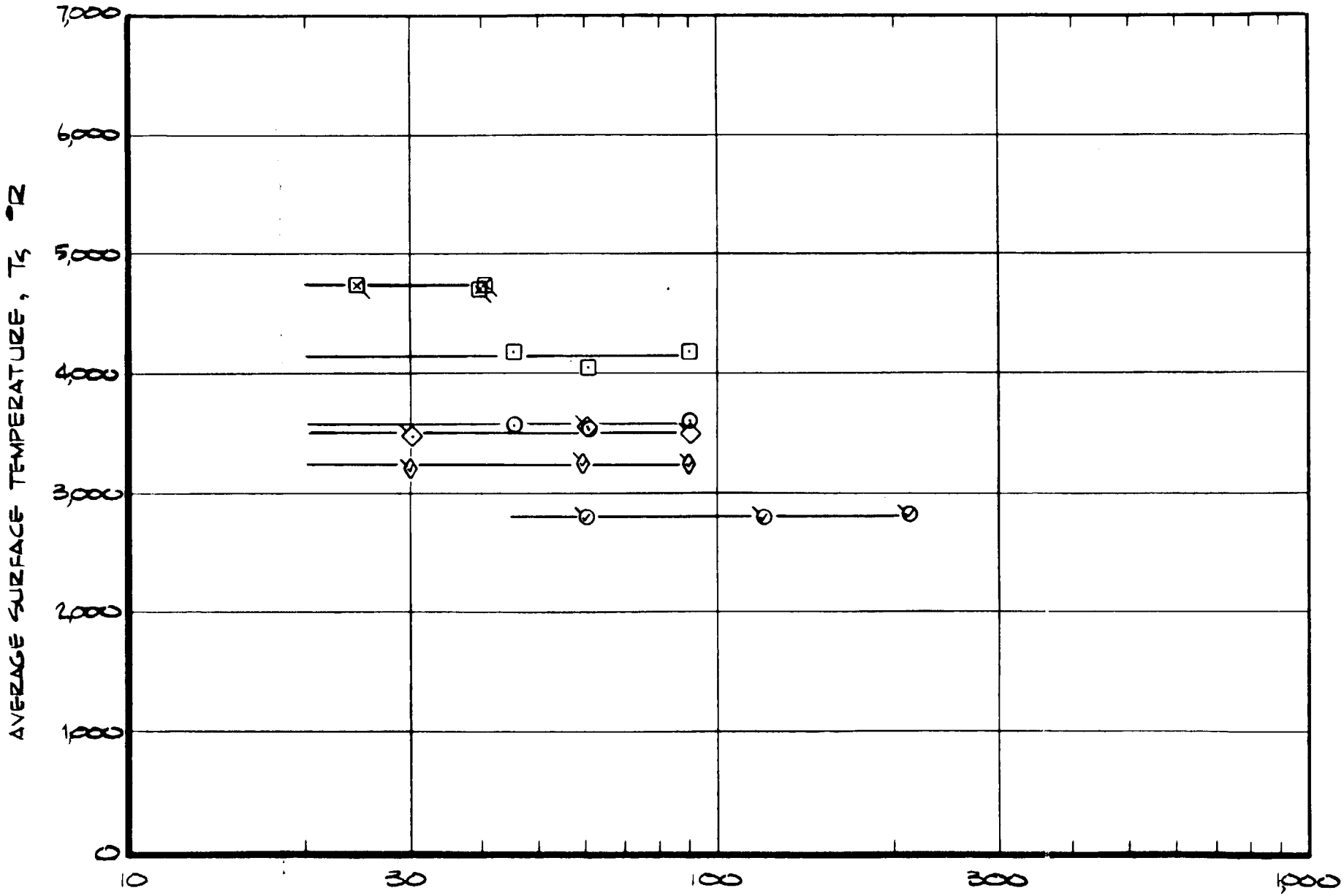

(c) SURFACE TEMPERATURE
FIGURE 9-18 CONCLUDED.

9.1.2.5 Model Size and Shape

The study of the effects of size and shape on the interpretation of test results and model response encompassed Phases IV - VI. Phase VII may also be included in this study although changes in size were also accompanied by changes in model stagnation pressure, contrary to the other appropriate phases. The summary of the test matrix for the size and shape investigation is presented in Table 9-5; the actual test results are included in Table 9-1 presented previously. Both the shroud and core of all models were the 5026-39HCG honeycomb material except for the 1-inch models for which the shroud was the 5026-39M molded material (Figures 4-2 and 4-3). There were no apparent problems in defining the test conditions, in the conduct of tests and in the measurement of model response which would affect the interpretation of the test results. The test results are presented and discussed in the following paragraphs.

The qualitative effect of model shape on the model surface recession response is illustrated in Figure 9-19 which presents pre- and post-test photographs of the three model shapes. The hemispherical shape (H) became more blunt and the flat face shape (FF) became less blunt, in both cases the final shape being close to that of the blunt hemisphere. The blunt hemisphere models (BH) retained their basic shape the best of the three. On the basis of these early test results (Figure 9-19), the blunt hemisphere was chosen as the standard shape for the rest of the tests. Note that for the hemisphere shape, the effective nose radius increased through a test and therefore the convective heat flux and heat transfer (and mass transfer) coefficients decreased. For the flat-face shape, the opposite was true and therefore the heat flux and heat transfer coefficient increased through a test.

The effect of model shape on surface recession rate at constant enthalpy (heat flux variable with shape) is presented in Figure 9-20. In all cases the flat-face and hemisphere points fall within the scatter of the blunt hemisphere results and therefore no significant effect of shape is apparent in these results. The effect of model shape at constant heat flux (enthalpy variable with shape) is presented in Figure 9-21. The same conclusion as for the previous results (Figure 9-20) is also apparent for these results. The effect of shape on the surface temperature response is presented in Figure 9-22. The results at constant enthalpy indicate that the surface temperature is a function of enthalpy only and not of heat flux, at least when this heat flux variation is accomplished by a change in model shape. This rather disturbing observation, in terms of correlating results for different model shapes, may be scatter in the data although the effect is quite consistent. Contrary to the above observation, the results at constant heat flux exhibit no definitive enthalpy effect with a change in shape within the groups of

TABLE 9-5

TEST MATRIX FOR SIZE AND SHAPE TESTS

NOMINAL TEST CONDITIONS

Phase	Shape/Size	Enthalpy h (Btu/lb)	Stagnation Pressure p_s (atm)	Heating Rate q_c (Btu/ft^{2}sec)	Nozzle d_e (inch)	Effect Studied
VI A	BH/2.0 (1)	5000	0.028	89	4.5	Shape at constant enthalpy
	FF/2.0			63		
	H/2.0			122		
	BH/2.0 (1)	10000		179		
	FF/2.0			125		
	H/2.0			244		
	BH/2.0 (1)	17500		313	6.0	
	FF/2.0			218		
	H/2.0			426		
VI B	BH/2.0 (1)	5000		89	4.5	Shape at constant heat flux
	FF/2.0	7200				
	H/2.0	3700				
	BH/2.0 (1)	10000		179		
	FF/2.0	14400				
	H/2.0	7400				
	BH/2.0 (1)	17500		313	6.0	
	FF/2.0	24400				
	H/2.0	12500				
VI A & V	BH/2.0	5000	0.028	89	4.5	Size at constant enthalpy
	BH/4.0			63	6.0	
	BH/2.0	10000		179	4.5	
	BH/4.0			127	6.0	
	BH/2.0	17500		313	4.5	
	BH/4.0			221	6.0	
IV A & V	BH/2.0	3500	0.008	33	8.0	Size at constant heat flux
	BH/4.0	5000				
	BH/2.0	10000		93		
	BH/4.0	14100				
VII	BH/2.0	25000	0.028	444	6.0	Size and shape at constant heat flux
	BH/1.0	10000	0.088		2.5	
	H/2.0					
	BH/1.0	3500	0.400		1.5	

(1) Results at these conditions are also included in Phase IV B.

(a) Pre-Test Models 33/H/2.0, 30/BH/2.0, 19/FF/2.0

h = 5000 Btu/lb

p_s = 0.028 atm

(b) Post-Test Models 33/H/2.0, 30/BH/2.0, 19/FF/2.0

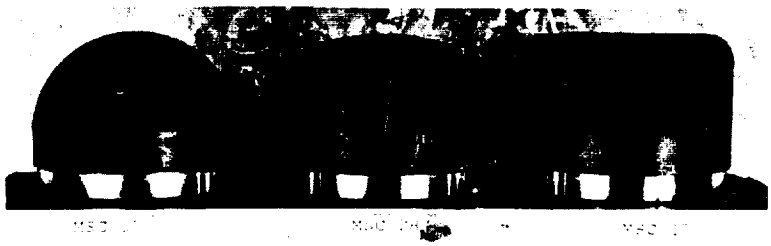

(c) Pre-Test Models 35/H/2.0, 28/BH/2.0, 17/FF/2.0

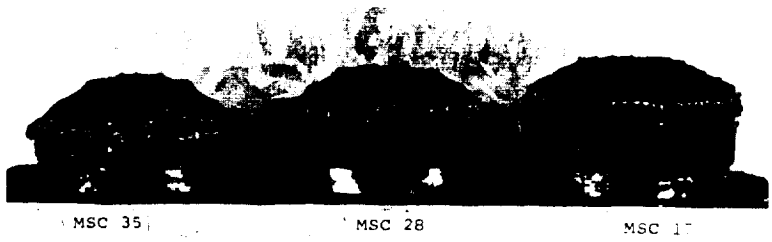

h = 10000 Btu/lb

p_s = 0.028 atm

(d) Post-Test Models 35/H/2.0, 28/BH/2.0, 17/FF/2.0

Figure 9-19. Pre- and Post-Test Photographs of the Model Shapes.

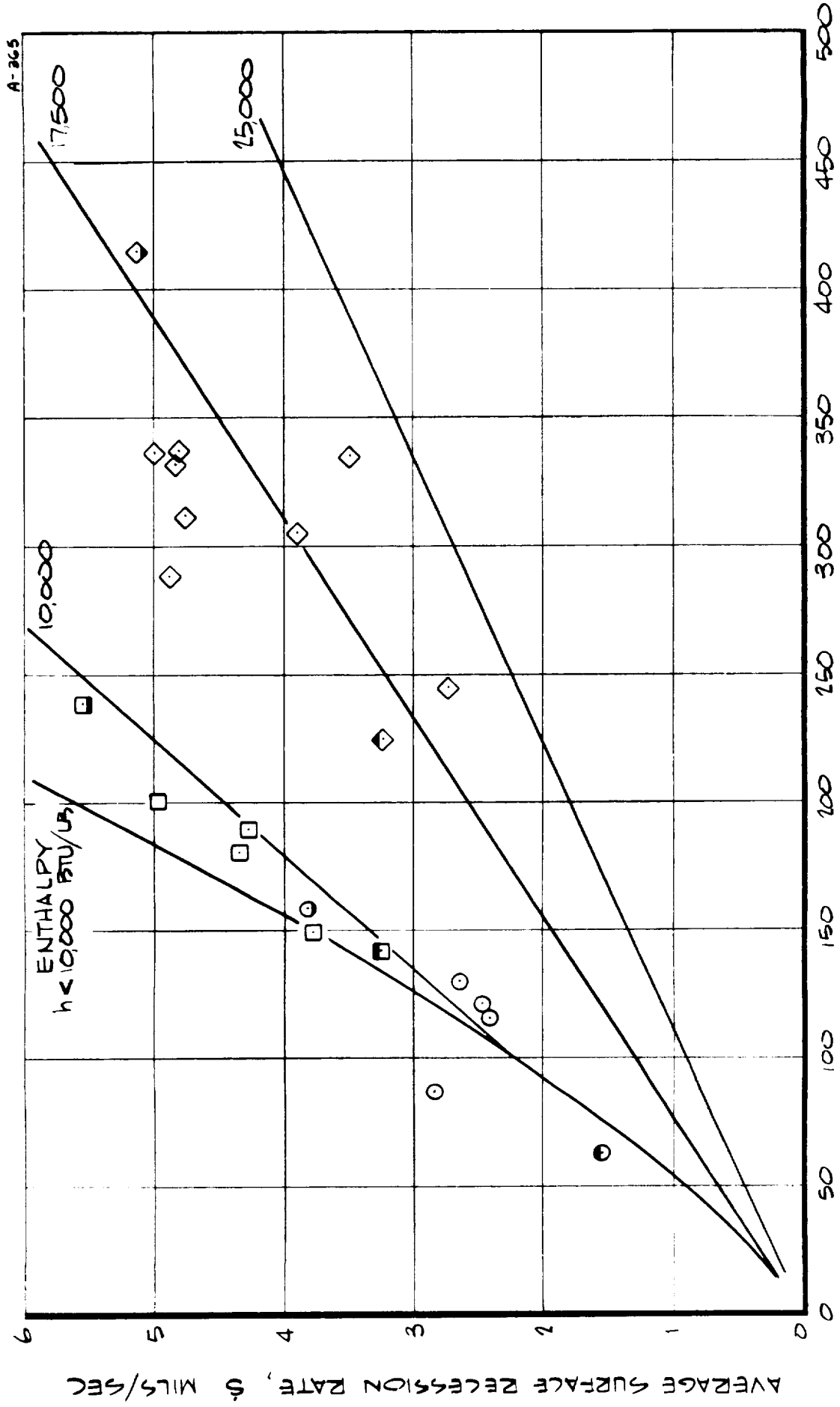

(a) $\dot{s}$ vs $(q_c)_{cw}$

FIGURE 9-10 EFFECT OF MODEL SHAPE AT CONSTANT ENTHALPY ON SURFACE RECESSION RESPONSE.

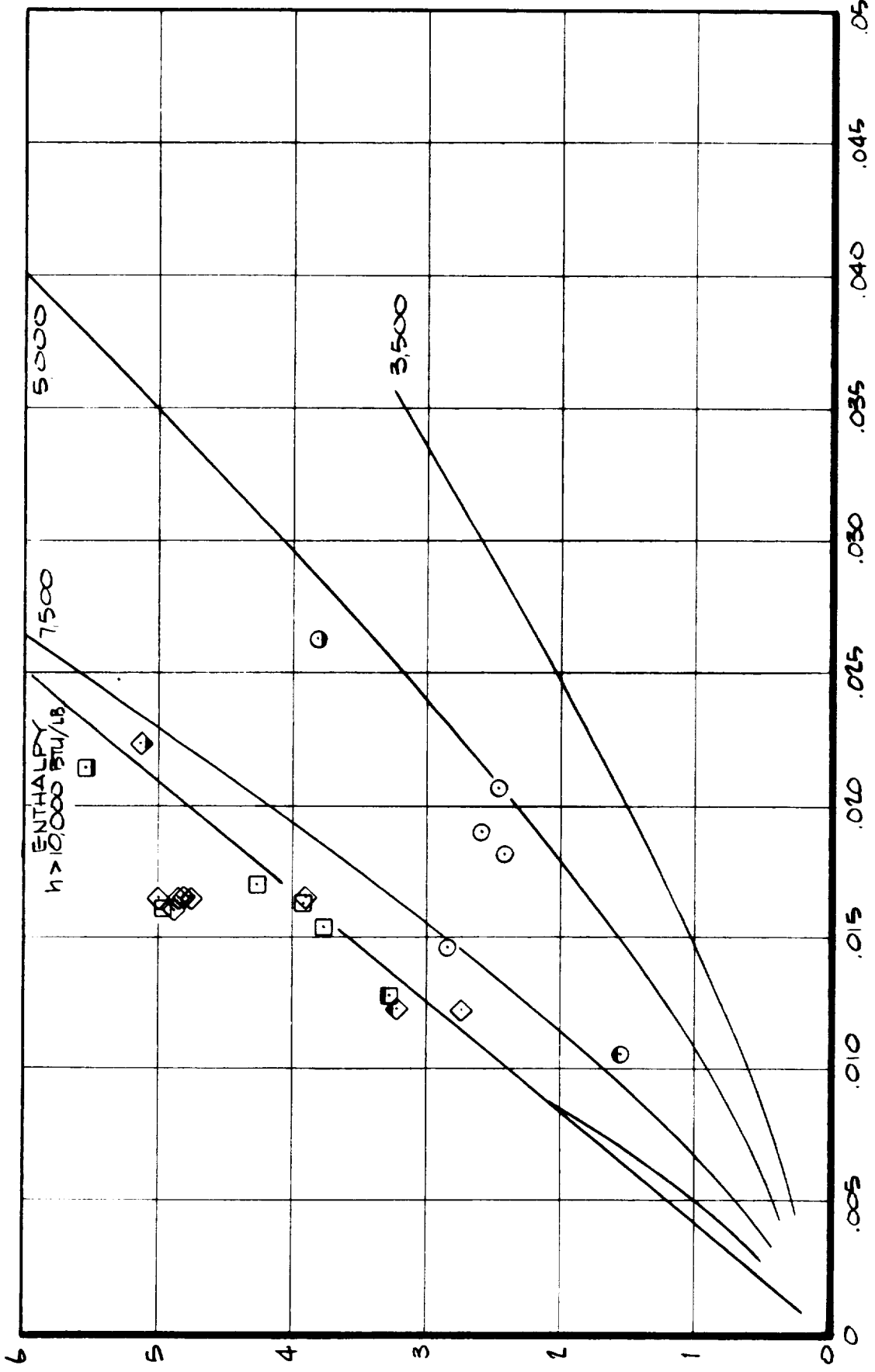

(b) $\dot{s}$ vs $(\rho_e u_e C_H)_{hw}$
FIGURE 9-10 CONTINUED

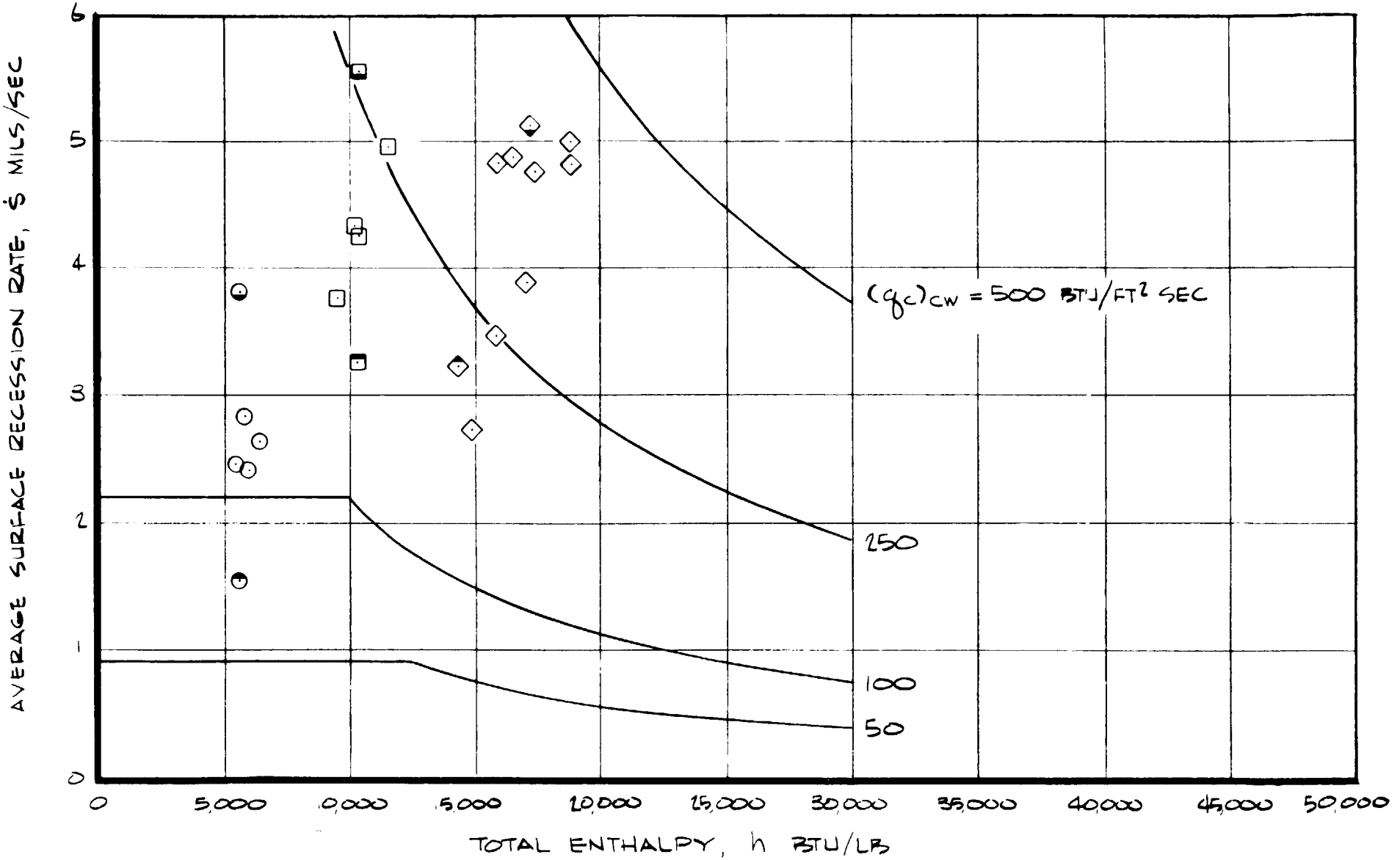

(c) $\dot{s}$ vs h

FIGURE 9-10 CONCLUDED

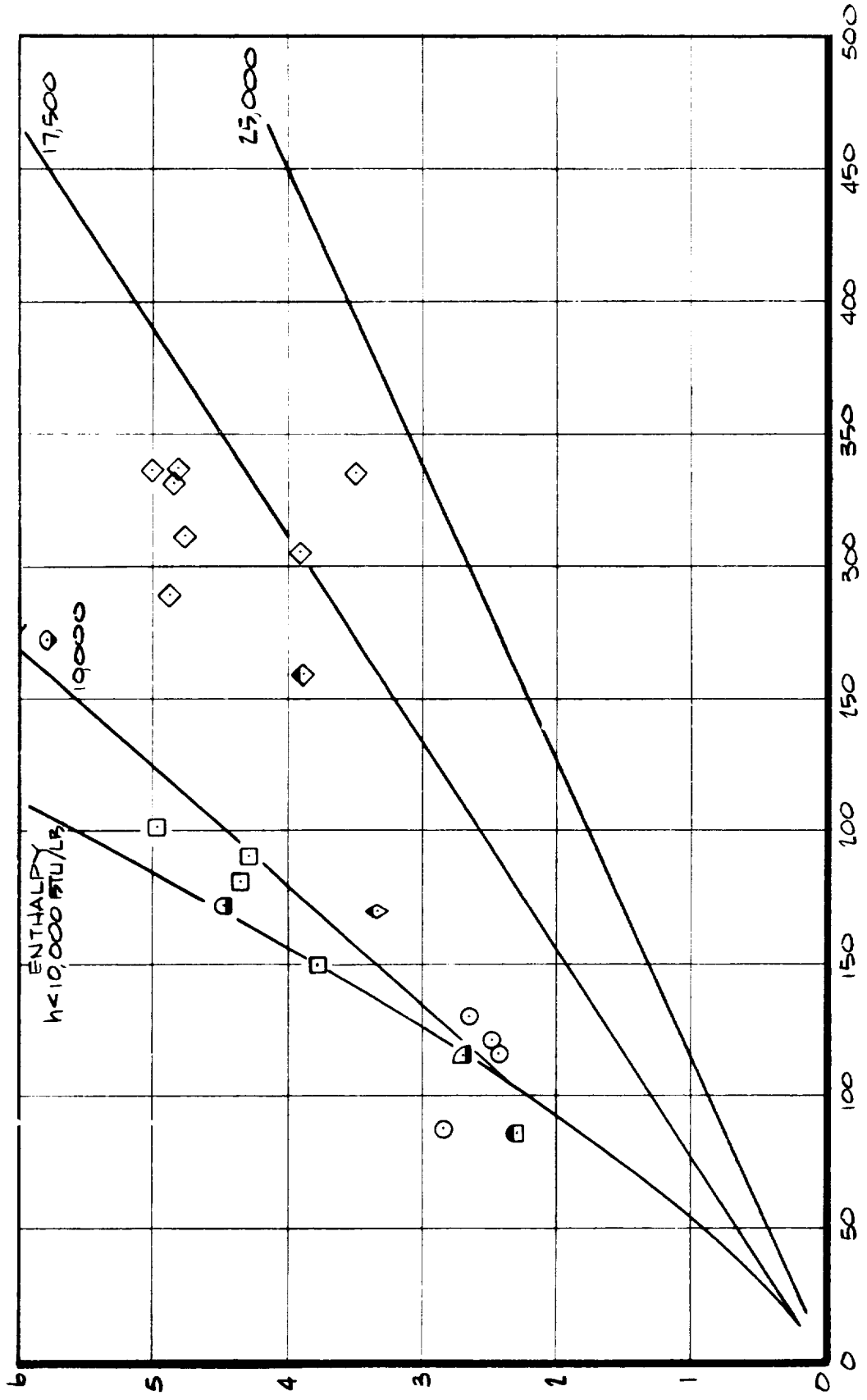

(a) $\dot{s}$ vs $(q_c)_{cw}$

FIGURE 9-21 EFFECT OF MODEL SHAPE AT CONSTANT HEAT FLUX ON SURFACE RECESSION RESPONSE.

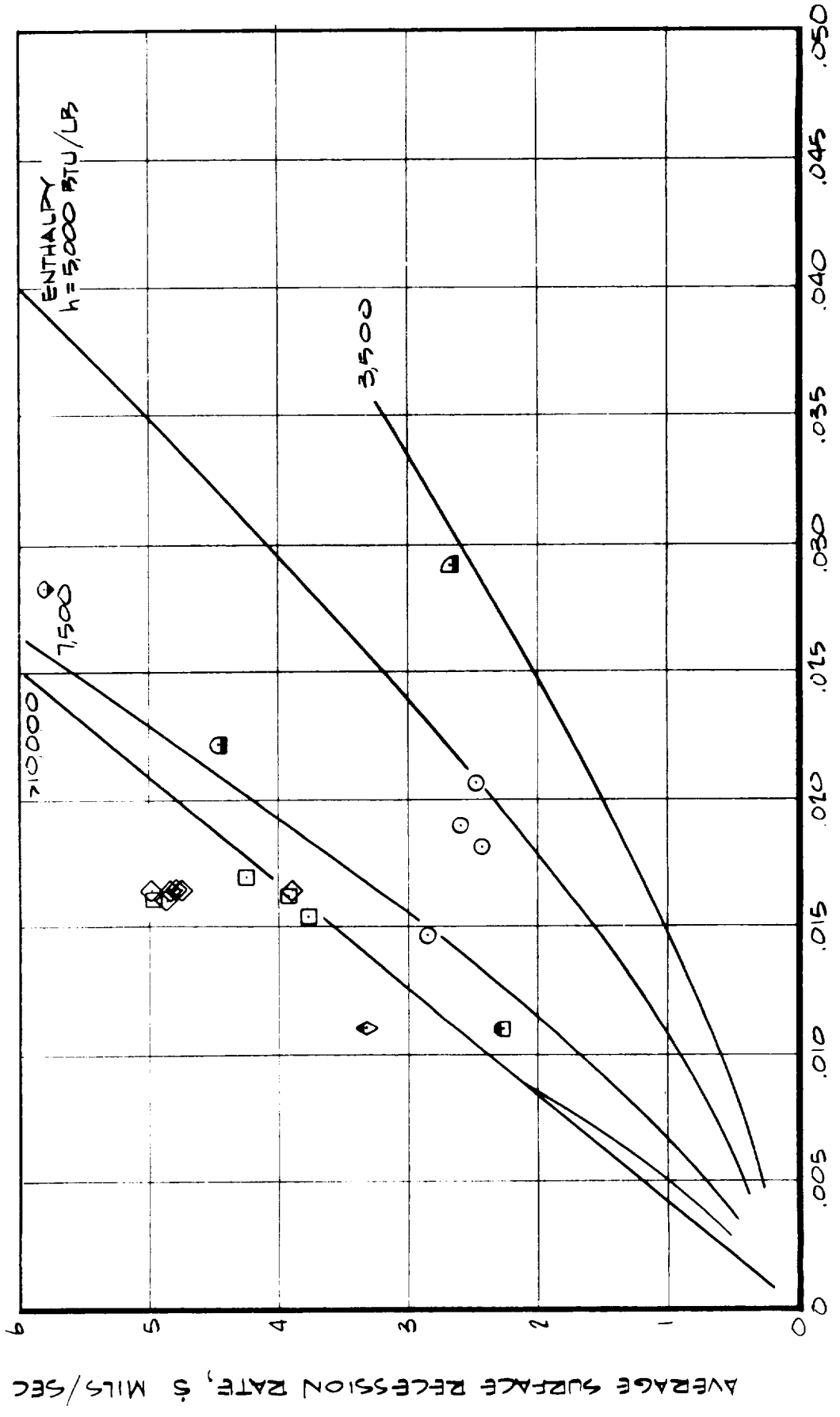

(b) $\dot{s}$ vs $(\rho u C_H)_{hw}$

FIGURE 9-11 CONTINUED

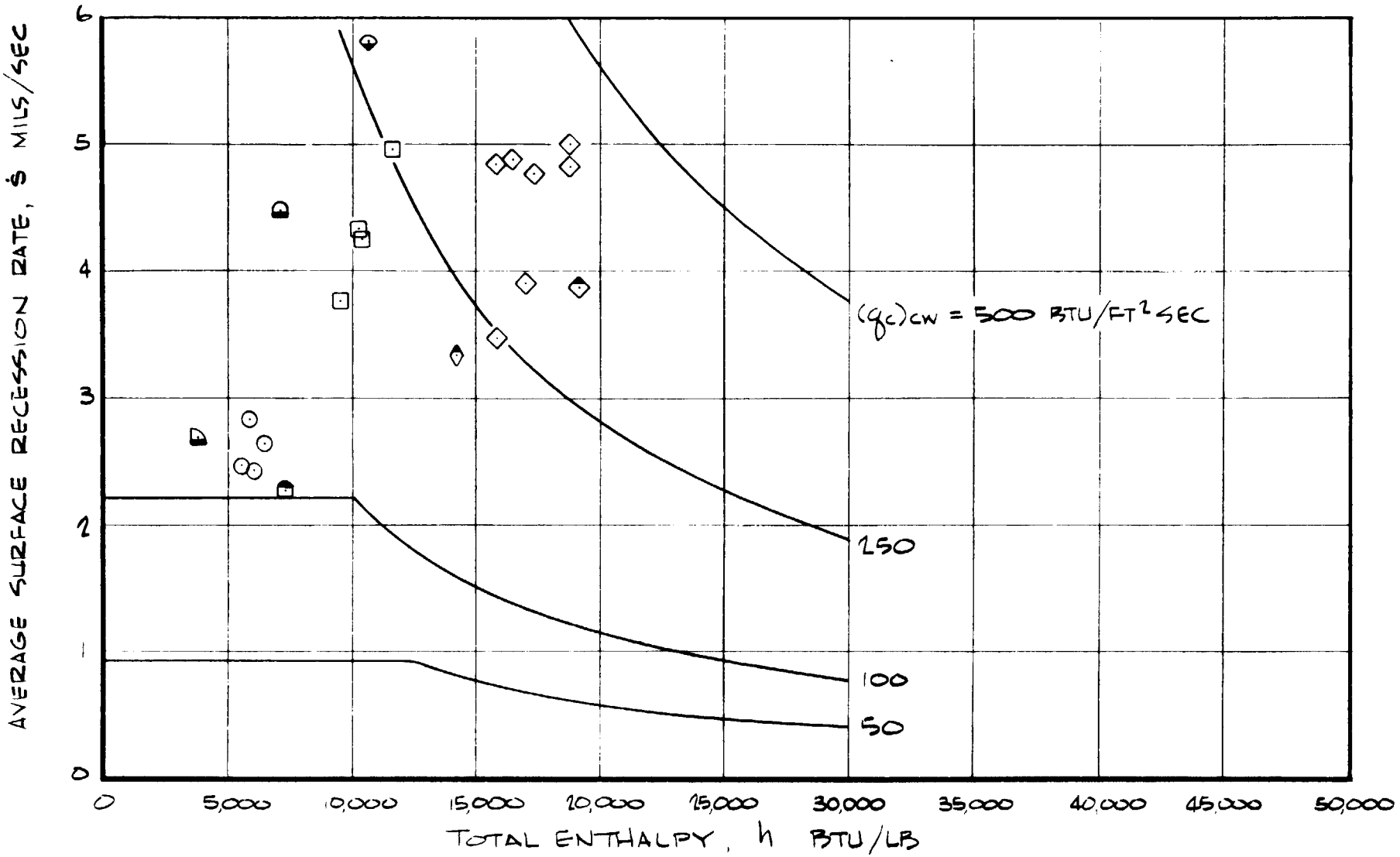

(c) ṡ vs h

FIGURE 9-21 CONCLUDED

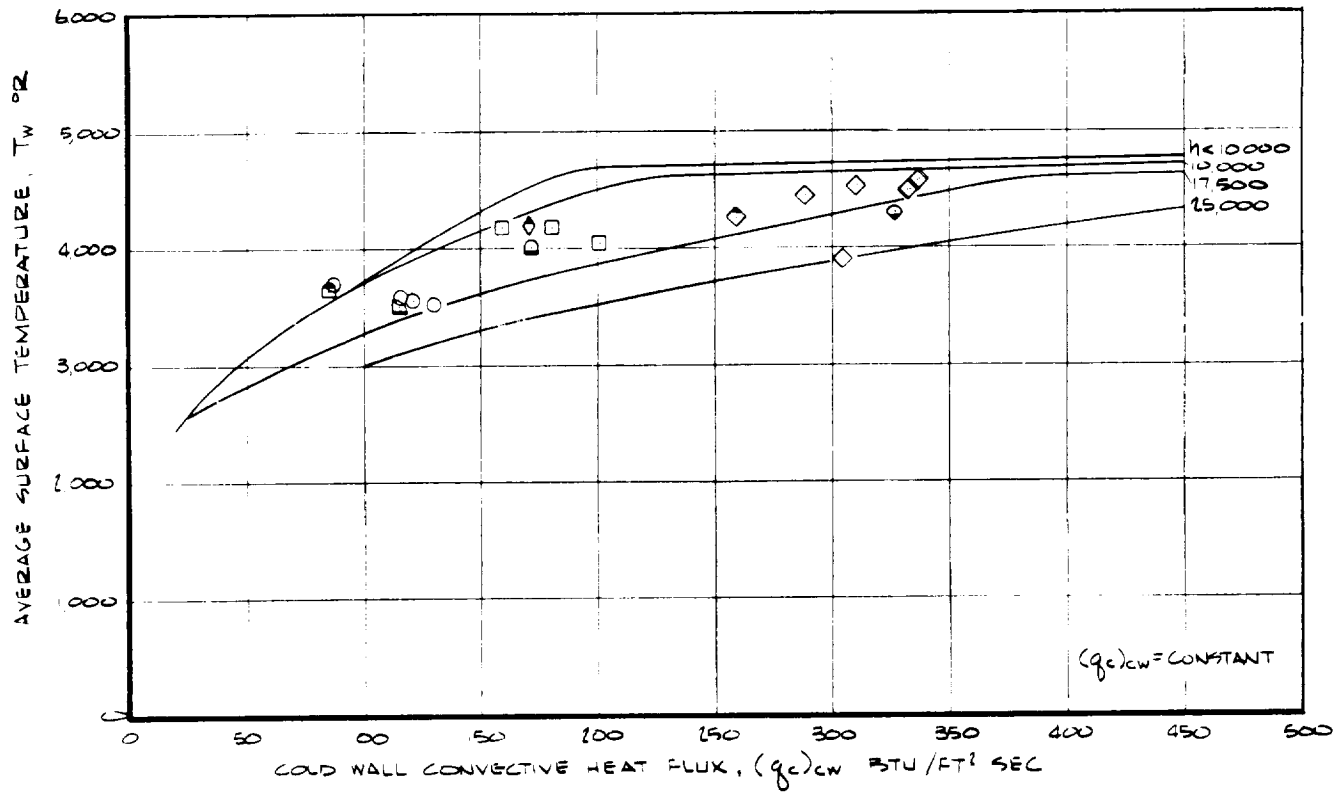

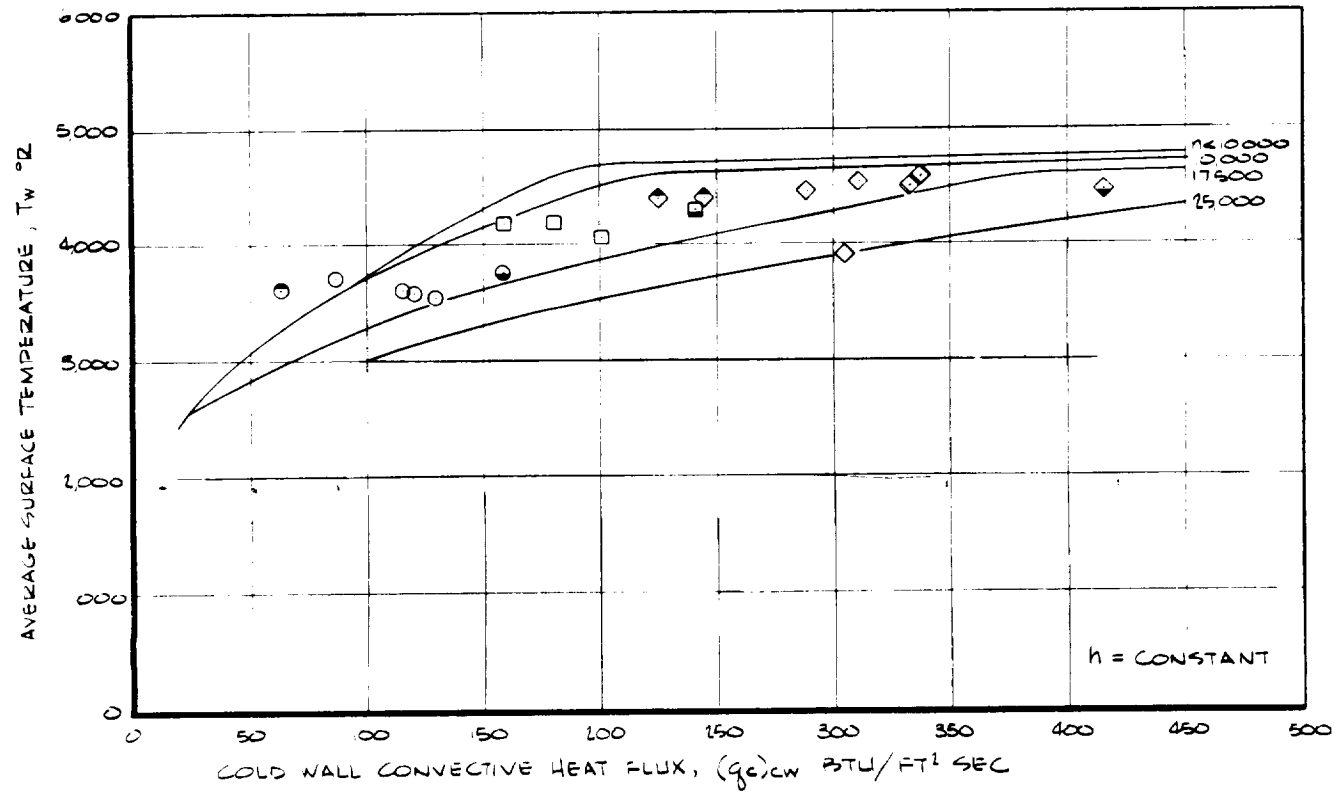

FIGURE 9-22 EFFECT OF MODEL SHAPE ON SURFACE TEMPERATURE RESPONSE.

approximately constant heat flux results. The effect of shape on surface temperature is therefore inconclusive; the effect on surface recession is apparently negligible.

The qualitative effect of model size on the model surface recession response reduces primarily to a shape effect. The 4-inch models exhibited a more uniform surface recession and retained their initial shape better than the 2-inch models. This observation is apparent from the photographs of Figures 6-25 and 27 through a comparison of models at comparable conditions for Phases IVA and V. The largest model size should therefore be selected within the limits of test conditions, acceptable model-diameter to nozzle-exit-diameter ratios, and facility capabilities.

The effect of model size on surface recession rate at constant enthalpy (heat flux variable with size) is presented in Figure 9-23. No major effect of size on the recession response is apparent although the results for the 4-inch models are generally slightly lower, relative to the correlation lines, than the 2-inch models. The effect of model size on surface recession rate at constant heat flux (enthalpy variable with size) is presented in Figure 9-24. No effect of size is apparent, at least for the few data points available. The effect of model size on surface temperature is presented in Figure 9-25. The results exhibit reasonable agreement with the correlation and among themselves, thus exhibiting no apparent effect of model size. No definite effect of model-diameter to nozzle-exit-diameter ratio is apparent in the results of Figures 9-23 - 9-25. The maximum D/d_e value for these results was 0.667 for the 4-inch models at a stagnation pressure of 0.028 atm.

The Phase VII results are presented in Figure 9-26; these results cover a broad spectrum of enthalpy and stagnation pressure and include 2-inch hemisphere and 1-inch and 2-inch blunt hemisphere models. The results exhibit no major effect of size or shape although the non-agreement with the correlations, where they exist, can be rationalized on these terms. The 1-inch models were fabricated with the 5026-39M molded material as the shroud. As discussed in Section 9.1.2.2, this construction technique might well inhibit the recession of the 5026-39HCG honeycomb core. The 3,500 and 10,000Btu/lb, 1-inch model points exhibit a lower than expected recession rate which can be rationalized on this basis. The 10,000 Btu/lb 2-inch hemisphere point can also be rationalized in terms of a shape change through the test as discussed earlier in this section. The hemisphere shape becomes more blunt with recession and therefore the average heat flux and heat transfer coefficients for the test are somewhat lower than that at the start of the test, the values at which the point is plotted. The point should therefore move

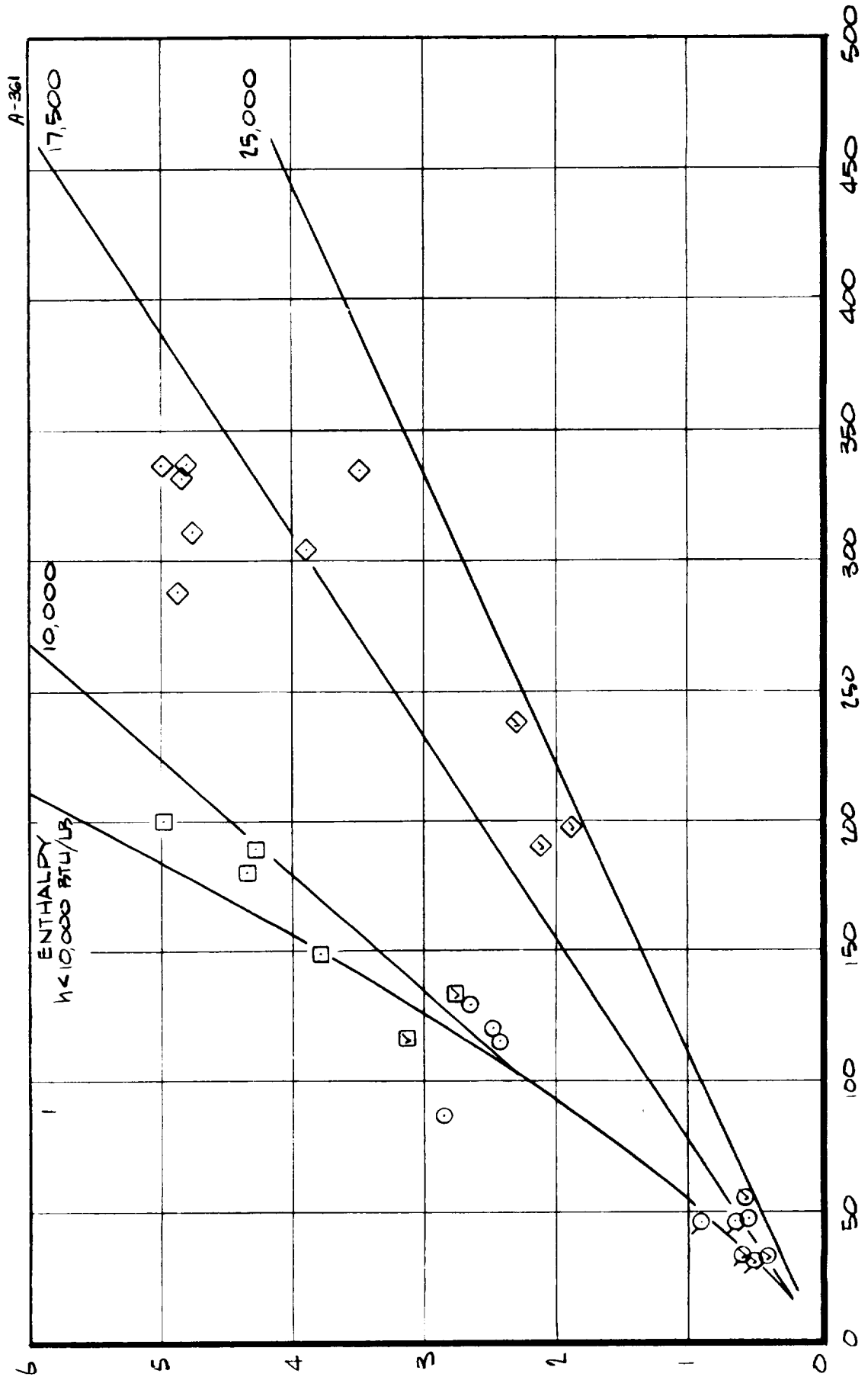

(a) $\dot{s}$ vs $(q_c)_{cw}$

FIGURE 9-23 EFFECT OF MODEL SIZE AT CONSTANT ENTHALPY

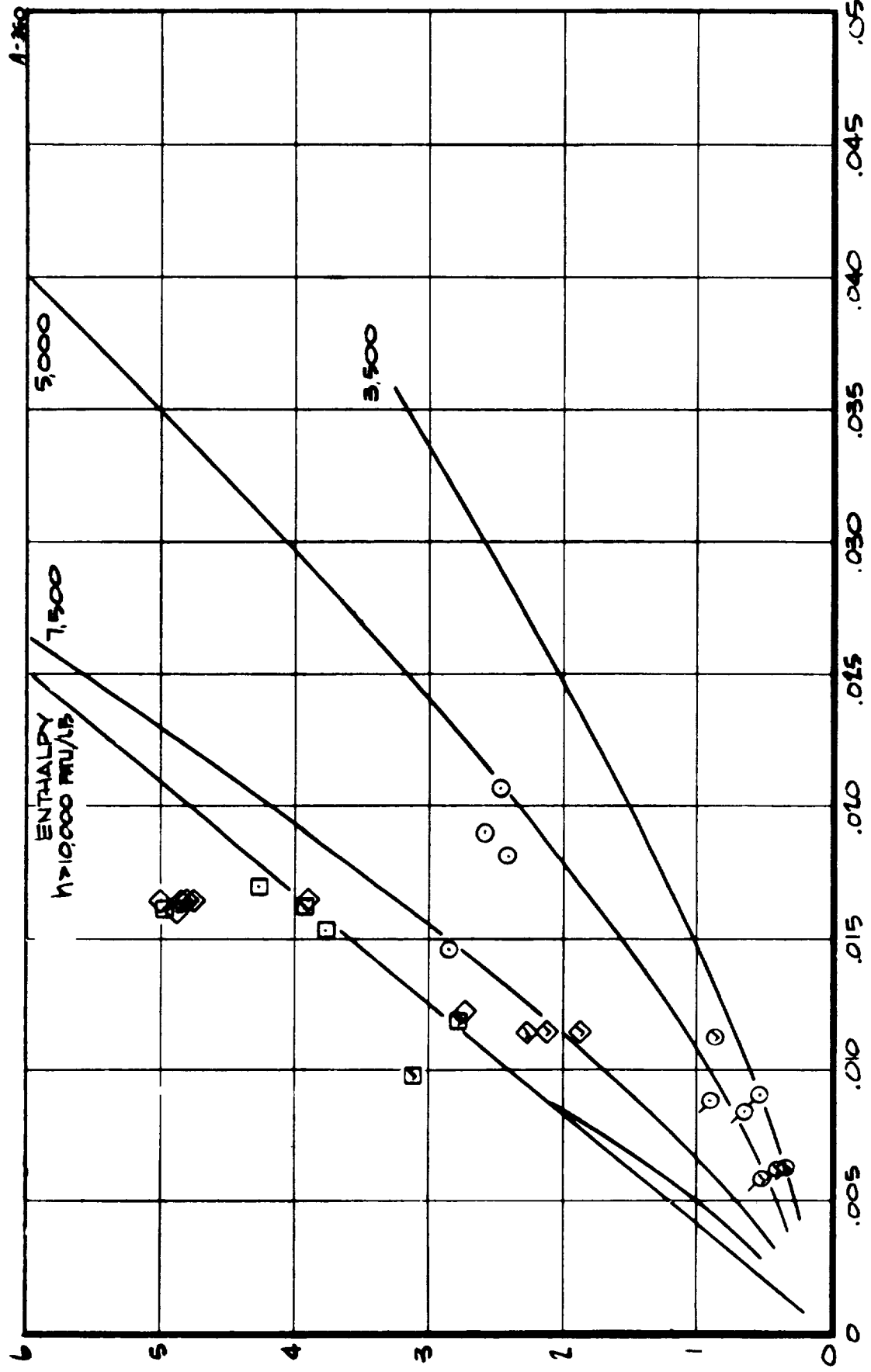

(b) $\dot{s}$ vs $(\rho_e u_e C_H)_{hw}$

FIGURE 9-13 CONTINUED

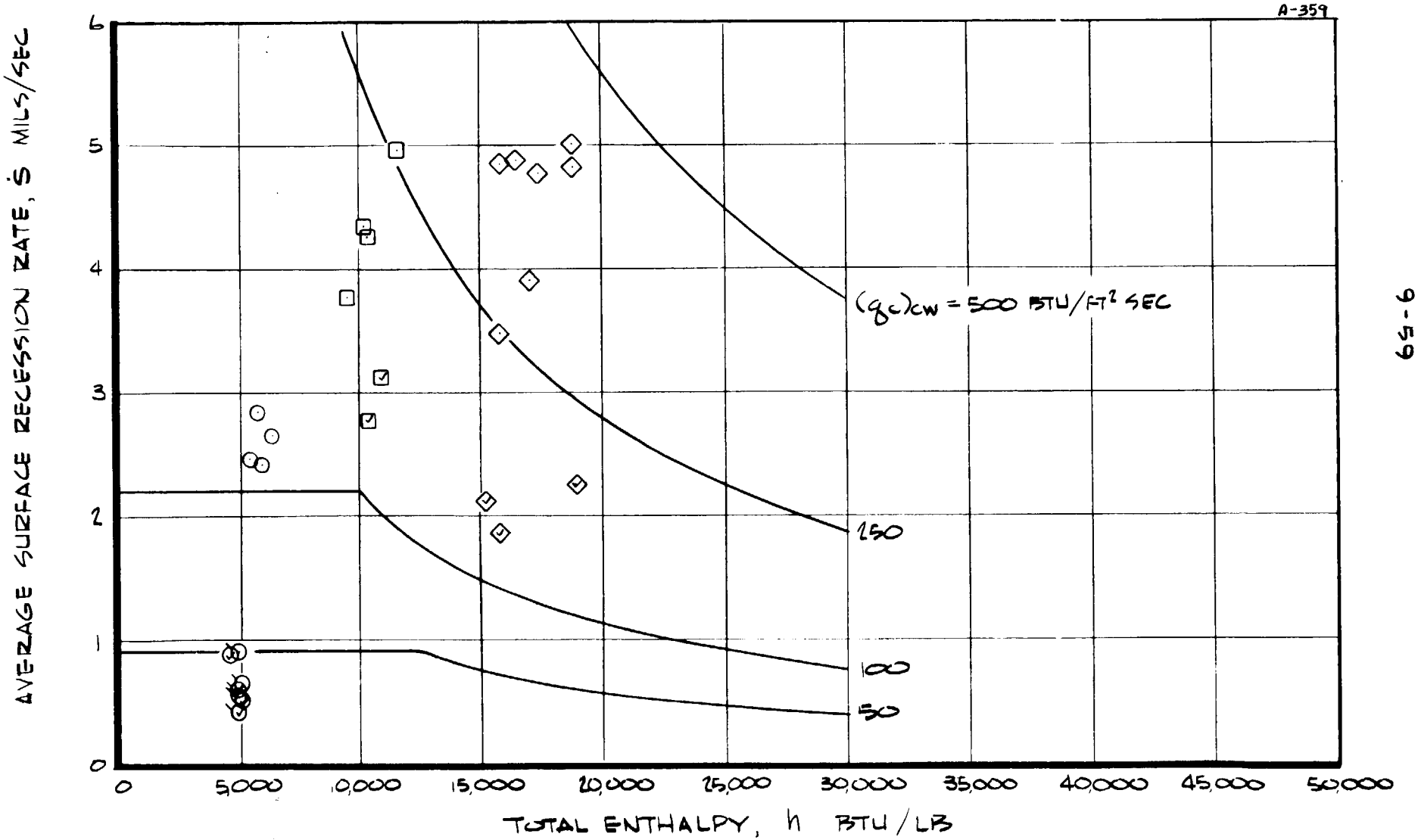

(c) ṡ vs h

FIGURE 9-13 CONCLUDED

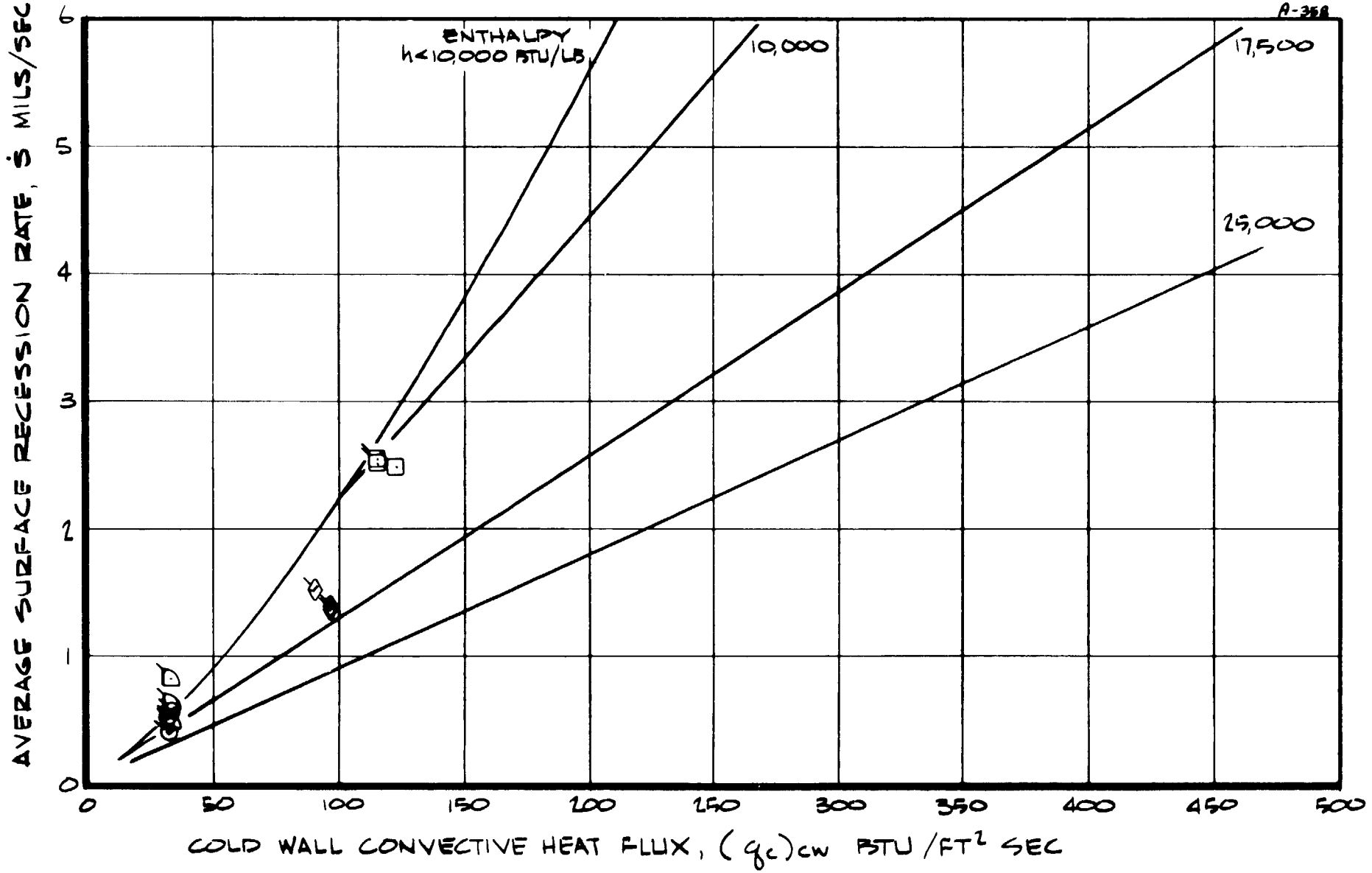

(a) $\dot{s}$ vs $(q_c)_{cw}$

FIGURE 9-24 EFFECT OF MODEL SIZE AT CONSTANT HEAT FLUX ON SURFACE RECESSION RESPONSE

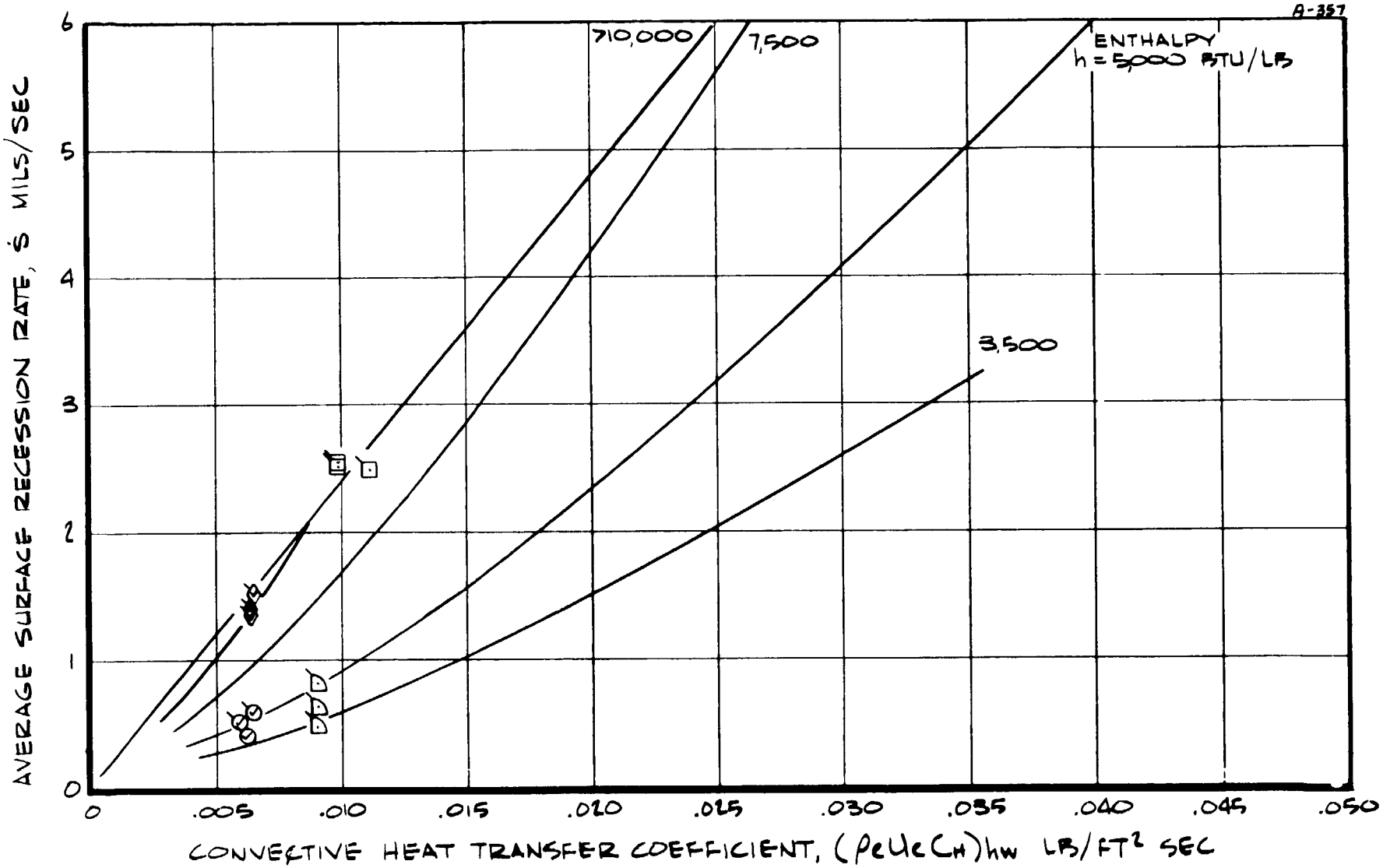

(b) ṡ vs $(\rho_e U_e C_H)_{hw}$

FIGURE 9-24 CONTINUED

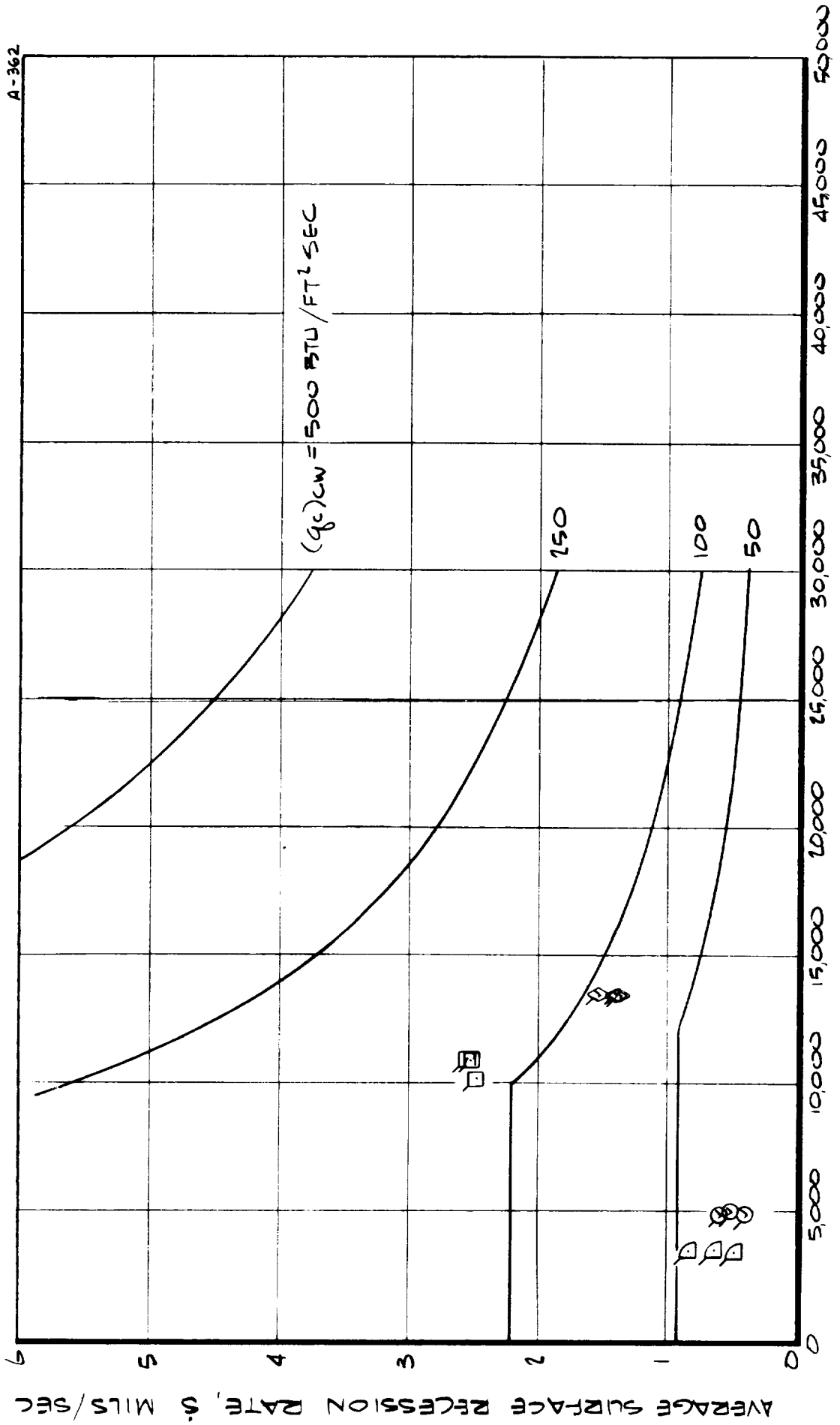

(C) ṡ vs h

FIGURE 9-24 CONCLUDED

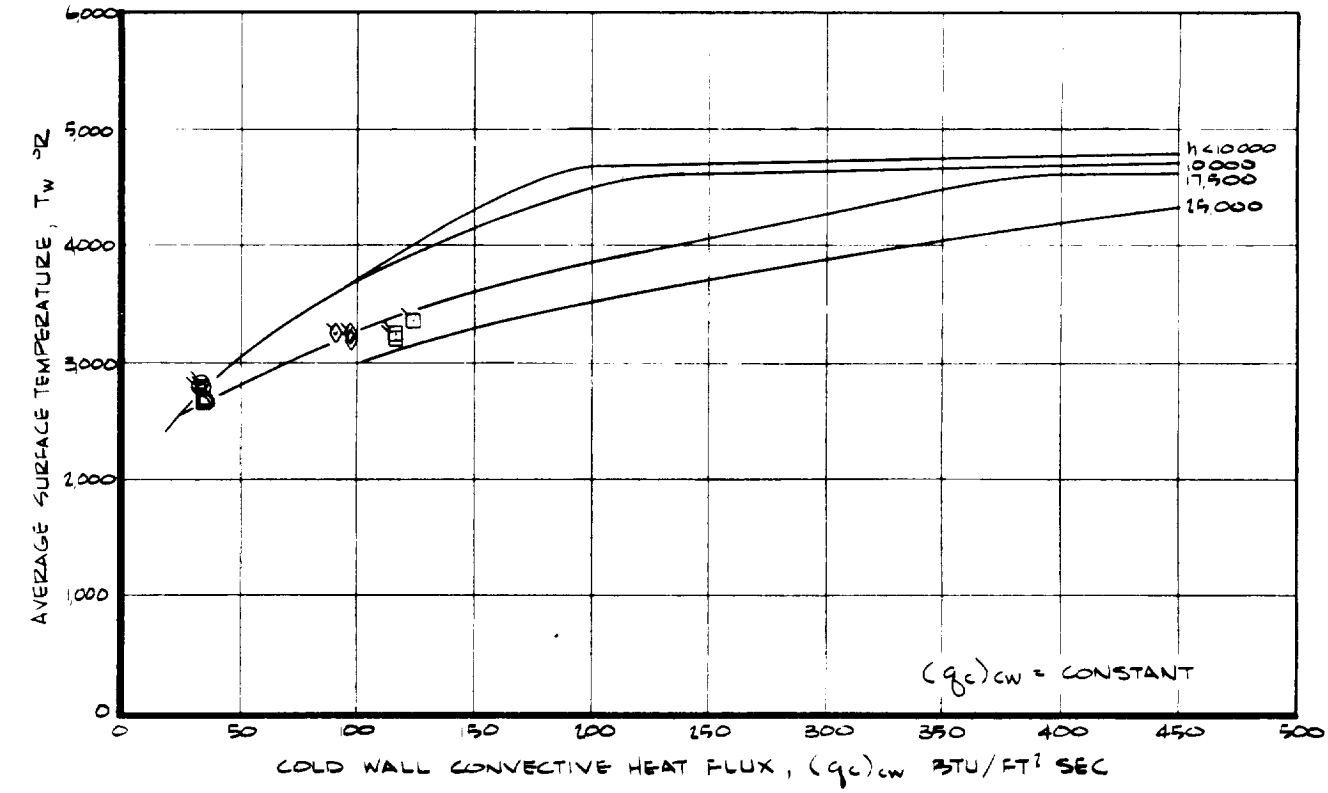

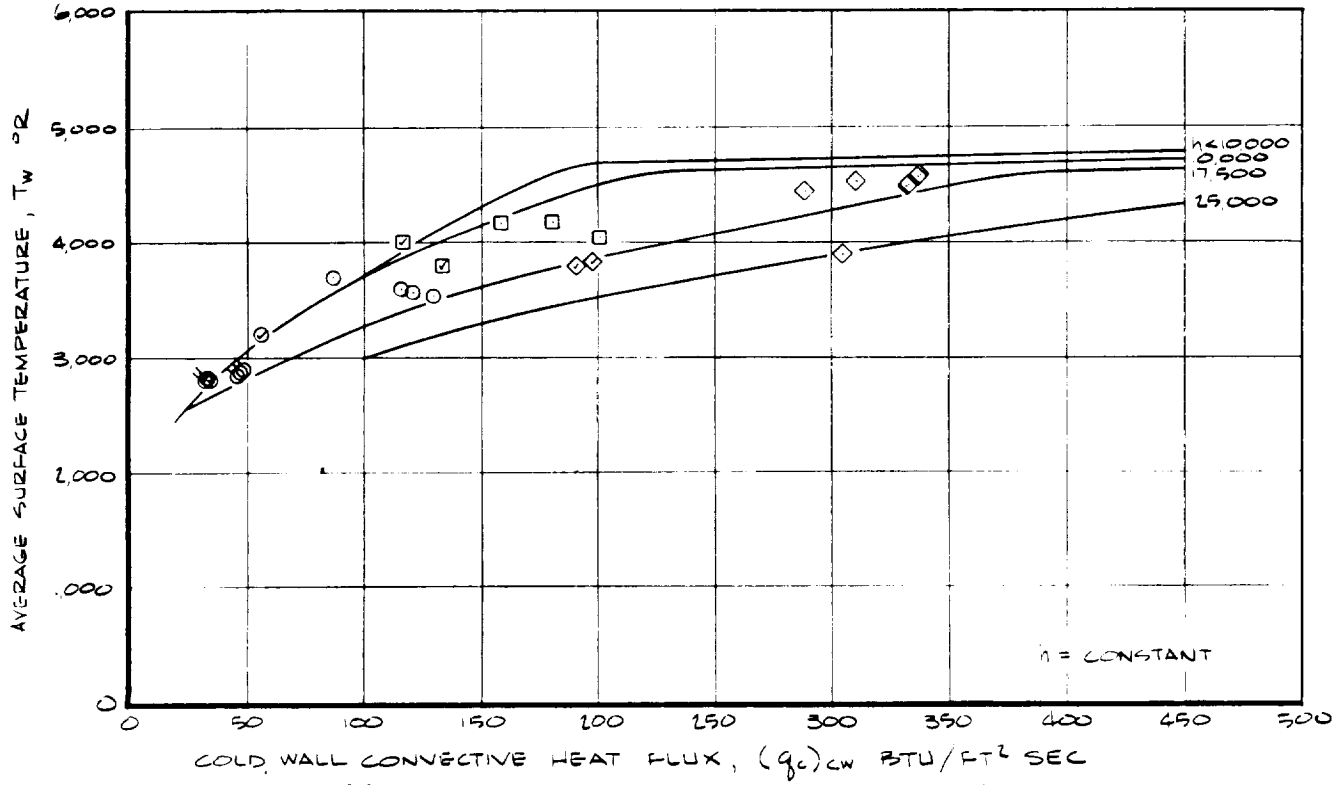

FIGURE 9-25 EFFECT OF MODEL SIZE ON SURFACE TEMPERATURE RESPONSE.

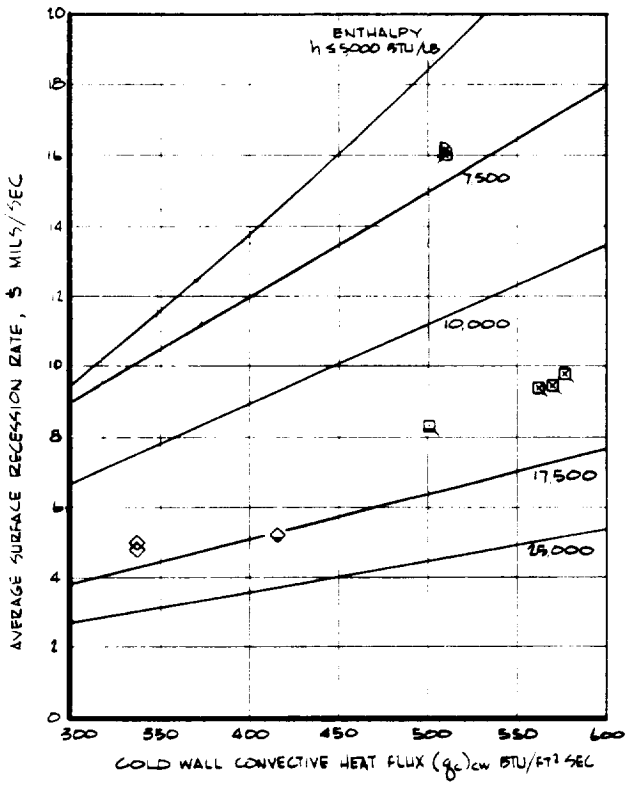

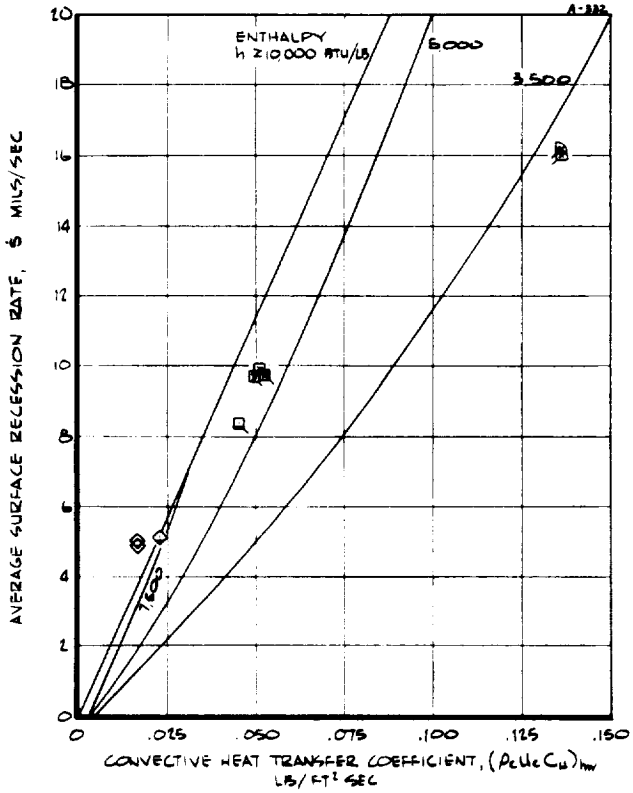

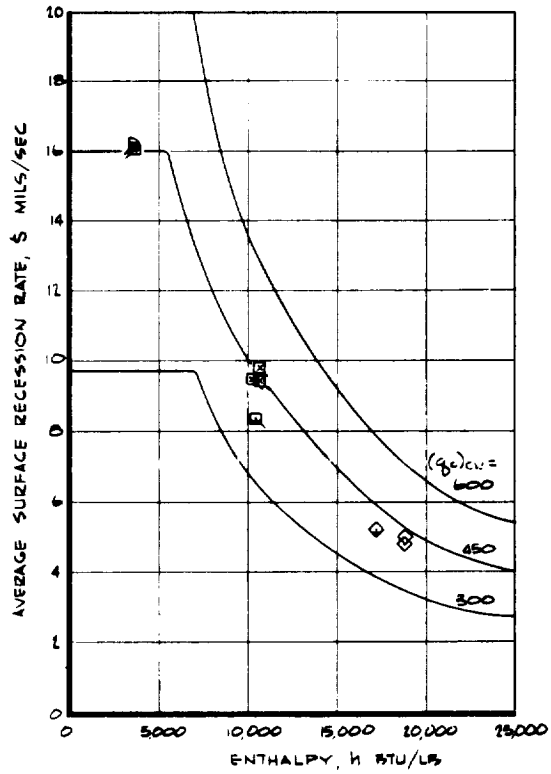

FIGURE 9-16 EFFECT OF MODEL SIZE AND SHAPE ON SURFACE RECESSION RATE, APPROXIMATELY CONSTANT HEAT FLUX TESTS.

to the left toward the proper correlation lines in each of the two appropriate plots of Figure 9-26. It should be noted that these size and shape effects observed from this figure are small and could be interpreted as experimental scatter.

In summary, the effect of model size and shape for the conditions herein is small or negligible.

9.1.2.6 Combined Convective and Radiative Heating

The effects of combined convective and radiative heating on material response were studied as Phase II. These tests were performed in the NASA-Ames Entry Heating Simulator as Gasdynamics Branch Test Series 56. Tests were performed for the range of enthalpy from 3,000 to 6,500 Btu/lb at model stagnation pressures of about 0.10 atm (Table 9-1b). Radiation only tests in a vacuum environment were also performed. Radiation heat flux levels up to 600 Btu/ft^2-sec where achieved. The 1 1/4-inch, flat face model configuration (Figure 4-2) was used in these tests; the core was 1/4 inch in diameter and the shroud was the 5026-39M molded material. The differential recession problem discussed with reference to the 1-inch models (Section 9.1.2.2) therefore also applies to the 1 1/4-inch models. The radiation flux covered an area 5/16 inch in diameter; this dictated the 1/4-inch core size and also further compounded the differential recession problem. Because of this, exposure times were relatively short and total surface recession small. The test results are presented and discussed in the following paragraphs.

Figure 9-27 presents the average surface recession rate results for the convective heating only cases and also includes those results obtained by NASA-Ames in their in-house program conducted concurrently with the Aerotherm program (Reference 9-3).[2] The results at all three conditions exhibit considerable scatter, the Aerotherm models falling within the scatter range but consistently on the high side.[3] This scatter is larger than that experienced at similar conditions in the other test program phases. Also the results generally fall below the appropriate correlation lines. This is probably due to the model configuration and short exposure times used. The core recession

---

[2] The NASA-Ames program employed the same model configuration as in the Aerotherm tests; the models were not instrumented with thermocouples, however. The test conditions were also the same but with convective heating only. The details of the test program and results are included in Reference 9-3.

[3] The models tested as part of the Aerotherm program were measured by Aerotherm; those tested under the NASA-Ames program were measured by NASA-Ames.

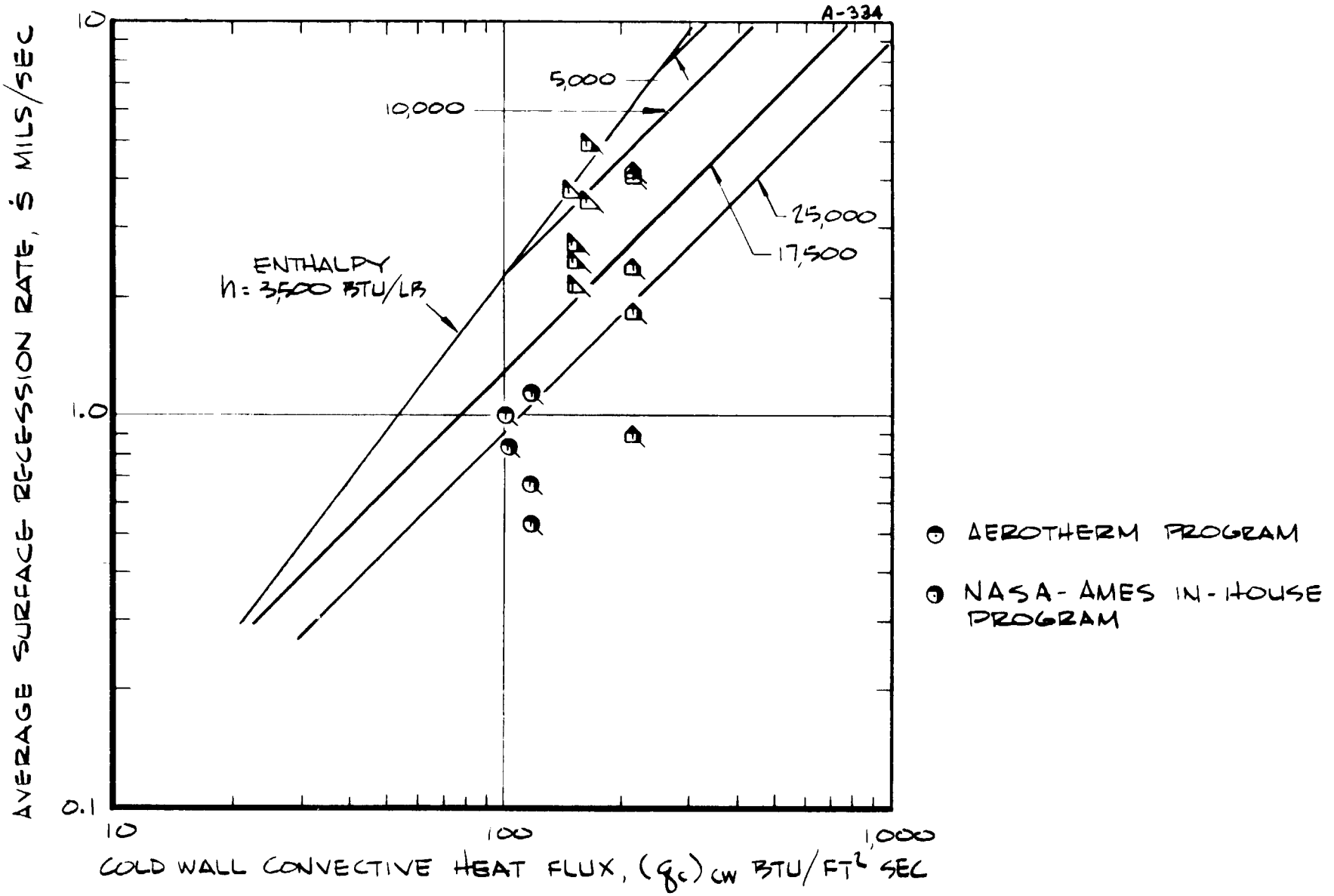

FIGURE 9-27 SURFACE RECESSION RATE FOR CONVECTIVE HEATING ONLY FOR THE COMBINED CONVECTIVE AND RADIATIVE HEATING TESTS INCLUDING THE NASA - AMES IN-HOUSE RESULTS.

was probably affected by the lower recession of the molded shroud. Also, any small errors in measurement of pre- and post-test core length could result in large errors in measured recession and recession rate. This then is felt to be the primary cause of the scatter and the lower than expected recession rates.

The surface recession rate variation with the inverse of surface temperature is presented in Figure 9-28 for all points in the Aerotherm program (Table 9-1b). The "kinetically-controlled" correlation lines of Figure 9-1 are also included for comparison purposes. The lowest recession rate points of each set are the convective heating only conditions (except, of course, for the radiation only set) and the lines connecting the points follow the path of increasing radiation flux. The results exhibit considerable scatter but are reasonably represented by the correlation line, particularly when viewed in the light of the surface recession being somewhat lower than expected. This observation includes the radiation heating only results as well as the combined heating results. This is certainly a somewhat surprising observation, indicating that the surface recession may well be closely coupled to surface temperature regardless of the external conditions. This tentative conclusion of course applies for the conditions of this program only and care must be taken in accepting it as a sweeping generalization.

For the case of a vacuum environment, the recession rate may be calculated theoretically from classical kinetic theory considerations. The number of molecules leaving a surface in a hard vacuum is given by (Reference 9-4)

$$N = \frac{p_v}{\sqrt{2\pi \bar{m} \bar{R} T}} \tag{9-7}$$

where N is the number of mols of gas per unit area per unit time, p_v is the vapor pressure of gases at the surface, and T is the surface temperature. Expressed in terms of mass loss, a computationally convenient form of Equation (9-7) becomes

$$(\rho v)_w = 122\, p_v \sqrt{\frac{m}{T}} \tag{9-8}$$

where $(\rho v)_w$ is in lb/ft^2-sec units, p_v in atm, and T in $^\circ R$. Calculations were made using the ACE computer program to define the vapor pressure as a function of temperature for the char decomposition products of the 5026-39HCG char in the absence of pyrolysis gases. The results of this calculation are presented in Figure 9-29. Equation (9-8) was then evaluated and expressed in terms of surface recession rate (char density = 16.0 lb/ft^3), these results

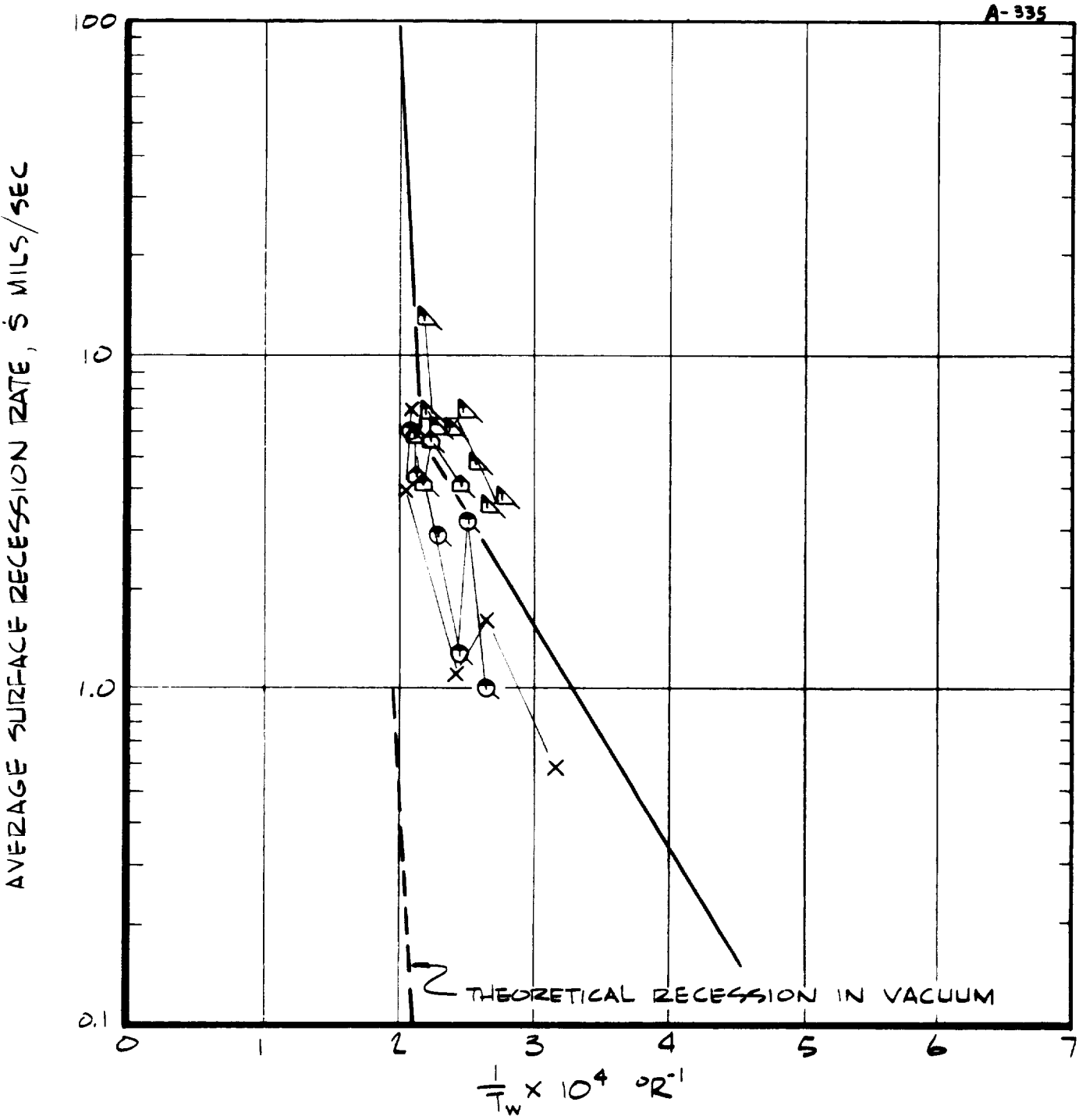

FIGURE 9-28 SURFACE RECESSION RATE - SURFACE TEMPERATURE VARIATION FOR THE COMBINED CONVECTIVE AND RADIATIVE HEATING TESTS, ALL COMINATIONS OF HEATING.

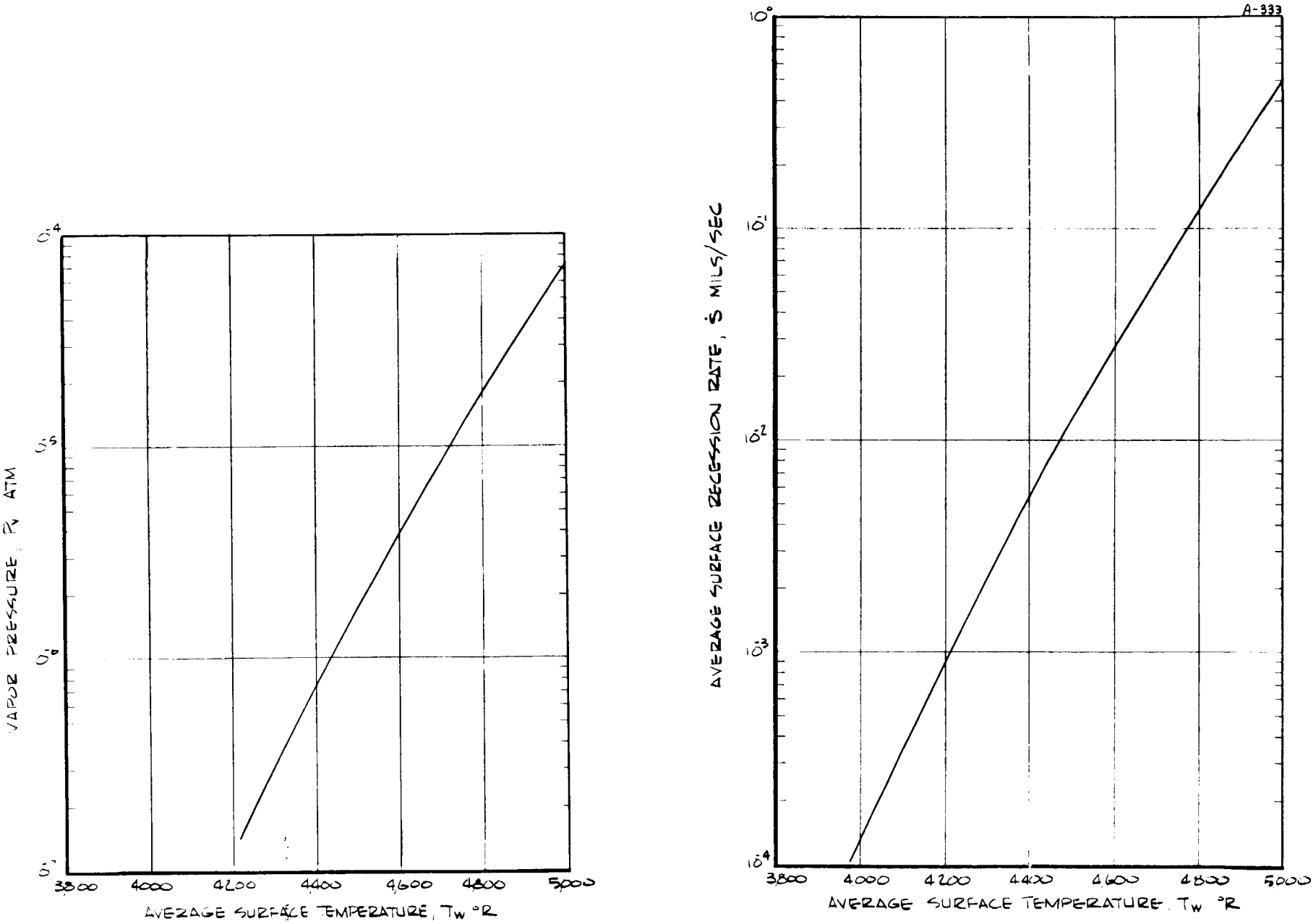

FIGURE 9-29 THEORETICAL RESPONSE OF CHAR IN A VACUUM ENVIRONMENT.

also being included in Figure 9-29 and in Figure 9-28. At a surface temperature of 5,100°R, the surface recession rate is rather significant, about 1 mil/sec, and decreases rapidly as the temperature decreases. This mechanism, though not insignificant at high temperatures, does not provide an explanation of the surface recession in the radiation-only environment. Note that the pryolysis gases were not considered in this analysis; if they had been the theoretical recession rate would probably have been lower, at least in the temperature range of these calculations.

The effect of radiative heating level on surface recession rate is presented in Figure 9-30. The total heat flux is the hot wall convective heat flux plus the radiative heat flux, this being the total flux to a non-ablating model at the measured surface temperature. In each case but the radiation only conditions, the lowest flux plotted is the convective heating only condition. It should be noted that for all but two conditions only one test was performed for the combined heat flux test conditions. The results should exhibit a scatter similar to that of Figure 9-27 and therefore the individual recession results cannot be interpreted as strictly quantitative. The trends however are felt to be real and valid in terms of interpreting the effect of radiative heating on the material performance.

From Figure 9-30, the recession rate increases with increasing total heat flux although, as expected, this increase is not as great as would occur if the additive flux were convective instead of radiative. In the convective case the additional flux would, of course, be accompanied by an increase in the heat and mass transfer coefficients whereas in the radiative case these coefficients are approximately constant as the radiative flux is increased. The radiative-heating-only results generally fall slightly below the combined-heating results. In the combined-heating results, no consistent effect of enthalpy is apparent; total heat flux seems to be the more important parameter in defining recession rate, at least for the limited range of conditions for which results are available.

The effect of total heat flux on surface temperature is presented in Figure 9-31. The trend is as expected and the results fall with respect to the correlation about as well as the convective heating only results presented previously (Figure 9-7).

In summary, the combined convective and radiative heating results exhibit trends that are quantitatively similar to the convective-only-heating results, at least for the range of conditions studied herein. The results correlate reasonably well with the two basic correlations defined in Section 9.1.1, where the total heat flux ($q_c + q_r$) is used in the correlation which relates surface response to environmental conditions.

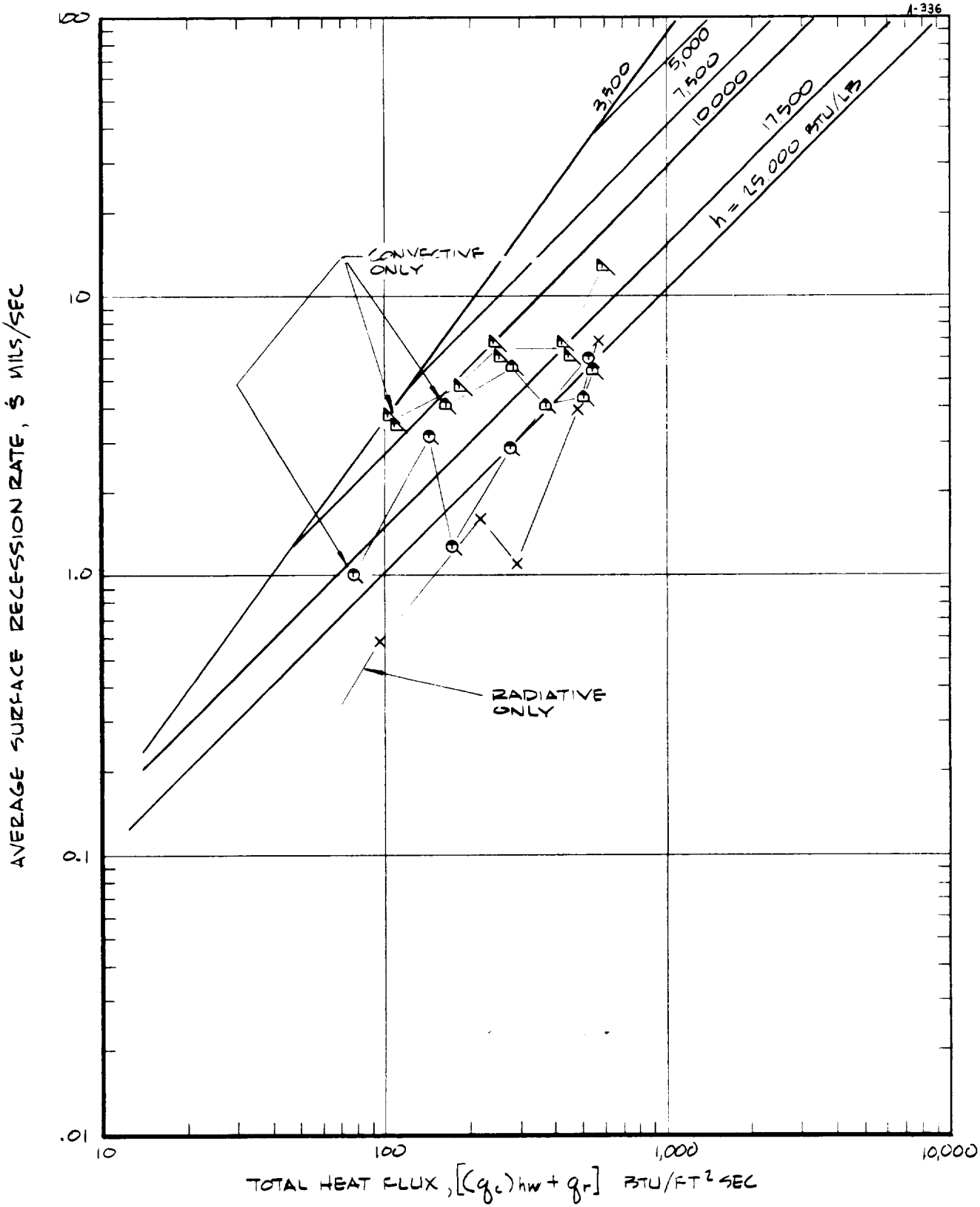

FIGURE 9-30 EFFECT OF TOTAL HEAT FLUX ON SURFACE RECESSION RESPONSE, COMBINED CONVECTIVE AND RADIATIVE HEATING RATE.

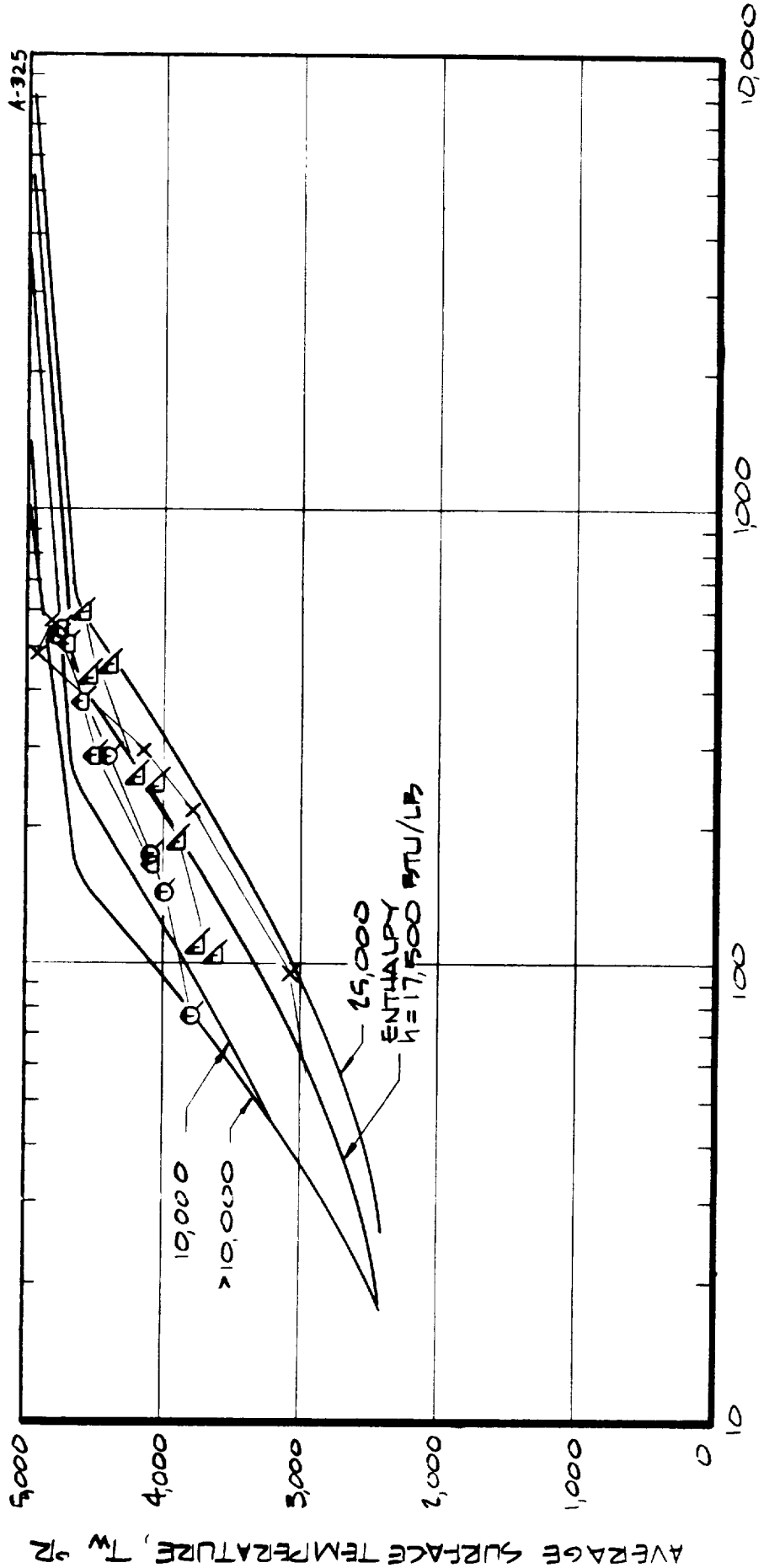

FIGURE 9-31 EFFECT OF TOTAL HEAT FLUX ON SURFACE TEMPERATURE RESPONSE, COMBINED CONVECTIVE AND RADIATIVE HEATING TESTS.

9.1.2.7 Shear

The study of the effects of shear on material response was performed as Phase I (Table 9-1a). The test conditions covered shear levels from 3 to 20 psf, enthalpies from 3,500 to 10,000 Btu/lb, total pressures from 1 to 5 atm, cold wall heat fluxes to 500 Btu/ft^2-sec, and chemical environments of nitrogen and air. Tests were performed primarily on the 5026-39HCG material; however, some tests were performed on the P2019 and 5026-22 materials. In all cases the model shroud and instrumented core were made of the same material. The two duct configurations shown previously in Figures 4-5 and 4-6 were used, the tests being designated Series A and Series B, respectively, according to the duct configuration.[4] The test conditions and configurations are summarized in Table 9-6. Note that in all but the subsonic cases the flow conditions on the model are difficult to define, particularly in the presence of surface recession, due to the particular duct configuration (Series A) and due to the unfortunate combination of chamber pressure, throat pressure, and exit pressure (Series B). This certainly casts at least some doubt on the validity of the results for these cases. Note also that the specified conditions (Tables 9-1a and 9-6) are initial conditions; the severity of conditions decreases as surface recession occurs except for the possible deleterious effects of shocks that might have occurred. The test results are presented and discussed in the following paragraphs.

The models tested in the air environment exhibited a generally uniform surface recession although some "scallops" occurred on the models both axially and locally at random.[5] The axial scallops may well have been due to the flow field problem mentioned previously. The locally random scallops occurred at the 7 psf shear level. The results for the nitrogen environment at the 7 psf shear level were very erratic and the material seemed to be removed in the form of discrete chunks of char. This could have been caused by the flow field problem or it could have been a mechanical removal phenomena related to the thick char that formed before this apparent "chunking" occurred. The possible mechanical removal mechanisms were discussed in Section 9.1.2.2 and this discussion is not repeated here. At the 3 psf shear levels in nitrogen, the surface recession was uniform and low.

---

[4] The results of Series A were presented previously in Aerotherm Technical Memorandum 6007-TM-1 (Reference 9-4).

[5] The qualitative comments apply primarily to the Series B tests. The Series A test models had already been forwarded to NASA-MSC and were not available for a second look at the time of this writing. Also, all recession results for the Series A tests are averages only; no minimum/maximum measurements were made.

TABLE 9-6

SUMMARY OF SHEAR TEST CONDITIONS

Series	Nominal Initial Test Conditions						Flow Conditions
	Enthalpy h (Btu/lb)	Chamber Pressure p_o (atm)	Sonic Pressure p_* (atm)	Exit Pressure p_e (atm)	Shear Stress τ_w (psf)	Heating Rate q (Btu/ft^2-sec)	
A	5,000	1.0	1.0	1.0	3	175	Subsonic
	3,000	2.0			10	300	"Transonic" upstream of model; "transonic or subsonic on model (Fig. 4-5)
		5.0	2.5		20	500	Sonic upstream of model; sonic, supersonic or subsonic on model (Fig. 4-5)
B	3,000	2.0	1.0	1.0	7	250	"Transonic" or subsonic on model (Fig. 4-6)
	4,000	1.0			3	200	Subsonic
	9,000					350	

The surface recession rate variation with heat flux and heat transfer coefficient is presented in Figure 9-32 for all results on the 5026-39HCG material in air. The stagnation point correlations presented previously are also included for comparison purposes. The actual conditions of the shear tests were sonic and subsonic flow with a turbulent boundary layer which of course do not correspond to the laminar, stagnation point conditions for which the correlations were developed. The correlations are sufficiently general however that there is no reason to believe that they should not be applicable to these conditions. As seen from Figure 9-32, the results fall well above the correlations except those for the 9,000 Btu/lb - 3 psf condition which fall very close to the correlation. Actually all other recession rates are a factor of about 2 higher than that indicated by the correlations. There is no obvious explanation for this observed difference in behavior relative to the correlations. The most likely possibility seems to be the pressure effect above 1 atm observed for the high pressure tests, Section 9.1.2.2. Of course, another possible expanation is the experimental problems discussed previously.

The effect of heat flux and heat transfer coefficient on surface temperature is presented in Figure 9-33, again for the 5026-39HC material in air. The surface temperatures are close to but consistently higher than those observed at similar conditions in stagnation point flow. The same possible rationalizations presented above for surface recession also apply here.

From Figure 9-32, it is apparent that recession rate varies approximately as the heat transfer coefficient ($\dot{s} \propto \rho_e u_e C_H$) at the 3,500 Btu/lb conditions, the only enthalpy level for which there are enough points to exhibit this trend. The shear stress also varies approximately as the heat transfer coefficient ($\tau_w \propto \rho_e u_e C_H$) as shown in Figure 9-34 and therefore it can also be said that the recession rate is proportional to shear stress ($\dot{s} \propto \tau_w$). It is difficult to definitively say which parameter is controlling, $\rho_e u_e C_H$ or τ_w, but intuitively $\rho_e u_e C_H$ seems to be the answer. The effect of shear, if it were important, would be expected to be non-linear with shear; that is, $\dot{s}$ would be expected to increase proportionately faster as the shear is increased. Again, however, the above observations and interpretations are somewhat clouded by the potential experimental problems discussed previously.

The surface recession rate and dimensionless recession rate parameter B' are plotted functions of shear stress in Figure 9-35 for all 5026-39HCG models tested in air. The observations discussed above are apparent in this figure; note that constant B' is equivalent to $\dot{s} \propto \rho_e u_e C_H$.

The comparison of the performance of the three materials considered, 5026-39HCG, P2019, and 5026-22, is presented in Figure 9-36 in terms of $\dot{s}$ and B'. The 5026-39HCG material consistently exhibits the highest recession

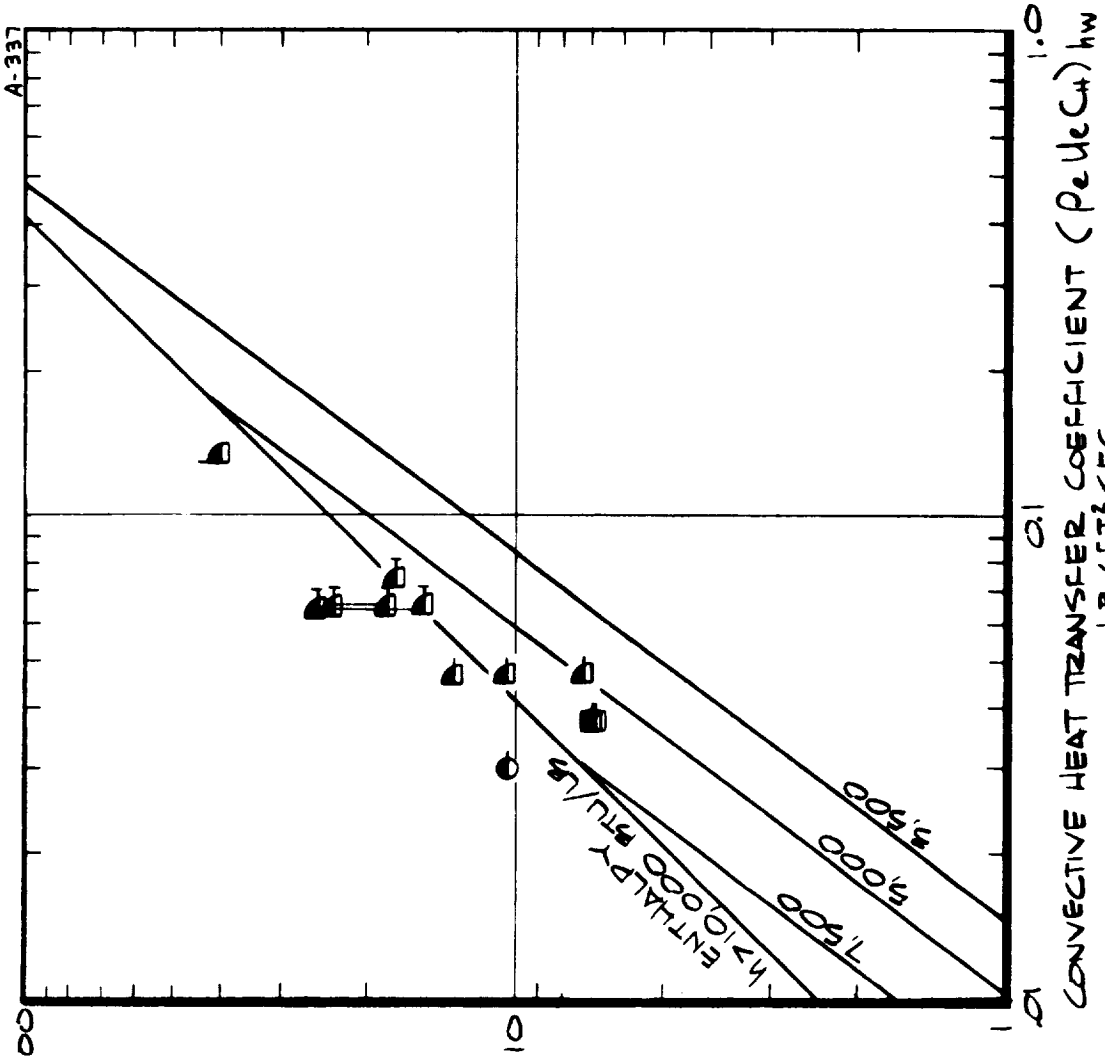

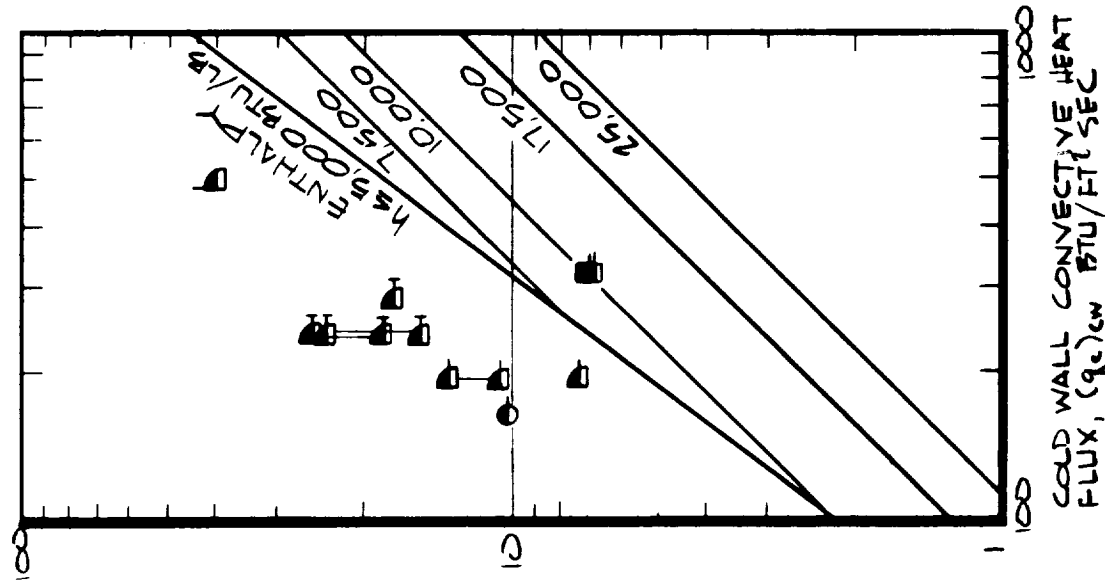

FIGURE 9-32 EFFECT OF CONVECTIVE HEAT FLUX AND HEAT TRANSFER COEFFICIENT ON SURFACE RECESSION RESPONSE, SHEAR TESTS.

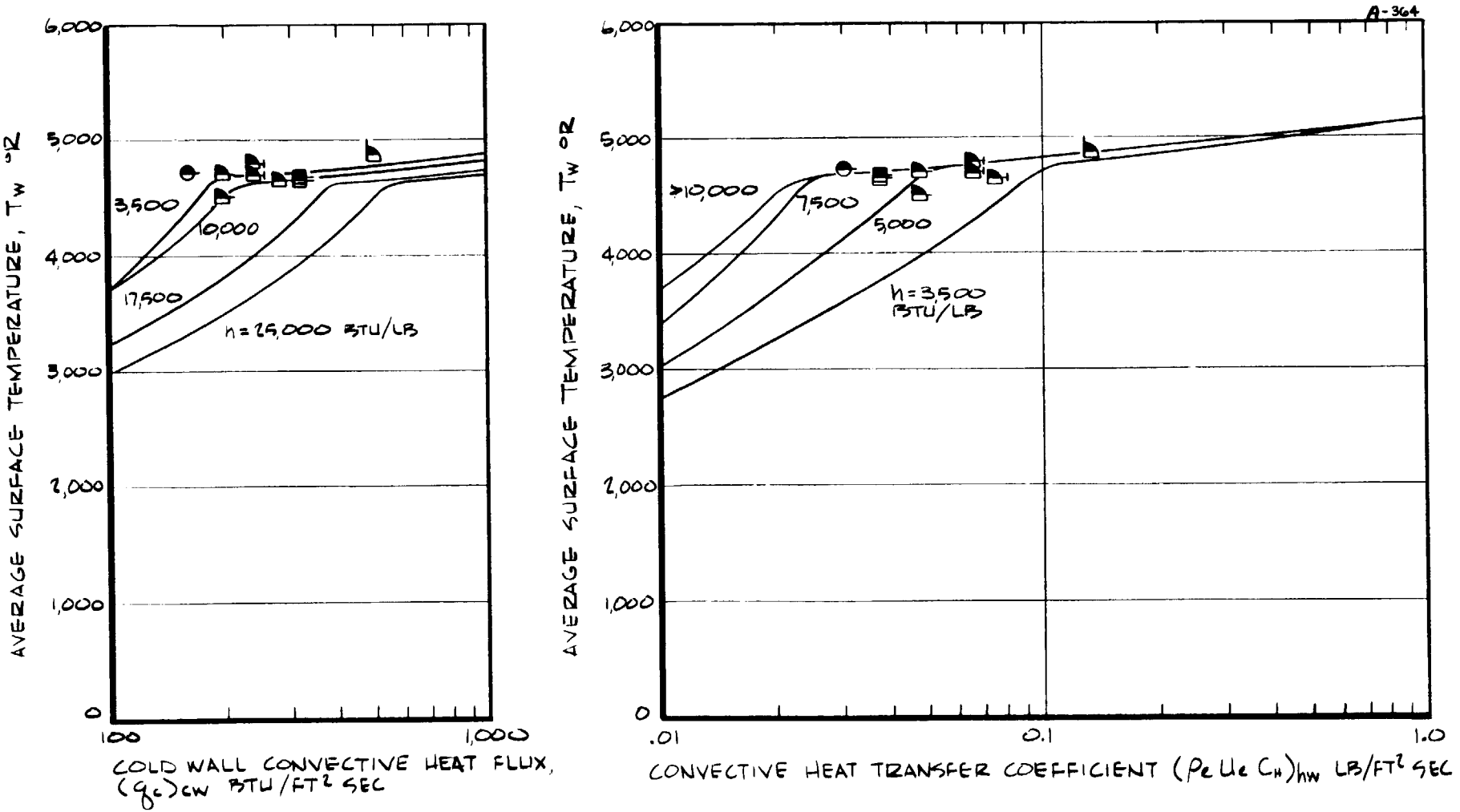

FIGURE 9-33 EFFECT OF CONVECTIVE HEAT FLUX AND HEAT TRANSFER COEFFICIENT ON SURFACE TEMPERATURE RESPONSE, SHEAR TESTS

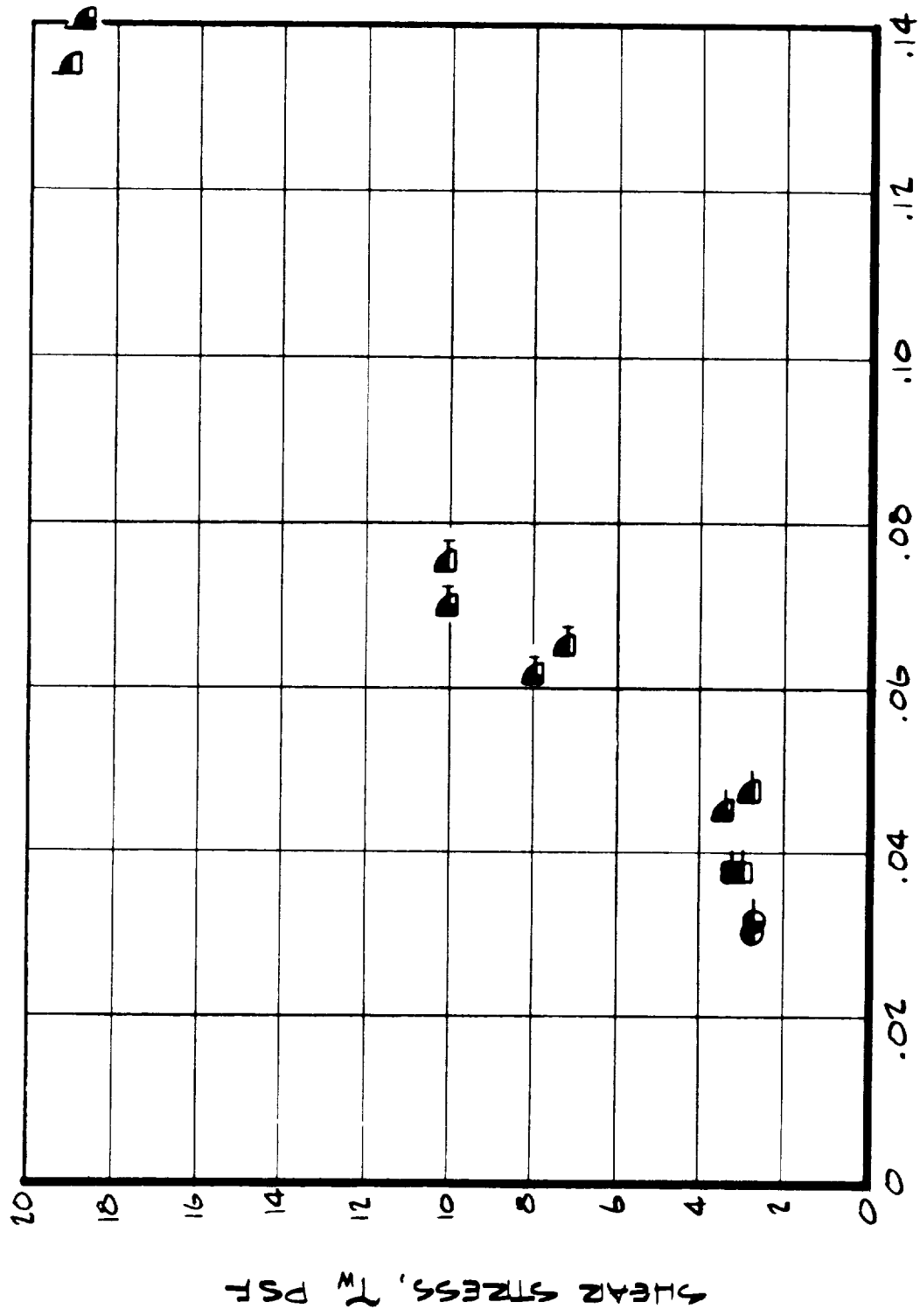

FIGURE 9-34 VARIATION OF HEAT TRANSFER COEFFICIENT WITH SHEAR STRESS.

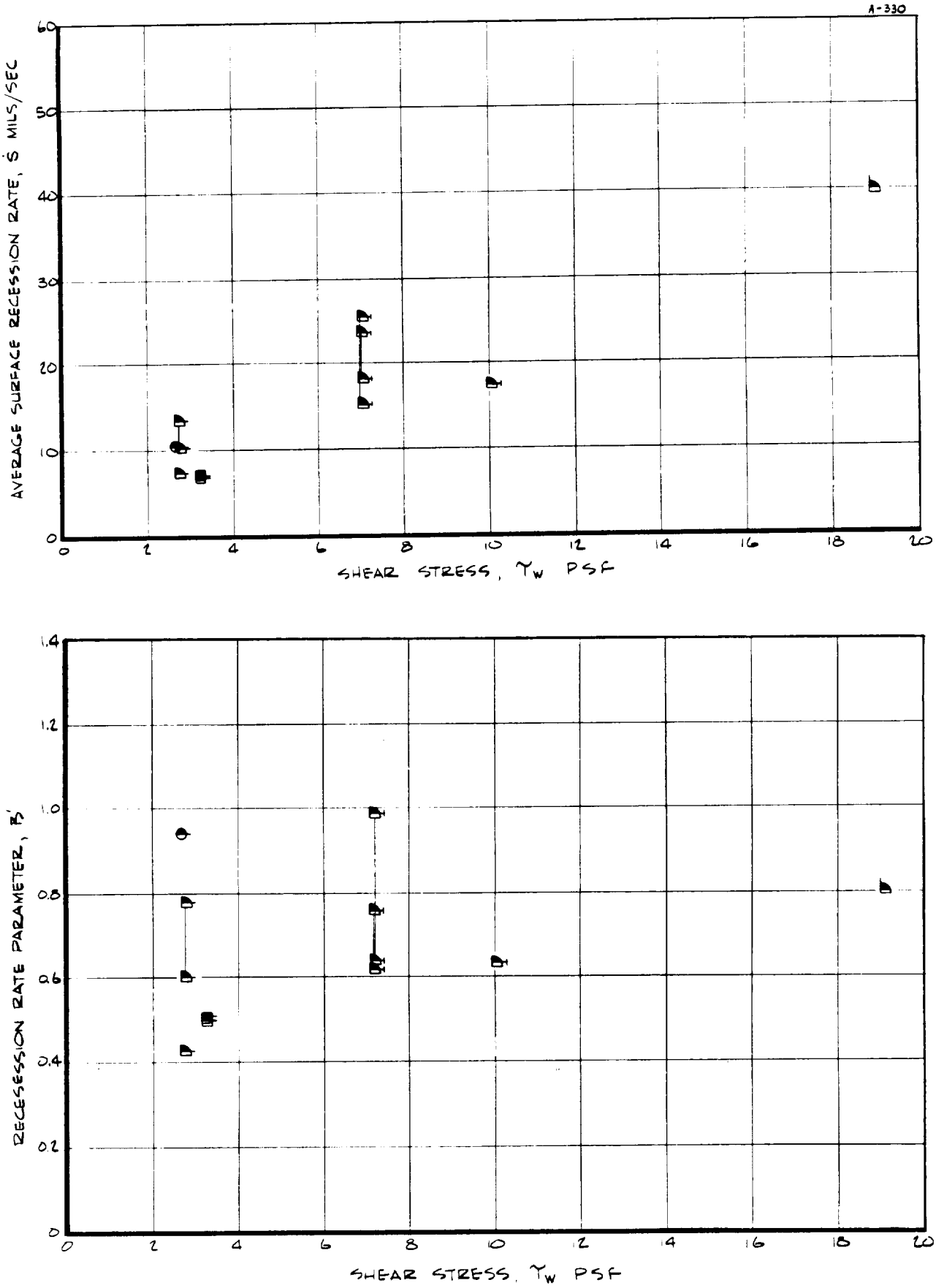

FIGURE 9-35 SURFACE RECESSION RESPONSE AS A FUNCTION OF SHEAR STRESS FOR THE 5026-39HCG MATERIAL.

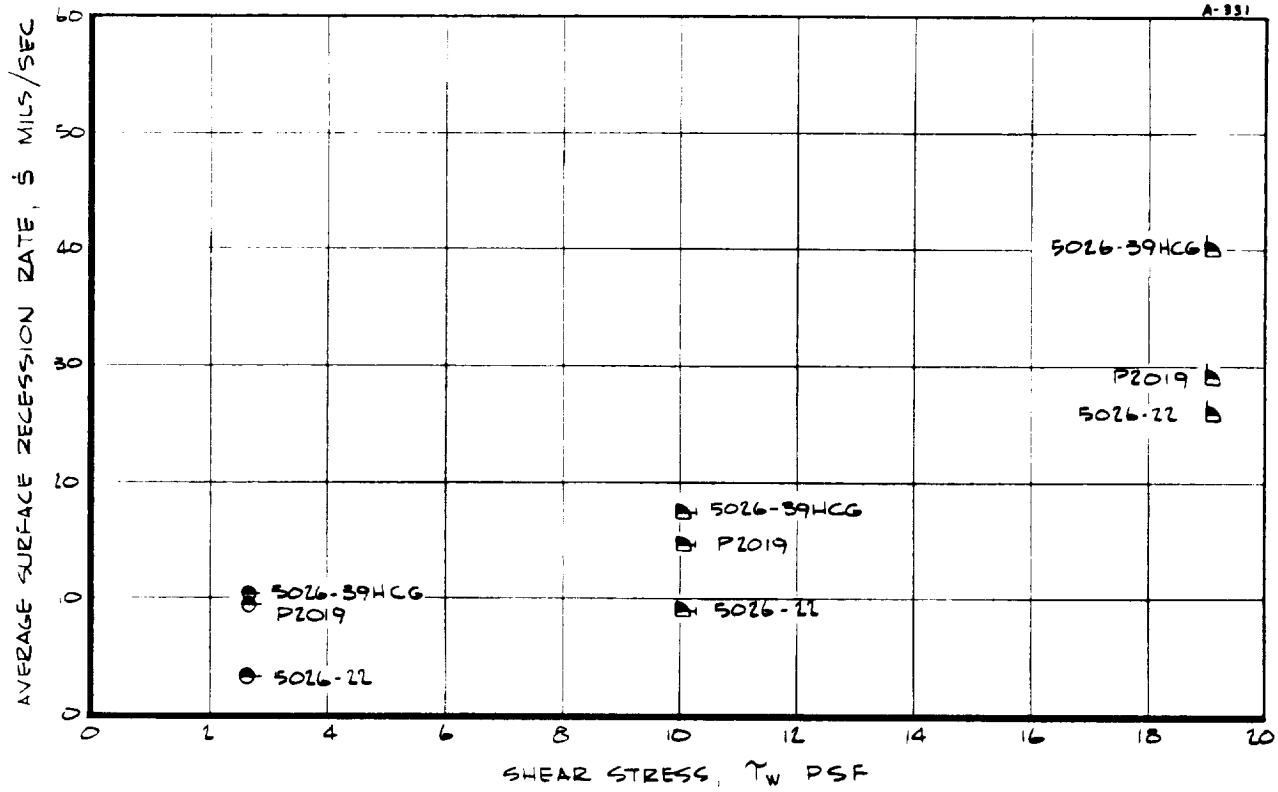

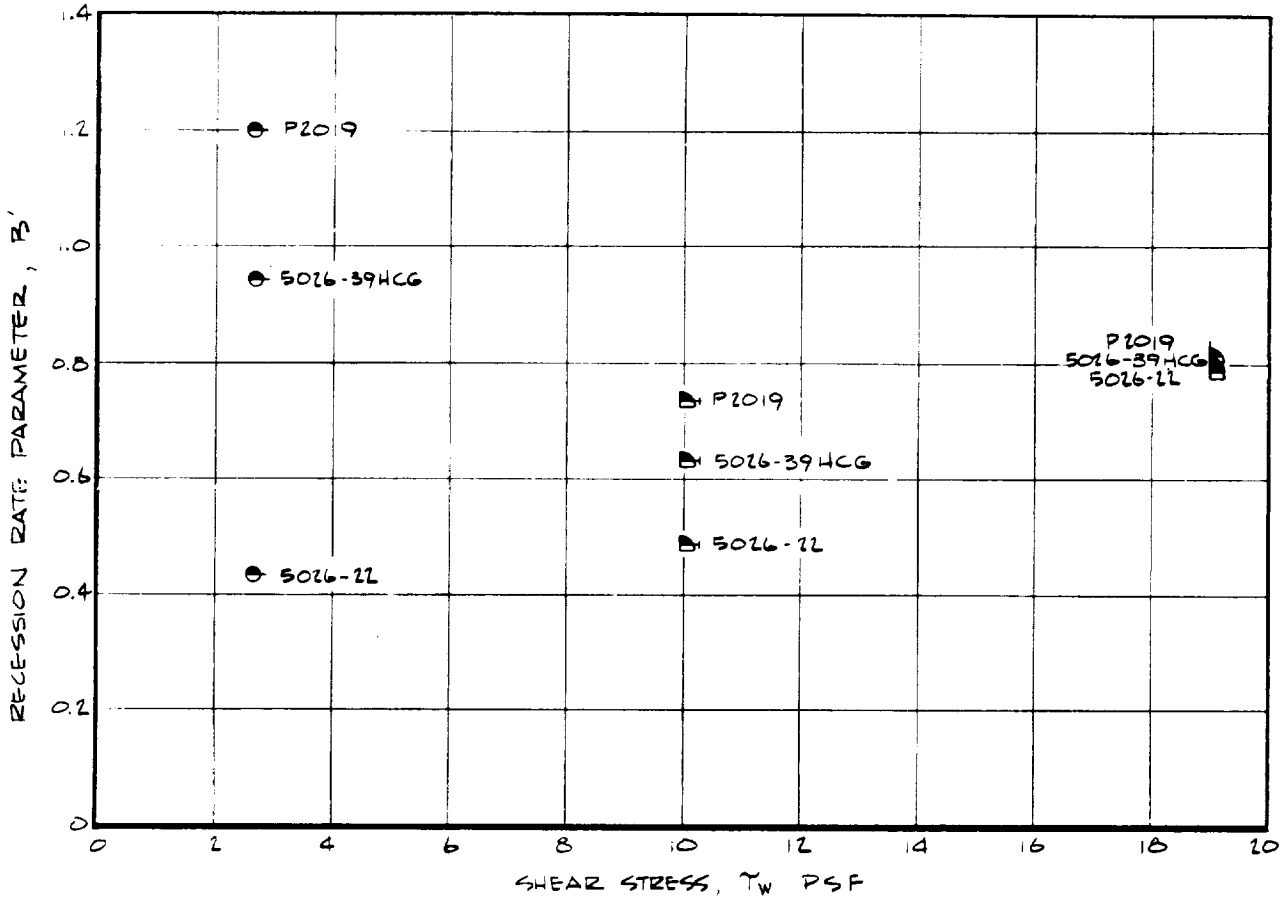

FIGURE 9-36 SURFACE RECESSION RESPONSE AS A FUNCTION OF SHEAR STRESS FOR THE 5026-39HCG, P2019 AND 5026-22 MATERIALS.

rate and the 5026-22 material the lowest. When viewed in terms of weight loss ($B' = \dot{s}\rho_p/\rho_e u_e C_H = \dot{m}_p/\rho_e u_e C_H$), the 5026-22 material still exhibits the lowest loss rate but the P2019 material now becomes the highest. The large differences in B' values at the 3 psf shear level are somewhat surprising in the light of the results at the higher levels. No definitive explanation appears possible based on the limited results available.

The comparison of results for the air and nitrogen environments is presented in Figure 9-37 for the 5026-39HCG material. The nitrogen results exhibit a lower $\dot{s}$ and B' in general, with the recession rate for nitrogen at the 3 psf shear level being less than 1 mil/sec. The results generally agree with the trends of the nitrogen-air comparisons for the stagnation point models presented in Section 9.1.2.3.

Because of the generally erratic recession response of the shear test models, it was difficult to assess the effect of exposure time. No definitive trend is apparent and no effect would be expected based on the stagnation point flow results.

9.2 ANALYTICAL PREDICTION RESULTS

The results of the analytical predictions of the 5026-39HCG material performance are discussed in the following sections. As presented previously in Section 7, the Aerotherm ablation computer programs, which are a detailed model of the surface and in-depth response of ablative materials, were used to make the predictions and the input information was provided by a thorough characterization of the properties of the 5026-39HCG material. The discussion of the prediction results is presented in two sections. Section 9.2.1 discusses the performance predictions corresponding to model tests performed under the experimental program and Section 9.2.2 discusses the parametric study results.

9.2.1 Comparisons with Test Results

The predictions corresponding to model tests were performed in two parts. First the measured surface recession rate and surface temperature were imposed as surface boundary conditions and the material in-depth response was calculated (CMA program, Option 2). Second, the measured heat transfer coefficient, recovery enthalpy, pressure, and the system chemistry were imposed as surface boundary conditions and the complete material surface and in-depth response was calculated (CMA program, Option 1). These two sets of calculations are discussed separately in Sections 9.2.1.1 and 9.2.1.2 respectively.

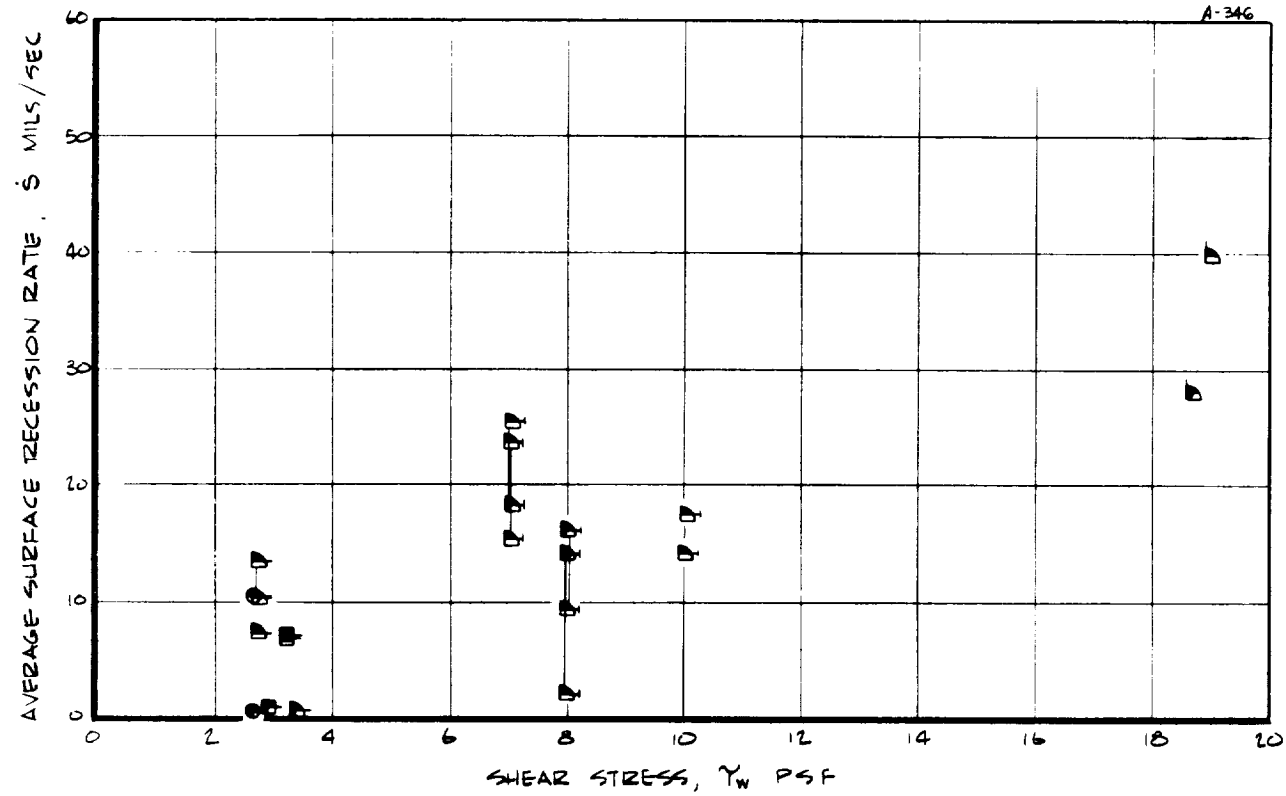

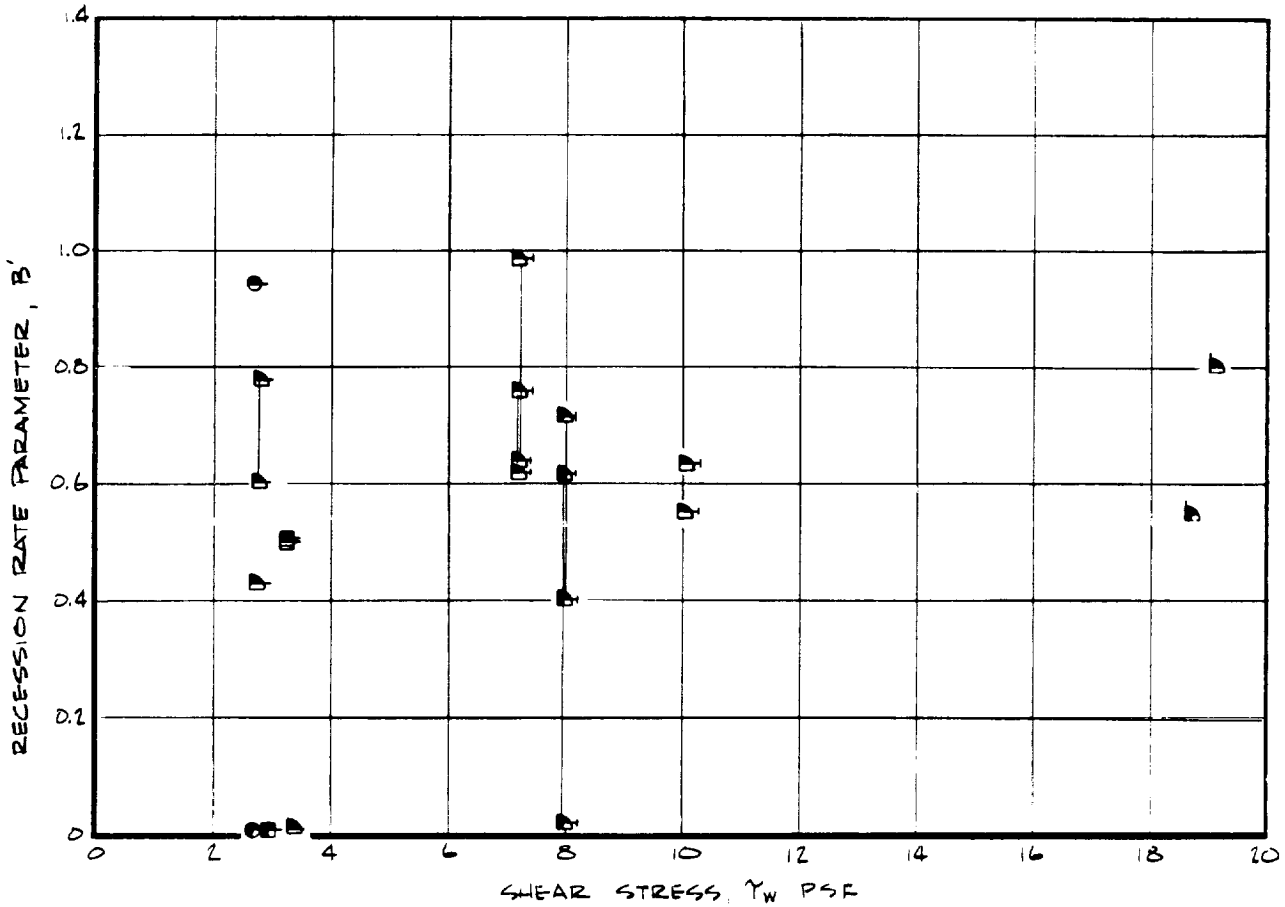

FIGURE 9-37 EFFECT OF CHEMICAL ENVIRONMENT ON SURFACE RECESSION RESPONSE, SHEAR TESTS.

C-2.

9.2.1.1 In-Depth Response

The predicted in-depth response for the 14 test models considered and the comparison with the measured model performance is presented in Table 9-7 and Figure 9-38. The table presents the in-depth post-test response and the figure presents the internal temperature histories. Note that the average surface recession rate presented in the table and the measured surface temperature history presented in the figure were the input surface boundary conditions. In the table, boundaries for defining the predicted char depth and pyrolysis zone depth were defined as

char - pyrolysis zone interface

$$\rho_{cpi} = \rho_c + 0.08\ (\rho_p - \rho_c) \tag{9-9}$$

pyrolysis zone - virgin material interface

$$\rho_{ppi} = \rho_p - 0.08\ (\rho_p - \rho_c) \tag{9-10}$$

where ρ_p is the virgin material density (34.0 lb/ft^3) and ρ_c is the char density (16.0 lb/ft^3). The predicted weight loss was determined from the calculated loss per unit surface area due to both char removal and in-depth decomposition and from the surface area of the model instrumented core. Note that all predicted performance results presented include the effect of heat soak after test. In Figure 9-38, the predicted internal temperature histories, the solid lines, are superimposed over the measured response, the symbols. The predictions correspond to the measured thermocouple locations. Note that the results for Models 158/BH/1.0 and 140/BH/1.0 are not included in Figure 9-38 since the measured surface temperatures were somewhat questionable and there were very little internal temperature data on which to make a comparison.

For all results presented, the calculated internal response was transient throughout the test, with the exception of the Phase III high pressure tests; that is, the char thickness and pyrolysis zone thickness were increasing throughout the test. The comparisons presented therefore represent a true test of the computer program treatment and property data used for transient response calculations. It is also interesting to note that the pyrolysis zone - virgin material interface, defined by Equation (9-10), corresponded very closely in all cases to the location of the 1,000°F isotherm.

From Table 9-7 and Figure 9-38, the general agreement for all variables for all 14 models considered is seen to be good. The results at low heat flux, Models 93/BH/2.0 and 114/BH/4.0, exhibit the greatest discrepancy

TABLE 9-7

COMPARISON OF PREDICTED AND MEASURED MATERIAL IN-DEPTH RESPONSE, OPTION 2

Phase	Model No.	Enthalpy h (Btu/lb)	Stagnation Pressure p_s (atm)	Heating Rate q_c (Btu/ft²-sec)	Chemical Environment	Exposure Time τ (sec)	Surface Recession		Average Recession Rate		Char Depth		Char Thickness		Pyrolysis Zone Thickness		Mass Loss	
							Measured s (inch)	Calculated s (inch)	Measured $\dot{s}$ (mils/sec)	Input $\dot{s}$ (mils/sec)	Measured (inch)	Predicted (inch)	Measured (inch)	Predicted (inch)	Measured (inch)	Predicted (inch)	Measured (gm)	Predicted (gm)
III	158/BH/1.0	5,030	1.06	1,170	Air	10.2	0.509	0.538	50.0	52.6	0.549	0.538	0.04	0	0.01	0.008	0.83	0.83
|	140/BH/1.0	5,150	3.10	1,770	|	2.9	0.418	0.419	144	144	0.428	0.419	0.010	|	0	0.001	0.72	0.60
IVA	93/BH/2.0	3,440	0.0082	33	|	210.2	0.100	0.100	0.48	0.474	0.325	0.375	0.22	0.275	0.10	0.147	1.69	—
|	91/BH/2.0	10,970	0.0079	116	|	60.5	0.152	0.152	2.51	2.51	0.237	0.279	0.085	0.127	0.08	0.066	1.27	1.66
	108/BH/2.0	16,300	0.008	154	|	60.4	0.147	0.148	2.44	2.45	0.247	0.291	0.10	0.143	0.07	0.067	1.52	1.70
IVB	84/BH/2.0	10,920	0.298	188	Helium	60.3	0.023	0.023	0.38	0.375	0.213	0.250	0.19	0.227	0.12	0.078	1.02	1.17
|	80/BH/2.0	9,960	0.0276	271	Nitrogen	60.6	0.172	0.172	2.84	2.84	0.292	0.366	0.12	0.194	0.11	0.068	1.77	2.06
V	114/BH/4.0	4,910	0.0112	33	Air	211.4	0.085	0.085	0.40	0.400	0.305	0.399	0.22	0.314	0.15	0.143	1.62	2.08
|	122/BH/4.0	10,430	0.0275	134	|	60.6	0.168	0.170	2.77	2.80	0.308	0.324	0.14	0.154	0.04	0.067	1.72	1.91
VIA	30/BH/2.0	5,937	0.0275	116	|	90.0	0.218	0.218	2.42	2.43	0.388	0.402	0.17	0.184	0.07	0.075	2.15	2.36
VIB	27/BH/2.0	10,270	0.0282	181	|	90.0	0.391	0.394	4.34	4.37	0.551	0.550	0.16	0.156	0.06	0.056	3.22	3.44
|	102/BH/2.0	16,520	0.0271	288	|	44.7	0.218	0.220	4.88	4.92	0.328	0.348	0.11	0.128	0.06	0.052	1.69	2.20
VII	96/BH/2.0	18,860	0.0285	337	|	30.8	0.148	0.148	4.81	4.81	0.258	0.265	0.11	0.117	0.03	0.050	0.92	1.57
|	111/BH/1.0	10,590	0.082	577	|	39.6	0.388	0.388	9.80	9.79	0.468	0.460	0.08	0.072	0.02	0.032	0.72	0.84

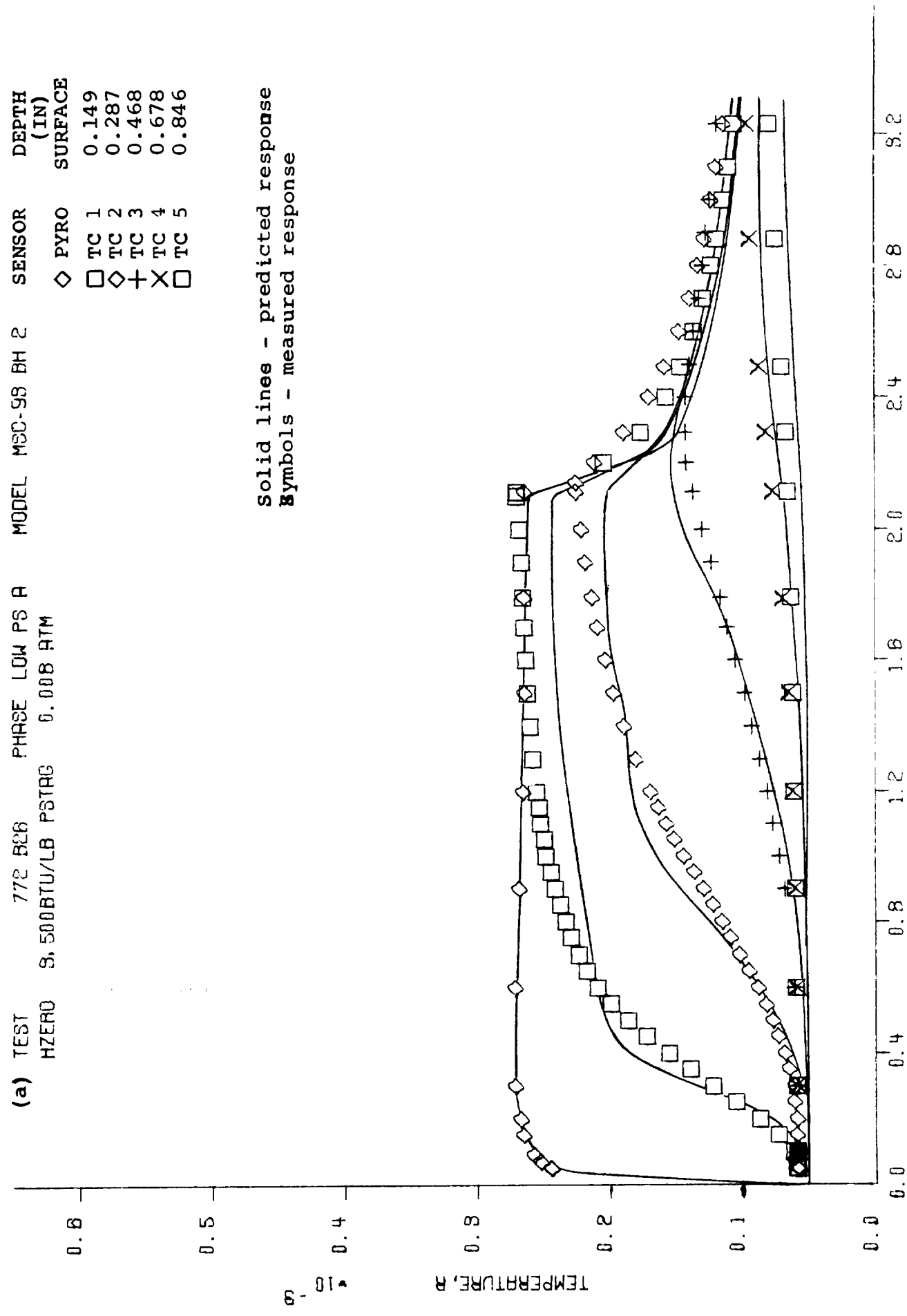

Figure 9-38. Comparison of Measured and Predicted Internal Temperature Response.

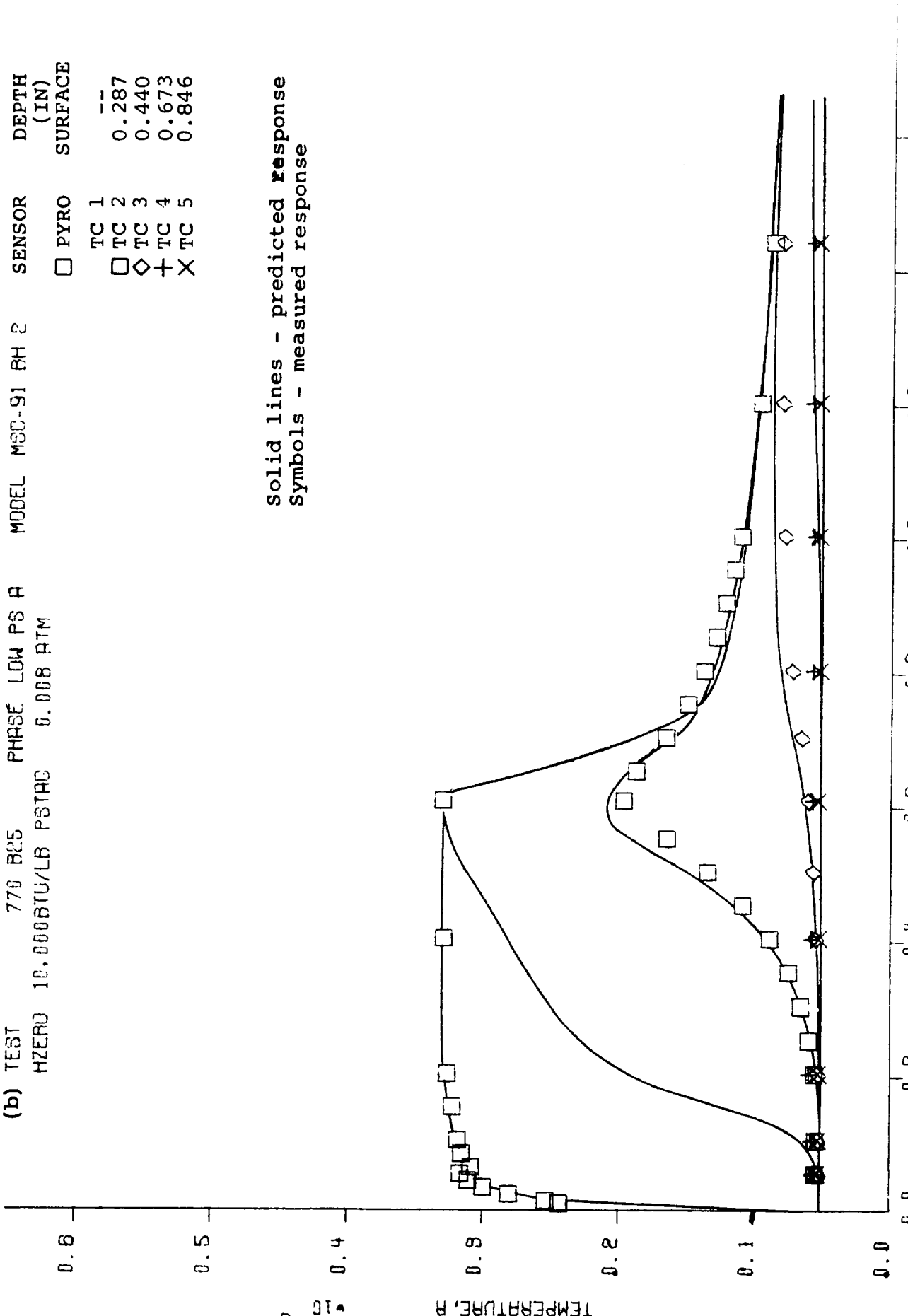

Figure 9-38. Continued.

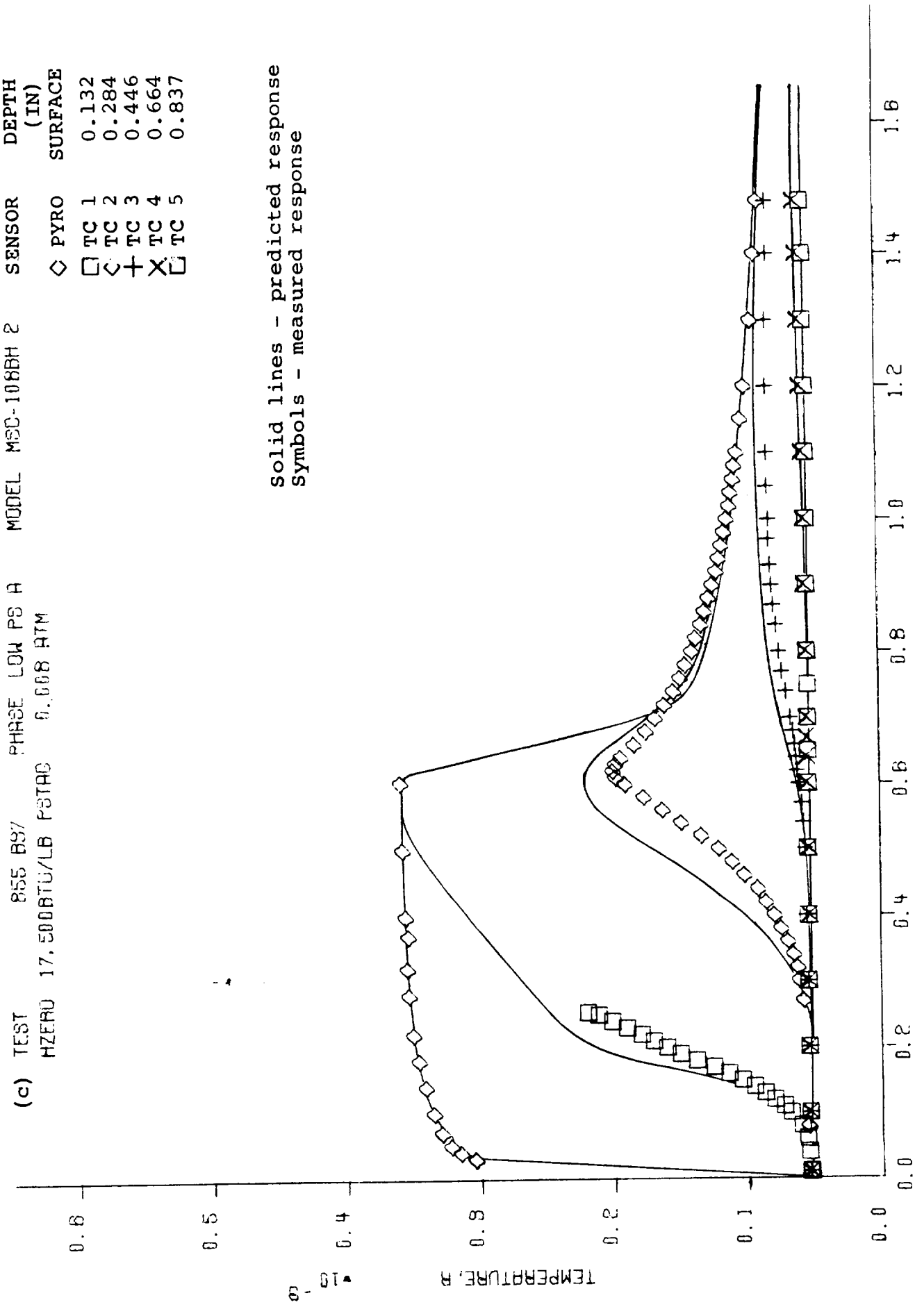

Figure 9-38. Continued.

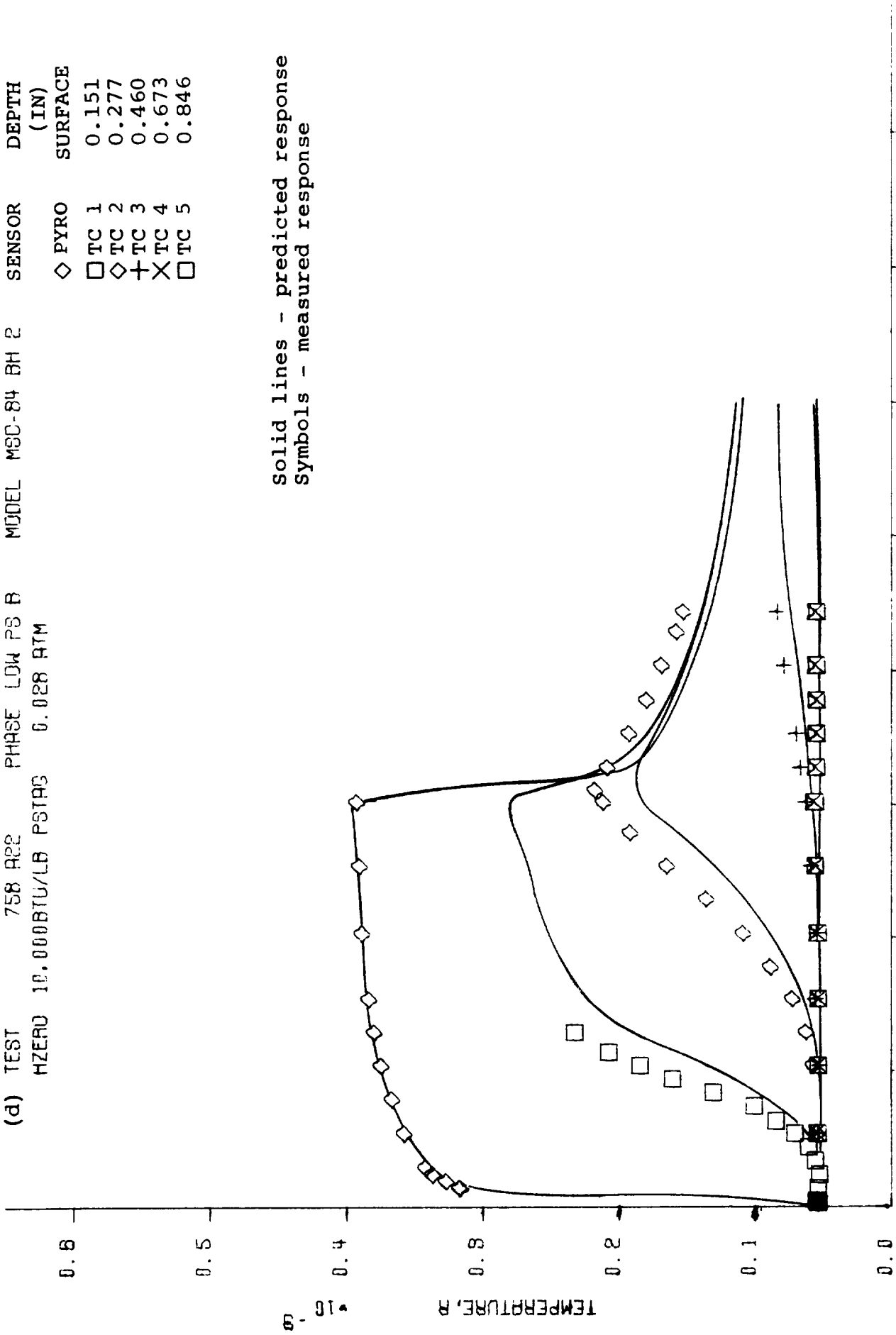

Figure 9-38. Continued.

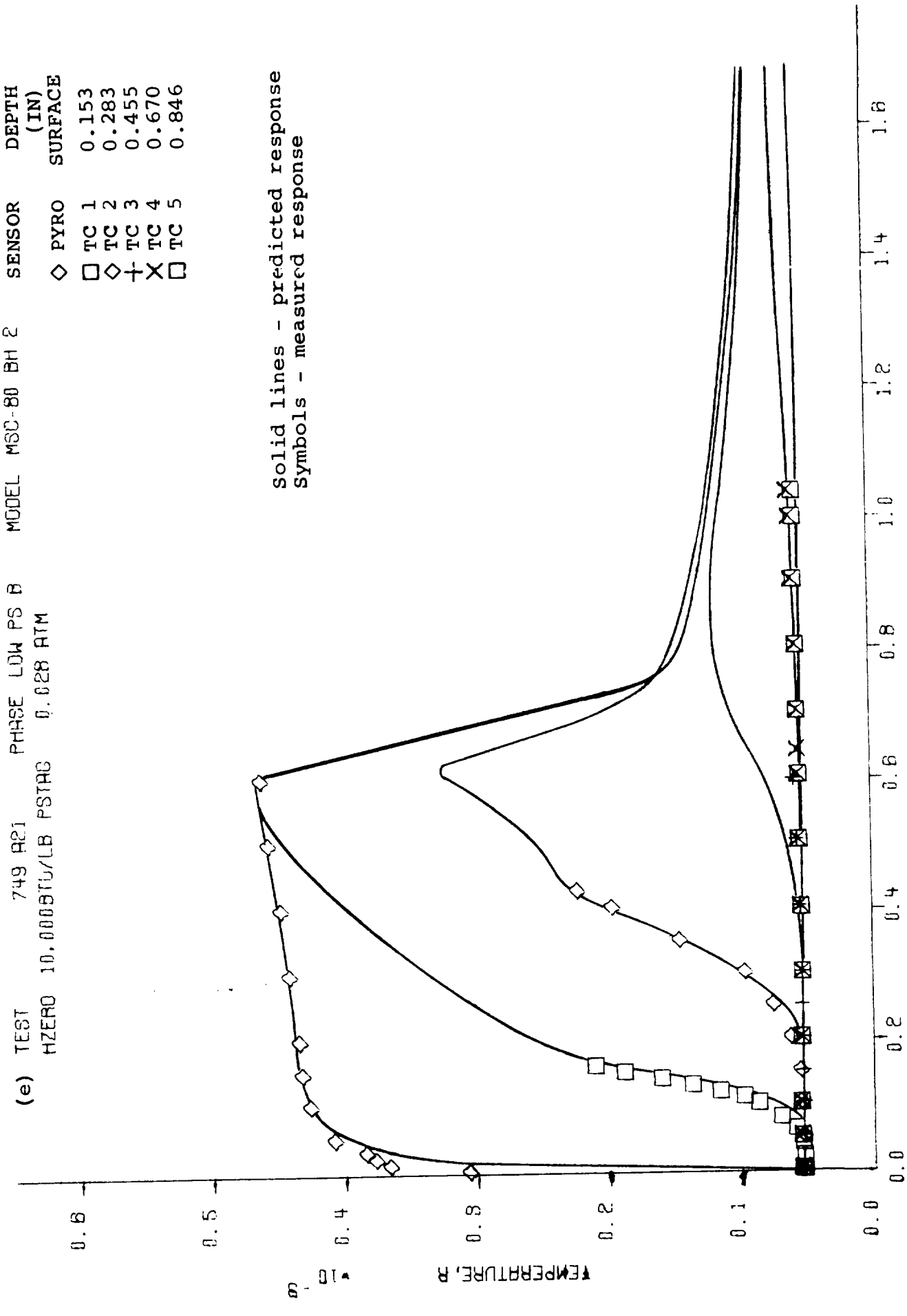

Figure 9-38. Continued.

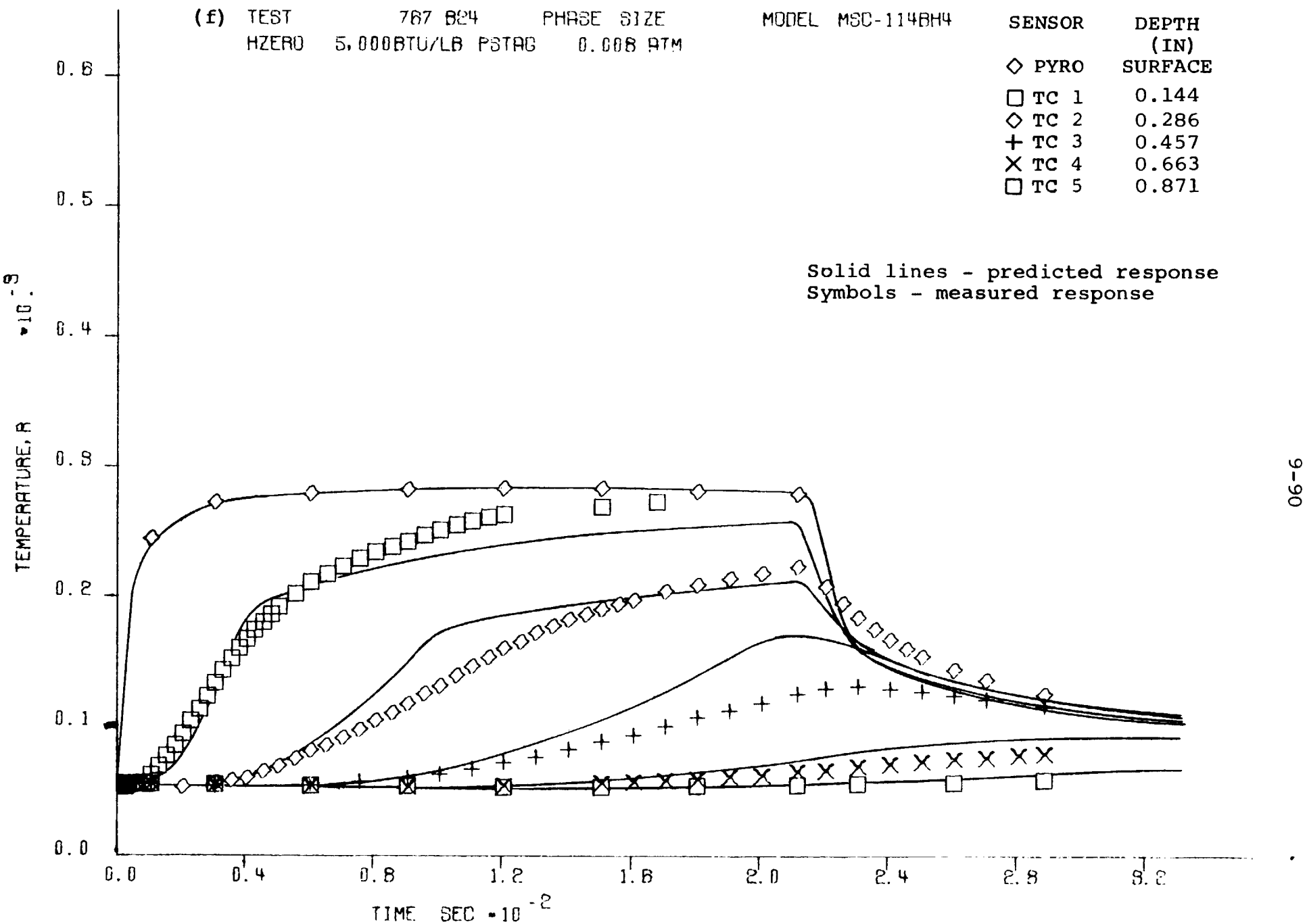

Figure 9-38. Continued.

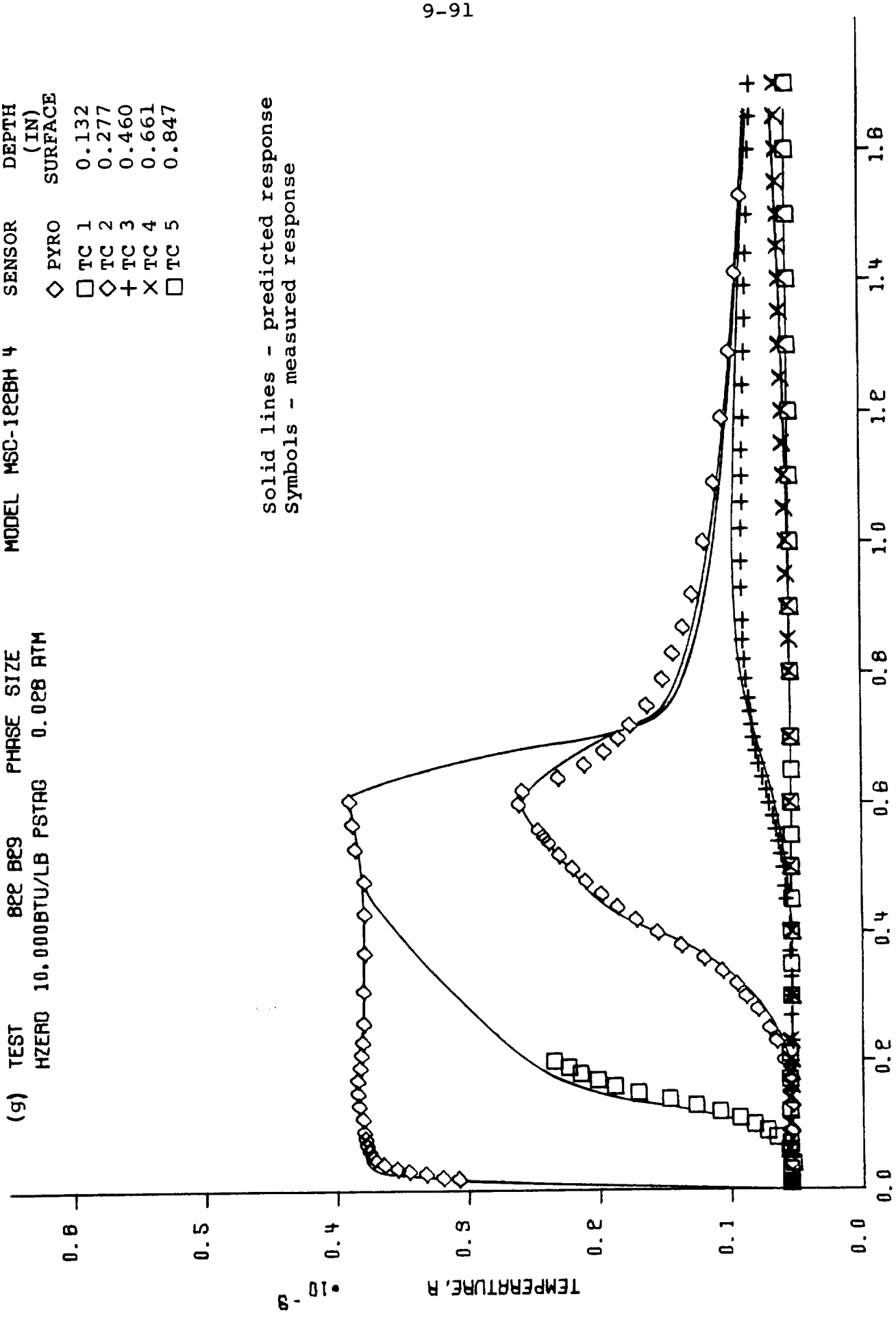

Figure 9-38. Continued.

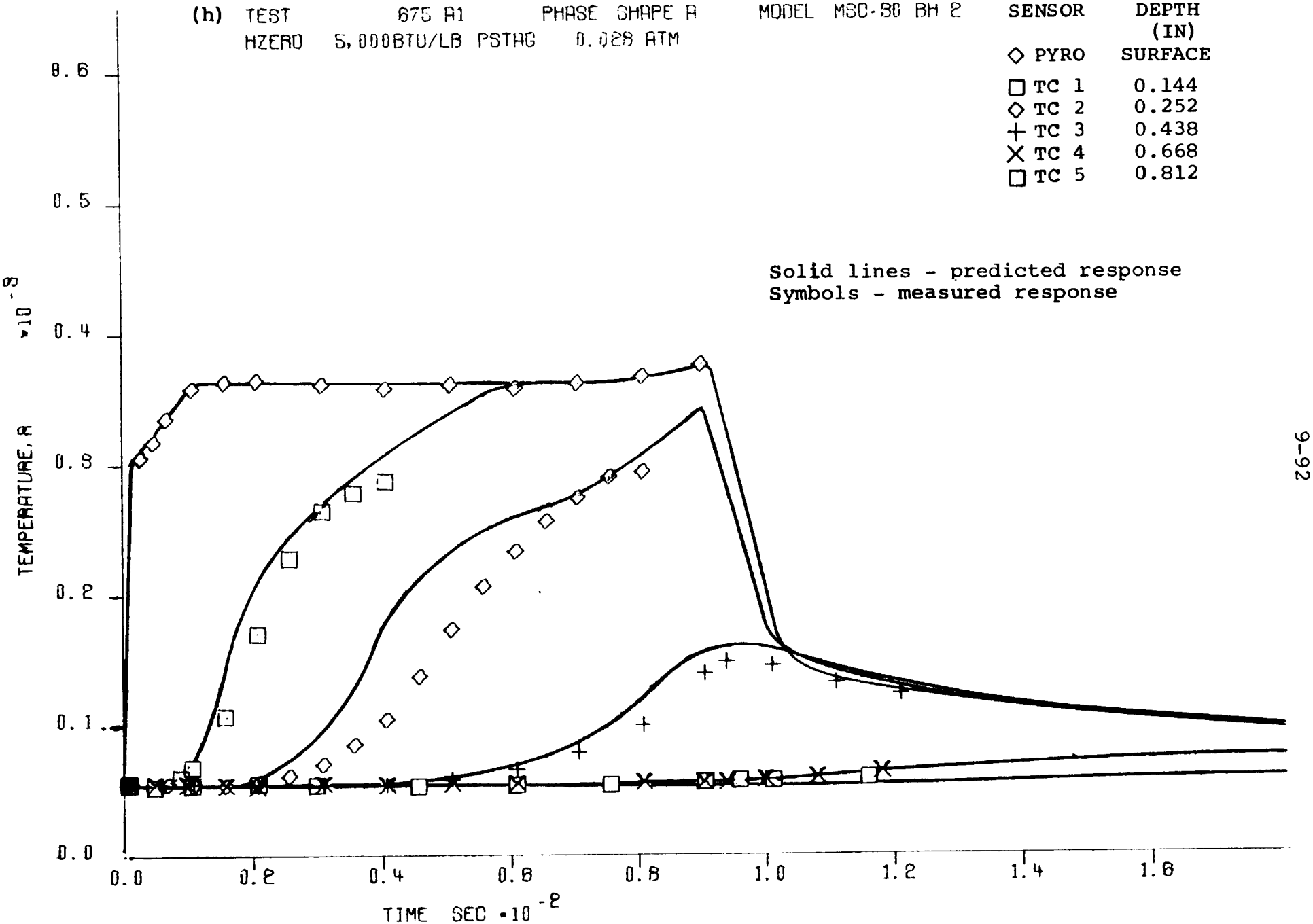

Figure 9-38. Continued.

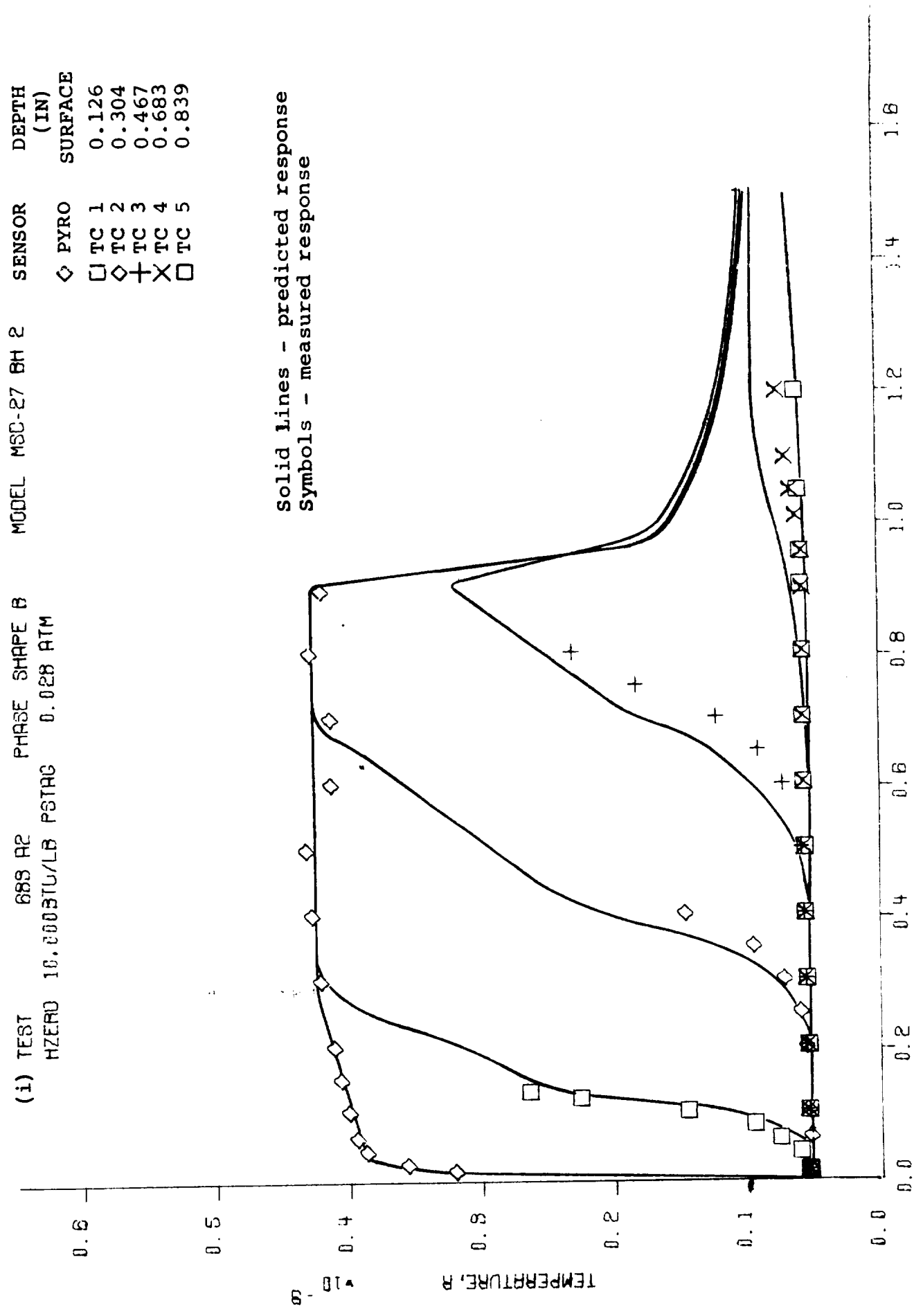

Figure 9-38. Continued.

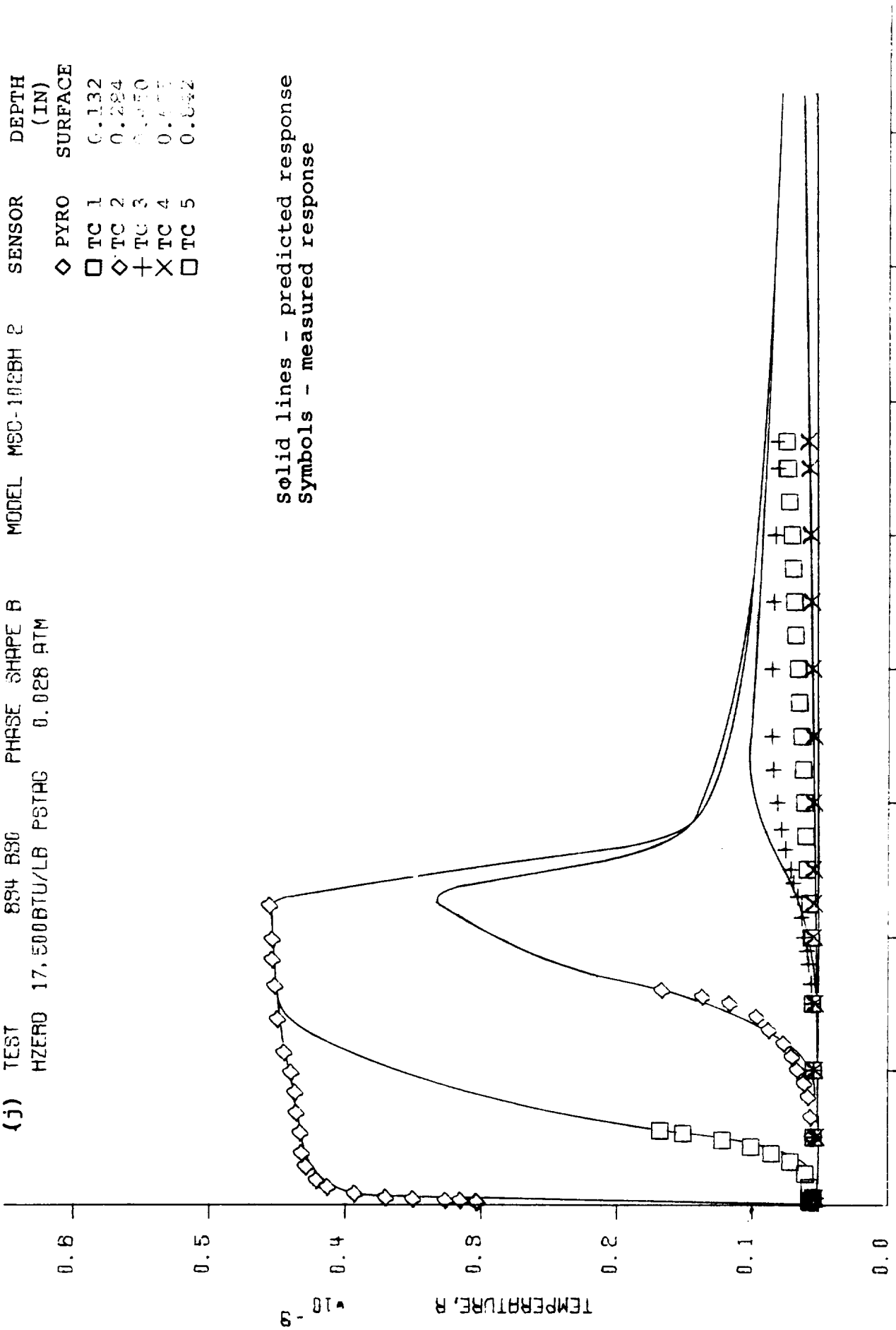

Figure 9-38. Continued.

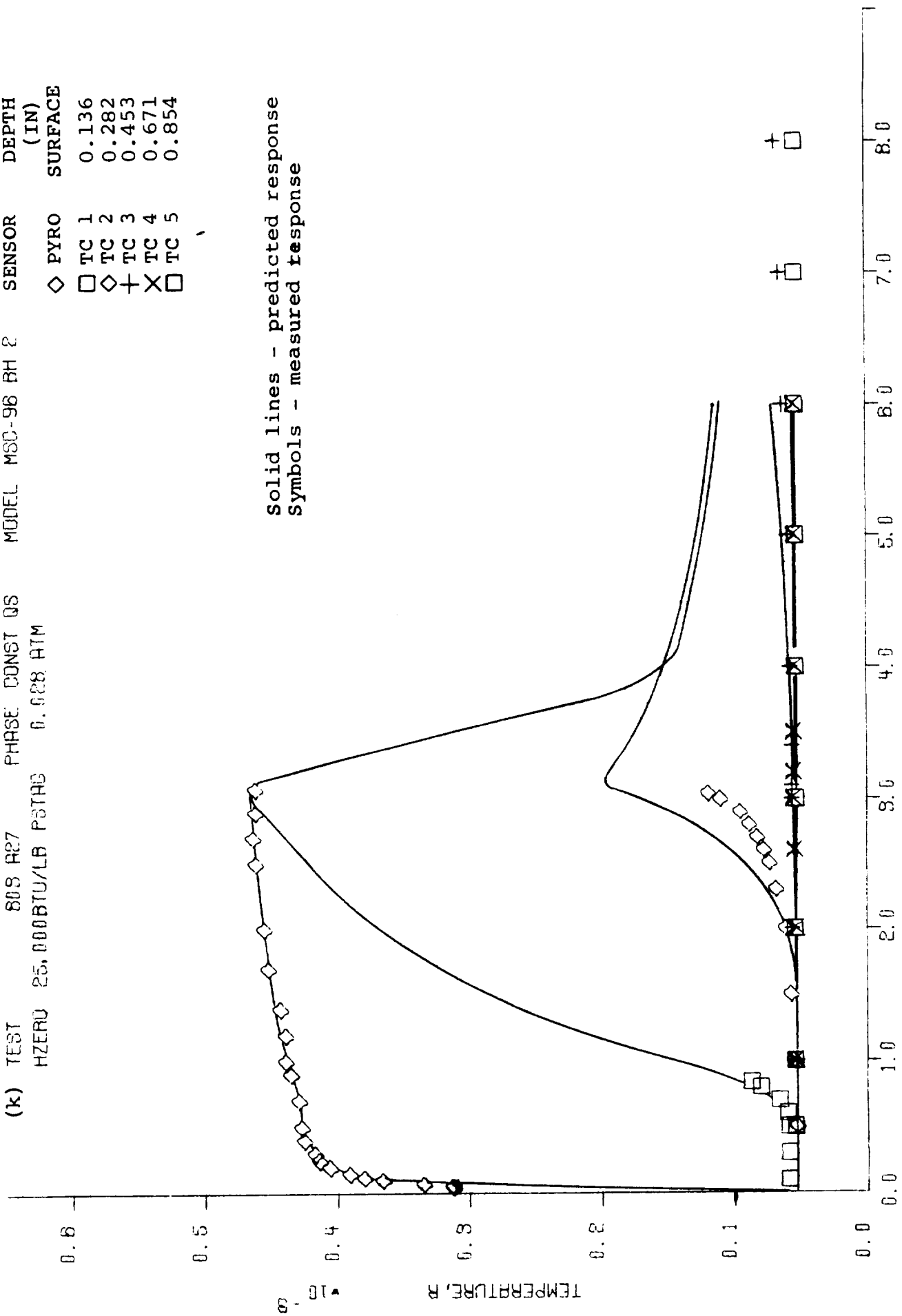

Figure 9-38. Continued.

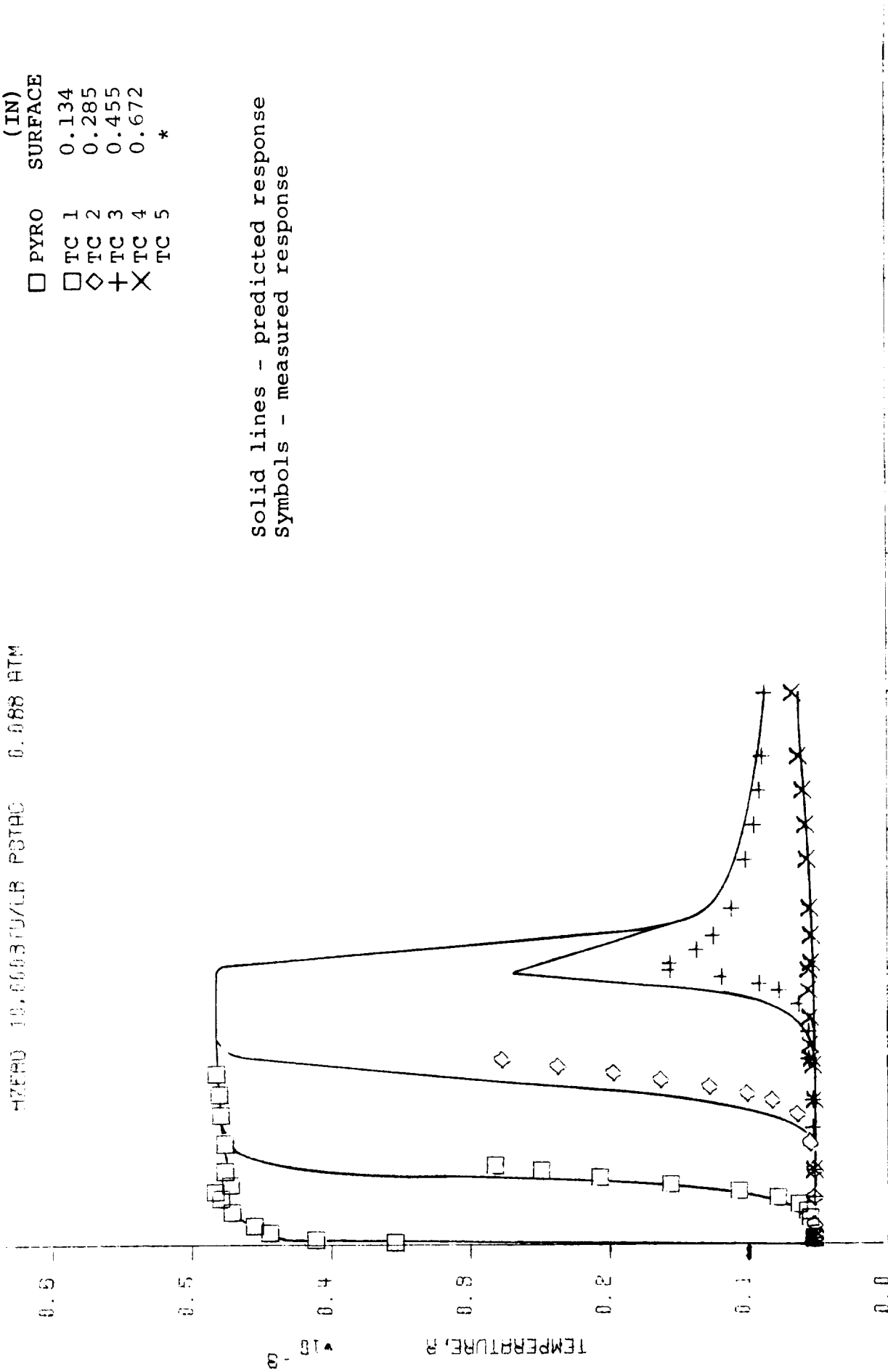

Figure 9-38. Concluded.

between measured and predicted performance, although this discrepancy is primarily limited to the char depth and thickness. This result is not too surprising since the surface scab which occurred in both of these tests was not characterized in the computer calculation; the scab was the surface and in-depth material for a considerable depth ($\leq$ 0.060 inch) and would be expected to have thermal properties far different from those of the char. Note that the models for which melt droplets were observed on the surface exhibited as good agreement with the predictions as those which did not. Also the models tested in the helium and nitrogen environments, for which the surface recession was small relative to the similar conditions in air, exhibit excellent agreement between measured and predicted performance.

In summary, the computer program treatment of the in-depth response of and the property data for the 5026-39HCG material, presented in Section 7, effectively characterizes the transient in-depth response of the material.

9.2.1.2 Surface Response

The predicted surface response and the comparison with the measured model performance is presented in Table 9-8 and Figures 9-39 through 9-42. The input surface boundary conditions for the predictions were the heat transfer coefficient, enthalpy, and pressure presented in the table and the char, pyrolysis gas, and free stream chemistry as presented in Section 7. The in-depth response is not presented since it was discussed in detail in the previous section and since any in-depth comparisons are not informative unless predicted and measured surface response agree. In the table, only the results for the particular model for which the prediction corresponded are presented whereas in the figures all experimental results at the same nominal conditions are included. The correlations defined in Section 9.1 are also included in the figures for comparison purposes.

Before discussing the comparisons between measured and predicted response in detail, a comment on the predicted surface recession rate as a function of exposure time is in order. Contrary to the observed experimental performance, the calculated recession rate for all test conditions but those in Phase III at high pressure is a strong function of exposure time. This is illustrated in Figure 9-39 for representative tests of Table 9-8. The comparison of measured and predicted response is therefore a function of the exposure time for all tests for which the comparison is made. It should be noted, however, that the predicted surface temperature is not a significant function of exposure time, in agreement with the experimental results. Computationally, the immediate reason for the $\dot{s} - \theta$ effect is the varying pyrolysis off-gas rate with time, high early in the test and decreasing with time, this rate directly affecting the surface thermochemical response. Recall that the

TABLE 9-3

COMPARISON OF PREDICTED AND MEASURED MATERIAL SURFACE RESPONSE, OPTION 1

Phase	Model No.	Enthalpy h_s (Btu/lb)	Stagnation Pressure p_s (atm)	Heating Rate $\dot{q}_c$ (Btu/ft^2-sec)	Heat Transfer Coefficient $\rho_e u_e C_H$ (lb/ft^2-sec)	Chemical Environment	Exposure Time t (sec)	Surface Recession Measured s (inch)	Surface Recession Predicted s (inch)	Average Recession Rate Measured $\dot{s}$ (inch)	Average Recession Rate Predicted $\dot{s}$ (inch)	Surface Temperature Measured T_w (°R)	Surface Temperature Predicted T_w (°R)	Observed Surface Condition	Surface Species Predicted	Surface Species Measured
III	158/BH/1.0	5,031	1.06	1,175	0.2185	Air	10.2	0.509	0.391	50.0	38.3	4,800	5,035	DG,NM	SiC or SiO_2	—
|	1.0/BH/1.0	5,151	3.10	1,775	0.322	|	2.90	0.418	0.2106	144.0	72.6	4,850	5,075	G,NM	SiC or C	—
IVA	93/BH/2.0	3,440	0.0082	33	0.009	|	210.2	0.100	0.0023	0.48	0.0109	2,650	2,975	S	SiO_2 or C	—
|	91/BH/2.0	10,969	0.0079	116	0.0098	|	60.5	0.152	0.0048	2.51	0.07933	3,250	3,700	DG,M	C or SiO_2	SiO_2/C
|	108/EH/2.0	16,301	0.008	154	0.0088	|	60.4	0.147	0.0006	2.44	0.00993	3,550	3,775	DG,(M)	C	|
IVB	84/BH/2.0	11,000	0.029	173	0.0114	Helium	60.3	0.023	0	0.38	0	3,875	3,650	BD,LC,NM	|	C/SiO_2/(SiC)
|	80/BH/2.0	9,960	0.0276	271	0.0253	Nitrogen	60.6	0.172	|	2.84	|	4,425	4,625	BD,NM	|	C/SiO_2/SiC
|	114/BH/4.0	5,910	0.010	83.2	0.0063	Air	211.4	0.085	0.0009	0.40	0.00425	2,825	2,875	LC,S	SiO_2 or C	SiO_2/C
|	121/BH/4.0	10,433	0.0275	134	0.0120	|	60.6	0.168	0.0159	2.77	0.26	3,800	3,850	G,NM	SiC or SiO_2	—
VIA	80/BH/2.0	5,500	0.028	89	0.0171	|	90.0	0.218	0.0958	2.42	1.07	3,600	3,625	G,(M)	SiO_2	SiO_2/C
VIB	77/BH/2.0	10,269	0.0282	189	0.0170	|	90.0	0.391	0.1342	4.34	1.49	4,175	4,125	BD,(G),NM	SiC	C/SiO_2/(SiC)
|	104/BH/2.0	16,513	0.0271	278	0.0156	|	44.7	0.218	0.0294	4.88	0.64	4,450	4,475	G,(BD),NM	C	|
VII	90/BH/2.0	24,300	0.0282	443	0.017	|	30.8	0.148	0.0727	4.81	2.36	4,575	4,275	|	|	|
|	111/BH/1.0	10,000	0.0842	|	0.0410	|	59.6	0.388	0.2526	9.80	6.38	4,750	4,775	G,NM	SiC or C	C/SiO_2

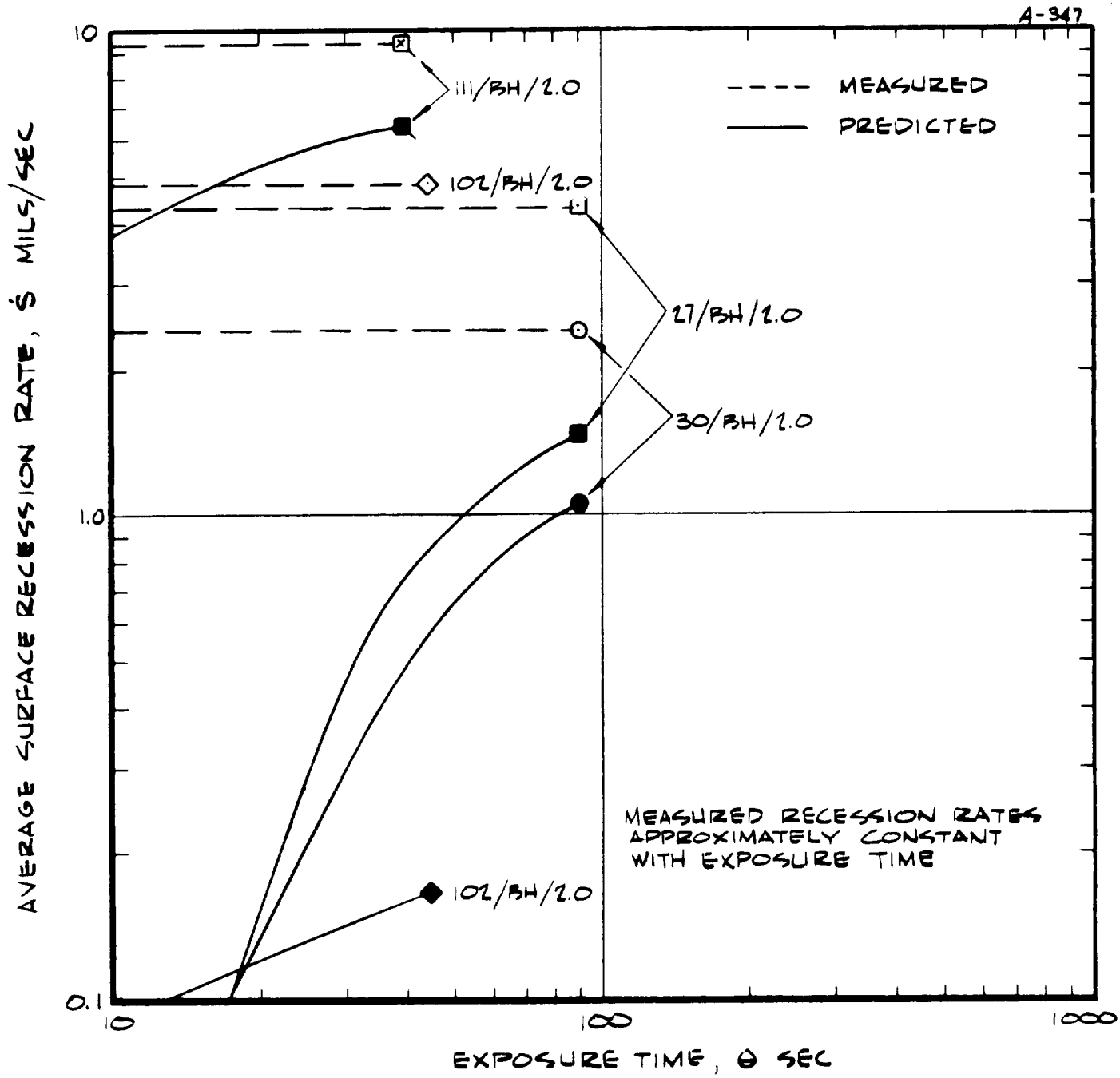

FIGURE 9-39 COMPARISON OF MEASURED AND PREDICTED SURFACE RECESSION RATES AS A FUNCTION OF EXPOSURE TIME.

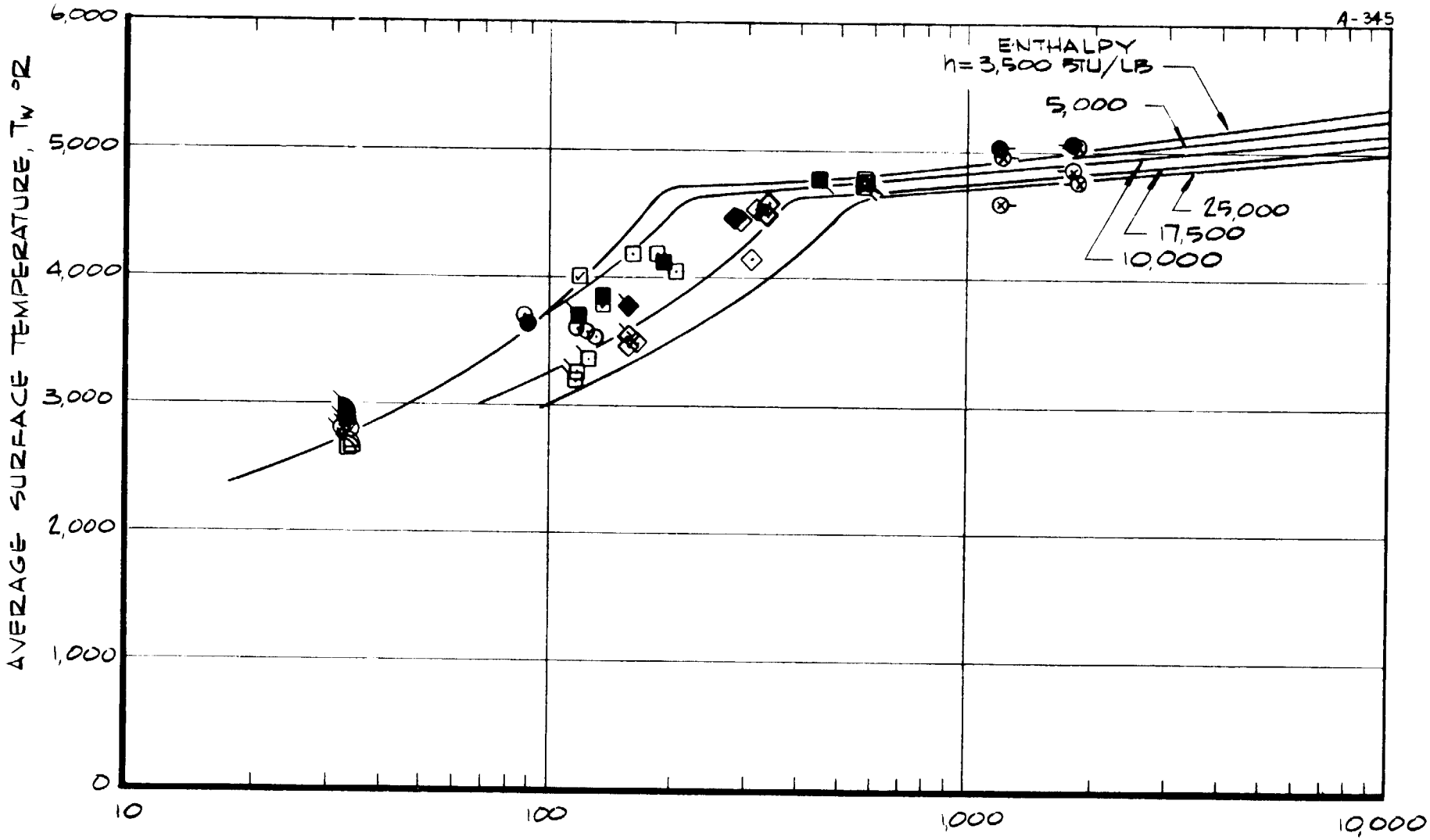

FIGURE 9-40 COMPARISON OF MEASURED AND PREDICTED SURFACE TEMPERATURE AS A FUNCTION OF HEAT FLUX.

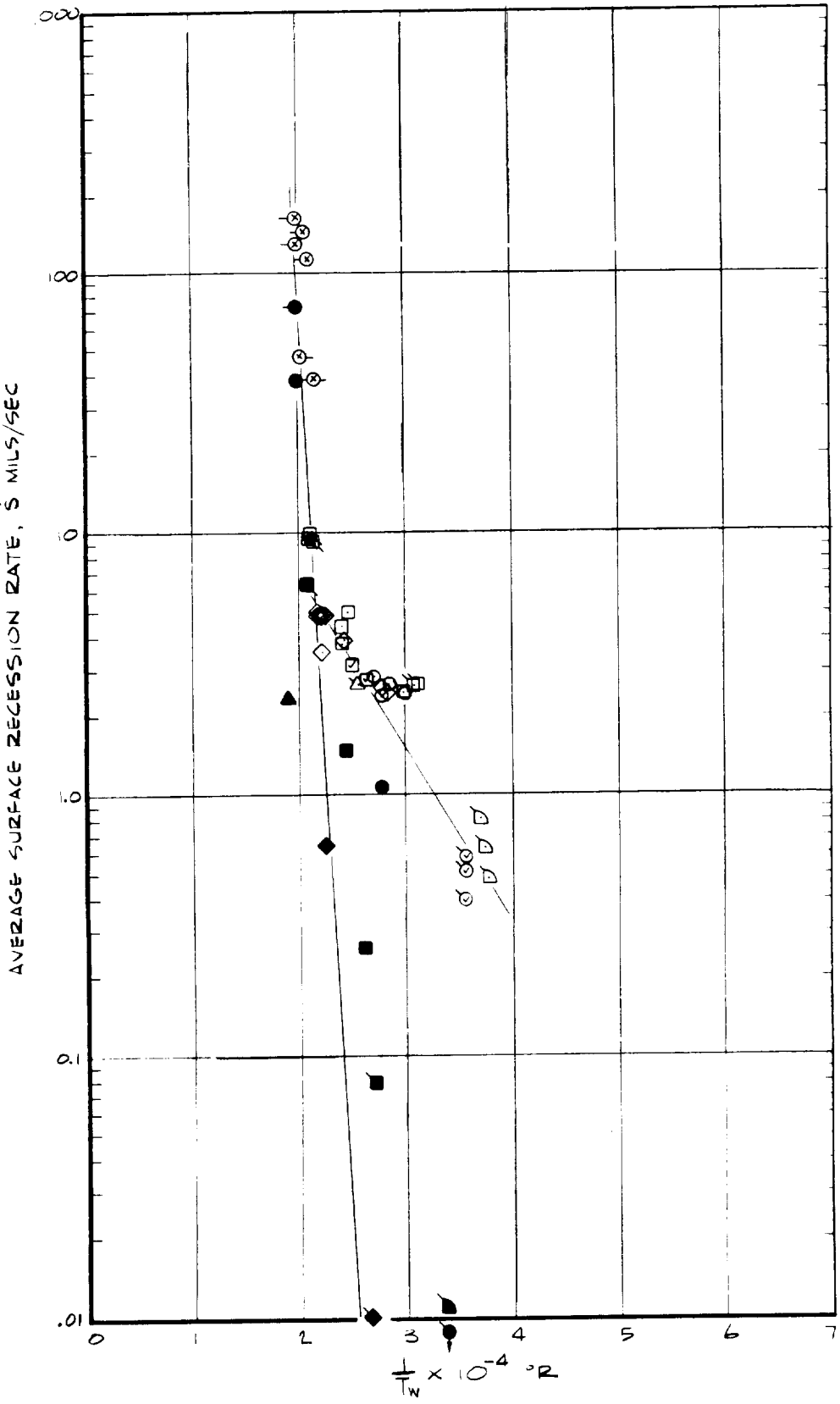

FIGURE 9-41 COMPARISON OF MEASURED AND PREDICTED SURFACE RECESSION RATE-SURFACE TEMPERATURE VARIATION

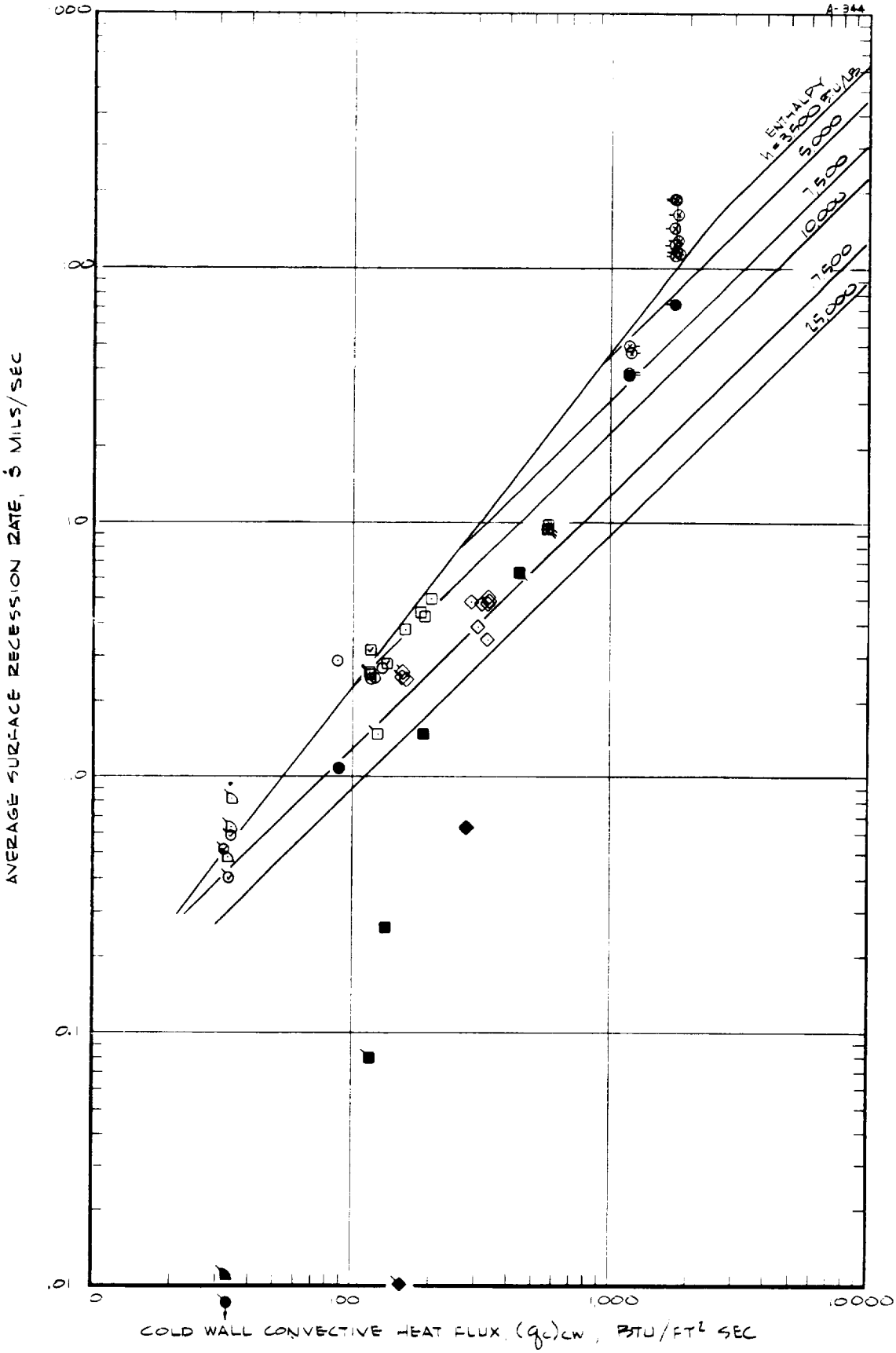

FIGURE 9-42 COMPARISON OF MEASURED AND PREDICTED SURFACE RECESSION RATE AS A FUNCTION OF HEAT FLUX.

boundary layer edge gases and the pyrolysis off-gases are treated as a gas phase in chemical equilibrium which in turn is in chemical equilibrium with the surface. One possible explanation for the predicted recession rate depending on time, contrary to measurement, may therefore be that this theoretical characterization of the pyrolysis gases and/or their interaction with the edge gases and surface is incorrect. Other possible assumptions that might characterize the pyrolysis gases more accurately include assuming the pyrolysis gases to be chemically inert with the edge gases and to be either reactive or non-reactive with the char surface, considering the pyrolysis gases to be frozen at the composition at which they are formed (corresponding to a temperature of about 1,200°R), and allowing coking in-depth and the resultant change in gas phase composition to occur (see Reference 7-2). These possibilities are discussed in detail in Section 9.3, based on the chemical and physical properties test results.

All predicted and corresponding measured results for surface temperature are presented in Figure 9-40 as a function of heat flux. The agreement between prediction and measurement is excellent for all tests in air but those at low heat flux. In these cases the surface scab occurred, the scab providing the apparent explanation for the non-agreement.

The variation of surface recession rate with the inverse of surface temperature is presented in Figure 9-41. The measured and predicted results exhibit good agreement at high surface temperature and recession rate but poor at low temperature and recession rate. This poor agreement is due to the significant underprediction of surface recession at moderate and low heat flux as noted from Table 9-8 and Figure 9-42. The theoretical model therefore appears to be reasonably correct at high surface temperature but deficient at moderate and low temperature. This will be discussed further in Section 9.3. Note that any changes in the theoretical model must result in little change in predicted surface temperature, both in magnitude and variation with exposure time.

The predicted and measured surface recession rates are presented in Figure 9-42 plotted against heat flux. The results at high heat flux (> 500 Btu/ft^2-sec) agree quite well although the general tendency to underpredict the measured performance is apparent. At low heat flux the measured recession rate is significantly below that predicted. It is also apparent that the higher the enthalpy at a given heat flux, the poorer the agreement. This certainly provides further information on which to analyze the adequacy of the theoretical model; however, taken alone, this observation provides no immediate rationale for changes to the model.

For the helium environment, the predicted surface recession rate was zero (Table 9-8). The measured recession for the helium case, however, was finite but also small and, as discussed in Section 9.1.2.3, could well be attributed to char shrinkage. It is interesting to attempt to quantify this effect and apply it to the measured recession for the air results. It is not unreasonable to assume that the shrinkage is proportional to char thickness and if so the measured performance in the helium environment indicates that the surface recession due to shrinkage is approximately 10 percent of the char thickness. The recession due to effects other than shrinkage may therefore be defined by

$$\text{(net surface recession)} = \text{(measured surface recession)} - 0.10\ \text{(char depth)}$$

For the test results in the air environment, the 0.10 of char depth correction is very small relative to the measured recession.[6] This shrinkage effect therefore does not explain the discrepancy between the measured and predicted surface recession and does not change the interpretations of the test results presented previously.

The predicted surface recession for the nitrogen free stream environment was also zero; however, contrary to the results for helium the measured recession was quite significant (Table 9-8). Some surface recession mechanism associated with nitrogen is apparently not being accounted for in the analytical predictions, its omission providing a potential explanation for the poor agreement of predicted and measured recession in air. The mechanism, if it exists, is probably chemical, either a gas phase - solid phase reaction (or reactions) or some effect which causes or influences condensed phase reactions at the surface. A brief search for possible gas phase and condensed phase species that might support the existence of such a mechanism was therefore made. Based on the available thermochemical data no gas phase species was overlooked that might have explained the observed performance. One condensed phase species which could have affected the surface response, Si_3N_4, was not included. This species would not be expected to occur, however, and as a further check the X-ray diffraction patterns were reviewed to specifically

[6] The low heat flux results demonstrate somewhat of an exception to this sweeping generalization. For the cases where the surface recession was less than 1 mil/sec the shrinkage correction can be as large as 30 percent of the measured recession. The correction is therefore small, however not negligible for these cases.

look for its existence in all surface samples (Section 6.3). No evidence of Si_3N_4 was found. It should be noted that the surface temperature was well below that at which the pyrolysis gases would be expected to react with the char. Further studies of this nitrogen environment phenomenon are certainly warranted but are beyond the scope of this contract.

The observed surface condition, the predicted surface material, and the measured surface materials (from the chemical analysis tests) are also included in Table 9-8. The predicted surface material is that species which is governing the surface recession, either chemically or through liquid removal. In the case where two materials are indicated, the solution fell between points such that one point was one of the indicated surface materials and the other, the other material. It was therefore impossible to define which one was governing the material response. In all cases where comparisons can be made, the specie predicted to be governing the material response was also found to be present as a surface material.

As discussed in Section 7, the possible surface species had a fail temperature corresponding to the temperature of phase change from solid to liquid. The most significant specie for the 5026-39HCG material in this regard is silica (SiO_2). Although silica exhibits no discrete phase change but rather a continual decrease in viscosity as temperature increases, a phase change temperature of 3,390°R was indicated (Reference 7-3) and taken as the fail temperature. Note however from Table 9-4, that flowing silica droplets began to appear somewhere in the temperature range of 2,900°R to 3,200°R, with an appropriate experimental fail temperature probably being on the low end of this range. This apparently provides at least a partial explanation for the low predicted surface recessions in the low and moderate heat flux range. If the lower fail temperature had been used, higher recession rates would be expected wherever SiO_2 appeared as a surface specie at or above the fail temperature. Additional calculations are required to check out the magnitude of this effect and its influence on surface temperature and other response results.

The results of the chemical and physical properties tests also shed light on the adequacy of the theoretical model. For instance, in some cases the char surface chemical composition was far from that assumed in the analytical prediction calculations. These results will be discussed in detail in Section 9.3.

In summary, the surface response of the 5026-39HCG material is not generally adequately characterized by the theoretical model used in the calculations performed herein, although the in-depth response is accurately characterized by the model. The comparisons of measured and predicted response

have suggested several possible reasons for the inadequacy, several possible approaches to eliminating it, and the constraints which must be followed in the process.

Prior to developing a completely accurate theoretical model, the results of this program allow a semi-empirical approach to material performance prediction which should provide reasonable accuracy. The surface response may be defined by the two basic correlations presented in Section 9.1 and, with these as boundary conditions, the in-depth response may be calculated using the theoretical model as demonstrated in Section 9.2.1.1. It is of course hoped, and expected, that the discrepancies in the surface response theoretical model are not too obscure and the inclusion of the phenomena in it not too difficult to allow an accurate, completely theoretical technique for predicting the response of the 5026-39HCG material. The results discussed in Sections 9.1 through 9.3 provide a firm basis for such an effort, but were beyond the scope of this study.

9.2.2 Parametric Study

The parametric study performed under the analytical predictions phase of the program employed the complete surface and in-depth theoretical model presented in Section 7 and discussed in Section 9.2.1. Based on the discussion of Section 9.2.1, the results presented herein cannot be expected to be quantitatively correct. The qualitative trends are felt to be reasonable however and therefore the results are valuable in this regard. The parametric study results are discussed in the following paragraphs; the results presented were tabulated previously as Table 7-2 which may be referred to for a complete description of the parametric study conditions.

The predicted effect of exposure time on surface recession rate and surface temperature is presented in Figure 9-43 for a broad spectrum of test conditions. The predictions exhibit the relatively small effect of exposure time on surface temperature discussed previously. The surface recession rate is dependent on exposure time, once it is predicted to occur, contrary to the measured surface recession response. It should be noted that all subsequent results must be considered in the light of the predicted exposure time effect.

The predicted effects of heat flux and heat transfer coefficient are presented in Figures 9-44 and 9-45 respectively. These results present no surprises. The surface recession rate and surface temperature increase with increases in both parameters. At a given heat flux, the recession rate increases with decreasing enthalpy as expected. The recession rate at a given heat transfer coefficient is relatively independent of enthalpy whereas the surface temperature increases with increasing enthalpy. Note that these trends are consistent with the correlations of Section 9.1.

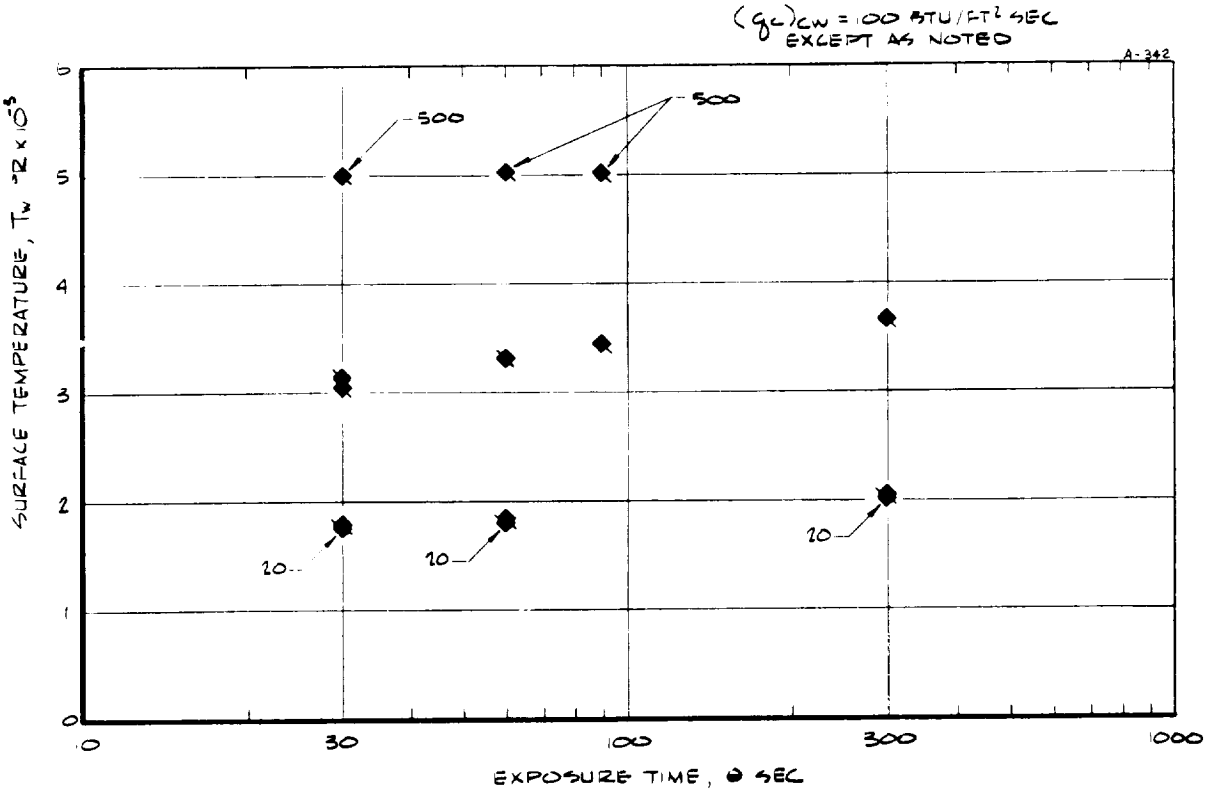

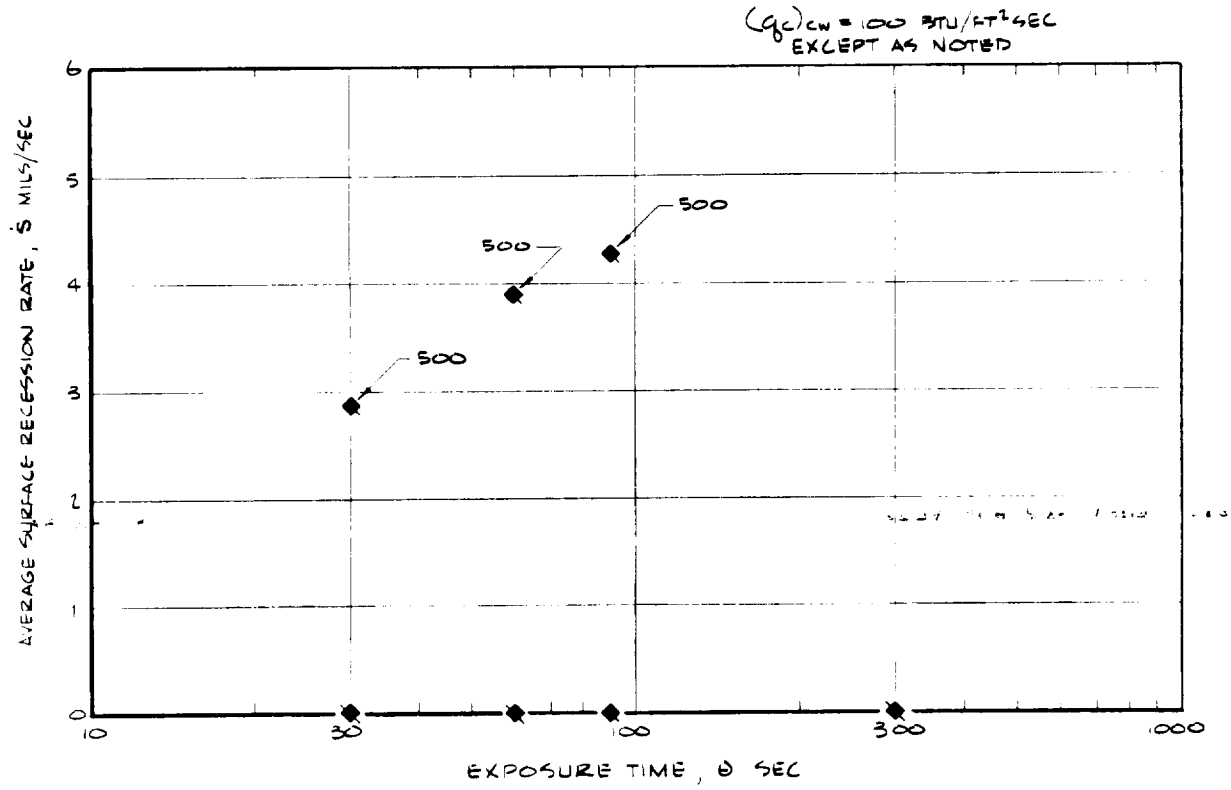

FIGURE 9-43 ANALYTICAL PREDICTION OF THE EFFECT OF MODEL EXPOSURE TIME ON MATERIAL PERFORMANCE.

FIGURE 9-44 ANALYTICAL PREDICTION OF THE EFFECT OF STAGNATION POINT HEAT FLUX ON MATERIAL PERFORMANCE.

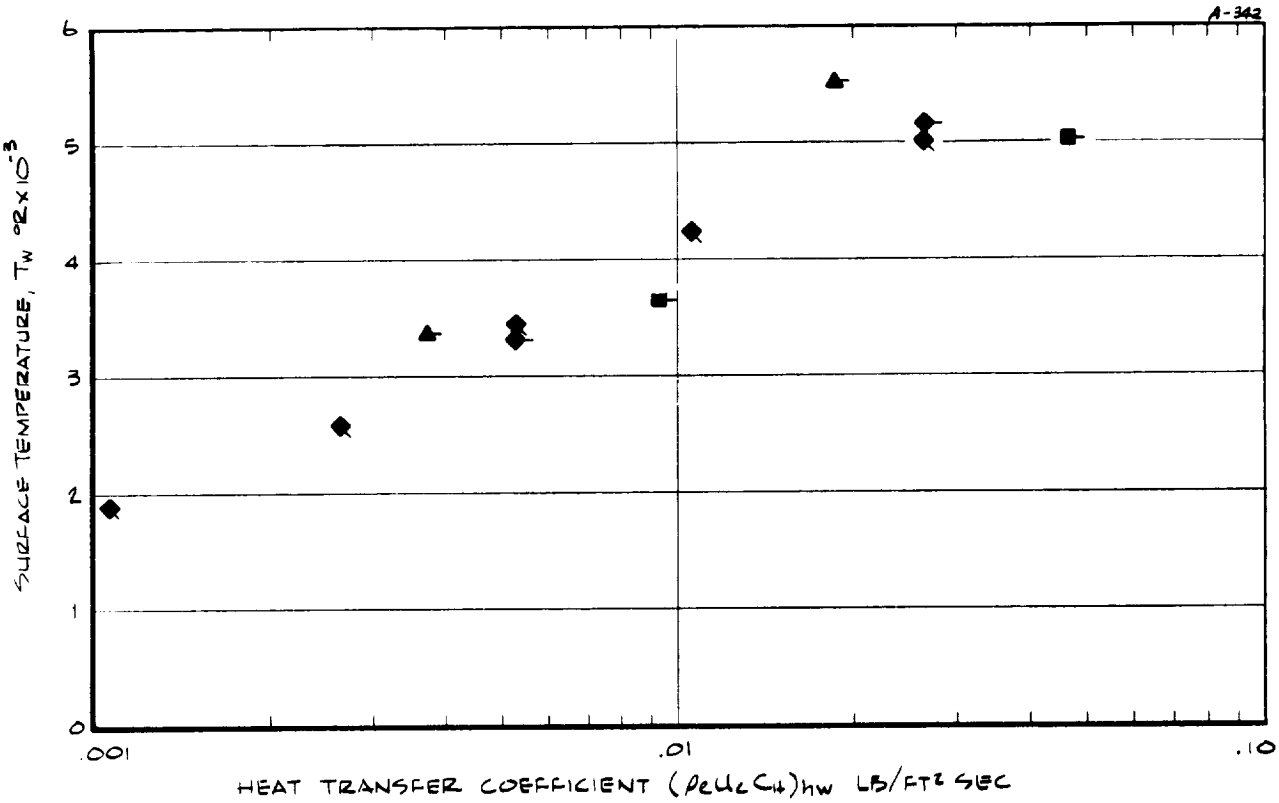

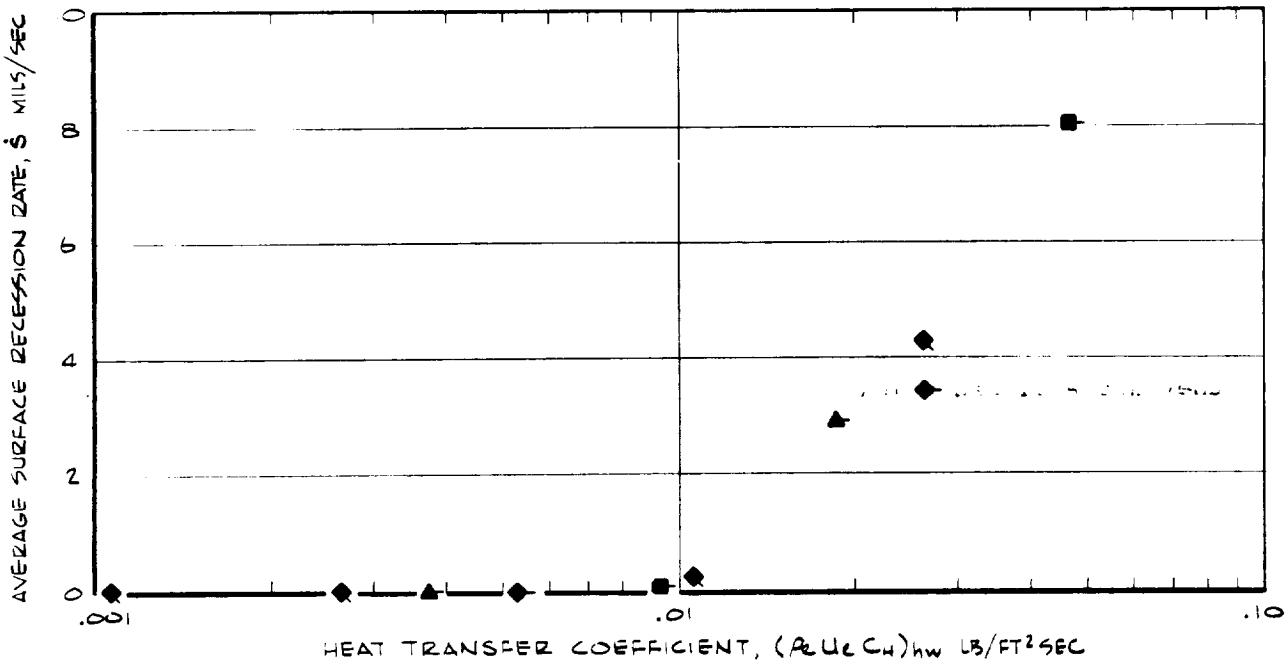

FIGURE 9-45 ANALYTICAL PREDICTION OF THE EFFECT OF STAGNATION POINT HEAT TRANSFER COEFFICIENT ON MATERIAL PERFORMANCE.

The predicted effect of enthalpy on material performance is presented in Figure 9-46. The surface recession rate at constant heat flux increases with decreasing enthalpy as noted above. The surface temperature at constant heat flux is relatively independent of enthalpy.

The predicted effect of pressure on the surface temperature is presented in Figure 9-47. As noted from the figure the effect of pressure is negligible; the exposure time is the primary variable that affects the surface temperature in the results presented.

The predicted effect of oxygen content on material performance is presented in Figure 9-48. The recession decreases with decreasing oxygen mass fraction, being zero or small for the pure nitrogen environment. The one case of finite recession in nitrogen occurs at high heat flux and high surface temperature. The surface temperature is related to oxygen content primarily through surface recession; the higher the surface recession rate the lower the surface temperature.

Finally, the predicted effect of combined convective and radiative heating on material performance is presented in Figure 9-49. The surface recession rate and surface temperature at a given convective heating rate increase with increasing radiative heating; for the case considered, an increase in radiative flux from 0 to 500 Btu/ft^2-sec (total flux from 200 to 700 Btu/ft^2-sec) results in an increase in recession rate of about 50 percent and in surface temperature of about 30 percent. The partition of the total flux between convective and radiative is seen to be important for surface recession rate but to have very little effect on surface temperature.

9.3 CHEMICAL AND PHYSICAL PROPERTIES TESTS RESULTS

The results of the chemical and physical properties tests performed on models exposed to simulated reentry conditions are discussed in the following sections. These tests included microchemical quantitative analysis and X-ray diffraction studies of surface materials and in-depth char, density distribution measurements as determined by X-ray transmission, infrared spectra measurements of the in-depth char and surface materials, and surface and in-depth photomicrographs. The results of this test program were presented in Section 6.3; they are analyzed below in terms of their description of the surface and in-depth response, the surface response being discussed in Section 9.3.1 and the in-depth response in Section 9.3.2.

Before discussing the specific results for the test models, it is informative to review the results for the virgin material. The measured chemical composition of the virgin material is presented in Table 9-9. The three "measured" compositions represent different approaches to handling the measured moisture content. Note that nitrogen was not measured and assumed to be negligible. The virgin material composition used in the analytical predictions is also included in the table for comparison purposes. The agreement between measured and assumed composition is good; however, the measured

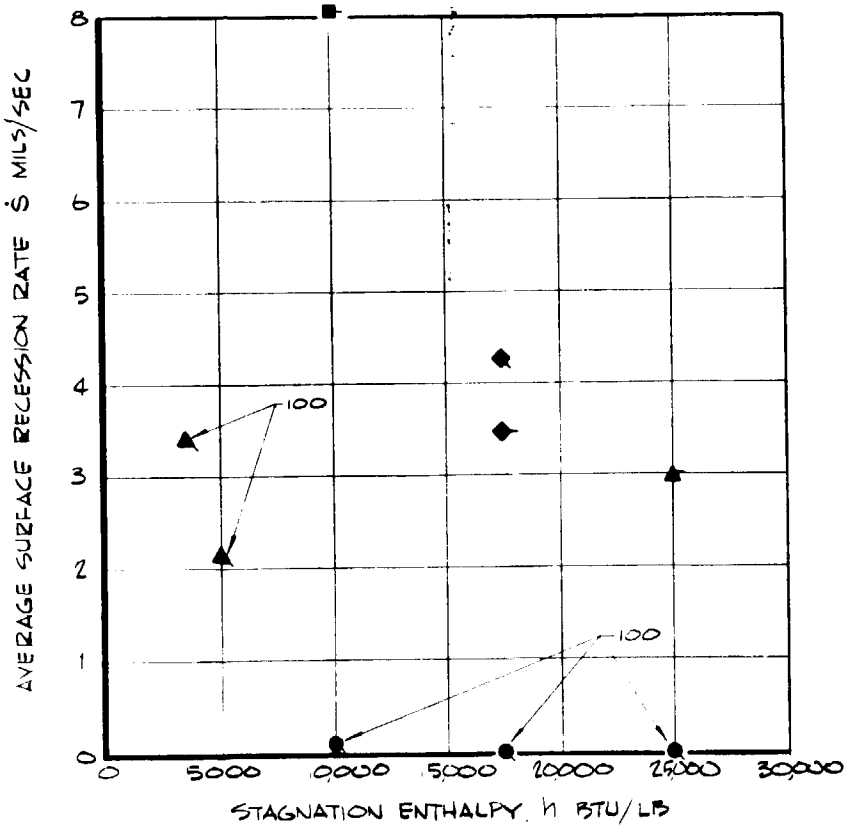

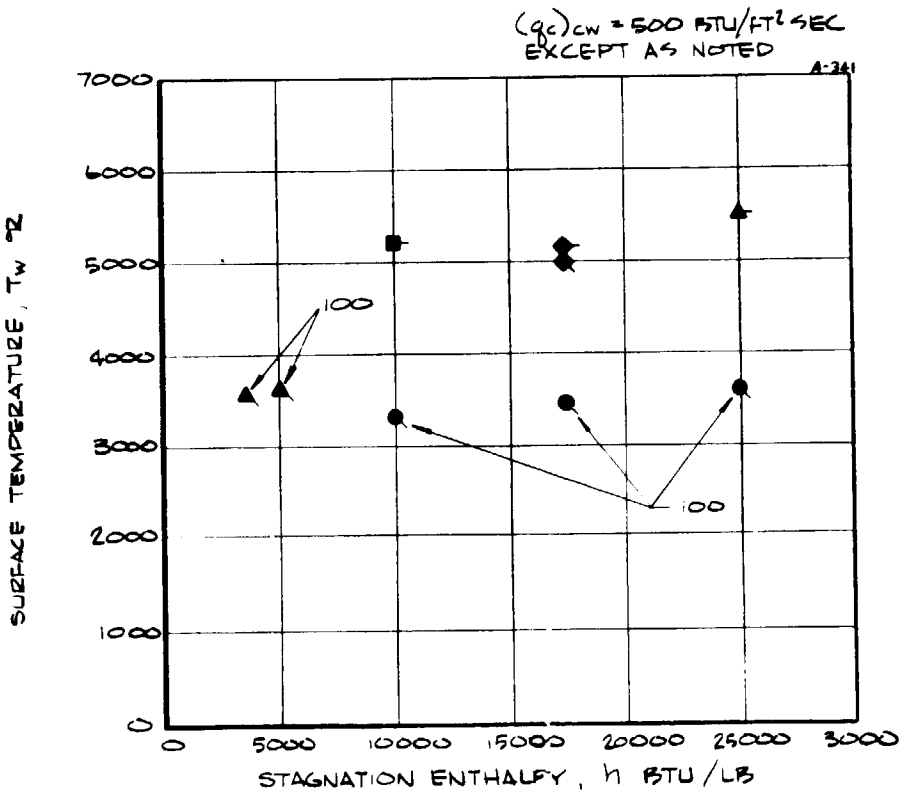

FIGURE 9-46 ANALYTICAL PREDICTION OF THE EFFECT OF STAGNATION POINT ENTHALPY ON MATERIAL PERFORMANCE.

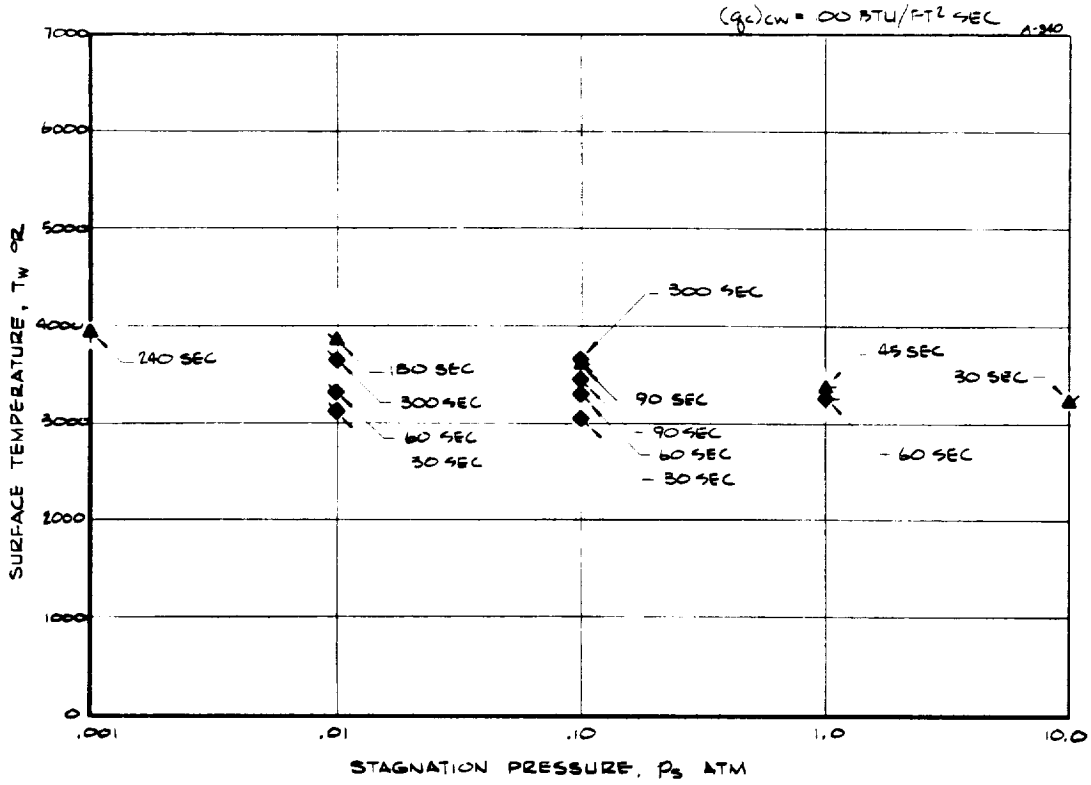

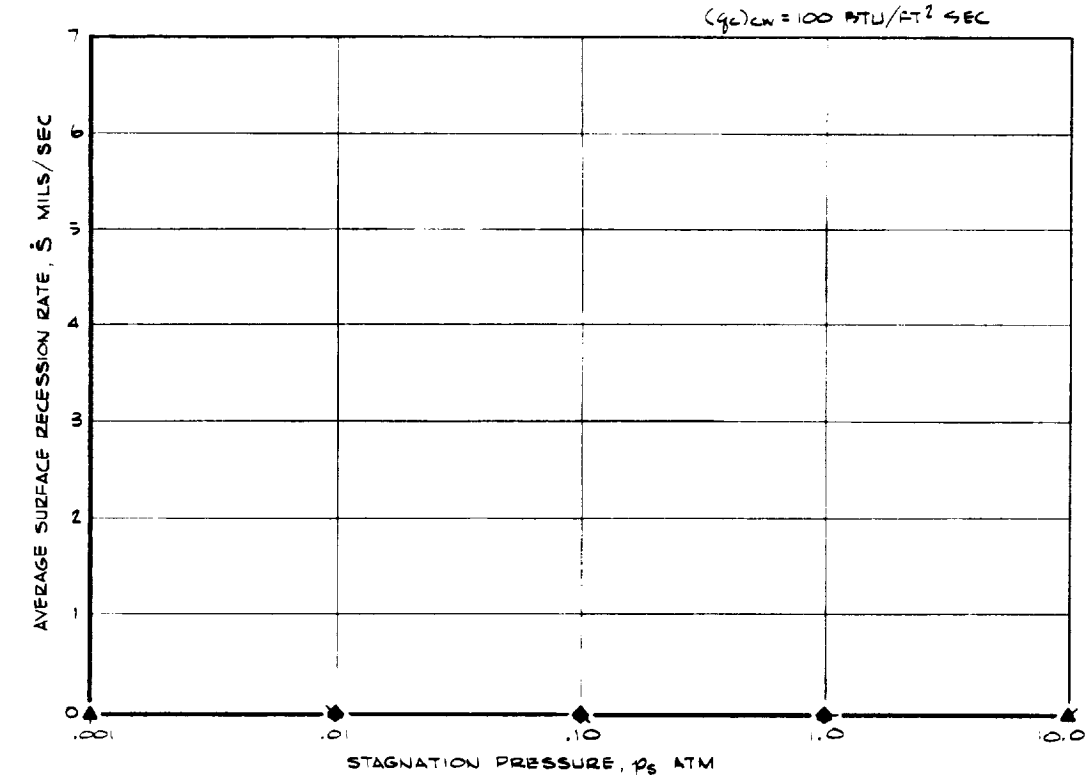

FIGURE 9-47 ANALYTICAL PREDICTION OF THE EFFECT OF STAGNATION POINT PRESSURE ON MATERIAL PERFORMANCE.

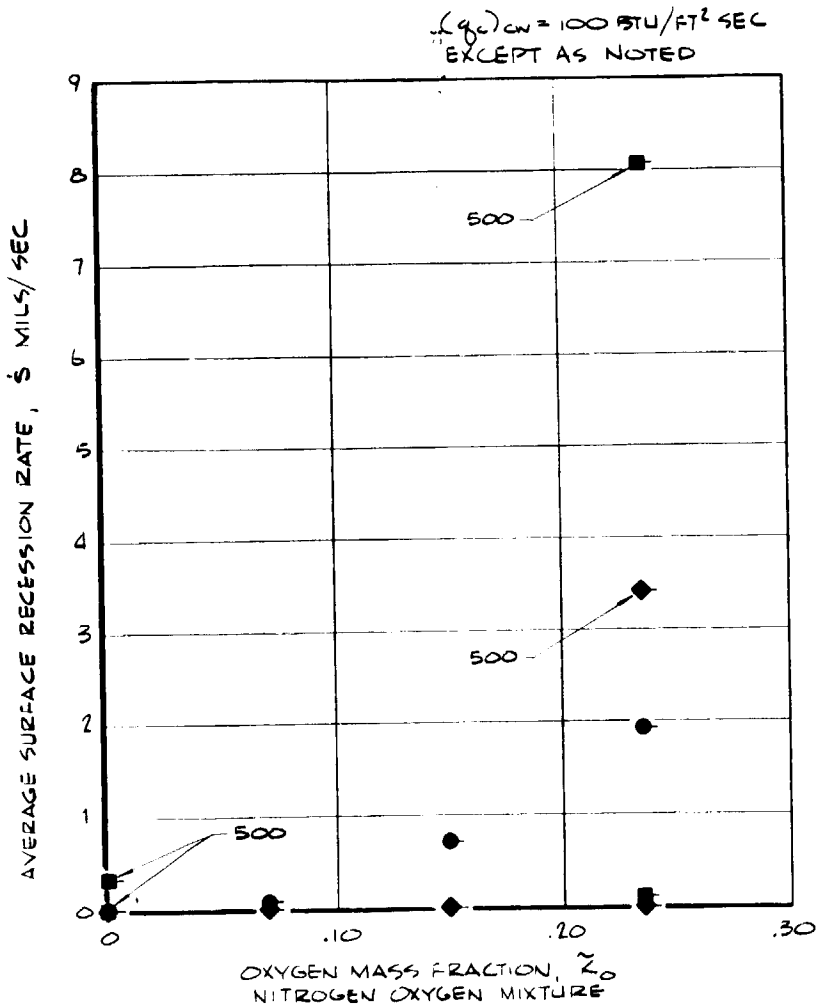

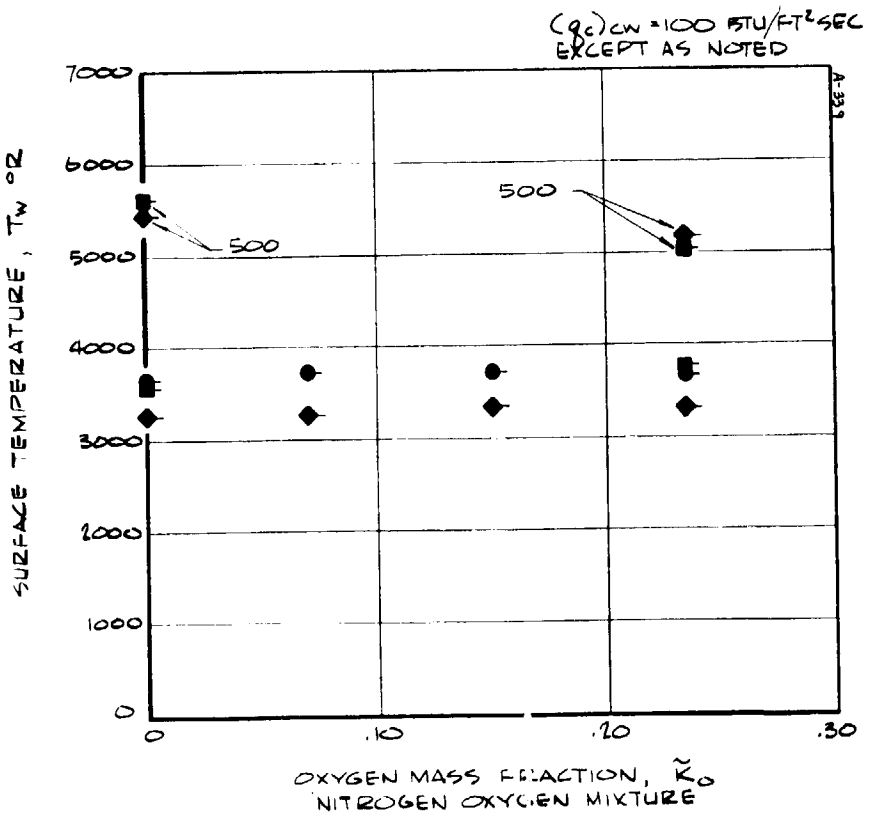

FIGURE 9-48 ANALYTICAL PREDICTION OF THE EFFECT OF OXYGEN CONTENT ON MATERIAL PERFORMANCE.

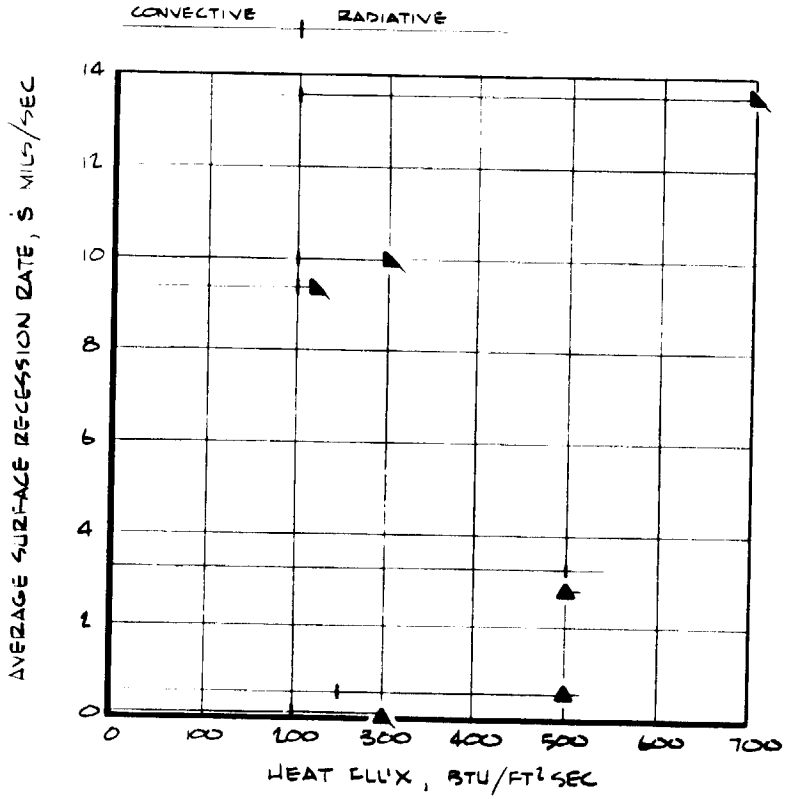

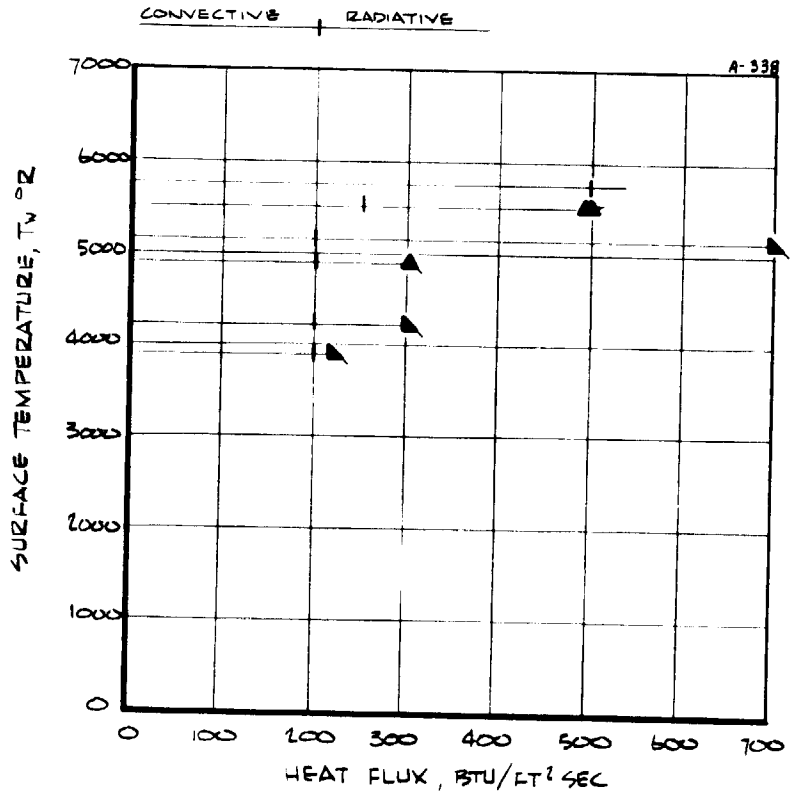

FIGURE 9-49 ANALYTICAL PREDICTION OF THE EFFECT OF RADIATION HEAT FLUX ON MATERIAL PERFORMANCE.

TABLE 9-9

CHEMICAL COMPOSITION OF THE VIRGIN MATERIAL

Material Description	Weight Percent						Ash / Carbon Ratio	Carbon / Hydrogen Ratio
	Ash	Carbon	Hydrogen	Oxygen	Moisture	Nitrogen		
Virgin Material, as Measured	25.7	48.3	4.23	18.5	3.2	—	0.53	11.4
Virgin Material, Less Moisture	26.6	49.9	4.4	19.0	0	—		11.4
Virgin Material, Moisture Included in Hydrogen and Oxygen Concentrations	25.7	48.3	4.6	21.3	0	—		10.5
Virgin Material, Assumed for Analytical Predictions	24.1	52.0	4.9	18.0	—	1.0	0.46	10.6
Char, Assumed for Analytical Predictions	51.2	48.8	0	0	—	0	1.05	—

Note: Virgin material was amorphous, no crystalline compounds were detected.

ash and oxygen content are slightly higher than that assumed, the carbon and hydrogen content slightly lower. Since the measured composition was based on a single test and the measured and assumed compositions are quite close, the assumed composition for the analytical predictions is felt to be a reasonably accurate chemical characterization of the virgin material. The char composition assumed in the analytical predictions is also included in the table for completeness; this composition will be referred to subsequently.

The virgin material exhibits large variations in silica content as indicated by the X-ray densitometer measurements (Figure 6-33). Recall that the X-ray density is basically an indicator of silica density and not overall material density. The magnitude of these variations was no less than $\pm$ 18 percent for the two models considered (Model Nos. 114 and 27), these variations occurring in regions as small as 0.005 inch in thickness.

9.3.1 Surface Response

The chemical test results pertinent to the analysis of the material surface response, including the microanalysis, X-ray diffraction, and infrared spectra measurements, are summarized in Table 9-10 for all models for which these tests were performed. The test conditions to which the models were exposed and their surface and in-depth response to these conditions is also included.

For the three models for which the surface scab and surface globules were observed (Models 91, 114, and 30), the scab or globule material was almost exclusively ash, this ash being primarily silica. Therefore, as expected, when melt removal occurred (the globule cases), this removal was due to the flowing "liquid" silica. Note from the photomicrographs (Figure 6-32) that the globules covered a large spectrum of size; as they flowed they apparently collected other globules and also entrapped some gases. Much of the char surface was not covered with a melt in these cases (Figure 6-32). Therefore two separate but interrelated surface recession mechanisms apparently occurred, these being melt removal as reflected by the globules, and surface chemical reactions at the exposed char surface not covered by globules. (The globules themselves are of course subject to decomposition and to reaction with the gas phase species.) This apparent duality in surface removal mechanisms is not currently treated in the theoretical model.

For the case of the scab, the entire char surface was protected by an agglomerated mass of primarily silica fibers. Because of the low surface temperature, silica was not removed in liquid globule form but apparently continued to build up with exposure time, this build up resulting in a decrease in recession rate with exposure time. Note that a small amount of

TABLE 9-10

SURFACE MATERIAL CHEMICAL ANALYSIS RESULTS

Phase	Model No.	Enthalpy h (Btu/lb)	Stagnation Pressure P_s (atm)	Heating Rate q_c (Btu/ft²-sec)	Chemical Environment	Exposure Time θ (sec)	Surface Recession s (inch)	Char Depth (inch)	Pyrolysis Zone Depth (inch)	Average Surface Temperature T_w (°R)	Weight Percent: Scab or Globules Ash	Scab or Globules Carbon	Char Ash	Char Carbon	Char Ash/Carbon Ratio	Crystal Form: Scab or Globules	Crystal Form: Char	Scab or Globule Material	Predicted Surface Species	Observed Surface Description
III	158/BH/1.0	5,030	1.06	1,170	Air	10.2	0.509	0.549	0.559	—	—	—	—	—	—	—	β-SiC,C	—	SiC or SiO_2	DG,NM
|	140/BH/1.0	5,150	3.10	1,770	|	2.9	0.418	0.428	0.428	4,850	—	—	—	—	—	— —	|	—	SiC or C	G,NM
IV	91/BH/2.0	10,970	0.0079	116		60.5	0.152	0.237	0.317	3,250	98.2	0.7	45.1	54.0	0.84	Amorphous	Amorphous	SiO_2 Globules	C or SiO_2	DG,M
|	108/BH/2.0	16,300	0.0088	154	|	60.4	0.147	0.247	0.317	3,550	—	—	34.4	65.1	0.53	— —	C	—	C	DG,(M)
|	84/BH/2.0	10,920	0.0298	188	Helium	60.3	0.023	0.213	0.333	3,875	—	—	18.3	81.2	0.23	— —	β-SiC,C	—	|	BD,LG,NM
|	80/BH/2.0	9,960	0.0276	271	Nitrogen	60.6	0.172	0.292	0.402	4,425	—	—	25.0	72.1	0.37	— —	|	—		BD,NM
V	114/BH/4.0	4,910	0.0112	33	Air	211.4	0.085	0.305	0.455	2,825	99.6	0.1	70.1	27.1	2.61	α-SiO_2	α-SiO_2	SiO_2 Scab	SiO_2 or C	LG,S
VI	30/BH/2.0	5,940	0.0275	116	|	90.0	0.218	0.388	0.458	3,600	98.6	0.1	58.3	41.1	1.42	Amorphous	Amorphous	SiO_2 Globules	SiO_2	G,(M)
|	27/BH/2.0	10,270	0.0282	181	|	90.0	0.391	0.551	0.611	4,175	—	—	28.6	71.4	0.40	— —	β-SiC,C	—	SiC	BD,(G),NM
|	102/BH/2.0	16,520	0.0271	288	|	44.7	0.218	0.328	0.388	4,450	—	—	23.2	75.6	0.31	— —	|	—	C	G,(BD),NM
VII	97/BH/2.0	18,860	0.0285	337	|	31.0	0.155	0.285	0.395	4,575	—	—	34.4	65.1	0.53	— —	β-SiC	—	|	G,DB,NM
|	111/BH/1.0	10,550	0.0831	562	|	40.7	0.382	0.468	0.488	4,750	—	—	43.8	54.0	0.81	— —	C	—	SiC or C	G,NM
—	Virgin Material	—	—	—	—	—	—	—	—	—	—	—	25.7	48.3	(0.53)	Amorphous	Amorphous	—	—	—
Char Composition used for analytical predictions											—	—	51.2	48.8	1.05					

surface recession was predicted to occur (Figure 9-42) due to silica decomposition and gas phase reactions with the silica. In this case the theoretical model was apparently consistent with the observed surface condition even though the predicted surface recession was too low. Two possible explanations for this discrepancy are apparent. The scab exhibited a rough surface and appeared to be porous; this could result in a large effective exposed surface area and therefore a higher surface recession. Also in the process of scab formation, agglomeration may result in a densification of the scab and the resultant shrinkage and apparent surface recession. Either or both mechanisms could provide the explanation for the differences between the measured and predicted surface recession as observed from Table 9-8 and Figure 9-42. There are also other possibilities as noted below.

As shown in Table 9-10, the scab is, at least in part, crystalline in form, α-cristobalite (α-SiO_2) having been identified by X-ray diffraction. At higher temperatures typical of globule formation, the silica is amorphous. At still higher surface temperatures, above about 3,500°R where no surface melt is observed, silicon carbide and carbon appear in crystalline form as β-SiC and graphite. The graphite formation could be the high temperature graphitization of the carbon in the char or it could be coking of the pyrolysis gases to form pyrolytic graphite (or it could be both). Note that the graphite content of the surface samples was no greater than 10 percent by weight of the total sample and therefore no greater than about 30 percent of the total carbon in the samples. This however does not preclude coking as a significant surface and in-depth response mechanism since amorphous carbon deposition can also occur. In the cases where silicon carbide occurred, the microanalysis indicated that this concentration was less than 2 percent by weight in all cases, with Model 80 tested in the nitrogen environment exhibiting the highest value (~ 1.9 percent). Silicon carbide formation therefore does not appear to be an important mechanism in influencing the surface response. Note that this conclusion does not necessarily apply to the high pressure test results (Phase III, Models 158 and 140) for which no results pertinent to quantifying the silicon carbide concentration were obtained.

As noted in Table 9-10, the char ash-to-carbon ratio measured is significantly less than that assumed in the analytical predictions for all models except those which exhibited the scab or globules on the surface. These measured results can be interpreted as reflecting a high carbon content at the surface due possibly to coking of the pyrolysis gases or to a depletion of silica at the surface. The depletion of silica certainly appears to be real based on the in-depth X-ray densitometer trace for Model 27 (the only model so studied for which a silica "melt" was not observed on the surface); this

trace was presented in Figure 6-33b. The silica content exhibits a significant, steadily decreasing trend through the char towards the surface. No quantitative density information is available to actually define the silica content. The mechanism of this apparent silica depletion is somewhat obscure. Possibilities include in-depth condensed phase reactions such as

$$SiO_2^* + C^* \rightarrow SiO + CO \qquad (9\text{-}11)$$

for which the products are in gas phase, silica decomposition in-depth to form gas phase species

$$SiO_2^* \rightarrow SiO + 1/2\ O_2 \quad , \qquad (9\text{-}12)$$

and in-depth silica at high temperature and therefore low viscosity being transported to the surface by the pryolysis gases and then removed by decomposition and chemical reaction. The former reaction has been observed and quantified as discussed in Reference 9-5.

The possibility of a higher carbon content at the surface, the other possible explanation for the low measured surface ash-to-carbon ratio, cannot be supported or refuted by the available test results. The X-ray densitometer measurements were not sensitive to carbon and no other measurements indicative of absolute quantitative carbon content are available. The source of the high carbon content, if it actually occurs, is more than likely coking of the pyrolysis gases.

Actually both effects - silica depletion and carbon deposition - are probably occurring in the real situation. The relative magnitude of these effects would be expected to be a function of the environmental conditions which in turn affect the temperature distributions and temperature histories. Once the surface temperature exceeds that for which a melt is apparent on the surface, however, no environmental or response variable, including surface temperature itself, seems to correlate with the ash-to-carbon ratio (Table 9-10). This lack of correlation could simply be scatter in the measurements; however, if it simply is scatter, the scatter seems to be unreasonably high.

The high ash-to-carbon ratio for the char surfaces on which the scab and globules were observed (Table 9-10) is apparently due to the surface and near in-depth temperatures being too low for the carbon deposition and silica depletion mechanisms mentioned above to be contributing significantly to the surface response. In the case of the scab there was, of course, no mechanism for silica to be removed in quantity. It is interesting to note that the char

surface ash-to-carbon ratio decreases with decreasing silica "melt" observed at the surface.

Based on the above discussion, it is apparent that the chemical characterization of the char assumed for the analytical predictions was in error certainly for cases where the surface temperature was above 3,500°R. The average measured ash-to-carbon ratio for models tested in the air environment and which exhibited surface temperatures above 3,500°R was 0.52, this value being just half of the value assumed in the predictions (1.05). The use of this average surface value in the predictions would certainly be expected to change the predicted surface response. It is interesting to note that, for the one model for which in-depth ash-to-carbon ratio measurements were made for the non-globule surface conditions (Model 27), the average ash-to-carbon ratio for the complete char layer was approximately 1.05, the value corresponding to the analytical predictions.

The surface char density assumed in the analytical predictions may also be in error. No results were available in the chemical and physical properties tests to define this density. Based on the comparisons of predicted and measured weight loss presented in Table 9-7, however, the overall char density characterization appears quite accurate.

The models exposed to the helium and nitrogen environments both exhibited very low surface ash-to-carbon ratios (Table 9-10). For the helium environment model, the surface exhibited significant quantities of silica in fiber form (Figure 6-32); it has the appearance of a virgin material in which the resin had pyrolized and the silica had been left undisturbed. The low ash-to-carbon ratio is therefore probably due to coking of the pryolysis gases. For the nitrogen environment model, no discrete fibers are apparent (Figure 6-32). In this case the low ash-to-carbon ratio may be attributed to both carbon deposition and silica depletion, the carbon deposition possibility being consistent with the black surface deposit observed on this model. It should be noted that the surface temperatures for the helium and nitrogen environment models were significantly different (3,875°R and 4,425°R, respectively). Visual inspection of Model 86 which was tested in a helium environment and for which the surface temperature was 4,600°R revealed the same surface appearance as the lower temperature helium environment model. Therefore, the above discussion is qualitatively a function of the chemical environment only and not surface temperature as well. Based on these results and as discussed in Section 9.2.1.2, there appears to be a significant effect of nitrogen on the surface response, an effect which apparently is not accounted for in the theoretical model and for which no explanation is currently available as discussed in greater detail in Section 9.2.1.2.

In summary, the chemical and physical properties tests results provided a detailed description of the 5026-39HCG material surface after exposure to simulated reentry conditions. This description allowed a preliminary definition of the material surface response mechanisms. When a surface melt occurs, in the form of a scab or globules, the melt is almost exclusively ash which, in turn, is primarily silica. For these cases, the char surface exclusive of the melt exhibits a high ash-to-carbon ratio which decreases with decreasing amount of observed melt. When globules are observed, two surface removal mechanisms may well be important; one being liquid runoff, the other being surface chemical reactions with the char surface not covered by globules. At conditions for which no surface melt is apparent (surface temperatures above about 3,500°R), the surface ash-to-carbon ratio is quite low, being about half the average ratio for the complete char layer. This low ratio at the surface is due to the probable combination of carbon deposition and silica depletion. The carbon deposition is apparently due to coking of the pryolysis gases at and near the surface; the silica depletion is apparently due to silica decomposition and/or silica-carbon or carbon gas phase reactions. Contrary to the theoretical surface response model, nitrogen exhibits a strong influence on the surface response of the material either directly or indirectly. Helium exhibits no such influence. Based on all the above results, the theoretical model used in the analytical predictions to characterize the surface and surface response is in error in some respects. The two primary problem areas are the assumed ash-to-carbon ratio being about twice that actually measured for the cases where no surface melt was observed, and the observed effect of nitrogen on surface response which was not apparent in the analytical predictions.

9.3.2 In-Depth Response

The chemical test results pertinent to the analysis of the in-depth material response, including the microanalysis, X-ray diffraction, and infrared spectra measurements, are summarized in Table 9-11 for the two models for which the in-depth tests were made. The test conditions to which the models were exposed and their surface and in-depth response to these conditions were presented in Table 9-10. The chemical compositions of the char and virgin material used in the analytical predictions are also included in Table 9-11 for comparison purposes. Further discussion of the virgin material test results is presented in the introduction to Section 9.3.

For Model 27 the ash-to-carbon ratio from the pyrolysis zone to the surface exhibits an increase from the virgin material value to a maximum in the central part of the char region followed by a decrease to a value at the surface which is less than the virgin material value. This variation

TABLE 9-11

IN-DEPTH CHEMICAL ANALYSIS RESULTS

Phase	Model No. (1)	Average Surface Temperature T_w (°R)	In-Depth Location	Weight Percent						Ash/ Carbon Ratio	Carbon/ Hydrogen Ratio	Temperature from C/H Ratio (°R)	Crystal Form	
				Ash	Carbon	Hydrogen	Oxygen	Moisture	Nitrogen					
V	114/BH/4.0	2,825	Scab	99.6	0.1	0	0	0.3	—	—	—	—	α-SiO_2	Chemical and Physical Properties Test
			Char 1 (surface)	70.1	27.1	0.17		2.6	—	2.61	> 100	> 1,900		
			2	49.5	48.7	0.25		1.4	—	1.02				
			3	53.8	41.4	0.26		1.6	—	1.30				
			4	52.3	39.6	0.46		5.1	—	1.32	86			
			5	51.4	37.6	1.27	6.3	4.4	—	1.37	30		amorphous	
			6	45.6	40.4	2.28	9.4	3.3	—	1.13	18	~ 1,550		
VI	27/BH/2.0	4,175	1 (surface)	28.6	71.4	0	0	0	—	0.40	> 100	> 1,900	Si, C	
			2	44.1	55.2	0.04		0.7	—	0.80				
			3	52.3	44.2	0.21		3.3	—	1.18			α-SiO_2	
			4	57.0	36.6	0.50	3.2	2.7	—	1.56	73		amorphous	
			5	45.2	40.5	2.48	8.1	3.7	—	1.12	16	~ 1,550		
			6	29.3	48.1	4.06	14.9	3.6	—	0.61	12	> 1,200		
—	Virgin Material	—	—	25.7	48.3	4.23	18.5	3.2	—	0.53	11	—		
—	Char	—	—	51.2	48.8	0	0	0	0	1.05	—	—	—	Analytical Predictions
—	Virgin Material	—	—	24.1	52.0	4.9	18.0	—	1.0	0.46	10.6	—	—	

(1) Test conditions and measured performance are included in Table 9-10.

is illustrated in Figure 9-50 which presents the ash-to-carbon ratio results in terms of the approximate locations at which the samples were taken. The maximum ash-to-carbon ratio corresponds to a maximum temperature in-depth of about 2,000°R. This is illustrated in Figure 9-51a which presents the predicted maximum in-depth temperature (from Option 2 predictions presented in Section 7.4) seen by the material during test or cooldown.[7] Model 114 also exhibits the same general trend, however, the peak is not as high and is spread out more than that for Model 27. The ash-to-carbon ratio decreases towards the surface once the peak is reached but at the surface jumps up to a high value. As mentioned previously, this very high ash-to-carbon ratio at the surface for Model 114 is due apparently to the absence of a mechanism to remove silica from the surface.

The region in which the maximum ash-to-carbon ratio occurs for Model 114 also corresponds to a temperature of about 2000°R. Based on these results for both models, resin decomposition and the associated loss of carbon in gas phase species apparently occurred up to temperatures of about 2000°R. This is in agreement with the Option 2 analytical predictions (Section 7.4) wherein pyrolysis was predicted to be complete at about 2200°R. Above about 2400°R, carbon deposition and/or silica depletion are apparently occurring. As discussed in Section 9.3.1, both of these in-depth mechanisms are probably important. Carbon deposition due to coking apparently occurs at an increasing rate with increasing temperature, at temperatures above about 2400°R. The pyrolysis gases are therefore carbon rich at temperatures of the order of 2400°R, their carbon content continually decreasing thereafter as coking occurs at higher temperatures. Additional discussion of the carbon deposition and silica depletion mechanisms was presented in Section 9.3.1 and is not repeated here.

From the results for Model 27 presented in Figure 9-50, the average ash-to-carbon ratio between the surface and the peak value is approximately 1.05, the value corresponding to the analytical predictions. The value at the surface is, of course, the proper one to be used in predicting the surface response, however. Based on the average ash-to-carbon ratio, the in-depth model corresponding to the analytical predictions appears to be correct on an average basis. This applies to the char chemical composition and may also be generalized to the pyrolysis gas chemical composition.

Figure 9-51 also relates the in-depth crystal structure and the infrared spectra results to the internal temperature. Below temperatures of about

---

[7] As seen from Figure 7-4, the in-depth temperature continues to increase after test at locations significantly below the surface. The maximum temperature at these locations is therefore achieved during the cooldown period, not during test.

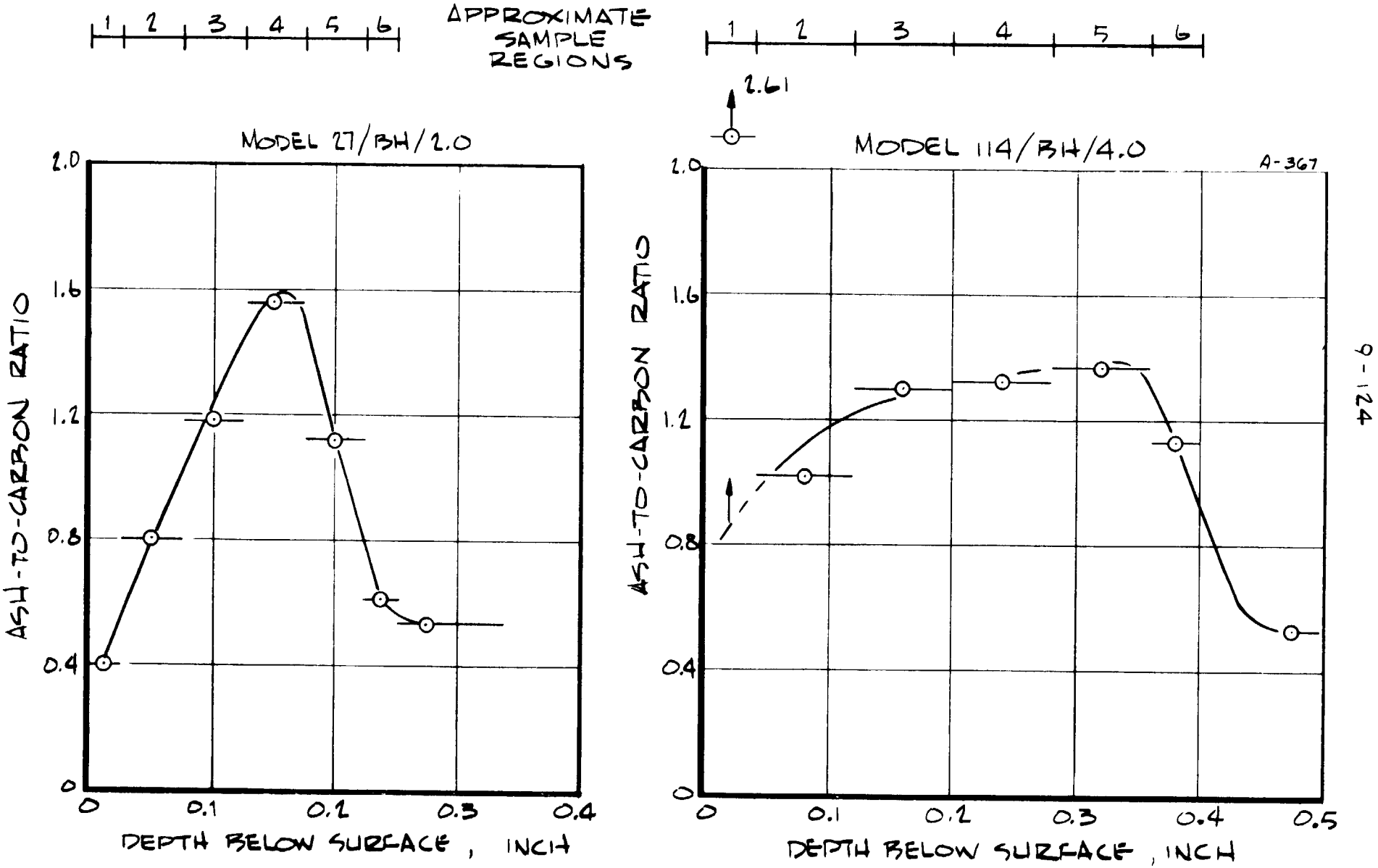

FIGURE 9-50 IN-DEPTH ASH-TO-CARBON RATIO DISTRIBUTION.

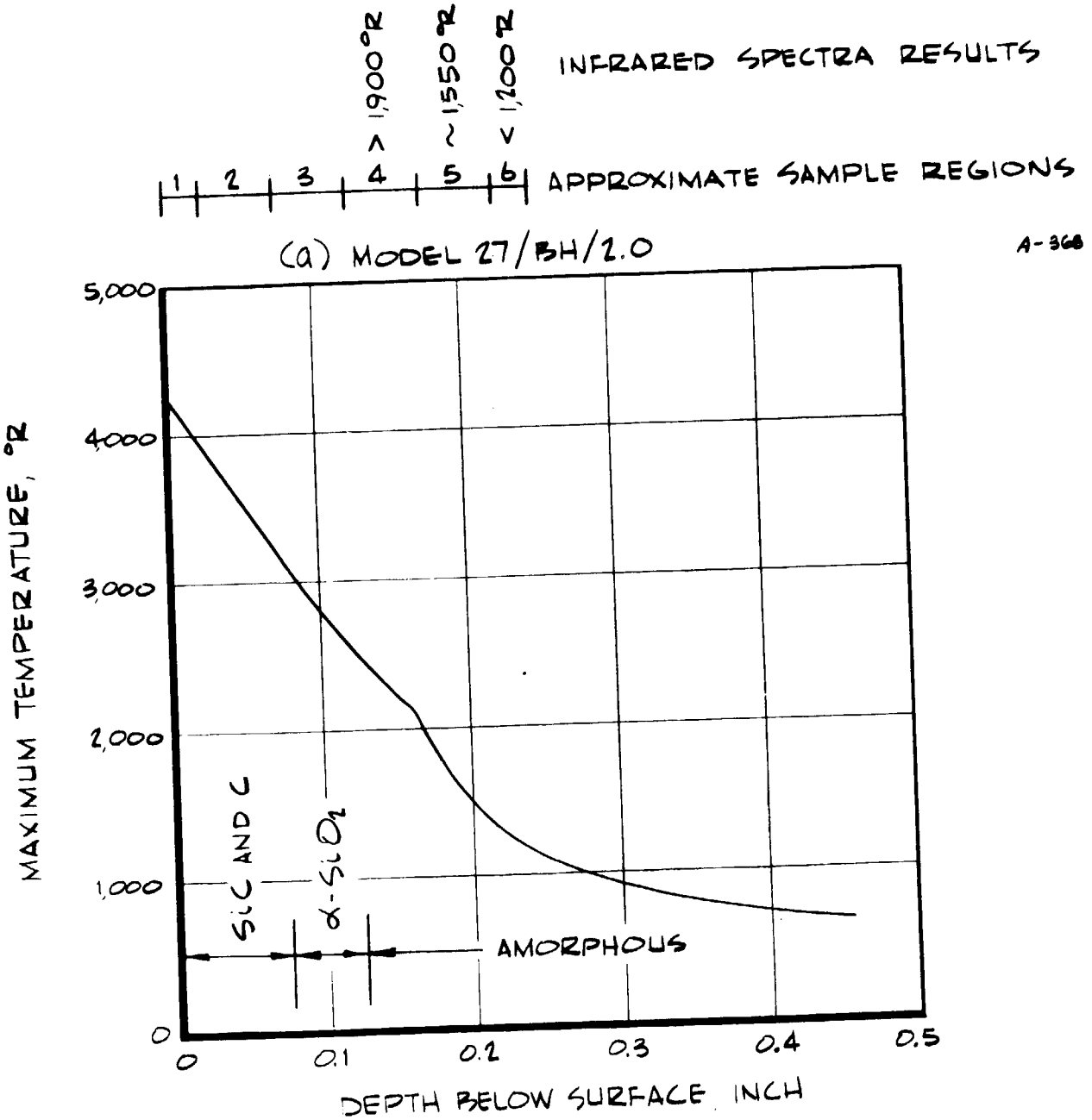

FIGURE 9-51 CORRELATION OF IN-DEPTH CRYSTALLINE STRUCTURE AND TEMPERATURE DISTRIBUTION

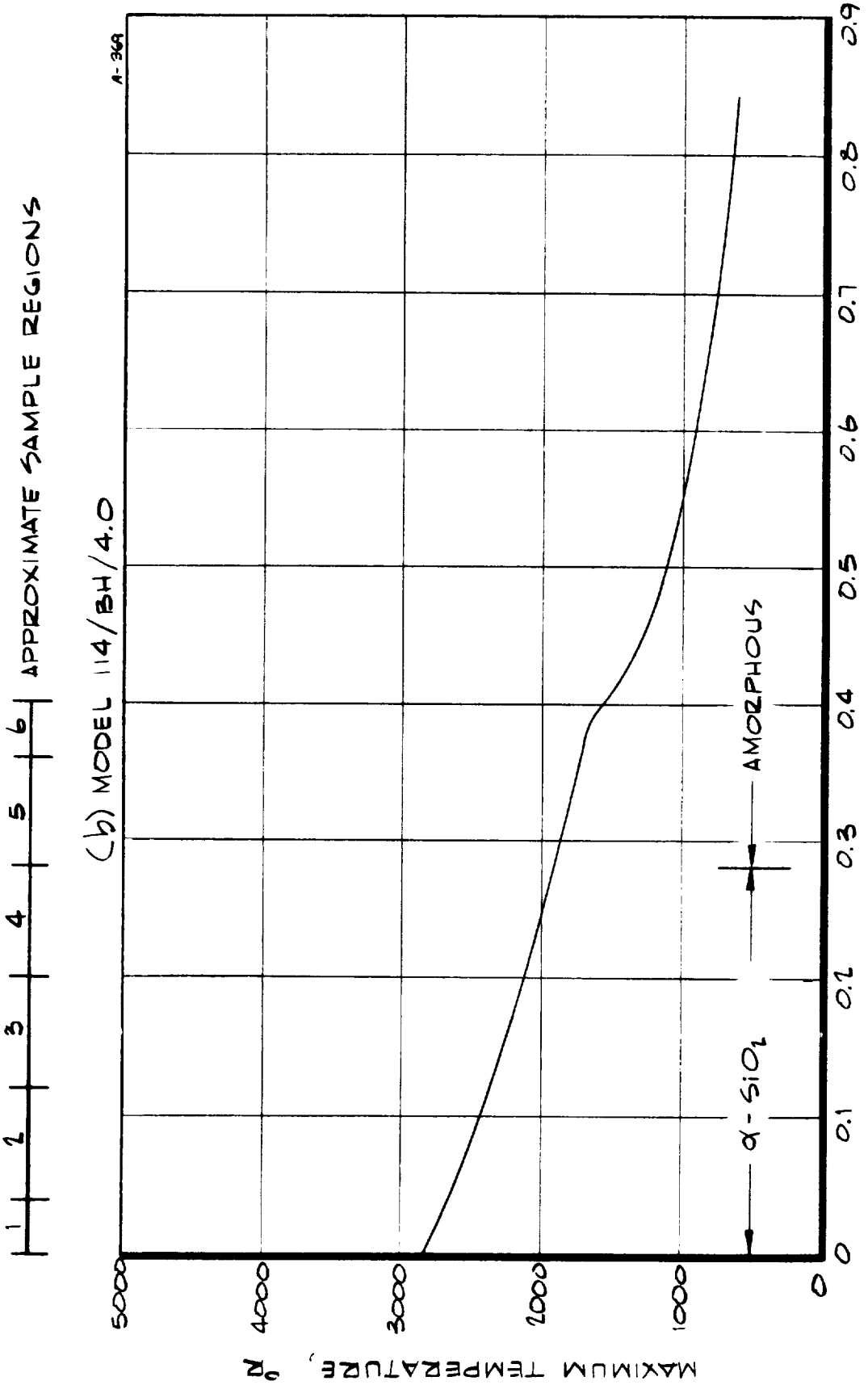

FIGURE 9-51 CONCLUDED

2,000°R the 5026-39HCG material is amorphous. From about 2,000°R to 3,000°R the silica in the material is, at least in part, in the form of α-cristobalite. Above about 3,000°R, graphite and β-silicon carbide are found in small quantities due to the graphitization of carbon or pyrolytic deposition (coking) of the pyrolysis gases and due to silica-carbon or carbon containing gas reactions. Note that the infrared spectra characterization of temperature agrees quite well with the analytical prediction of temperature.

In summary, the chemical and physical properties test results provided a detailed description of the in-depth response of the 5026- 39HCG material after exposure to two simulated reentry conditions. This in-depth response is intimately related to the surface response and therefore many of the conclusions pertinent to the in-depth response were presented previously in Section 9.3.1. The in-depth ash-to-carbon ratio exhibits a considerable variation with depth, the maximum value being achieved in a region where the maximum temperature was about 2,000°R. The decrease towards the virgin material is due to resin pyrolysis; the decrease towards the char surface is due to the carbon deposition and/or silica depletion mechanisms discussed in Section 9.3.1. Based on the test results, in-depth theoretical characterization of the char used in the analytical predictions appears to be correct on an average basis.

REFERENCES

9-1 Schaefer, J. W.: A study of Chunking Mechanisms in MX4926 Carbon Cloth Phenolic. Vidya Report No. 175, Vidya Project No. 8026, Itek Corporation, Vidya Division.

9-2 Munson, T. R., et al: An Advanced Analytical Program for Charring Ablators, Final Report, Avco Space Systems Division, Lowell, Massachusetts. AVSSD-0172-67-RR, 1967.

9-3 NASA Transmittal Letter, to Manned Spacecraft Center, (Attention Dave Greenshields), from Ames Research Center. Description of Test and Data, Ablation Tests of Avcoat 5026-39 HCG Conducted at Ames. Contract NAS9-5430, April 21, 1967.

9-4 Flood, D. T.: Phase I Evaluation of Apollo Materials Subjected to a Moderate Shear Stress Environment. Aerotherm Technical Memorandum 6007-TM-1, April 27, 1966.

9-5 Rindal, R. A., Clark, K. J., Moyer, C. B., Flood, D. T.: Experimental and Theoretical Analysis of Ablative Material Response in a Liquid Propellant Rocket Engine, Final Report Contract NAS3-7945, Aerotherm Report 67-15, September 1967.

7-2 Kendall, R. M.: A General Approach to the Thermochemical Solution of Mixed Equilibrium-Nonequilibrium, Homogenous or Heterogenous Systems, Part V of Final Report, Contract NAS9-4599, Aerotherm Project No. 6002, March 14, 1967.

7-3 JANAF Thermochemical Tables. The Dow Company, Midland, Michigan, August 1965.

SECTION 10
CHARACTERIZATION OF MATERIAL RESPONSE

The analysis of the 5026-39HCG material response is summarized in this section through a characterization of the surface and in-depth material performance. This characterization is based on the analysis of the program results presented in Section 9 and draws on all program efforts - reentry simulation tests, analytical predictions, and chemical and physical properties tests. The adequacy of the theoretical characterization of the material response is also reviewed.

This summary is divided into three sections. The characterization of the surface response is presented in Section 10.1 and the characterization of the in-depth response is presented in Section 10.2. Section 10.3 summarizes a technique for predicting the complete material response based on these characterizations.

10.1 SURFACE RESPONSE

The surface response of the 5026-39HCG material under stagnation point heating conditions in air is reasonably well characterized by two basic correlations, one relating the surface recession rate to the surface temperature and the other relating these surface response parameters to the environmental conditions. The relationship between the surface response parameters of recession rate and temperature is presented in Figure 10-1. The two correlation lines adequately represent the reentry simulation results of this program. The relationship of the surface response parameters to the environmental conditions of heat flux, heat transfer coefficient, and enthalpy is presented in Figure 10-2. This correlation adequately represents the results of this program and corresponds to surface recession rate proportional to heat transfer coefficient together with a cutoff limit beyond which this proportionality no longer applies. The surface temperature can be related to the environmental conditions through the combination of Figures 10-1 and 10-2.

The two basic correlations are essentially independent of stagnation pressure over a broad range. Above a stagnation pressure of about 1 atmosphere, however, the correlations no longer apply. The response of the material becomes pressure sensitive and mechanical removal of the surface char apparently occurs. The measured recession at these conditions is the order of 2 1/2 times that indicated by the correlation (Figure 10-2).

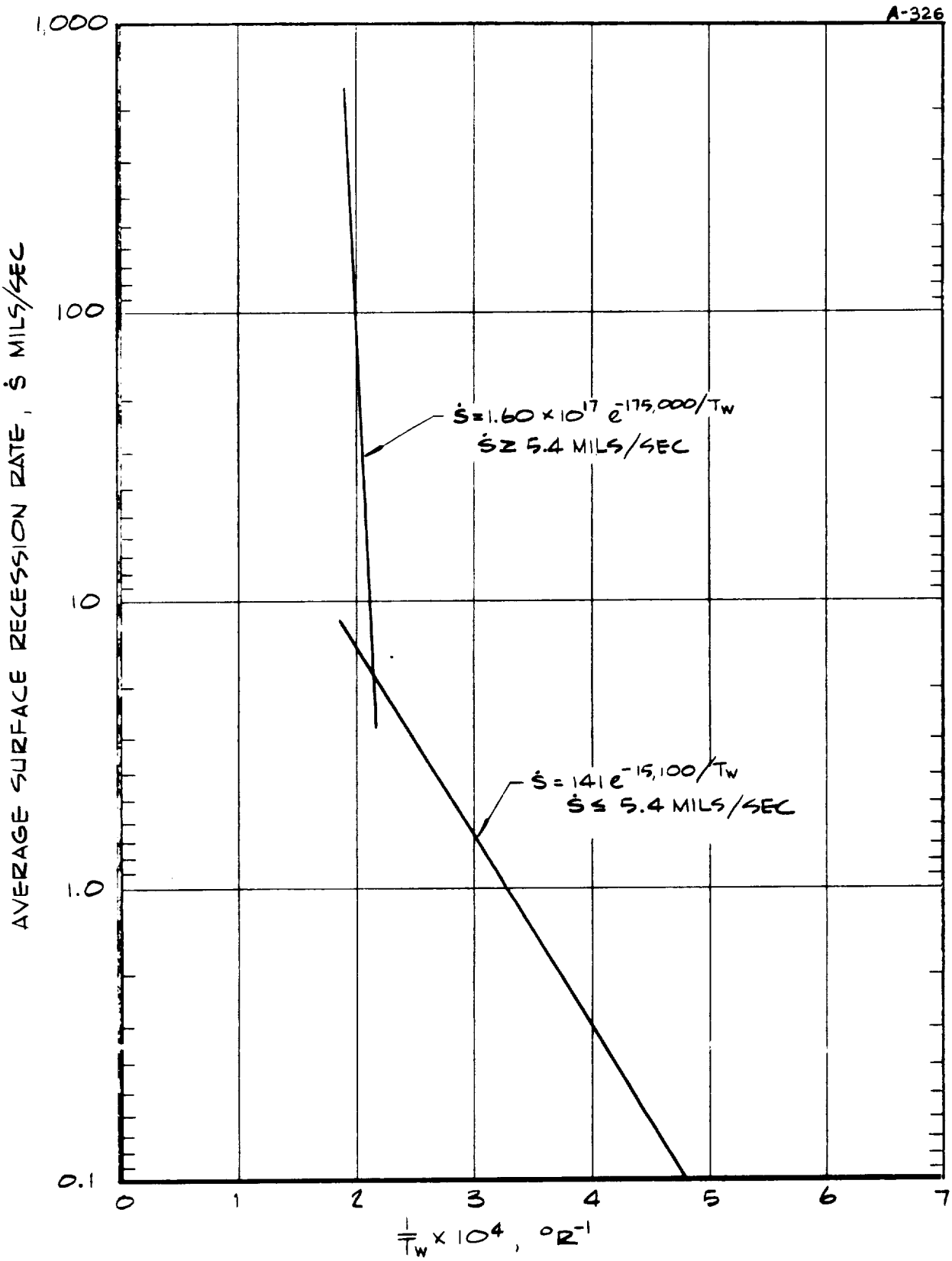

FIGURE 10-1 SURFACE RESPONSE CORRELATION FOR THE 5026-39HCG MATERIAL IN AIR.

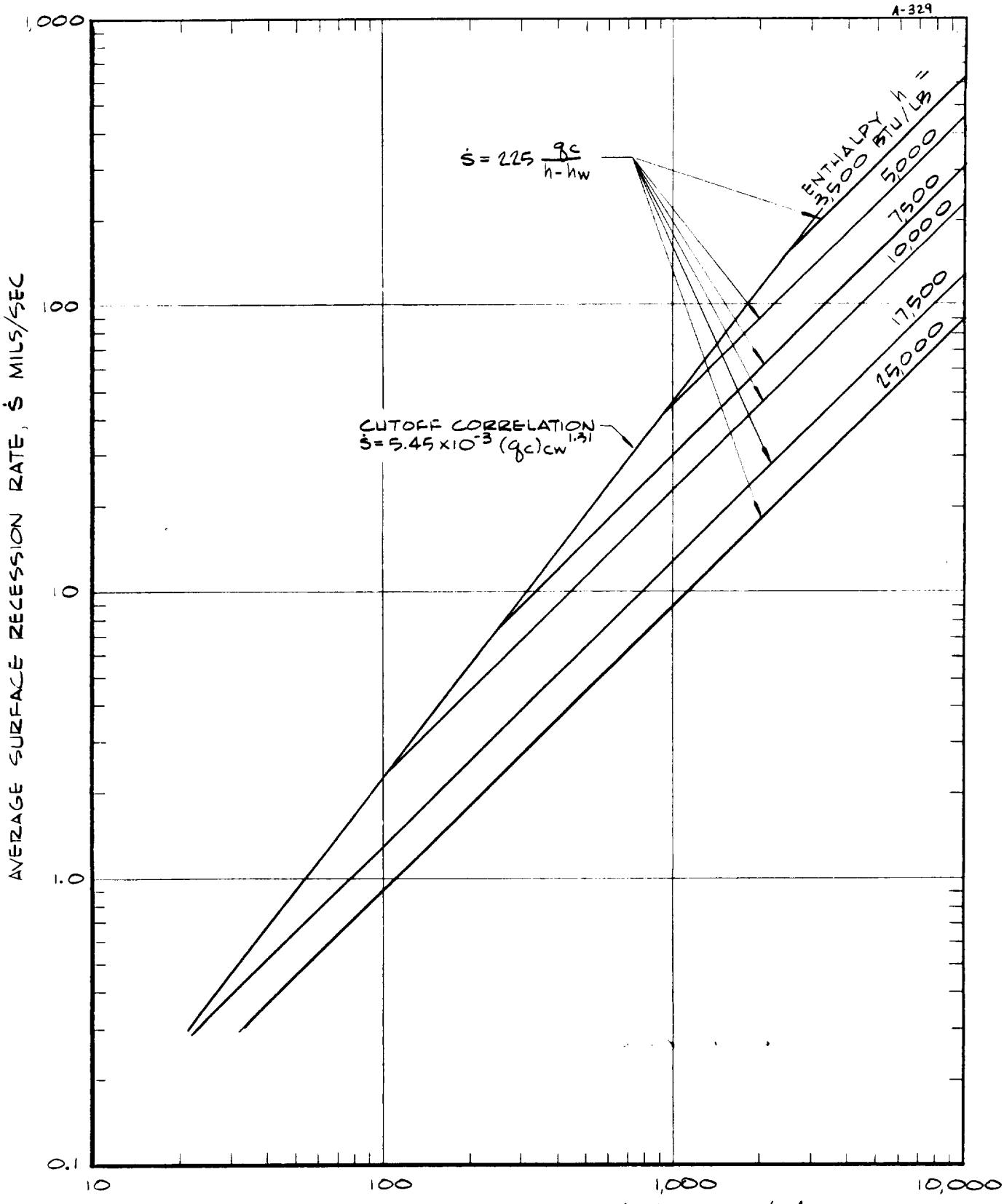

(a) IN TERMS OF COLD WALL CONVECTIVE HEAT FLUX

FIGURE 10-1 SURFACE RESPONSE - ENVIRONMENTAL CONDITIONS CORRELATION FOR THE 5026-39 HCG MATERIAL IN AIR

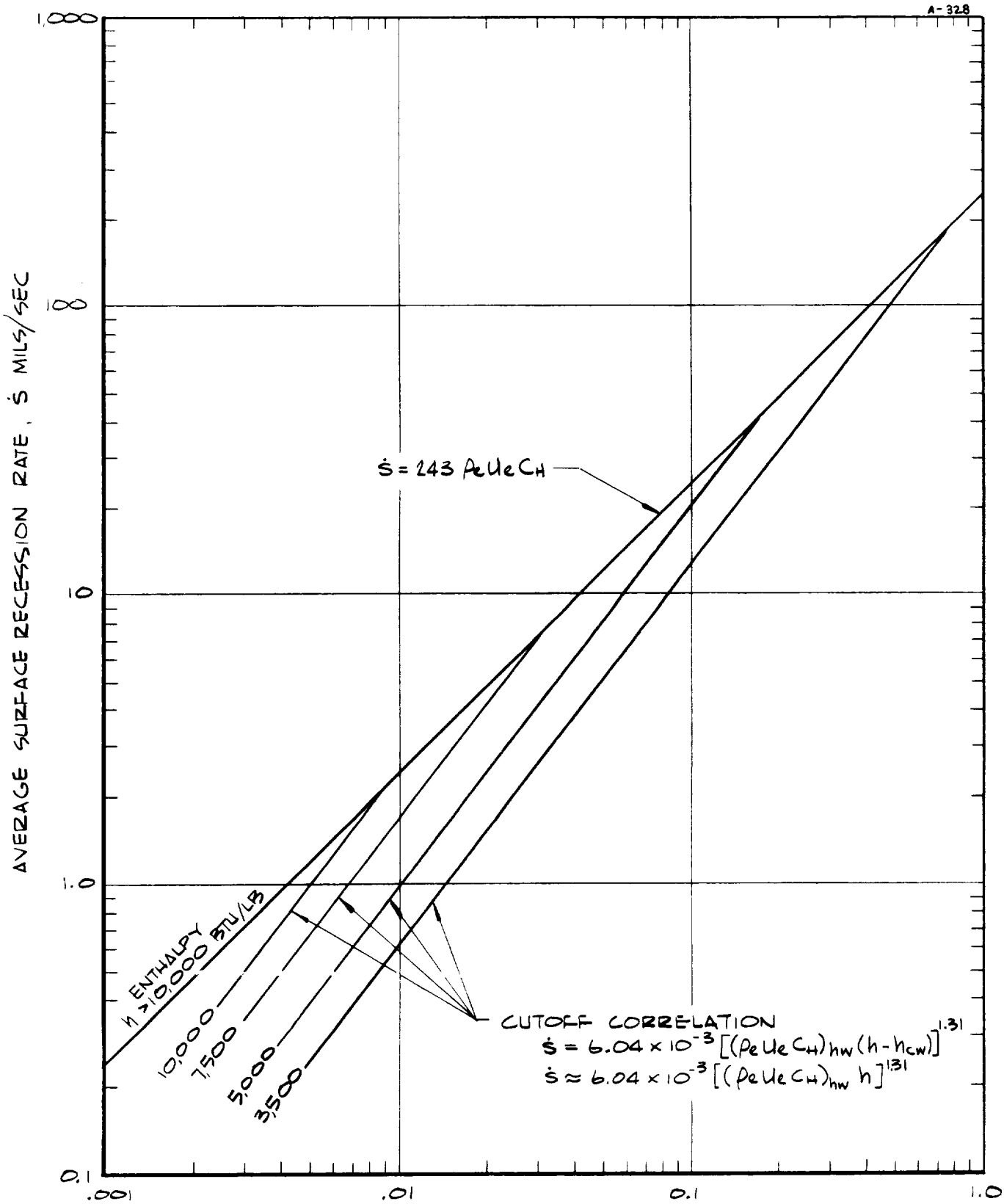

(b) IN TERMS OF CONVECTIVE HEAT TRANSFER COEFFICIENT

FIGURE 10-1 CONCLUDED

It is important to note that the above correlations were derived from the results of this program and therefore strictly apply only for the range of conditions considered. The correlations are felt to have a general validity over a broader spectrum of conditions however.

The surface recession rate and surface temperature response of the 5026-39HCG material is essentially independent of exposure time except at low heat flux - below a cold wall convective heat flux of about 50 Btu/ft^{2}sec. At tnese conditions a surface scab of agglomerated fibers that are primarily silica occurs. The scab apparently builds up with time providing protection to the char surface and resulting in a decreasing recession rate with increasing time. The surface scab is observed to occur at surface temperatures of about 2900°R and below, the approximate temperature at which silica begins to flow on the surface.

In the approximate surface temperature range of 3200°R to 3800°R, a surface melt in the form of globules occurs on the surface. These globules are primarily silica and flow along the surface and in the process coalesce with other globules and entrap gases. Above a surface temperature of about 3800°R, no surface melt is apparent. The char surface is primarily silica and carbon in the approximate ratio of 0.52.

The crystal structure at the surface can also be characterized by temperature. The silica at the surface is at least in part α-cristobalite in the approximate temperature range 2000°R to 3000°R. Silicon carbide (β-SiC) and graphite appear above about 3000°R. The β-silicon carbide occurs in only small quantities ($<$ 2 percent) whereas the quantity of graphite can be as high as about 30 percent of the carbon in the char. The graphite formation is apparently due to coking of the pyrolysis gases or graphitization of the carbon in the char.

Char shrinkage is apparently a real but small contributor to the surface recession. Based on results in a helium environment, this shrinkage is no greater than about 10 percent of the char thickness.

The surface recession in a nitrogen environment is significant, being much higher than that for helium at comparable conditions. This recession is apparently due to gas phase reactions with the char or to an effect on condensed phase reactions at the char surface. The actual mechanism has not been identified.

The correlations presented in Figures 10-1 and 10-2 also represent reasonably well the surface recession rate and surface temperature response of the material under combined radiative and convective heating conditions. In relating the surface response to the environmental conditions the correlation should be used in terms of heat flux where the convective heat flux is replaced by the total combined heat flux.

The theoretical characterization of the 5026-39HCG material response used in this program did not accurately represent the surface response of the material. The predicted surface temperature agreed closely with that measured but the predicted surface recession was always lower than that measured. The most obvious problems in this theoretical characterization were in the area of input information. The assumed char surface chemical composition was in error; the silica-to-carbon ratio is approximately 0.52, not 1.05 as used in the analytical predictions (the approximate average value for the char in-depth). This discrepancy also reflects a discrepancy between the actual and assumed pyrolysis gas chemistry at the surface. Finally, the actual flow temperature for SiO_2 was found to be lower than that assumed; approximately $3000^{\circ}R$ actually rather than the $3390^{\circ}R$ assumed. Also a more basic problem apparently exists although it could be related to the above input problems. The significant effect of nitrogen on the surface recession response mentioned previously is not accounted for by the theoretical model and the mechanism that should be included has not yet been identified. Additional analytical predictions using the above updated input information are required for further assessment of the theoretical model. This additional effort was beyond the scope of the contract.

10.2 IN-DEPTH RESPONSE

The in-depth response of the 5026-39HCG material, contrary to the surface response, is transient except at high heat flux. This response is therefore in general a strong function of exposure time and hence not subject to simple correlations such as developed for the surface response. The in-depth theoretical characterization of the material response is an accurate representation of this response however. This theoretical model therefore provides an accurate means of predicting the in-depth response for a given surface response.

Because of the transient nature of the in-depth response any detailed quantitative summary of this response is not sufficiently general to be included here. Other general information pertinent to its characterization is summarized below, however.

Resin decomposition occurs at in-depth temperatures up to about $2200^{\circ}R$. At this temperature the silica-to-carbon ratio is high and steadily decreases toward the surface, as temperature increases, approaching a value at the surface of about 0.52. The decrease in silica-to-carbon ratio is due to carbon deposition and/or silica depletion. The source of carbon deposition is apparently coking of the pyrolysis gases. The source of silica depletion is more obscure although its existence is apparently real. It is probably due to silica decomposition to gas phase species or due to condensed phase reactions between silica and carbon, also yielding gas phase species.

The in-depth formation of a crystalline structure occurs at approximately the same temperature conditions as indicated in Section 10.1 for the surface.

10.3 PREDICTION OF MATERIAL RESPONSE

The surface response and environmental conditions correlations presented in Section 10.1 and the in-depth theoretical model discussed in Section 10.2 provide a complete characterization of the response of the 5026-39HCG material The correlations define the surface recession rate and surface temperature response for given environmental conditions. The in-depth theoretical model, with this surface response as input, then defines the in-depth response. These surface and in-depth characterizations taken together therefore provide a means of predicting the complete response of the material to stagnation point reentry heating conditions. This prediction technique allows the calculation of material response for a broad spectrum of environmental conditions, including transient conditions typical of a reentry trajectory.

The results summarized in Section 10.1 also provide information necessary to checking out and improving an even more powerful prediction technique - the combined surface and in-depth theoretical model. This complete model will provide a prediction technique which is generally applicable and reliable for the complete spectrum of conditions to be experienced by the Apollo thermal protection system.

SECTION 11
RECOMMENDATIONS FOR FUTURE WORK

The results of this program have provided a quantitative characterization of the 5026-39HCG Apollo thermal protection material over a broad spectrum of reentry heating conditions. The program has also pointed out several questions regarding its response to reentry heating and several problems in theoretically characterizing this response. The answers to these questions and solutions to these problems were beyond the scope of this program but should certainly be the subject of future studies. Areas where a better definition of test conditions is desirable were also identified under the program and should also be the subject of future studies. The recommendations for future work, based on the results of this program, are presented in this section. These recommendations are outlined briefly below in two categories. The first, Section 11.1 presents recommendations pertinent to the further characterization of the material response to reentry heating conditions. The second, Section 11.2 presents recommendations pertinent to improved test and instrumentation techniques and to a better definition of test conditions. Concluding remarks are presented in Section 11.3.

11.1 DEFINITION AND CHARACTERIZATION OF MATERIAL PERFORMANCE

11.1.1 Further Evaluation of Empirical Correlations

The two basic empirical correlations of surface response presented in Sections 9 and 10 were based exclusively on the results of this program. These correlations should be checked against the results of other reentry simulation tests to establish their validity and generality.

11.1.2 Study of the Material Response in Nitrogen

The cause of the significant surface recession observed herein in the nitrogen environment has not been identified. A study should be initiated to define the mechanism or mechanisms of this recession. The possible chemical reactions should be investigation further, including the possibility of unaccounted for carbon-nitrogen species, unaccounted for interactions with the pyrolysis off-gases, and effects on possible condensed phase reactions. Tests in nitrogen over a broader spectrum of conditions and possibly including other materials such as a carbon - epoxy novalac - phenolic material or a very high purity silica - epoxy novalac - phenolic material would be informative in defining the mechanism. The study should also include additional and more detailed chemical analysis of the char surface material.

11.1.3 Study of Shear Effects

The response of the 5026-39HCG material under off-stagnation-point heating conditions in both laminar and turbulent flow should be studied more definitively and over a broad spectrum of conditions. A sonic duct configuration, in conjunction with a vacuum system, should be used for the majority of tests. This combination would allow an accurate definition of the material response over a broad spectrum of well defined test conditions. Some tests should be performed in subsonic and supersonic duct configurations to allow a differentiation between shear level and heat flux effects and identify any effect of Mach number.

11.1.4 Further Study of In-Depth Response

The analysis of in-depth response performed herein identified carbon deposition and silica depletion as two apparently important in-depth response phenomena. The mechanisms of these phenomena should be identified definitively. Detailed density measurements coupled with detailed chemical analysis would quantitatively define the mass distribution of carbon and silica and the distribution of molecular composition in the char. Laboratory tests which isolate each of the two mechanisms would certainly be informative. Pyrolysis gas sampling and subsequent mass-spectrometer analysis at in-depth locations could identify the elemental carbon distribution through the char and the existence of gas phase silicon compounds.

11.1.5 Further Study of Surface Response

The program herein resulted in a partial characterization of the surface response. This characterization should be completed through more detailed tests and analyses than possible under this program. The low heat flux region in which the scab and globules occur at the surface should be studied in detail. The scab should be characterized more thoroughly including an approximate definition of its properties and rate of formation. Its response to transient heating typical of trajectory conditions should also be studied to define its integrity and performance as the severity of heating conditions increases. The surface globules should be better characterized including an improved definition of the surface temperature at which they begin to form. The existence and importance of the dual surface recession mechanism - melt removal plus chemical reactions with the exposed char - should be studied. A more detailed characterization of the high surface temperature char should also be accomplished.

11.1.6 Study of the Effects of Transient Conditions on Material Response

All reentry simulation tests performed in this program were at constant environmental conditions. The effects of transient conditions typical of a reentry trajectory should also be studied. To define these effects, portions of a trajectory would be simulated through the controlled variation of test conditions. The measured response would then be compared with predictions of this response based on the correlations presented herein and on the theoretical characterization of the material response. These comparisons would then provide a definition of the transient effects, if any.

11.1.7 Study of Char Shrinkage

The results of this program indicate that char shrinkage is a significant though small surface recession mechanism. Tests should be performed to better quantify this mechanism and to define whether it occurs during heating or during the cooldown period after test.

11.1.8 Analysis of the Theoretical Model in the Light of New Input Information

The results of this program demonstrated that some of the input information used in the analytical predictions performed herein was in error. These predictions should be performed again using this better input information and possibly parametrically varying this input within the limits indicated by the program results. The input to be considered would include the char surface chemistry, pyrolysis gas chemistry, pyrolysis gas molecular composition (e.g. equilibrium or frozen), pyrolysis gas interaction with the boundary layer edge gas and surface material, and fail temperature above which melt removal is allowed.

11.1.9 High Pressure Tests

Tests at high stagnation pressure ($p_s \geq 1$ atm) should be performed in a multi-megawatt facility to allow reasonably large model sizes to be used. This would reduce the apparent problems encountered herein in such high pressure tests.

11.1.10 Combined Convective and Radiative Heating Tests

Tests at combined convective and radiative heating conditions should be performed for a broad spectrum of conditions and with a radiation beam that covers the complete model surface. This would reduce the problems encountered in this program in such tests.

11.2 TEST AND INSTRUMENTATION TECHNIQUES

11.2.1 Definition of Properties and Heat Transfer Parameters for Non-Air Streams

The definition of test conditions under this program for non-air environments was incomplete in that mass flux and heat flux enthalpies were not able to be defined and heat flux and heat transfer coefficient calculations were not possible. Calculations to define sonic flow conditions, supersonic expansion properties, transport properties, and heat transfer coefficients should be performed for non-air gas systems such as helium, argon, nitrogen, and nitrogen-oxygen mixtures to allow the complete definition of test conditions for these systems.

11.2.2 Measurement of Local Enthalpy and Mass Flux

The current state-of-the-art at the start of this program did not allow definitive local measurements of enthalpy and mass flux to define the radial distribution of these properties. Sharp-tipped probes should be developed to provide definitive measurements of these properties in supersonic streams and once developed should be used for the further analysis and detailed definition of test stream properties.

11.2.3 Diagnostics of High Enthalpy Conditions

Tests at high enthalpy (> 15,000 Btu/lb) for which the supersonic anode configuration was used resulted in significant radial nonuniformities in stream properties and the relation between energy balance enthalpy, mass flux enthalpy, and heat flux enthalpy was not able to be defined. Further characterization of these streams should be performed through detailed measurements (e.g., Section 11.2.2) and theoretical calculations of constrictor arc properties distributions and expansion characteristics.

11.3 CONCLUDING REMARKS

The above recommendations for future work were based on the results of this program and covered the major problem areas and areas of question indicated by the program. Further effort is required to completely characterize the 5026-39HCG material response to reentry heating conditions and to provide a more detailed description of arc heated test streams in which this response is determined. The above recommendations cover many of the requirements for future work in these areas; the list, though thorough, cannot be regarded as complete.